CRPP

CENTRE DE RECHERCHES EN PHYSIQUE DES PLASMAS
FACULTÉ DES SCIENCES DE BASE
ASSOCIATION EURATOM - CONFÉDÉRATION SUISSE

ÉCOLE POLYTECHNIQUE FÉDÉRALE DE LAUSANNE

ANNUAL REPORT

2011

Table of contents

Préface

Cher Lecteur,

C'est avec grand plaisir que je vous présente notre Rapport Annuel 2011. Dans le domaine de la fusion, notre stratégie est focalisée sur l'avancement de la physique et de la technologie ayant pour but la réalisation commerciale d'une centrale. ITER, qui est en construction à Cadarache, signifie clairement que notre quête de l'énergie de fusion est proche de son aboutissement. Le lancement du « Power Plant Physics and Technology Programme» est un autre signal fort de l'engagement du programme de fusion européen à préparer la construction de la centrale de démonstration DEMO. Dans les deux cas, le CRPP joue un rôle important dans cette stratégie.

De nombreux nouveaux résultats importants se trouvent dans le Rapport Annuel 2011. Je remercie toutes les institutions et les organismes de financement pour leur support. J'exprime également ma gratitude envers tous mes collègues, dont l'engagement a rendu possible notre succès collectif.

Prof. M.Q. Tran
Directeur Général

Foreword

Dear Reader,

It is with great pleasure that I present you our 2011 Annual Report. In the field of fusion, our strategy remains focused on the advancement of physics and technology aiming at the commercial realization of a power plant. ITER, under construction in Cadarache, is the clear sign that our quest for fusion is within reach. The launch of a Power Plant Physics and Technology Programme is another clear signal of the commitment of the European Fusion Programme to prepare for the construction of DEMO fusion power plant. In both cases, the CRPP is playing an important role as part of its strategy.

Many novel and important results can be found in the 2011 Annual Report. I would like to thank all institutions and funding agencies for their support. I also express my gratitude to all colleagues, whose commitment has made our collective success possible.

Prof. M.Q. Tran
General Director

Vorwort

Liebe Leserin, lieber Leser,

Es freut mich, Ihnen hiermit unseren Jahresbericht 2011 vorlegen zu können. Wie bereits in den vergangenen Jahren ist unsere Strategie auf Fortschritte der Fusionsforschung sowohl in der Physik als auch in der Technologie ausgerichtet und hat die Verwirklichung eines Fusionsreaktors zum Ziel. Der Beginn der Konstruktionsphase von ITER in Cadarache, Frankreich, setzt ein klares Zeichen dafür, dass die Verwirklichung der Fusion in Reichweite liegt. Mit dem Start des Programms zur Entwicklung von Physik und Technologie des Fusionkraftwerks (Power Plant Physics and Technology Programme) wurde ausserdem deutlich gemacht dass im europäischen Programm Entschlossenheit zur Vorbereitung eines Reaktor-Prototyps (DEMO) besteht. Innerhalb dieser Strategie kommt dem CRPP eine wichtige Rolle zu.

Der vorliegende Jahresbericht 2011 enthält eine Vielzahl neuer und bedeutender Ergebnisse. Für die erforderliche finanzielle Unterstützung möchte ich allen betroffenen Organisation und Institutionen meinen Dank aussprechen. Meine dankbare Anerkennung gilt auch allen Kollegen und Mitarbeitern, durch deren unermüdlichen Einsatz diese Resultate zustande gekommen sind.

Prof. M. Q. Tran
Generaldirektor

Prefazione

Caro lettore,

è con grande piacere che Le presento il nostro Rapporto Annuale 2011. Nel campo della fusione, la nostra strategia è focalizzata sul progresso della fisica e della tecnologia, puntando alla realizzazione commerciale di una centrale. ITER, in corso di costruzione a Cadarache, indica chiaramente che l'utilizzo dell'energia di fusione è alla nostra portata. Il lancio del «Power Plant Physics and Technology Programme» è un altro limpido segnale dell'impegno del programma di fusione europeo nella preparazione della costruzione della centrale prototipo DEMO. In entrambi i casi, il CRPP svolge un ruolo importante in questa strategia.

Molti nuovi risultati di rilievo sono descritti nel Rapporto Annuale 2011. Ringrazio tutte le istituzioni e gli organismi di finanziamento per il loro sostegno. Esprimo inoltre la mia gratitudine a tutti i miei colleghi, il cui impegno ha reso possibile il nostro successo collettivo.

Prof. M.Q. Tran
Direttore Generale

1 INTRODUCTION

1.1 The international frame and its relation to the Swiss programme

1.1.1 ITER

In Europe, the funding of ITER for the last two years of the 7th Framework Programme (2012-2013) was decided at the end of 2011. This decision will allow the European Domestic Agency Fusion for Energy (F4E) to plan for procurement in 2012-2013.

The devastating earthquake and tsunamis in Japan forced the ITER Organisation to revise the time schedule, since some components are manufactured in Japan. First plasma is now foreseen in November 2020.

1.1.2 Euratom

In parallel with the decision on the budget of ITER for 2012-2013, Euratom has also decided the fusion budget for the last two years of the 7th Framework programme. This budget is relatively tight compared to the past one. The 2012-2013 workprogramme will include a new element, the Power Plant Physics and Technology programme under the auspices of the European Fusion Development Programme Agreement. The programme's aim is the design of a demonstration fusion power plant capable of delivering electricity by the mid of the century. Formally, Switzerland has now to negotiate with Euratom on its participation to the Euratom programme for 2012-2013, including ITER. Such negotiation will take place in 2012.

In view of the preparation of the Euratom programme in the years 2014-2020 (known as Euratom - Horizon 2020) the main objectives of fusion research have been discussed within the community. They encompass:

- the construction of ITER within scope, schedule and cost
- the preparation for a successful scientific operation of ITER
- the preparation of ITER generation of scientists, engineers and operators
- the laying of the foundation for fusion power plant
- the promotion of innovation and of the competitiveness

A more detailed work plan will be prepared in 2012.

Switzerland has also to decide about its participation in Euratom Horizon 2020.

1.2 A brief summary of the CRPP activities

The activities of the CRPP during 2011 are in line with a strategy, which was endorsed in an audit performed in 2010 by a panel of high level international scientists. For the fusion part, they are oriented towards:

a) the successful construction of ITER through focused contributions in the CRPP fields of expertise;
b) the preparation of the scientific exploitation of ITER, the exploration of novel physics for DEMO;
c) the education of the young scientists and engineers;
d) the fulfilment of tasks assigned by the Swiss government in the frame of the "Broader Approach".

The lines a) to c) are fully in line with the 2011 Workprogramme of the Euratom-Swiss Confederation Contract of Association.

Applications of the knowledge and know-how through fusion- based activities are also a main component of our work, as in the past.

The Annual Report gives a detailed description of our scientific results in the various fields. They encompass, in the domain of plasma and fusion physics, experimental tokamak physics using the TCV device, basic plasma physics on the Torpex machine, theory and numerical modelling. The construction of ITER and DEMO involves high technology in the field of heating, material science and technology and superconductivity. The interested reader will find the contributions of the CRPP in all these key fields.

Transfer of technology and application of the knowledge gained through fusion R+D are, as in the past, an important part of our scientific and technological activities: besides industrial processes based on plasma, our traditional field of excellence, high T_C superconductivity applications and sub-millimeter wave sources for NMR applications are two other fields which have obtained interesting results in 2011.

The wealth, diversity and importance of the results obtained in 2011 render a selection of highlights difficult, if not impossible. We kindly refer the reader to the separate chapters, where they are detailed.

1. INTRODUCTION

1.1.1 ITER

En Europe, le financement d'ITER pendant les deux dernières années du 7e Programme Cadre (2012-2013) a été décidé à la fin de 2011. Cette décision permettra à l'Agence Européenne « Fusion for Energy » (F4E) de planifier les acquisitions pour les deux prochaines années.

Le tremblement de terre, suivi du tsunami dévastateur, qui a ravagé le Japon, a contraint l'Organisation ITER de réviser le calendrier, étant donné que certains composants y sont fabriqués. Le premier plasma est maintenant prévu en novembre 2020.

1.1.2 Euratom

En parallèle à le décision du budget d'ITER pour 2012-2013, le budget Euratom a aussi été décidé pour ces années-là. Comparé au précédent, ce budget est assez serré. Le programme de travail 2012-2013 inclura un nouvel élément, le « Power Plant Physics and Technology programme », qui sera effectué sous les auspices de l'EFDA (European Fusion Development Agreement). Son but est la conception d'une centrale électrique basée sur la fusion pour le milieu du siècle. La Suisse doit maintenant négocier avec l'Euratom sa participation au programme 2012-2013, y compris ITER. Ces négociations auront lieu en 2012.

Afin de préparer le programme Euratom pour les années 2014-2020, appelé « Horizon 2020 », les objectifs principaux de la recherche en fusion ont été discutés dans la communauté. Ils englobent :

- la construction d'ITER en respectant les spécifications, le calendrier et les coûts ;
- la préparation de l'opération scientifique réussie d'ITER
- la formation de la « génération ITER » de scientifiques, d'ingénieurs et d'opérateurs ;
- de jeter les bases d'une centrale électrique à fusion ;
- la promotion de l'innovation et de la compétitivité.

Un plan de travail plus détaillé sera préparé en 2012.

La Suisse doit également se prononcer sur sa participation à « Horizon 2020 ».

1.2 Un bref résumé des activités du CRPP

Les activités du CRPP en 2011 sont en accord avec la stratégie approuvée par une commission d'experts de scientifiques de haut niveau international, lors d'un audit effectué en 2010. Pour la partie fusion, elles sont orientées vers :

a) La construction réussie d'ITER, par des contributions spécifiques aux domaines d'expertise du CRPP ;
b) La préparation de l'exploitation scientifique d'ITER et l'exploration de la nouvelle physique pour DEMO ;
c) la formation de jeunes scientifiques et ingénieurs ;
d) l'accomplissment des tâches allouées par le gouvernement suisse dans le cadre de l' « approche élargie ».

Les points a)-c) ci-dessus sont en plein accord avec le programme de travail effectué dans le cadre du contrat d'Association Euratom – Confédération Suisse.

Le Rapport Annuel donne une description détaillée de nos résultats scientifiques dans différents domaines. Ils comprennent la physique expérimentale du tokamak en utilisant l'installation TCV, la physique des plasmas de base sur la machine Torpex, la théorie et la simulation numérique. La construction d'ITER et de DEMO implique de la haute technologie pour le chauffage, la science des matériaux et la supraconductivité. Le lecteur intéressé trouvera les contributions du CRPP dans tous ces domaines clés.

Le transfert de technologie et l'application des connaissances acquises par la recherche et le développement en fusion sont, comme par le passé, une partie importante de nos activités scientifiques et techniques. En plus des procédés plasmas pour l'industrie, qui est notre champ d'excellence traditionnel, nous avons également obtenu des résultats intéressants pour la supraconductivité à haute température et les sources d'ondes sub-millimétriques appliquées à le résonance magnétique nucléaire.

La richesse, la diversité et l'importance des résultats obtenus en 2011 rendent pratiquement impossible la sélection de l'un ou l'autre point fort. Le lecteur est donc prié de se référer aux chapitres correspondants, où ceux-ci sont présentés plus en détail.

1 EINLEITUNG

1.1 Das internationale Umfeld und dessen Einfluss auf das schweizerischen Forschungsprogramm

1.1.1 ITER

Der europäische Beitrag zur Finanzierung des ITER Projekts für die letzten zwei Jahre des 7. Europäischen Rahmenprogramms (2012-2013) wurde am Ende des Jahres 2011 verabschiedet. Auf der Basis dieser Entscheidung wird die europäische Agentur zur Verwirklichung der Fusion (Fusion for Energy, F4E) ihre Ausgaben in den Jahren 2012-2013 planen können.

Die Situation in Japan nach dem katastrophalen Erdbeben und Tsunami zwangen die ITER Organisation zur Revision des Zeitplans, denn bedeutende Komponenten für ITER werden in Japan hergestellt. Damit verschiebt sich das vorgesehen Datum für ein erstes Plasma in ITER auf November 2020.

1.1.2 Euratom

Gleichzeitig mit der Entscheidung über das Budget von ITER für den Zeitraum 2012-2013, hat EURATOM auch die Mittel der Fusionsforschung für die letzten zwei Jahre des 7.europäischen Rahmenprogramms festgelegt. Im Vergleich zu den vorangehenden fällt dieses Budget recht knapp aus. Das Arbeitsprogramm für den Zeitraum 2012-2013 enthält als neues Element das Programm zur Entwicklung von Physik und Technologie des Fusionskraftwerks, das im Rahmen des europäischen Abkommens zur Fusionsforschung durchgeführt werden soll. Ziel dieses Programms ist die vorbereitende Planung eines Reaktor-Prototyps, mit dem Ziel bis zur Mitte des Jahrhunderts elektrische Energie aus einem Fusionskraftwerk zu gewinnen. Für die Schweiz stehen im Lauf des Jahres 2012 Verhandlungen mit EURATOM über die Beteiligung am Fusionsforschungsprogramm 2012-2013 und am ITER Projekt bevor.

Mit Aussicht auf die Vorbereitungen des EURATOM Programms für die Jahre 2014-2020 (EURATOM Horizont 2020) legten die beteiligen Partner die Zielsetzungen fest. Dazu gehören :

- Der Bau von ITER unter Berücksichtigung von wissenschaftlichem Ziel, Zeitplan und Kostenplan
- Die Vorbereitungen für einen erfolgreichen wissenschaftlichen Betrieb von ITER
- Die Ausbildung einer “ITER-Generation“ von Wissenschaftlern, Ingenieuren und Technikern
- Vorarbeiten zur Verwirklichung eines Fusionskraftwerks
- Die Förderung der Innovation und der internationalen Konkurrenzfähigkeit

Ein ausführliches Arbeitsprogramm wird im Jahr 2012 ausgearbeitet werden.

Im Jahr 2012 ist die Schweizerische Eidgenossenschaft aufgefordert eine Entscheidung über die weitere Beteiligung am EURATOM Programm (Horizont 2020) zu treffen.

1.2 Eine Zusammenfassung der Forschungsergebnisse des CRPP

Auch im Jahr 2011 folgten die Forschungsarbeiten am CRPP einer bewährten Strategie, die bereits 2010 im Rahmen einer Beurteilung durch eine international zusamengesetzte Gruppe von renommierten Wissenschaftlern befürwortet wurde. Für den Bereich Fusionsforschung gilt folgende Ausrichtung :

a. gezielte Beiträge zum ITER Projekt unter Berücksichtigung spezieller Kenntnisse am CRPP
b. Vorarbeiten zum wissenschaftlichen Betrieb von ITER ;
   Suche nach neuen Erkenntnissen für DEMO
c. Ausbildung von jungen Wissenschaftlern und Ingenieuren
d. Arbeiten im Rahmen des Erweiterten Forschungprogramms zur Fusion (broader approach), in Erfüllung des Auftrags der schweizerischen Bundesregierung.

Die Positionen a) bis c) stehen voll im Einklang mit dem Arbeitsprogramm 2011 der Assoziation zwischen EURATOM und der Schweizerischen Eidgenossenschaft.

Dieser Jahresbericht stellt eine Zusammenfassung unserer wissenschaftlichen Ergebnisse aus den verschiedenen Bereichen dar. Auf dem Gebiet der fusionsorientierten Plasmaphysik gehören dazu experimentelle Untersuchungen am Tokamak TCV, sowie an TORPEX, einer Anlage zur Untersuchung von grundlegenden Plasmaeigenschaften, und Forschungsarbeiten in Plasmatheorie und numerischer Simulation.
Der Bau von ITER und DEMO basiert auf Technologie auf hohem Niveau ; insbesondere auf dem Gebiet von Plasmaheizung und in Bezug auf Materialien, wie z.B Supraleiter. Der interessierte Leser wird auch zu diesen Themen wesentliche Beiträge vom CRPP finden.

Wie bereits in früheren Jahren bildet die Anwendung von Kenntnissen und Fähigkeiten, die im Rahmen unserer Forschungstätigkeiten erworben wurde, einen wichtigen Bestandteil unseres Auftrages. Untersuchung und Entwicklung industrieller Verfahren auf Plasmabasis sind seit langem eines unserer Spezialgebiete, das bedeutende Beiträge hervorgebracht hat. Ausserdem spielen technische Anwendungen von Hochtemperatur-Supraleitern und von leistungstarken Strahlungsquellen im Bereich der Mikrowellen eine wichtige Rolle. Das bezeugen einige bemerkenswerte Ergebnisse aus dem Jahr 2011.

Die Zahl und Vielfalt der im Jahr 2011 erzielten Ergebnisse machen es schwer, eine Auswahl hervorragender Beiträge zu treffen. Wir überlassen es dem Leser, aus den verschiedenen Kapiteln nach eigenem Interesse auszuwählen.

1 INTRODUZIONE

1.1 La situazione internazionale e il suo rapporto con il programma Svizzero.

1.1.1 ITER

In Europa, il finanziamento di ITER per gli ultimi due anni del settimo Programma Quadro [2012-2013] è stato deciso alla fine del 2011. Questa decisione permetterà all'Ente Europeo Fusion for Energy [F4E] di pianificare gli appalti per il 2012-2013.

Il devastante terremoto e tsunami in Giappone ha costretto l'Organizzazione ITER a modificare il programma e le scadenze, poiché alcuni componenti vengono fabbricati in Giappone. Il primo plasma è ora previsto per il novembre 2020.

1.1.2 Euratom

In parallelo alla decisione sul budget di ITER per il 2012-2013, l'Euratom ha stabilito anche il budget della fusion per gli ultimi due anni del settimo Programma Quadro.
Il budget è relativamente ristretto rispetto a quello precedente. Il programma di attivitá comprenderà un nuovo elemento, il programma di Fisica e Tecnologia della Centrale Elettrica a Fusione sotto gli auspici dell'Accordo Europeo per lo Sviluppo della Fusione. Lo scopo del programma è la progettazione di una centrale elettrica a fusione di prova, in grado di fornire elettricità per la metà del secolo. Formalmente, la Svizzera deve ora negoziare con l'Euratom la sua partecipazione al programma Euratom per il 2012-2013, comprendente ITER. Questi negoziati si svolgeranno nel 2012.

Nella prospettiva della preparazione del programma Euratom per gli anni 2014-2020 [noto come Euratom – Orizzonte 2020], gli obiettivi principali della ricerca sulla fusione sono stati discussi in seno alla comunità. Questi comprendono:
- la costruzione di ITER nei termini, tempi e costi previsti
- la preparazione dell'operazione di ITER
- la formazione della generazione ITER di scienziati, ingegneri e operatori
- la posa delle fondazioni di una centrale elettrica a fusione
- la promozione dell'innovazione e della competitività

Un piano di lavoro più dettagliato sarà formulato nel 2012.

La Svizzera deve inoltre prendere una decisione sulla sua partecipazione all'Euratom – Orizzonte 2020.

1.2 Un breve riassunto delle attività del CRPP

Le attività del CRPP durante il 2011 sono in linea con la sua strategia, avallata da un'analisi effettuata nel 2010 da un pannello internazionale di scienziati di alto livello. Per quanto riguarda la fusione, queste attività volgono a:

a) la costruzione compiuta di ITER attraverso contributi focalizzati nelle aree di competenza del CRPP;
b) la preparazione dell'utilizzo scientifico di ITER e l'esplorazione di nuova fisica per DEMO;
c) l'educazione di giovani scienziati e ingegneri;
d) l'adempimento di mansioni assegnate dal governo svizzero nel quadro del "Broader Approach".

Le linee da a) a c) sono completamente coerenti con il programma di attività del Contratto di Associazione tra l'Euratom e la Confederazione Svizzera.

L'applicazione delle nostre conoscenze e competenze attraverso attività basate sulla fusione rimangono una componente importante del nostro lavoro, come in passato.

Il Rapporto Annuale fornisce una descrizione dettagliata dei nostri risultati scientifici nelle diverse aree. Questi comprendono, nel campo della fisica del plasma e della fusione, la fisica sperimentale del tokamak usando l'installazione TCV, la fisica del plasma di base sul dispositivo Torpex, la teoria e la modellizzazione numerica. La costruzione di ITER e di DEMO fa ricorso ad alte tecnologie nei campi del riscaldamento ausiliario del plasma, della scienza e tecnologia dei materiali e della superconduttività. Il lettore interessato troverà i contributi del CRPP in tutte queste aree cruciali.

Il trasferimento tecnologico e l'applicazione di conoscenze acquisite attraverso ricerca e sviluppo nella fusione costituiscono, come nel passato, una parte importante delle nostre attività scientifiche e tecnologiche: oltre ai processi industriali basati sul plasma, il nostro campo d'eccellenza tradizionale, le applicazioni della superconduttività ad alta temperatura e lo sviluppo di sorgenti elettromagnetiche sub-millimetriche per applicazioni RMN sono due aree che hanno visto risultati interessanti nel 2011.

La ricchezza, varietà e importanza dei risultati ottenuti nel 2011 rendono difficile, per non dire impossibile, effettuare una selezione ridotta di quelli piú importanti. Preghiamo il lettore di consultare i capitoli individuali in cui troverà tutti i dettagli.

2 RESEARCH ACHIEVEMENTS OF THE CRPP IN 2011

2.1 The TCV tokamak

Experimentation on TCV, the largest research facility on EPFL campus, continues to be the main effort of the CRPP Team. The TCV tokamak has been operational since 1992 and is characterized by the most extreme plasma shaping capability worldwide, the highest Electron Cyclotron (EC) power concentration in the plasma, and by a large degree of flexibility in its heating and control schemes. The main mission of TCV is to contribute to the physics basis for a more efficient ITER exploitation, and for the optimization of the tokamak concept and relevant plasma scenarios, heating and control techniques, for the establishment of the step following ITER, a demonstration power plant called DEMO, expected to be the last one before the commercial fusion power plants.

TCV operation in 2011 started in February, after a short interruption due to the need to replace one of the primary transformers feeding the flywheel generator. Apart from a planned five-week break during the summer holidays, which was employed for in-vessel repairs and diagnostic installations, TCV has been operated continuously since that date within the conventional 3-weeks-on, 1-week-off schedule (4 operation days per week). Despite the continuing unavailability of an X3 gyrotron, still under repair, and of the diagnostic NBI since May, the plant availability has been very high, of the order of 80%, until the end of the year.

The experimental campaigns have been conducted along a rich variety of specific missions proposed and selected during discussions within the CRPP and with a number of European and international collaborators. These missions are structured according to the following general themes: transport in shaped L- and H-mode plasmas, scenarios with internal transport barriers and developments towards steady-state operation, H-mode and ELM control, ECH and ECCD physics, advanced plasma control, edge and core electron-dominated turbulence, advanced shaping and innovative divertor concepts, and related edge physics, and the preparation for medium term developments and upgrades.

As is typical in the flexible TCV environment, a significant fraction of the experimental time has been dedicated to exploring ideas that were not anticipated a priori. We also note that during 2011 several PhD theses based on TCV experiments were successfully brought to completion, and that approximately 40% of TCV experiments were officially conducted by PhD students.

The highlights of the many notable results obtained in 2011 are given in the following paragraphs, through which emerges the significance of the parallel progress in the physics understanding and in the development of control methods and capabilities.

2.1.1 Scenarios with internal transport barriers

Development work has taken place to establish electron internal transport barriers at a location centred in the TCV vessel, where ion temperature and rotation measurements can be performed owing to the presence of a diagnostic neutral beam injector (DNBI). While these scenarios have been routinely produced in TCV for many years in the upper part of the chamber, shifting them to the centre is more challenging because of reduced passive wall stabilisation of axi-symmetric instabilities and less optimal ECRH launching geometry. However, a robust target configuration has now been developed, and ion measurements are planned for the last few weeks of this year after the ongoing repairs on the DNBI are completed.

2.1.2 H-mode physics

As in previous campaigns the study of H-mode physics has played an important and central role in the experimental run of 2011. The H-mode physics topic was split into several sub-topics ranging from the practical matter of establishing an ELMy H-mode close to the geometric centre of the TCV chamber to the study of ELM control using edge electron cyclotron resonance heating.

Z=0 H-mode, double null H-mode

The TCV machine has enormous flexibility in plasma shaping and plasma position control. A gateway has been found on TCV, to regularly and routinely establish diverted, single and double null, Ohmic, stationary, ELMy H-mode plasmas in the upper part of the machine (plasma centre typically 23cm above the machine mid-plane), but it has proven difficult to routinely and reliably create similar discharges near the machine centre. The reasons for this are not fully understood. In addition to providing a possible contribution to the basic understanding of H-mode physics, the development of a quasi-stationary ELMy H-mode at the machine mid-plane (Z=0cm) is motivated by two main reasons.

The first reason is related to intrinsic plasma rotation, which plays an important role in regulating plasma confinement and whose study is an important part of the TCV programme. Rotation in L-mode and in the presence of internal transport barriers has been extensively studied. The charge exchange recombination spectrometer (CXRS), with its diagnostic neutral beam, is the means by which plasma rotation is measured in TCV. Unfortunately, this offers only edge measurements of intrinsic impurity (carbon) rotation and impurity temperature in standard TCV H-mode discharges placed in the upper part of the vacuum vessel. Despite the fact that some analysis can be done under these circumstances, the limited radial coverage compromises the scientific study of discharges in the upper part of the machine. If it were possible to establish quasi-stationary ELMy H-modes near the chamber mid-plane then the measurements of intrinsic impurity rotation and temperature would extend from the plasma edge to the plasma centre completing diagnostic coverage of these discharges.

The second reason is related to plans to install approximately one mega-Watt of neutral beam heating (NBI) on TCV in the near future. This will be installed with the beam near the chamber centre, thus it will be necessary to be able to achieve ELMy H-mode near the machine centre as a target for the NBI heating.

Some considerable time has been spent developing strategies for creating ELMy H-mode at Z=0cm. Initially efforts concentrated on establishing a double-null divertor and toggling the active divertor leg. Initial results show that the toggling certainly modifies the H-mode from ELMy to ELM-free but the discharges were not sustainable due to external ideal modes that caused disruptions. Figure 2.1.1 shows an example of such a discharge.

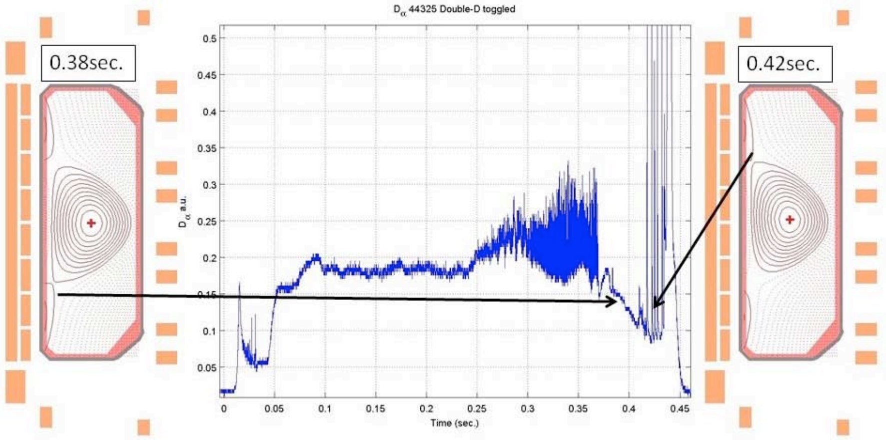

Fig. 2.1.1 *D_α evolution flanked by reconstructions of the plasma equilibrium caclulated at 0.38sec. and 0.42sec during the ELM-free and the ELMy H-mode phases respectively. They differ by the location of the active X-point. In the first instance, the lower X-point is active, in the direction favourable for H-mode but non-favourable for ELMs while in the second case the opposite is true.*

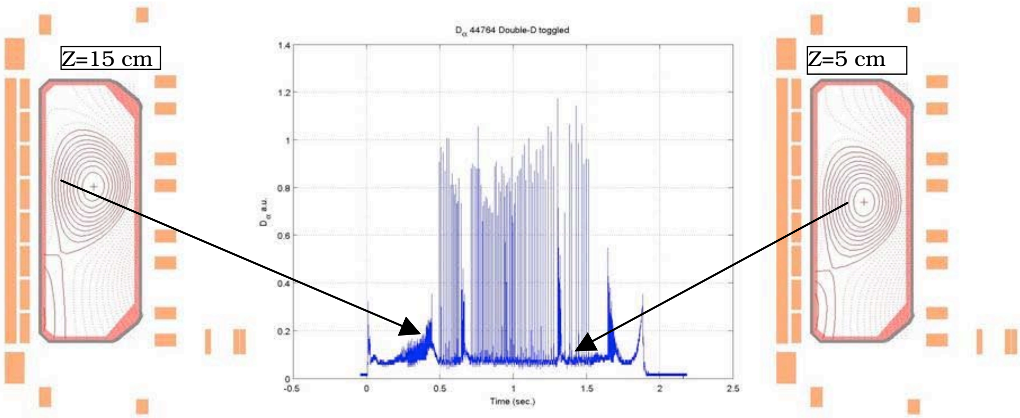

Fig. 2.1.2 *D_α signal flanked by equilibria calculated at 0.52sec (plasma at Z=15cm) and 1.5sec (plasma at Z=5cm). The ELMy H-mode was establised when the plasma centre was at 15cm, after which it was moved down to 5cm. At 5cm the discharge transitioned to an ELM-free H-mode.*

The double-null solution to achieving ELMy H-mode at Z=0cm in TCV is a promising avenue of exploration. It is planned to continue exploring this path by conducting plasma current, elongation and triangularity scans to find the optimum route to ELMy H-mode while avoiding the external modes that have led to disruption.

Another methodology that is being explored is to establish ELMy H-mode in the upper part of the chamber and then to move the plasma close to Z=0cm. Initial results are very promising. Shown in Fig. 2.1.2 is an example of a discharge established close to Z=15cm and then moved down to 5cm. This methodology will be pursued by completing detailed density, plasma current and triangularity scans in an attempt to find an optimum route to Z=0 while maintaining the ELMs.

ELM control by edge EC heating

In order to reduce the heat load on the first wall of present and future tokamak devices it is essential to be able to control the frequency of ELMs. Indeed, it has been observed that the amount of energy dumped on the walls by each ELM decreases with increasing frequency. Techniques like resonant magnetic perturbations, pellet pacing and vertical plasma jogging can achieve this goal but at the cost of reduced operational windows. Edge localised (ρ>0.85) electron cyclotron resonance heating might influence the edge pressure and/or current density profiles sufficiently to allow ELM pacing. Under certain conditions, ECRH can be injected into the extreme edge of H-mode plasmas on TCV.

Efforts in 2011 focused on examining how ECRH might affect the edge MHD stability and how ECH power modulation might affect the ELM frequency and phasing. Figure 2.1.4 shows the ECRH set up used for these experiments. One mega-Watt of electron cyclotron heating at the third harmonic in X-mode (X3) was launched from the top of the vessel along the X3 resonance to provide bulk plasma heating. One MW of second harmonic heating was launched form the outboard machine mid-plane aimed at the plasma edge near the X-point. In this way the deposition location of the X2 power could be varied from the X-point inward.

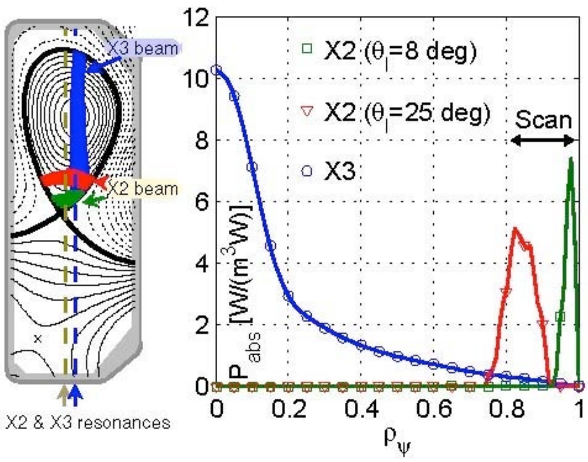

Fig. 2.1.3 *Equilibrium reconstruction of the snowflake-like diverted configuration. X3 beam, in blue, launched from the top of the vacuum vessel to heat the bulk plasma. X2 beam launched from the low field side and swept from $\rho(\psi)$=0.85 (red) to $\rho(\psi)$=1 (green). Absorbed power of the different beams as a function of the normalised radius.*

In Type-I ELMy H-modes it was observed that the ELM frequency increases as the X2 power deposition location is moved closer to the plasma edge. Stated otherwise, the ELM frequency increases as the absorbed power decreases and the power loss per ELM decreases at the same time. The density remains approximately constant during the scan in X2 deposition location and therefore does not play a role in the ELM frequency change.

In X2 power modulation experiments it was shown that the frequency of Type-I ELMs could be controlled by X2 power modulation. ECH X2 power was modulated at different frequencies and duty cycles. The ELM frequency varied accordingly with the variation of the averaged power but ELMs did not synchronize with power pulses. Real-time control of the X2 heating modulation was used. Figure 2.1.4 shows a typical example of a modulated X2 power case, showing the variation of ELM frequency and the standard deviation of the ELM frequency during various phases of continuous and modulated X2 heating. That average delivered power determines the Type-I ELM frequency was confirmed by comparing the results of continuous wave X2 heating and pulsed X2 heating, both delivering the same average power.

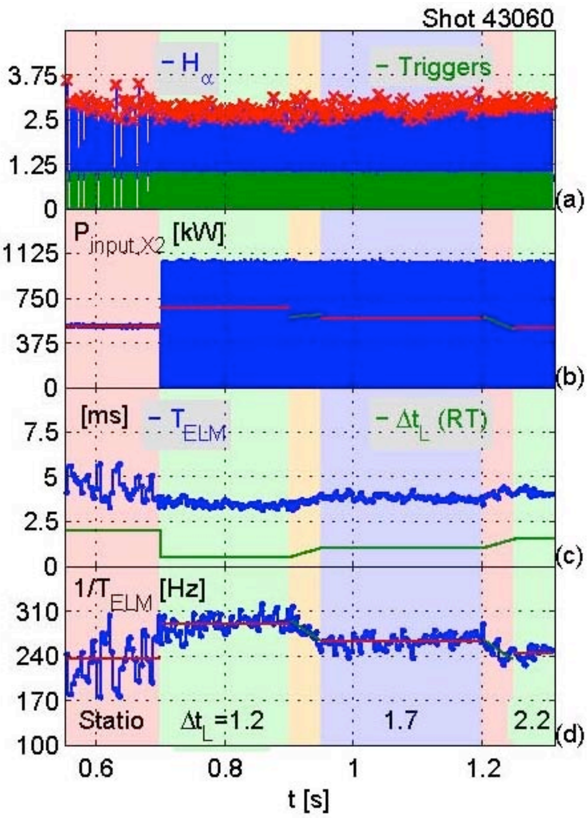

Fig. 2.1.4 *(a) D_α signal (blue) and real time X2 power triggers (green). (b) Average and actual X2 power. (c) ELM period and the X2 power on-time. (d) ELM frequency. In real time X2 power triggering experiments the ELM frequency can be controlled by the average X2 power. X2 power modulation serves to make the control more precise (small standard deviation on the average ELM period) than with constant X2 power.*

H-Mode threshold in H, D and He

During the early phases of ITER operation it is planned to operate in Helium so that neutron production rates will remain low. Although the database of Helium operation is sparse, it is known that the L- to H- mode transition threshold determined from different machines (JET, ASDEX, DIII-D) do not agree with the expected isotope scaling. There is a clear need to enlarge the database. Using the favourable ion grad-B drift direction, experiments were conducted to obtain the required Ohmic power for the L- to H-mode transition for the three gases as a function of line average density.

It was found possible to achieve H-mode using only Ohmic power for all three gases, although quasi-stationary ELMy H-mode in hydrogen was never obtained.

For H and He it was possible to achieve H-mode only in a narrow window of line-averaged density. Figure 2.1.5 summarises the results for L- to H-mode power threshold values for the three gases.

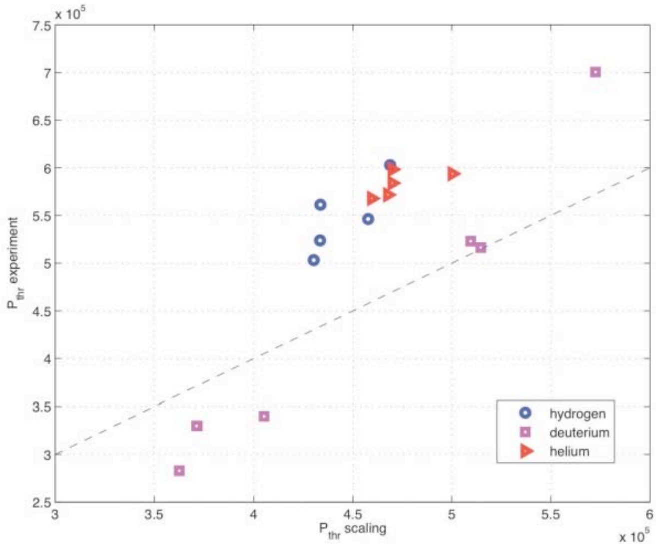

Fig. 2.1.5 *The loss power (P_{OHM}-dW/dt) required for L- to H-mode transition for the gases H, D and He. In the small window where H-mode was obtained there is no discernible difference in threshold power for H and for He. There is a substantial increase (≈30%) in the required power for H and He.*

Influence of the divertor leg length on the L- to H-mode transition

ITER auxiliary heating power could be marginal to achieve H-mode in the initial non-nuclear phase of operation. The prediction of the threshold power P_{LH} is based on scaling laws that only include the line averaged density $< n_e >$, magnetic field B_T and plasma surface S,

$$P_{LH} = 0.0488 < n_e > [10^{20} m^{-3}]^{0.717} B_T[T]^{0.803} S[m^2]^{0.941}$$

However, it is well known that P_{LH} can be significantly modified by other parameters. One of these parameters is the X-point height. Understanding the effect of geometry could lead to techniques that will facilitate H-mode access in ITER. TCV, with its high shaping capability could significantly contribute to develop such an understanding.

This activity is conducted in the framework of an international joint experiment (ITPA-JEX). While changing the X-point height modifies the L-H transition, it is likely that it is one or several correlated (or *hidden*) parameters that are responsible for the variation in threshold power.

In TCV H-mode access also depends on details of the divertor geometry. It is particularly sensitive to the radial position of the X-point. Contrary to observations in other devices, the power threshold in TCV is therefore a non-monotonous function of the divertor leg length.

We note that the typical TCV divertor differs from divertor configurations in other tokamaks. Due to the absence of dedicated divertor coils the inner divertor leg usually hits a vertical C-tile. The H-mode standard divertor configuration has one vertical and one horizontal leg with the outer divertor leg length (DLL) being much greater than the inner DLL.

We documented the influence of the outer divertor leg length (DLL) on the L-H transition and tried to link the geometric effect to hidden parameters. A clear reduction in power threshold for the L- to H-mode transition is observed (Fig. 2.1.6).

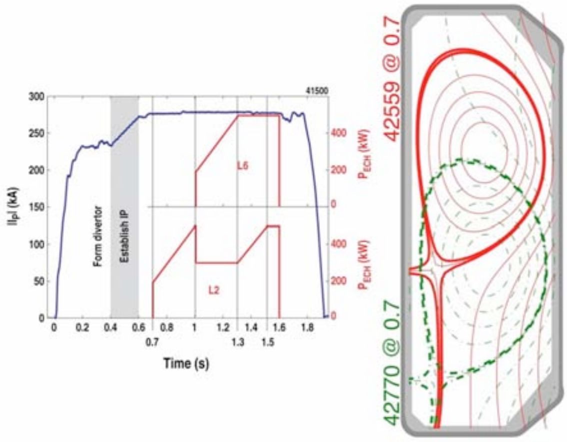

Fig. 2.1.6 *Two similar H-mode discharges were developed, one at Z=23cm (long divertor leg: in red) and the other at Z=-16cm (short divertor leg : in green). The heating power was smoothly ramped up to measure the L- to H-mode transition threshold power.*

In the experiment illustrated in Fig. 2.1.6 two H-mode discharges were created, one at Z=+23cm (long divertor leg) and the other at Z=-16cm (short divertor leg). Everything else being held constant, the X2 heating power was ramped until the H-mode transition. To achieve the H-mode transition two X2 gyrotrons were required and the total power supplied by the two gyrotrons had to be balanced: this explains the relative complexity of the X2 power traces. A 60% increase in the threshold power in going from -16cm to + 23cm was measured.

2.1.3 Plasma rotation

A strong rotation programme on TCV was curtailed early in 2011 by the failure of the DNB arc source. Much of the early run-time was dedicated to automation and systems analysis of the behaviour of the new Andor iXon CCD cameras providing only limited research data. Although the source's repair was initially expected for June 2011, at the time of writing, operations are only expected in the last 4 weeks of 2011 before the 2012 machine opening.

Following up on an initial measurement of the toroidal rotation profile across a sawtooth crash, a further sequence of experiments were performed using EC power to stabilise the sawtooth period to obtain long sawtooth cycles. Figure 2.1.7 shows a summary of these measurements, illustrating the change in toroidal rotation profile (i.e. the profile just before the sawtooth crash subtracted from that 2ms later) for a series of plasma discharges. The core co-current "kick" at the sawtooth crash is always observed, coherent with the behaviour of the co-current average toroidal profile previously reported.

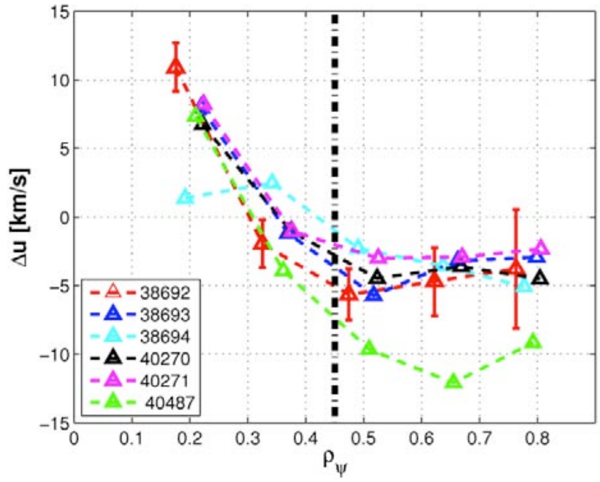

Fig. 2.1.7 *Toroidal rotation profile change across a sawtooth (ST) crash. Profile change is calculated over several ST events for a particular shot. The profile inside the ST inversion radius (indicated by the vertical line) is in the co-current direction whereas the plasma outside this radius goes in the counter-current direction implying some degree of local momentum conservation*

2.1.4 Heat and particle transport in TCV

The dependence of electron confinement on EC power deposition profile has been investigated in TCV, in collaboration with the Kurchatov institute. The main question was if broader deposition profiles, similar to Ohmic profiles, have better confinement properties. EC power density profiles as shown in Fig. 2.1.8 have been tested.

It was shown that broader profiles do not have better confinement properties and that the more centrally peaked profiles are beneficial. This is understood as the consequence of the better local confinement observed near on-axis than off-axis. In addition, it was shown that there is a large difference between cases in which heating is deposited inside the inversion radius and cases in which it is deposited outside. However, in both circumstances the power degradation is similar. The main findings can be summarized as follows:

- Ohmic and ECRH discharges with similar heating profile width have different confinement properties;
- Discharges with ECR heating have similar confinement properties and power dependences irrespective of the heating power profile width, as long as a significant fraction of the heating power is absorbed inside the q=1 radius.

The difference between core transport and edge transport is also being studied in more details. It is shown in particular that heat transport is stiff in the region between the inversion radius and a normalized ρ of about 0.8-0.9, but not between 0.8-0.9 and 1. This non-stiff behaviour was already observed in L-mode and can lead to very high R/L_{Te} values near the edge, which in turn raise the core temperature for the same core R/L_{Te}.

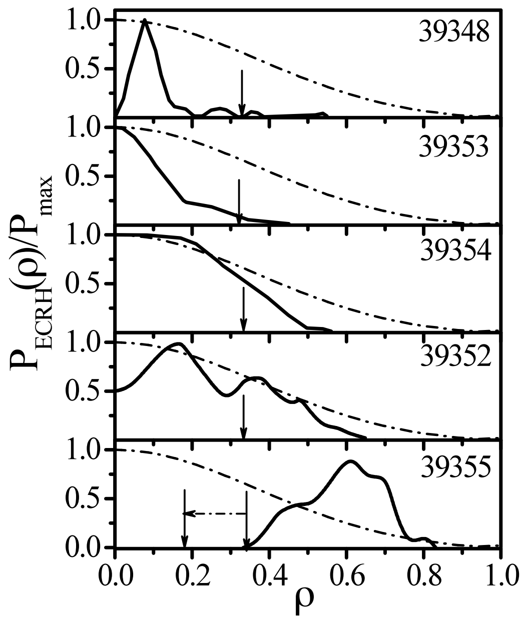

Fig. 2.1.8 Normalized power density profiles used in different TCV shots. The dash dotted line gives the normalized Ohmic power density profile.

The study of electron particle transport in TCV H-modes has been conducted using the same quasi-linear theory as used to explain TCV L-modes and eITBs. Very good qualitative agreement is reached, but better ion temperature measurements are required for further studies. In addition, it was possible to explain why density peaking does not necessarily decrease with increasing collisionality.

New experimental studies on impurity transport have been started on TCV. The fast valve is used with small opening times in order to be able to perform transport studies. Distinct or repetitive injections are used for transient and stationary studies.

Argon and Neon, in particular, have been injected in plasmas with different shapes, plasma current, density and EC heating. In most cases, the time evolution and the profiles measured with soft X-ray diagnostics show little difference with varying experimental conditions. A fast increase in emissivity is detected (~10ms) followed by a slow decay time (~300ms) much longer than the electron confinement time. On the other hand, Neon behaves very differently from Argon. The decay time is about one order of magnitude longer and therefore consecutive injections lead to rapid accumulation. This can lead to significant increase of electron density and often to disruption. These effects will be studied in detail next year.

In addition, Argon and Neon have also been injected at the edge of electron internal transport barriers. Preliminary analysis shows that the barrier is not strongly affected, except if it leads to a global slow increase of the electron density. In that case, the ECCD efficiency decreases and the eITBs degrades. The effective causes and effects need more detailed studies.

2.1.5 Physics of ECH, ECCD and of suprathermal electrons

ECH transmission measurements as observers of ECH absorption efficiency

EC heating relies on the correct polarisation of the launched radiation. X-mode polarised waves are absorbed far more efficiently than O-mode waves and are thus the optimal choice in most heating scenarios. The polarisation orientation in the laboratory frame that corresponds to X-mode launching is a complex function of the launching direction and of the plasma parameters, and is pre-calculated on the basis of the planned discharge characteristics. On future devices such as ITER, it is expected that the polarisation will be adjusted in real-time to maximise absorption in time-varying scenarios. The TCV team has now acquired fast polarisers and is ready to test them for such a real-time application. Accordingly, work has commenced on developing a reliable and quantitative measure of the power absorption efficiency.

A related quantity is the amount of EC radiation that is not absorbed and escapes the plasma, which can be measured by external microwave detectors placed at opportune locations around the torus. Initial experiments have been performed to assess whether such detectors can provide an adequate, quantitative observer for this purpose. As an added benefit, these tests can be expected to indicate whether the same method can be used for the purpose of machine protection by shutting down the power sources in case of excessive losses. At a more basic level, these measurements can serve to validate the launcher alignment and the polarisation calculations.

For this work, a microwave detector was coupled to a steerable receiver. Scans of both the launcher and receiver angles, as well as of the polarisation, were performed. Smooth variations with angle were observed (Fig. 2.1.9), and different maxima could be identified, corresponding to different component modes and mode conversions upon reflections from the vessel wall. The method appears to be sensitive and reliable, and further tests are planned for the remainder of the present TCV campaign.

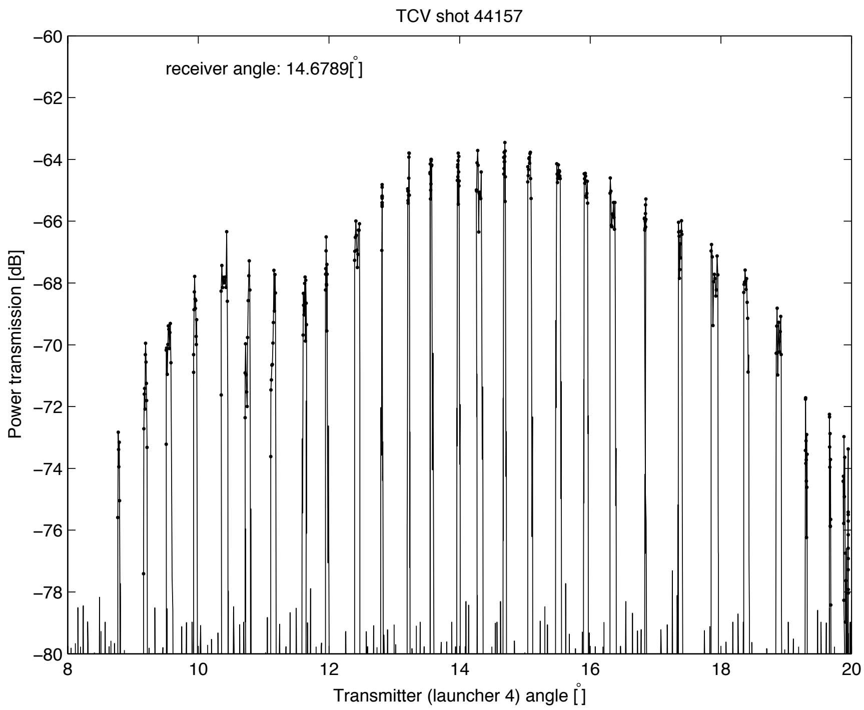

Fig. 2.1.9 *Power detected by a microwave receiver as a function of the EC launching angle. Power is applied in short periodic bursts.*

Study of 3rd harmonic ECH absorption enhancement by 2nd harmonic heating at the same frequency

Experiments were performed in the past in TCV to test whether a measurable synergy could be found between 2nd and 3rd harmonic absorption. In particular, an appropriate choice of the toroidal magnetic field permits both resonances to exist in the plasma simultaneously for the same launching frequency. These experiments typically employed the strategy of varying the magnetic field during the discharge to ensure that at some point in time the two resonances would lie on the same flux surface. Because of the extremely low intrinsic 3rd harmonic absorption efficiency in these conditions, the signature of synergy was sought in hard X-ray (HXR) signals from bremsstrahlung emitted by suprathermal electrons.

Extensive modelling of these discharges was performed this year using the quasi-linear Fokker-Planck code LUKE. Synergistic effects are indeed predicted, and they display a complex dependence on velocity-space dynamics that allow them to be at play over a broad spatial range and not only when the two resonances are on the same flux surface. The simulations, however, lead to the conclusion that none of the features observed in the HXR signals could be unambiguously attributed to synergy and that in fact any variations due to synergy are expected to be too small to be outside the experimental error bars. In spite of this negative outcome, the work has shed considerable light on the dynamics of EC wave-plasma interaction and can form the basis for future synergy tests under more favourable conditions.

Characterisation of the suprathermal electron population during ECCD

The first of an eventual set of four HXR cameras was installed on TCV during 2011. While the complete set will be required to perform tomographic reconstructions of HXR emissions for the first time, the first camera has already produced high-quality initial results. The camera features an array of 24 viewing chords, which can be distributed in any plane between horizontal and vertical by a simple rotation of the assembly. Initial results have confirmed the well-established generation of suprathermal electrons during ECCD in the high-power environment of TCV. However, the rotational freedom of the instrument has allowed for the first time a comparison between HXR emission within the poloidal plane and emission with a significant component parallel to the magnetic field. While ECRH accelerates electrons only in the perpendicular direction, pitch-angle scattering is expected to result in significant distortion of the distribution function in the parallel direction as well. This is indeed observed; additionally, we have determined for the first time the asymmetry that exists in the toroidal direction when non-inductive current is generated, and observed the reversal of this symmetry as the current direction is reversed. This asymmetry is shown in Fig. 2.1.10, which also evidences the significant role played by the Ohmic electric field. Indeed, the parallel distortion does not undergo mirror reversal from co- to counter-ECCD. This effect is qualitatively predicted by Fokker-Planck modelling. The agreement is still quantitatively imperfect, which may require refinements in the simulations, particularly concerning the treatment of spatial electron transport.

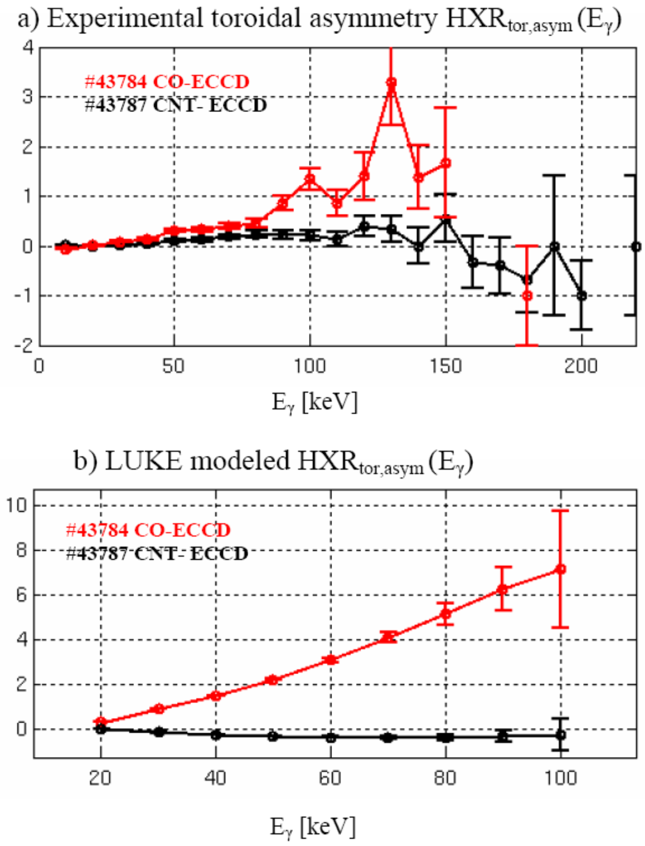

Fig. 2.1.10 *Toroidal HXR asymmetry factor (normalised difference between emission in the co- and counter-current directions) for discharges featuring, respectively, co- and counter-ECCD: (a) experiment and (b) simulation.*

2.1.6 Advanced plasma profile and instability control

Using the new control capabilities available on TCV, significant experimental progress was made on the control of plasma profiles and MHD instabilities, both of which are essential for the operation of ITER.

A new real-time control technique was tested for control of the sawtooth period using sawtooth-stabilizing ECCD deposited just outside the q=1 surface. A real-time controller was designed which periodically removes the stabilizing ECCD power whenever a given time has expired after the previous sawtooth crash. The sawtooth crash reproducibly occurs a short time thereafter; thus, this technique is referred to as “sawtooth pacing”. The delay between the power removal and the sawtooth crash depends on other stabilizing influences on the sawtooth period, for example the presence of a second ECRH source. The sawtooth pacing technique has allowed demonstration of precise control of individual sawteeth, showing that the sawtooth cycle lacks memory of previous crashes. In a related control scheme, a pre-programmed EC power modulation waveform is used which can cause the sawtooth cycle to lock to the modulation period for certain combinations of period and duty cycle. TCV experiments confirmed the simulation results, showing that a well-defined locking range in terms of period and duty cycle exists.

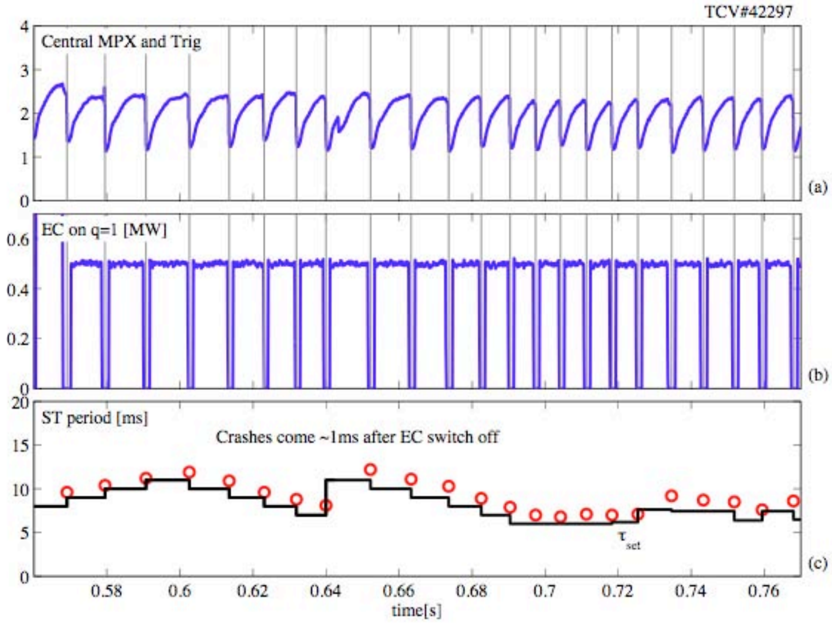

Fig. 2.1.11 *Control of individual sawtooth period using the sawtooth pacing technique. The sawtooth-stabilizing ECCD (centre) is removed when a time (tau_set) has passed since the last crash. The sawtooth crash occurs soon after the removal of power (bottom). X-ray traces (top) show the characteristic sawtooth signature.*

As an extension of the work above, the pacing control scheme has been applied to ELMs, showing that the ELM period can be strongly regularized by adding EC power at a pre-defined time interval after occurrence of each ELM. This has the beneficial effect of smoothing out heat load transients and provides a stringent benchmark for models of the ELM cycle.

Work on NTM (Neoclassical Tearing Mode) control has progressed further, particularly focusing on the pre-emption of tearing mode formation that results from large, long-period sawtooth crashes. This validates a possible MHD control strategy on ITER wherein long-period stabilized sawteeth can become acceptable if their negative consequences are mitigated. An experiment demonstrating combined sawtooth pacing and NTM prevention has been carried out: one set of gyrotrons was used for sawtooth pacing near the q=1 surface using the techniques discussed above, while a separate gyrotron was programmed to deposit power around the time of the sawtooth crash, at the rational surface where modes would otherwise appear. This successfully prevents NTMs from forming even for long sawtooth periods that would otherwise engender deleterious MHD activity.

A real-time estimate of the q profile, based on a real-time flux diffusion simulation from the new RAPTOR (RApid Plasma Transport simulatOR) code, recently installed in the TCV control system, was also integrated in a closed-loop feedback control scheme for the simultaneous control of the internal inductance, l_i, (a moment of the current distribution) and the electron temperature, T_e. Two gyrotrons, one oriented to provide co-ECCD and the other counter-ECCD, were used as actuators. The independent control of both quantities (l_i and T_e) was experimentally demonstrated.

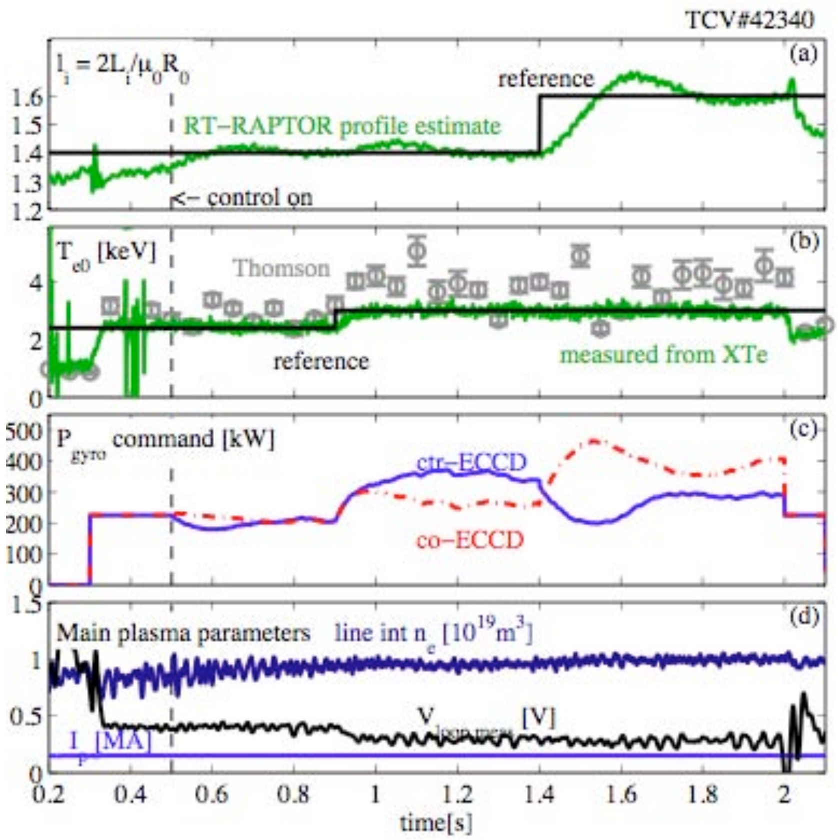

Fig. 2.1.12 *Real-time independent control of internal inductance (Li, top panel) and electron temperature (Te, second panel). The internal inductance is estimated by the real-time RAPTOR flux profile diffusion simulation. Co- and counter current drive is added as appropriate (thid panel). Other plasma parameters are also indicated (bottom).*

In a parallel effort, a real-time observer for the internal inductance based on Shafranov integrals was developed (CIEMAT collaboration). This observer was then used in l_i control experiments in Ohmic plasmas using the primary transformer ramp-rate as an actuator. Linear and nonlinear (sliding-mode) controllers were successfully tested in the ramp-up, flat top and ramp-down phases of the discharge. These controllers provide the ability to precisely navigate through the tokamak operational space and follow appropriate trajectories avoiding instabilities and physical limits.

Exploiting the rapidity of the above-mentioned RAPTOR code, numerical investigations were carried out to determine an optimum trajectory, given certain physical and technical operational constraints, in the tokamak parameter space using an automated technique. This can be of great importance in optimizing scenario trajectories without relying excessively on trial-and-error experimental approaches, as is mostly done today.

To this aim, a predictive version of RAPTOR was developed, which simulates the time evolution of both electron temperature and poloidal flux profiles, includes the main nonlinear coupling mechanisms between the two such as bootstrap current, neoclassical conductivity and q-profile dependent thermal conductivity. After defining a cost function and constraints reflecting requirements on the plasma time evolution, this is used in a numerical optimization routine that computes an optimal set of actuator trajectories that minimize the cost function while satisfying constraints. By applying these techniques to TCV scenarios that ramp up to a stationary q profile with low magnetic shear in the centre, it was shown that a current overshoot is beneficial for yielding flat and broad q profiles, and that carefully-tuned, early EC heating helps obtain the desired q profile while avoiding the formation of a q=1 surface. Future experimental investigations of these actuator trajectories should provide a benchmark for this tool.

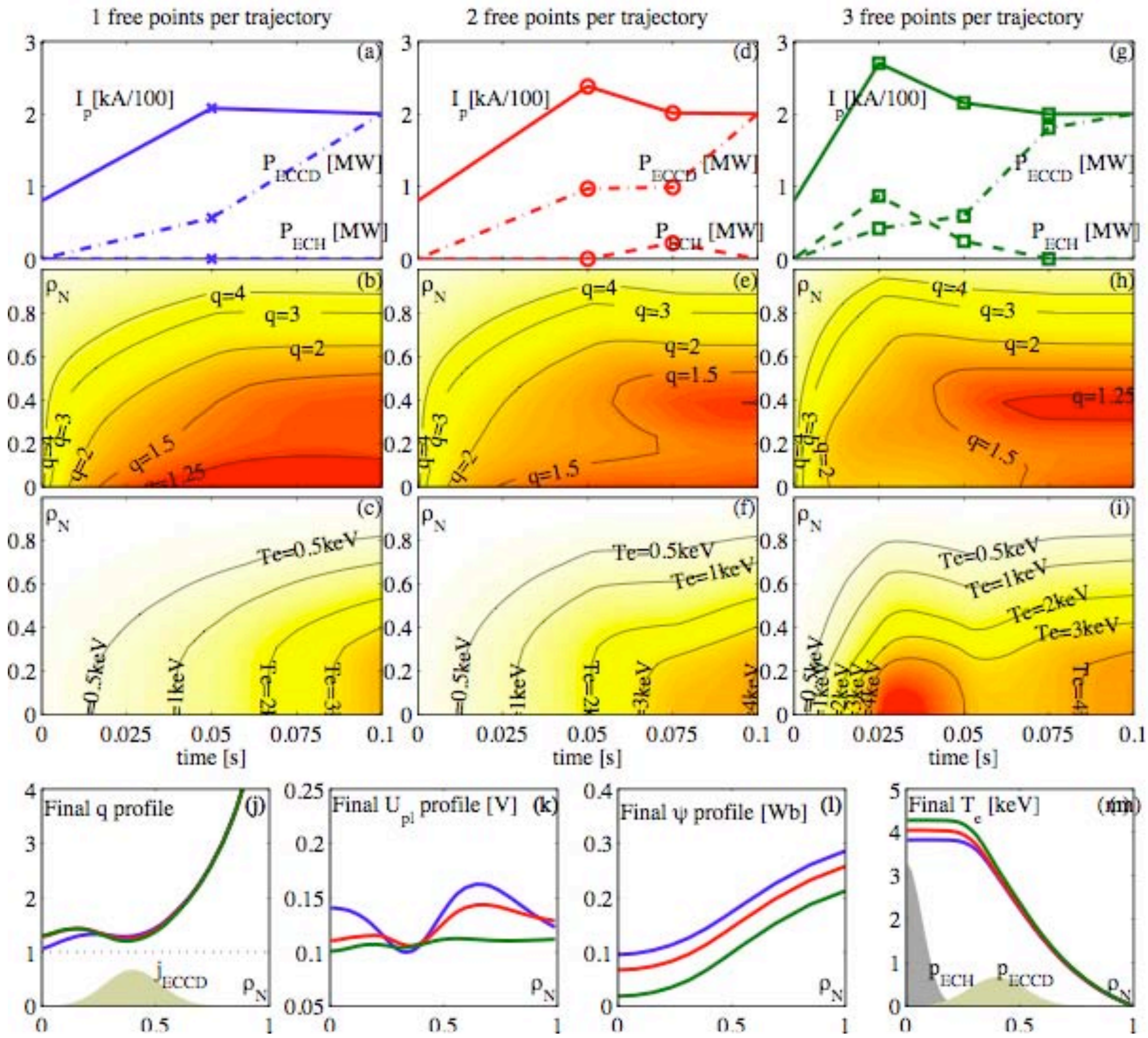

Fig. 2.1.13 *Computed optimal trajectories of plasma current, EC off-axis current drive and central heating to obtain a stationary, broad q profile with low central shear on TCV. The optimization algorithm attempts to minimize the final loop voltage profile derivative and resistive flux dissipation, while keeping q above 1 and the edge loop voltage positive. Trajectories with increasing degrees of freedom (left to right) yield increasingly better final profiles.*

2.1.7 Exploration of new shapes and configurations

Characterisation of the snowflake divertor plasma configuration

The snowflake (SF) divertor is an innovative divertor configuration, which attempts to solve the problem of reducing the heat fluxes into the divertor of DEMO. Conventional divertors do not extrapolate favourably to DEMO, with heat fluxes expected to reach intolerable levels. The problem is particularly serious for edge localized modes (ELMs), which usually occur in H-mode plasmas and result in even higher transient heat loads. In a SF divertor the spatial derivatives of the poloidal magnetic field also vanish at the null point. The separatrix then splits the poloidal plane into six rather than four sectors, resembling a snowflake. This new magnetic configuration has several characteristics that promise to facilitate the heat flux management. A longer connection length can increase the radiated power fraction, facilitate detachment and, consequently, reduce the heat flux density on the divertor plates. A larger flux expansion around the null point, with a divertor target plate placed in its vicinity, can lead to an additional decrease of the heat flux density. Finally, a larger magnetic shear near the edge is predicted to positively affect ELM activity. The snowflake configuration has been successfully created for the first time in TCV.

Recent experiments focused on measuring the power repartition among the four divertor legs of the SF+ divertor. In the SF+ configuration the spatial derivatives of the poloidal field do not completely vanish at the X-point, but are small. The configuration is characterized by two adjacent X-points with one being located outside the last closed flux surface. The distance between these two X-points (normalized to the minor radius), σ, indicates the proximity to a perfect SF configuration. The divertor legs define the scrape-off layer (SOL) and three private flux regions. In the typical SF+ configuration shown in Fig. 2.1.14 the strike points are numbered counter-clockwise starting at the top of the centre post. Only strike points 1 and 4 are in direct contact with the SOL. Key edge diagnostics in TCV are Langmuir probes (LP) and infrared (IR) cameras.

In the investigated SF+ configuration, shown in Fig. 2.1.14, the TCV Langmuir probes only cover the strike points 1 through 3. Experiments using L-mode discharges that are stationary except for a small movement of the strike points provide an estimate of the heat flux profile in the vicinity of theses strike points, Fig. 2.1.15. The heat flux $q_\perp = \gamma j_{sat} T_e/e \sin\alpha$ [Labit2011] depends on the sheath heat transmission coefficient γ, which is here assumed to be 5. The electron temperature is obtained from $T_e = eV_{float}/\ln\left(1 - j_0/j_{sat}\right)$. The floating potential V_{float}, the ion saturation current j_{sat} and the probe current with zero bias j_0 are directly obtained from the Langmuir probe. The angle α is the grazing angle of the magnetic field line at the probe tip. The LP measurements reveal a measurable heat flux at the secondary strike points (SP2 and 3), even though they are not in direct contact with the SOL. This demonstrates that it is possible to distribute the exhaust power on more strike points than the two of conventional divertor configurations. However, the total heat flux at strike point one, Fig. 2.1.15(a) is still an order of magnitude larger than the other two, Figs 2.1.15(b,c). The heat flux profiles at the three diagnosed strike points can be well described by an exponential decay with different characteristic scale lengths to either side of the strike point.

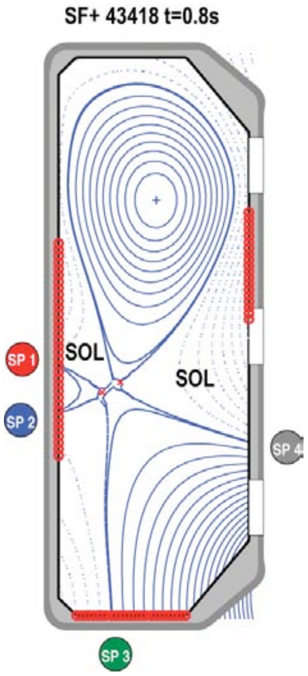

Fig. 2.1.14 *Typical snowflake+ (SF+) configuration investigated in TCV. The locations of the Langmuir probes are indicated with red circles.*

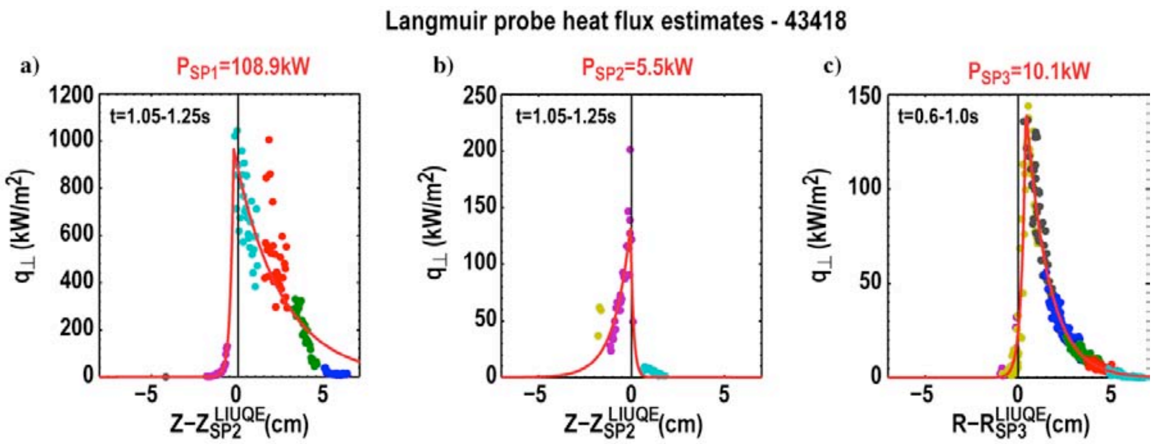

Fig. 2.1.15 *Heat flux profiles derived from Langmuir probe measurements during strike point sweeps of the strike points 1 (a), 2 (b) (both centre post) and 3 (c) (floor) during an Ohmic L-mode discharge. The measurements (dots) are fitted to an exponential decay with different characteristics lengths at either side of the SPs (red lines).*

Small modifications of the magnetic configuration show that the heat flux at strike point 3 is very sensitive to the strike point separation σ. Decreasing σ from 0.5 to 0.25 increases the heat flux by a factor of four, Fig. 2.1.16. Further experiments are necessary in order to see to how much of the heat can be exhausted at the secondary strike points as the magnetic configuration approaches a perfect snowflake.

Even though TCV has currently no means to directly measure the heat flux at the strike point on the outside wall (SP 4), a global power balance calculation can be used to obtain an estimate of the total heat flux at SP 4. In addition to the heat fluxes at SP 1-3, and the Ohmic heating power the radiated power has to be known. An estimate of P_{rad} is obtained from a tomographic reconstruction of the foil bolometer measurements. The power balance calculation in an Ohmic L-mode indicates a value of P_{SP4} of approximately 50kW. However, the uncertainty of this estimate is relatively high.

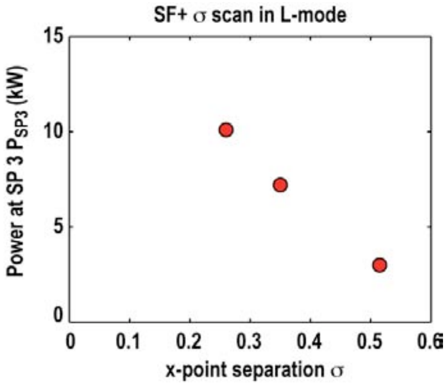

Fig. 2.1.16 *Langmuir probe estimates of the power deposition at strike point 3 (floor) during Ohmic L-modes.*

The Langmuir probe measurements are complemented with IR imaging of divertor targets. TCV is equipped with a fast-framing IR camera and two views, Fig. 2.1.17(a). In collaboration with FOM-Rijnhuizen a second IR camera was temporarily installed for a two-week period in 2011 to allow for simultaneous IR measurements of the strike points on the centre post and on the floor.

The interpretation of the IR images requires modelling of the temperature evolution of the PFCs (graphite tiles), which is carried out using the THEODOR code. This modelling is complicated by the poorly known thermal characteristics of a surface layer that forms during plasma operation. An initial cross comparison between heat flux measurement by IR imaging and Langmuir probes in stationary L-mode discharges yields reasonably good agreement provided that the power flux is sufficiently large.

The simultaneous IR measurements are particularly useful in the study of peak heat fluxes caused by ELMs. Figure 2.1.17(b-e) shows time traces along a slow variation of σ. During such a variation the type-I ELM frequency and the average ELM loss power decreases and confinement increases. The fast tile temperature increases associated with ELMs, Fig. 2.1.17(d), show when significant power arrives at the secondary strike point. This happens surprisingly quickly and at a surprisingly large value of σ, approximately 0.6, well before a perfect snowflake has been formed.

The measurements in H- and L-mode will be complemented by the addition of fourth Langmuir probe array, planned for 2012. This new array will be located to diagnose strike point 4 and promises a complete dataset that can test SOL transport models in the snowflake configuration.

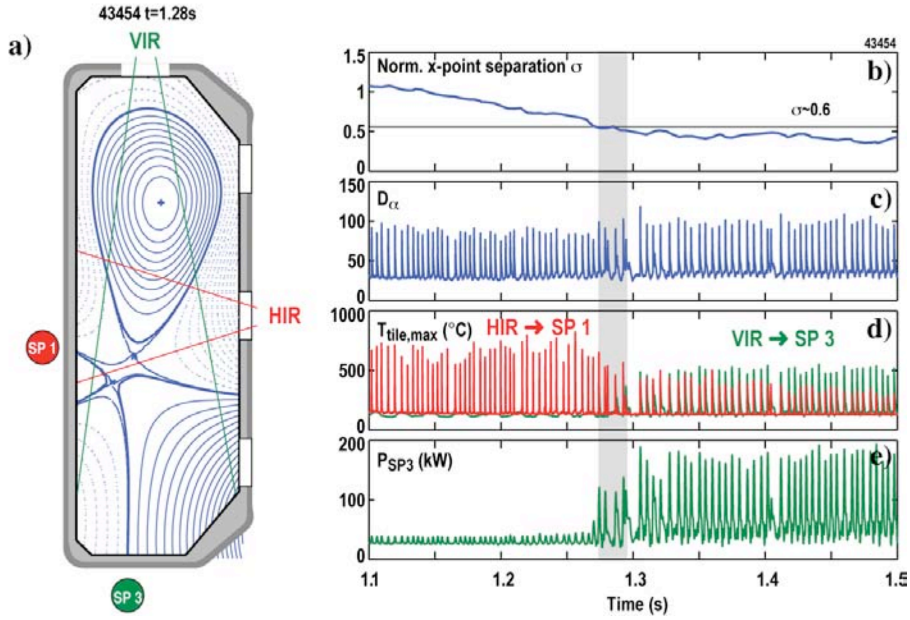

Fig. 2.1.17 *(a) Simultaneous measurements with the horizontal and vertical infrared camera systems (HIR and VIR) of strike point 1 (centre column) and 3 (floor) during (b) a slow variation of the strike point separation σ during c) type-I ELMy H-mode yield (d) the temperature of the divertor target. Once s becomes sufficiently small each ELM leads to significant temperature increases at strike point 4. Modelling of the temperature evolution of the floor tile yields (e) the power flux onto the floor tiles.*

Development of H-modes at negative triangularity

Core-plasma confinement has been found to improve, in TCV, in low-collisionality L-mode discharges at negative triangularity δ when in the TEM turbulence regime – a regime likely to occur in reactor conditions. At the same time it is known that, in H-mode, both the pedestal height and ELM size increase as δ increases. Therefore it is of high interest to explore properties of H-modes at negative δ to assess the ELM behaviour and investigate pedestal properties. However, the collisionality in TCV negative triangularity H-mode is probably too high to establish a clear TEM dominated transport. In addition, to get the favourable effect of negative triangularity, global transport effects should persist at the higher ρ^*-values of a reactor. Whether this will be verified is not known today, but should soon be in the reach of HPC gyrokinetic calculations.

Reliable H-mode operation with negative triangularity has been obtained this year, so far in centred single null (SNC) discharges, a plasma shape that provides good accessibility to the present electron cyclotron heating system, in particular to the 2nd harmonic (X2), even in the H-mode, at densities relatively higher than in the corresponding L-mode triangularity experiments. Thus, the core plasma is heated with 3rd harmonic (X3) and robust X2 absorption inside the separatrix enables control over the H-mode regime. This allows operating in high-power ELM regime (type I ELMs), the ELM regime that can cause, if not mitigated, excessive erosion of the plasma-facing components in a reactor. In TCV, it was possible to study the triangularity δ dependence of these ELMs, by changing gradually the upper triangularity in the range $-0.2<\delta_{top}<+0.2$. As expected from previous ideal stability calculation with KINX for such kind of equilibria (with SNC and $\delta_{top}<0$), the 2nd

stability region gradually disappears towards $\delta_{top}<0$, leading to a decrease of the height of the edge pressure pedestal, and consequently of the ELM amplitude (Fig. 2.1.18). These initial experiments show already that H-mode with negative triangularity $\delta_{top}<0$ has the potential to mitigate ELMs. However, other shapes, with a single or double null (SN and DN) located on the LFS seem even more promising with respect to edge ideal stability, since SN or even more DN by increasing the edge shear, allow for substantially larger edge pressure gradients. A very good candidate, in terms of edge stability (both pressure gradient and $j_{||}$) and of a large wetted surface for dumping the power is a snow flake divertor positioned on the LFS, compatible with TCV coil current requirements.

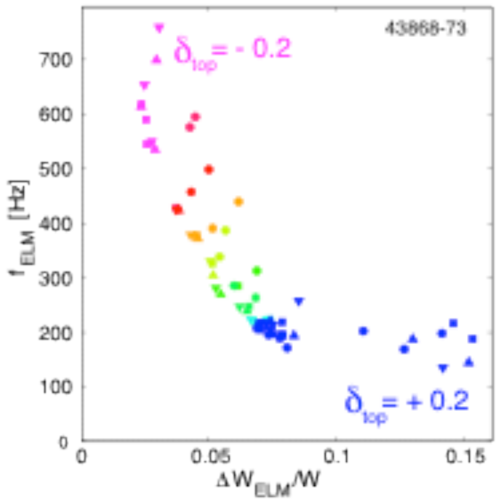

Fig. 2.1.18 *ELM amplitude and frequency (normalised to non-dimensional power) for different triangularity ™top. Towards negative triangularity, the ELM frequency increases and the ELM power fluxes decrease, both with by a factor of 3 over the range ™top=+0.2 to -0.2.*

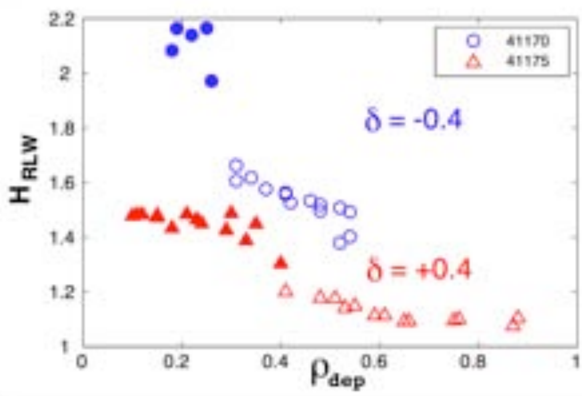

Fig. 2.1.19 *Dependence of H_{RLW} in a radial EC-power-deposition-location sweep in a discharge, for negative and positive triangularity δ, showing improved confinement at negative δ for deposition to the very core. Open symbols represent deposition outside the q=1 region, and solid symbols inside.*

Recent experiments in TCV have again shown the improvement of confinement resulting from negative triangularity (at low collisionality in L-mode), but in a new way, from measurements of the confinement response to a radial sweep of the power deposition. This is shown in Fig. 2.1.19, where the improvement factor over the standard L-mode, H_{RLW}, is shown as a function of the radius of power deposition. Confinement is improving for deposition close to plasma axis, typically inside q=1, and degraded for deposition close to the edge, as expected. More interestingly, the H-factor is substantially higher at negative triangularity (δ=-0.4) compared to positive (δ=+0.4), and the beneficial effect on confinement penetrates deep in the core. Surprisingly, the effect is not limited to the edge, as for the “geometric” triangularity penetration that remains confined to the edge. This represents an evidence of the relevance of global effects in transport.

2.1.8 Edge plasma physics

Statistical properties in L-mode plasma

In L-mode plasmas, intermittent particle and heat SOL transport is associated with the presence of blobs propagating in the radial direction. To investigate these phenomena, statistical properties of J_{sat} fluctuations measured in SN and SF configurations with Langmuir Probes in the SOL at the LFS mid-plane have been compared. The radial distance between the last closed flux-surface (LCFS) and the LP is about 2 cm. In order to investigate the influence of the plasma collisionality on the intermittent transport, a density scan was performed. The average and rms values of J_{sat} increase with density (Fig. 2.1.20), while the skewness, which is a measure of the intermittency, remains almost constant at a high level (not shown). Moreover, the level of fluctuations is significantly lower for the SF configuration compared to the SN, suggesting that large amplitude blobs are less frequent 2cm from the LCFS in the SF configuration. Two reasons might be invoked to explain this observation: either blobs are convected faster to the strike points in the SF than in a SN configuration and therefore do not have time to reach the wall, or, since the magnetic shear is larger for the SF plasma, blobs are more efficiently sheared-off and dissipated.

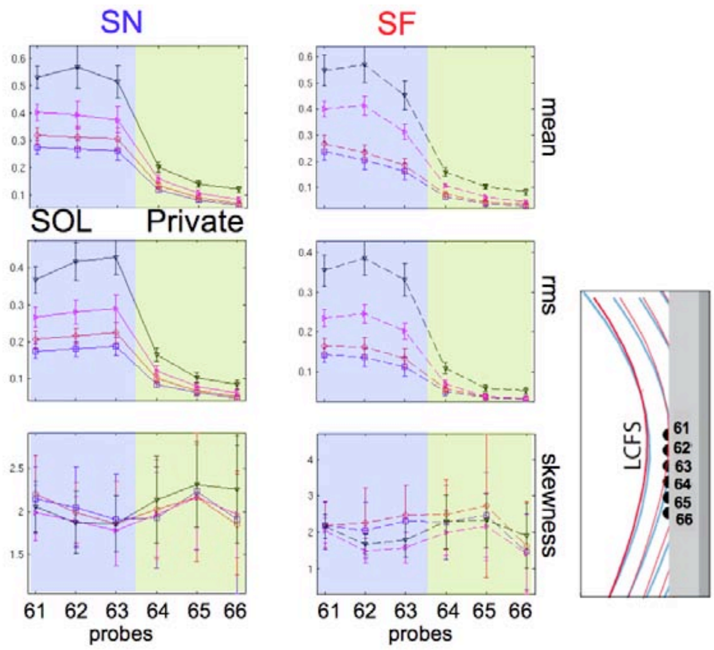

Fig. 2.1.20 *Statistical properties of J_{sat} measured in the SOL at the midplane in L-mode plasmas with both divertor configurations*

First measurements using a fast framing camera (Photron APX- RS) in the edge of SN/SF L-mode plasmas were performed in 2011. The camera observes the plasma with a wide angle of view (Fig. 2.1.21), recording unfiltered visible radiation. With a 30kf/s framing rate the recorded region corresponds to 86 x 140 pixels (white rectangle in Fig. 2.1.21). The normalised level of light fluctuations is slightly higher in the SN phase than for SF, and appears localised at the plasma edge. Tomographic inversion is under consideration for a clearer interpretation. A plot of the skewness shows a clear change from negative to positive values as the separatrix is crossed, similar to that observed from LP measurements on other tokamaks. The frequency spectrum of the fluctuations of the measured light from a region of almost zero skewness exhibits some coherent fluctuations around 6 kHz. It should be noted that this mode is also detected on magnetic probes.

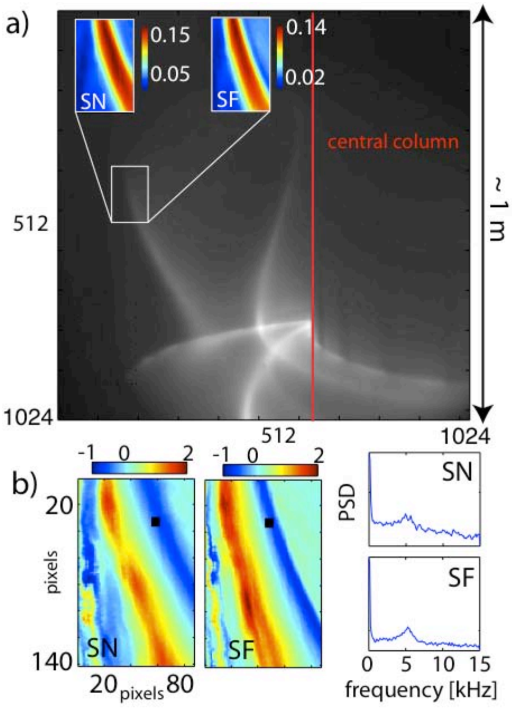

Fig. 2.1.21 *a) Fast camera image (1024 1024 3kf/s); Inset) Light r.m.s. normalized to the average light; b) 2D plot of the skewness and frequency spectrum of measurement at the black square.*

Estimation of heat loads for ELMy H-modes

On TCV, SN and SF configurations were observed to have similar H-mode power thresholds, whereas the SF confinement is 15% higher. The most striking difference is in the ELM frequency, reduced by a factor 2-3 with the snowflake divertor, while the ratio of the energy lost per ELM to the plasma energy is only increased by 20-30%. The Langmuir probes mounted on the central column (34 probes, 4mm tip diameter, vertically separated by 17.3mm) provide a good coverage of the inner divertor target zones for the SN/SF diverted configurations. For ELMy SN/SF plasmas, LP measurements at the inner target zone are performed on a shot-to-shot basis. Two quantities are directly measured: the ion saturation current density J_{sat} and the floating potential V_{fl}. Both quantities are coherently averaged over ELMs detected on the Dα signal. Knowing the ELM-averaged J_{sat} and V_{fl}, the temperature evolution is estimated from I-V characteristics measurements. Finally, the heat load is estimated with the formula: $P_{perp}=\gamma J_{sat}(T_e/e)\sin\alpha$ where $\gamma=5$ is the sheath heat transmission factor and $\alpha\sim3–5^{\circ}$ is the angle between the total magnetic field and the wall. Results are summarised in Fig. 2.1.22. From Dα, it is seen that the duration of the ELM cycle is shorter (~1ms) for the SN configuration compared to the SF (~4ms), consistent with the change of ELM frequency between the two configurations. In the SF case, the estimated heat power on SP1 is reduced by more than a factor of two. Moreover, some heat flux is measured on the additional strike points (SP2 and SP3) associated with the SF configuration, suggesting that this configuration is able to redistribute efficiently the heat losses between the strike points.

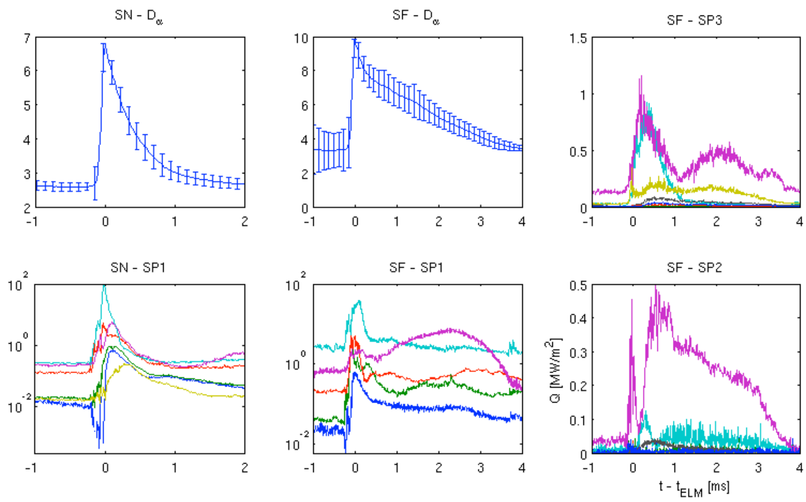

Fig. 2.1.22 *Coherently averaged Dα traces over ELMs for SN and SF H-mode plasmas. Average heat load during ELMs at SP1 (log scale) for SN and SF and at SP2 and SP3 (lin scale) for SF divertor.*

2.2 Theory and numerical simulation

2.2.1 Physics underlying anomalous transport

Interaction of neoclassical and turbulent transport

Collisional gyrokinetic simulations of microturbulence in the ITG-regime (assuming adiabatic electrons) starting from a neoclassical equilibrium are now being carried out with the ORB5 code on a regular basis. This is achieved by dividing the runs into two separate phases. In an initial phase only the n=0 toroidal Fourier mode is retained, enabling the system to reach an axisymmetric neoclassical equilibrium in the presence of ion-ion collisions. These are modeled by linearized Landau collision operators conserving locally the density, parallel momentum and kinetic energy. In a second phase both axisymmetric (n=0) and non-axisymmetric non-zero toroidal modes are allowed to evolve freely, enabling the system to enter its turbulent regime. A coarse graining procedure has been implemented and has proven to be effective at maintaining the signal to noise ratio at a significant level throughout the whole run and thus to ensure the physical validity of the simulation results.

Collisional simulations of microturbulence in the ITG regime have been carried out with the ORB5 code, both above the non-linear collisionless critical ion temperature gradient, as well as in the so-called Dimits-shift region (gradient region between the linear critical gradient and the up-shifted non-linear critical value). Poloidally rotating zonal flows, generated by the turbulence, but at the same time shearing the associated eddies and thus limiting the associated transport, provide the basic saturation mechanism of microturbulence in the ITG regime. We observe that the shearing effect of zonal flows results in nearly isotropic density perturbations in the poloidal plane (see e.g. Fig.2.2.1).

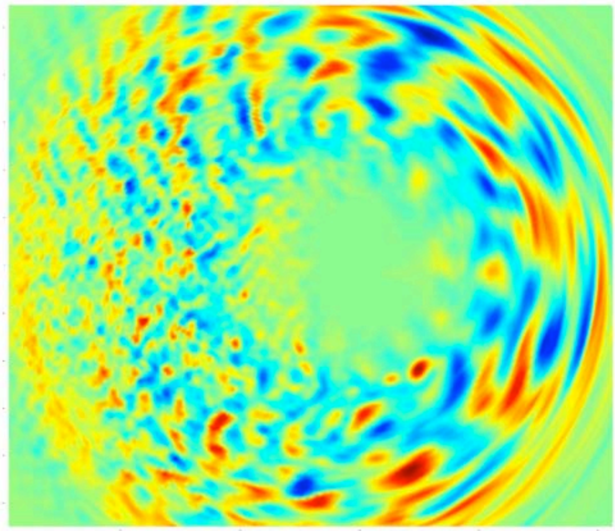

Fig. 2.2.1 *A snapshot of a global gyrokinetic simulation of ITG turbulence with the ORB5 code showing contours of the density perturations in the poloidal cross-section.*

These self-generated zonal flows are in fact the origin of the non-linear up-shift of the critical gradient. Ion-ion collisions damp these zonal flows thus reducing their shearing effect, which in turn leads to increased transport levels. Collisional ORB5 simulations have revealed finite turbulent transport levels in the Dimits shift region, confirming previous findings, as well as increased transport for gradients above the Dimits shift (Fig. 2.2.2).

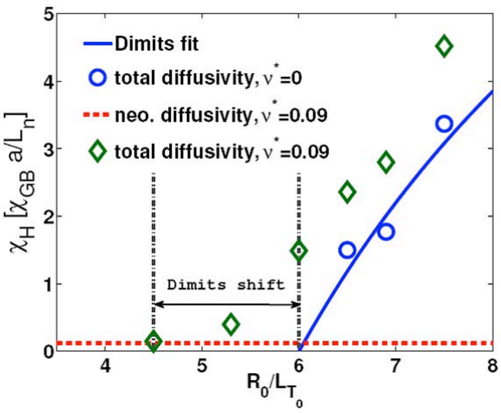

Fig. 2.2.2 *Heat diffusivity in ITG turbulence as a function of ion temperature gradient. In the "Dimits shift" region, collisionless turbulent transport vanishes, whereas a finite turbulent transport level is found when ion-ion collisions are taken into account*

Finite collisionality may also lead to a repetitive bursting behavior, with a period time scale of the order of the i-i collision period. Turbulence and associated transport levels at first increase; zonal flows are generated limiting the turbulence; zonal flows get damped by collisions and turbulence may grow again. Such bursting behavior has clearly been observed in ORB5 runs in the Dimits shift region. Systematic scans in ion temperature gradient strength and collisionality have revealed a synergetic effect of collisions and turbulence: the level of heat transport in nonlinear simulations of ITG turbulence in the presence of ion-ion-collisions systematically exceeds the sum of neoclassical and collisionless turbulent transport considered separately (see Fig. 2.2.3).

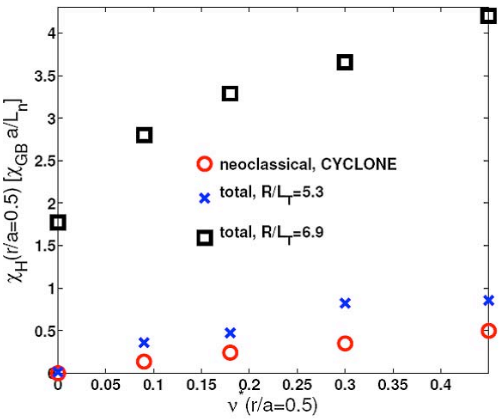

Fig. 2.2.3 *Heat diffusivity in ITG turbulence as a function of ion-ion collisionality. The turbulent transport in the presence of collisions is larger than the sum of collisionless ITG transport and neoclassical transport considered separately.*

In regimes dominated by the Trapped Electron Mode (TEM), the main collisional effect is that of electron-ion collisions. This is a much more challenging case than pure ITG, because both electron and ion dynamics, with their very disparate time scales, have to be resolved simulataneously. Linear collisional TEM runs have been carried out with the ORB5 code and compared with the Eulerian-based GENE code, showing good agreement in the relevant long wavelength regime. The stabilizing effect of collisions on TEM has been thus confirmed. First nonlinear global TEM simulations with the ORB5 code have been initiated.

Effects of electron dynamics on microinstabilities and turbulence

In the ORB5 code, four different models for electron dynamics have been implemented: (1) all electrons are adiabatic; (2) passing electrons are adiabatic and trapped electrons are kinetic; (3) all electrons are kinetic and perturbations are assumed purely electrostatic; (4) all electrons are kinetic and parallel current perturbations are taken into account, giving rise to an electromagnetic response. The “hybrid” model (2) has proven to be useful for TEM cases. Indeed, TEM is essentially electrostatic, and the model allows for larger time steps to be taken because passing electron modes (e.g. ETG) are not present. The success of this model, already implemented in ORB5, has prompted a similar development in the Eulerian code GENE. A fourth order accurate velocity integration scheme, correctly accounting for cut cells at the trapped-passing boundary has been implemented. This reduced electron model provides a useful “button” to turn off kinetic passing electron dynamics, and thus to better quantify the effect of non-adiabatic electron response near mode rational surfaces. Pairs of nonlinear turbulence simulations with full kinetic response and using this reduced model, respectively, are currently being carried out and compared.

Parallel performance of gyrokinetic turbulence simulation codes

The scalability of our numerical simulation codes with the number of processors, and with physical system size, has been the subject of important analysis and developments in view of, on the one hand, their running on the forthcoming IFERC-CSC supercomputer (a 1.3 PetaFlops machine dedicated to European and Japan magnetic fusion programmes, to start operation in 2012) and, on the other hand, for their possible application to ITER-size cases. In the frame of the procurement procedure, target specifications of the IFERC Computational Simulation Center were defined on the basis of series of benchmark runs with the ORB5 code on several platforms. On HPC-FF (a 100 TeraFlops machine in Juelich dedicated to European Fusion Research) the ORB5 code showed the best scalability performance of all European codes tested so far. The ORB5 code was thus selected as one of the High Level Benchmark Codes for capability tests, which will be part of the acceptance procedure of the IFERC-CSC 1.3 Peta Flops supercomputer. Finally, the ORB5 code was selected to be one of the 4 codes to be run as “Lighthouse Project” with access to the machine during the first three months of its operation, before other users are allowed in.

A detailed profiling of the ORB5 code was made, focusing on the inter-processor communications pattern. A kernel was extracted for these, and extensive testing was made on Cray XT5 and Cray XE6 architectures. The bottleneck preventing the extension of scalability to hundreds of thousands of processors was identified as a lack of scalability with increasing number of domain cloning. The related data communications pattern was optimized in several ways, and a substantial reduction of the non-scalable operations was achieved. These improvements were introduced into the ORB5 code and a reduction of cpu wall clock time by almost a factor of 2 for the largest number of clones used (24) could be demonstrated.

In another development, also aiming at reducing the amount of data to be communicated across processors, a field solver based on a finite element approach in magnetic field-aligned coordinates has been implemented in a simplified test problem, namely a 3-dimensional Poisson equation in a cylindrical system. This test problem has proven the feasibility of this approach, in particular in dealing with the non-periodic boundary conditions in the parallel direction, leading in general to a fractional overlap (in units of grid size) of the basis elements. The problem of imposing unicity of the solution at the magnetic axis has also been addressed and solved. The implementation of the relevant gyrokinetic Poisson operator in toroidal coordinates is under way.

Benchmarking of gyrokinetic transport simulation codes

Besides the benchmarking effort reported in the previous paragraph, further comparisons between the two global, gyrokinetic codes ORB5 (PIC-based) and GENE (Eulerian-based) have been undertaken. In collaboration with the IPP Garching, neoclassical simulations carried out with ORB5 have been repeated with GENE. These have enabled us to identify non-physical modes in GENE resulting from the discretization of the linearized collision operators. Potential solutions to this problem have been identified and are currently being tested.

Furthermore, in view of performing non-linear microturbulence simulations in the TEM-regime including electron-ion collisions, linear collisional TEM runs have been carried out with the ORB5 code and compared with the Eulerian-based GENE code. Results have shown good agreement at sufficiently long perpendicular wavelengths compared to the thermal ion Larmor radius. The quasi-neutrality equation implemented in the ORB5 code currently still makes use of a long wavelength approximation for the polarization drift term, which may thus be expressed as a differential operator. This limitation may be removed in the future by considering the full integral form of the polarization drift term, valid to all orders in the ratio of Larmor radius to perpendicular wavelength.

Turbulent transport of fast ions

The interface between the GENE code and the VENUS code, specifically tailored to simulate the turbulent fast ion motion in a global plasma environment, has been completed. A Monte Carlo scheme has been implemented in the VENUS code to simulate the stochastic diffusion of energetic particles under the influence of microturbulent fields. Velocity space dependent (i.e. kinetic) transport quantites are calculated with the GENE code and ported to VENUS. The single particle motion is simulated with VENUS also including the effect of the equilibrium magnetic fields and Coulomb collisions, now modeled with a new numerical scheme recently benchmarked with the ASCOT code. Turbulence transport, slowing down and pitch angle scattering phenomena are extremely important and must be treated in synergy. Collisions reduce the velocity of the particle, which then experiences stronger anomalous diffusivities (see Fig. 2.2.4). Previous simulations of the NBI system in ITER have been extended, confirming good beam ion confinement. Different conclusions are drawn from the numerical analyses of DEMO. Relative to ITER, DEMO will be characterized by reduced Efast/T ratio (thus increasing turbulent diffusivity) and longer slowing down times (increasing the exposure to the turbulence). The effect is a broader NBI deposition profile with respect to simulations where microturbulence is ignored. Similar phenomenology is observed for the Tokamak a Configuration Variable. It has been shown that redistribution is most important for scenarios with longer slowing down times, typically at large temperature and low density. This would put TCV in an advantageous position to investigate fast ion turbulent transport in the future.

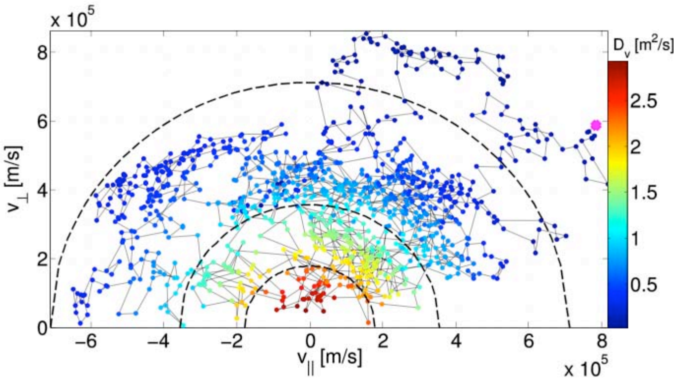

Fig. 2.2.4 *Slowing down of a neutral beam particle (birth position is indicated in magenta) in the TCV tokamak. The 25keV deuterium particle transfers its energy until background thermal velocities are obtained (dashed lines represent multiples 1, 2 and 4 of the thermal ion velocity). The color code represents the corresponding kinetic diffusion coefficient experienced by the particle during the thermalization process, in m^2/s.*

2.2.2 RF waves

ICRF waves in 2D and 3D configurations

The SCENIC ICRH package has been applied to predictions of heating and stability properties in baseline scenarios in ITER (see Fig. 2.2.5). SCENIC is capable of self consistently treating the interaction between the wave fields, fast ion heating and equilibrium. The code has been applied to He3 minority heating, with the line of resonance on the low field side of ITER. Such heating scenarios will be beneficial for control of sawteeth in ITER. The simulations have been compared favourably with the SELFO code. Relatively strong fast ion currents are predicted, and this in turn indicates the presence of an imbalance of co and counter passing ions with large orbit widths. These orbit widths reduce as the He3 concentration is increased, and this in turn reduces the favourable controllability of the internal kink mode. If the He3 concentration is too low however the wave-particle coupling is too weak. A major milestone has been to identify an optimal He3 concentration of around 1 percent, and this in turn has been verified by similar JET experiments.

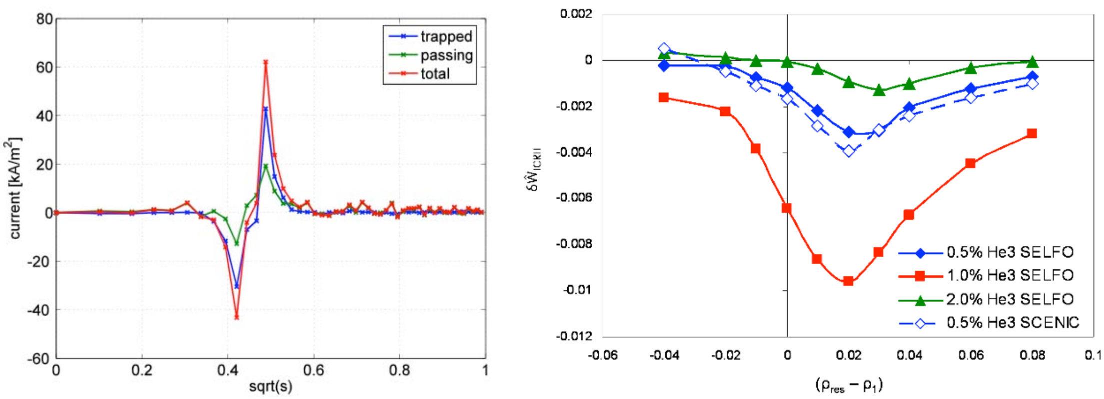

Fig. 2.2.5 *Left: Showing fast ion currents generated with the SCENIC code. ITER baseline scenario was assumed, with 1 percent He3 minority with resonance on the high field side. Right: The SELFO and SCENIC codes are compared favourably in these calculations of the internal kink stability over moving He3 minority resonance position and He3 concentration.*

2.2.3 Operational limits

MHD equilibrium and stability computations of TCV plasmas

In support of the TCV experimental campaign aiming at studying advanced shaping H-mode plasmas, global pressure driven kink mode and edge stability studies were performed at various separatrix shapes including negative triangularity single null (SN) and snowflake (SF) divertor configurations. An essential difference was discovered in the n=1 global beta limits between up/down negative/negative and up/down positive/negative triangularity SN equilibria (assuming that the X-point is in the lower part of the plasma). This is due to a milder influence of the negative triangularity of the X-point onto the core plasma stability, compared to the upper negative triangularity of smooth plasma boundary. In the family of up/down positive/negative SN equilibria, the efficiency of the n=1 mode wall stabilization decreases towards more negative triangularity. However, independently on the gap between ideal beta limits without/with wall stabilization, the growth rates of n=1 RWM modes for different boundary shapes were found to follow a simple general scaling. The up/down positive/negative SN equilibria with moderate X-point negative triangularity look suitable candidates for RWM studies on the TCV, provided that H-mode confinement conditions are reached. The sensitivity studies of the edge stability show that even moderate negative triangularity closes the second stability access in the edge stability diagram, so that high-n ballooning modes always become unstable before the medium-*n* kink/ballooning modes responsible for the type-I ELM triggering. Thus, different types of ELM behaviour can be expected dependent on the sign of the triangularity.

New equilibrium free boundary computation capabilities have been added as a support of the TCV experiment aiming in particular at advanced plasma shaping. The SPIDER free boundary code was upgraded to include the possibility to prescribe either locations of two X-points or the coordinates of a second order null of the poloidal field. This provides additional flexibility in the edge stability control for single null (SN), double null (DN) and Snowflake (SF) configurations. For example, SF-minus-like configurations with moderate negative triangularity, while preserving the positive triangularity of the plasma core, similar to the outside divertor equilibria in a previous ELM-free DIII experiment, can be investigated with the TCV magnetic system. The inverse equilibrium problem, i.e. fitting of PF coil currents, is solved with prescribed plasma profiles. In addition to the positions of the poloidal field nulls a target plasma shape or a number of limiter points can be prescribed to control the plasma geometry. The values of PF coil currents can be optimized to satisfy TCV hardware requirements.

The performance of stability diagram computations based on the KINX code was improved. In support of the edge stability calculations for TCV equilibria an updated version of the KINX code was developed: adaptive eigenvalue shifts in the inverse iterations were used to compute the lowest ideal MHD growth rate starting with an arbitrary initial guess. In particular, it facilitates massive automatic growth rate computations by allowing taking into account the diamagnetic stabilization by checking a simple condition for the ideal growth rate.

The development of a code package based on the KINX stability code, the CAXE fixed boundary equilibrium code and the SPIDER free-boundary equilibrium code has been initiated. The workflow for edge stability calculations includes the plasma shape and X-point position extracted from the TCV database, the SPIDER free-boundary inverse equilibrium solution with standard pedestal profiles for the initial equilibrium, series of fixed boundary equilibria (the boundary may coincide with the separatrix) computed with the CAXE code, ballooning and external kink mode stability computations with the KINX code (for different toroidal wave numbers) and, finally, the stability diagram generation based on the stability computation results. The workflow has been applied to the analysis of recent TCV experiments with varying negative triangularity.

Equilibrium and stability with helically symmetric islands

Helically symmetric equilibria with magnetic islands induced by helical plasma boundary shaping were computed. The helically symmetric plasma option was implemented into the MHD_NX ideal stability code. Ideal stability calculations with helical magnetic islands showed a weak influence of the islands on the external kink mode stability, but revealed a family of two-dimensional instabilities winding with the equilibrium islands (*n*=0 helical). Investigations of the ways to improve the numerical approximation of the ideal MHD condition of a vanishing parallel electric field in the MHD_NX code were continued. The edge-based condition (in contrast to the node-based one) was found to be advantageous in terms of eigenvalue accuracy. In particular, the edge-based option for structured grids aligned to magnetic surfaces gives results as accurate as hybrid finite elements in flux coordinates. The numerical stability of the method with the edge-based condition still needs improvement in order to provide efficient computations on irregular adaptive grids.

MHD Stability and Kinetic effects

The effect of energetic ions on the stability of macroscopic MHD modes has been calculated in terms of the force associated with pressure around a flux surface. This has enabled visualization of the effects of collisionless trapped ions and asymmetrically distributed passing ions on MHD modes (see Fig. 2.2.6). This study enables the successful modeling of sawtooth control with fast ions to be extended to other MHD modes including interchange modes, quasi-interchange modes, infernal modes and resistive wall modes.

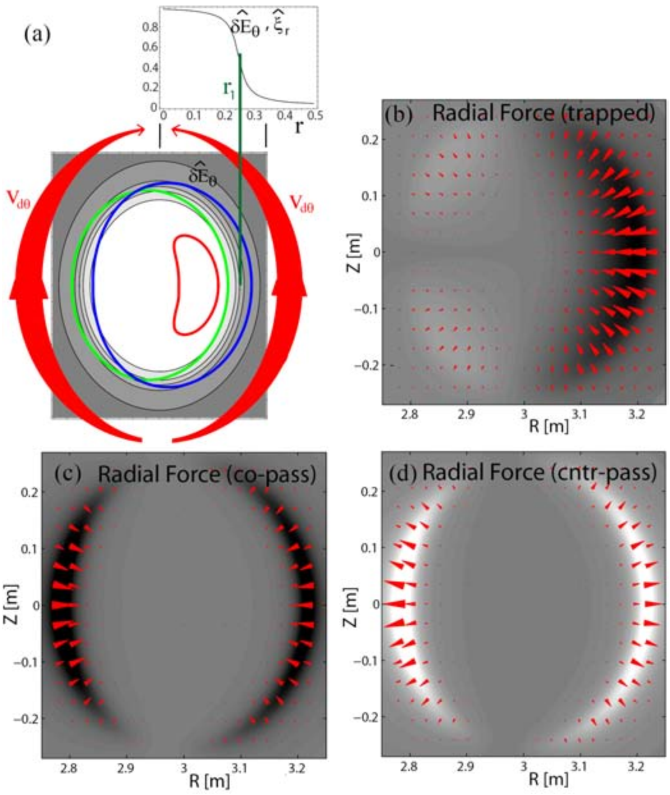

Fig. 2.2.6 *Showing the interaction between fast ions and an MHD mode with poloidal electric field profile shown in (a). Also, a contour plot of the poloidal electric field across the poloidal cross section is shown in (a) in conjunction with trapped (red), co passing (green) and counter passing (blue) ion orbits, together with an illustration of the direction and amplitude of the poloidal drift velocity. (b) plots the radial component of the trapped ion contribution to the response force of fast ions to the mode, while (c) and (d) plot the corresponding contributions due to the radial excursion of respectively co and counter passing ions.*

Sawtooth behaviour and internal kink stability in the presence of fast ions

Simulations examining recent sawtooth control experiments in JET, and predictions for ITER have been assisted by the integration of codes that allow calculations of the internal kink mode to be made in the presence of fast ion populations. Particularly demanding are calculations of realistic distributions of minority ions generated by ICRH. We have used the SCENIC code to generate ICRH driven fast ions with large orbit widths. A class of co or counter passing ions with large orbit widths can be used to control the internal kink mode instability and sawteeth. These results have been passed to a stability code that has evaluated the stability of important JET experiments where sawteeth have been controlled in conditions that would otherwise have led to distruption or confinement limiting neoclassical tearing modes. Moreover, we have been able to predict the effect of similar deployment of ICRH in ITER, and thereby establish that ICRH could be used as effective tool to combat the unfavourable effects of alpha particles and neutral beam ions on sawteeth (see Fig. 2.2.7).

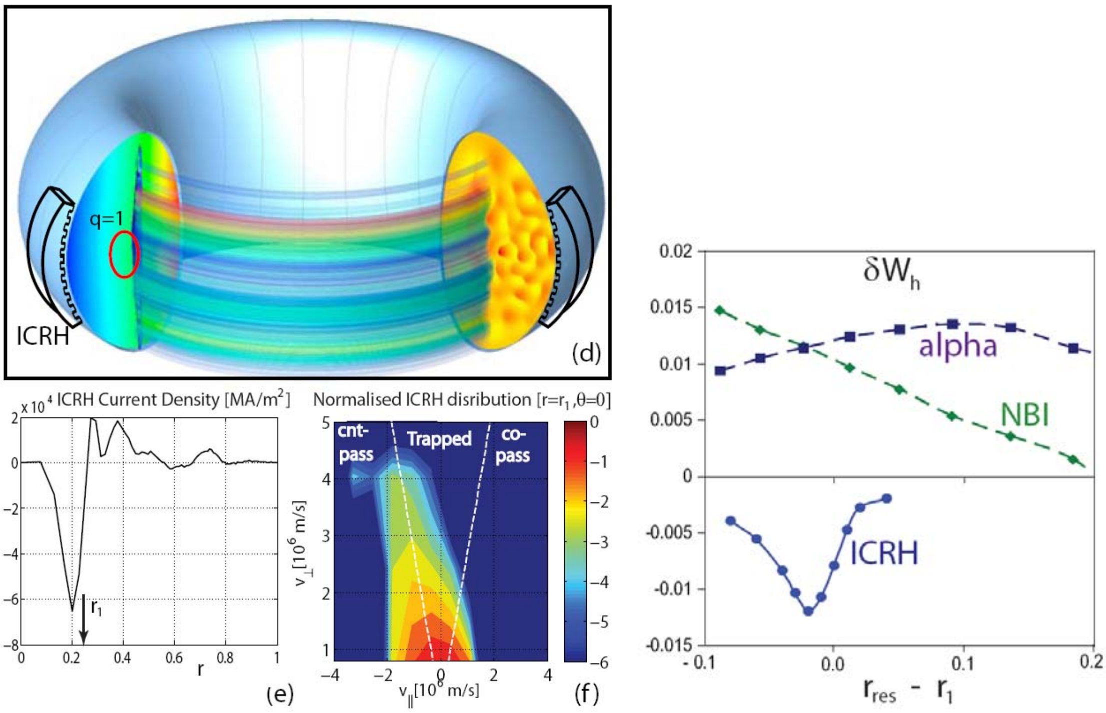

Fig. 2.2.7 *Showing on the left SCENIC simulations of ICRH in JET He3 minority pulses. The current shown in (e) arises due to the parallel velocity asymmetry of passing ions, which in turn destabilises the internal kink mode and triggers sawteeth. The asymmetry in the distributions function in (f) is consistent with the currents shown in (e). On the right, ITER calculations for the response of fast ion populations on the internal kink mode are shown. Due to its sign and magnitude of delta W, it is seen that ICRH can cancel the stabilising effect of alpha particles.*

MHD Stability Limits in Toroidally Rotating plasmas

We have examined MHD stability in strongly rotating plasmas typically found in spherical tokamaks such as MAST, and in future spherical tokamak power plants. Stability boundaries are found against the external kink mode and the Kelvin

Helmholz (KH) instability by using analytic expansions of a rotating torus and the CASTOR-FLOW code using equilibria derived from the DIVA code. As shown in Fig. 2.2.8, with both analytic and numerical treatments it is found that the self consistent treatment of the plasma rotation in the equilibrium and stability codes is required. While strong flows stabilize the external kink mode, they tend to destabilize the KH mode. A window of safe operation has been found with moderate plasma rotation. The external kink mode is highly sensitive to plasma beta, while the KH instability is not. Consequently this safe operation window is only accessible for low or moderate plasma beta.

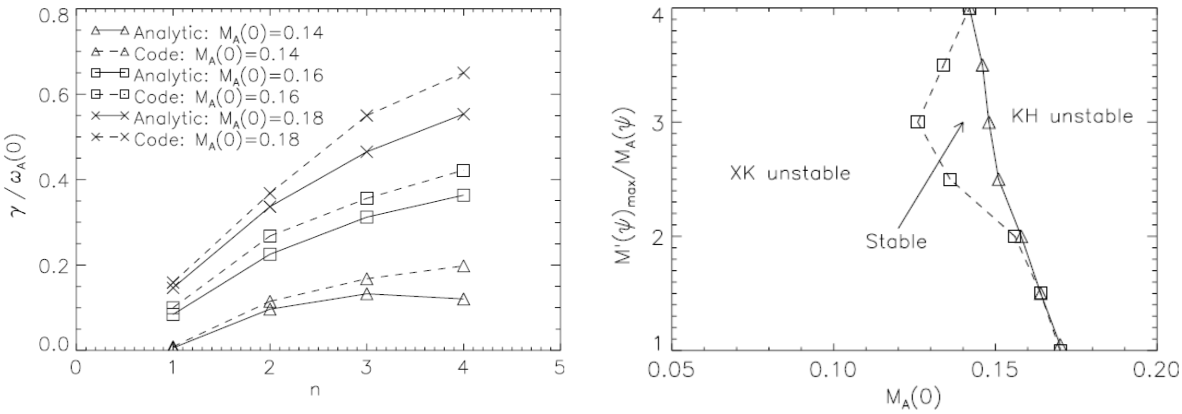

Fig. 2.2.8 *Left: Comparison of analytically and numerically derived growth rates for the KH instability for various toroidal mode numbers and flow rate Mach numbers. Right: The stability window of safe operation against KH and external kink instability shown as a function of Mach number and rotation shear. The stability window opens wider for reduced plasma beta, but closes for enhanced plasma beta.*

2.2.4 Optimization of 3D configurations

Optimization of quasi-isodynamic stellarator configurations

The optimization of a high-β, high aspect ratio quasi-isodynamic stellarator with a number of periods N=18 has been completed. The requirements of small neoclassical effective ripple are found to conflict with those of MHD stability. This implies that for a required value of effective ripple, the secondary currents cannot be diminished below some critical value. The dipole secondary current can be made negligible when no constraint is imposed on the effective ripple. And vice versa, the imposition of a small effective ripple leads to an increase of the secondary current. Several configurations were found with different values of effective ripple, and the corresponding values of the stability parameters were obtained - the higher ripple, the better stability. These configurations were Mercier and resistive interchange mode stable for the value of plasma pressure considered, $\langle\beta\rangle\approx 0.2$, so that $\beta(0)\approx 0.5$. For all the cases treated up to now with the resonant surface ι=3 outside the plasma, but with ι value at the boundary very close to 3 (from 2.8 up to 2.95), free boundary modes were found to be unstable.

Neoclassical transport in 3D stellarators

Energy scattering and the full energy and moment conservative operator have been implemented into the VENUS bootstrap current simulation routine. Bootstrap currents have been calculated for test W7X cases and for LHD configurations based on real experimental discharges.

Energetic particle physics

ITPA TAE linear benchmark cases with eigenmode toroidal index n=1,2 have been successfully reproduced by the VENUS+TAE code with different energetic particle charges. Good agreement has been obtained against the NOVA, CKA, TAEFL and CAS3D-K codes. Detailed results were presented in the 6th Meeting of the ITPA energetic particle physics (Frascati, ENEA, Italy, April 2011).

Alpha particle orbits in ITER

Preliminary calculations of alpha particle orbits and the corresponding closed second adiabatic invariant contours in ITER with a 3D helical core based on ANIMEC equilibria have been calculated with the VENUS code. Collisionless confinement in this non-symmetrical configuration is the same as in ITER with the exact axial symmetry.

2.2.5 Integrated tokamak modelling (ITM)

Contributions to the Integrated Tokamak Modelling (EFDA-TF-ITM Task Force)

In the frame of the ITM EFDA project #IMP12 the updated versions of the CAXE and KINX codes with input code parameters in XML format and the corresponding actors for the Kepler workflow manager were built and tested on the ITM TF gateway computer. In particular, the new KINX version takes into account some changes in the output MHD CPO (ITM data structure and UAL versions 4.08b and 4.09a).

The CHEASE code has also been updated to the most recent UAL version 4.09a. It is being coupled to the two versions of the ETS solver. Resolution of errors in the convention of the signs of the various components (I_p, B_φ, q) still needs further work and discussion. Since the convention is different from most previous assumptions and from ITER's convention. Since the departure of the main developer of the HELENA code, CHEASE might be more extensively used and might require increased support and maintenance efforts.

The spline interpolation is extensively used as a library and this works well. Another tool to enable easy plotting and analysis of CPOs has been developed and is available for the community.

Two specific modules for the ETS solver, sawteeth and NTM, have been updated to version 4.09a and are being coupled to the ETS solver. They now have all the physics and flexibility required for modelling studies. Therefore it is planned to use these new modules, with the ETS, for physics studies in 2012, in collaboration with the ISM group.

Support for the IMP5 group has also started. The first aim was the porting of the LEMAN code on the ITM database. After some analyses, it became clear that without CPOs related to 3D geometry and related equilibrium/stability codes like VMEC/ANIMEC and TERPSICHORE, the effort would be too large. On the other hand, there is a request to have the LION coded ported on the ITM platform. The code is being modified to meet F90 standards and to be compatible with the ITM database.

2.2.6 Tokamak simulations with 3D field effects

Bifurcated helical core equilibria

Fixed boundary MHD equilibrium states with bifurcated helical core solutions have been obtained in ITER and MAST configurations with weak reversed core magnetic shear and $q_{\min}\approx 1$. The pressure and the toroidal current profiles are prescribed and the ANIMEC code is applied to generate the bifurcated solutions. Internal helical cores are computed at a radial position of $q_{\min}\approx 1$ closer to one quarter of the minor radius at tighter aspect ratio.

JET snake structure

JET snake structures are reproduced with the ANIMEC code. The equilibrium state is similar to the bifurcated helical core configurations computed previously in TCV, ITER and MAST, except that the pressure profile prescribed is peaked (consistent with peaked density generated with pellets or impurity accumulation). The structures obtained are also compatible with observations of snakes in Tore-Supra which occur well inside the position detected for the q=1 surface. The pressure profile at the midplane of a computed JET equilibrium is displayed as a function of the toroidal angle v (through 4 toroidal transits) in Fig. 2.2.9.

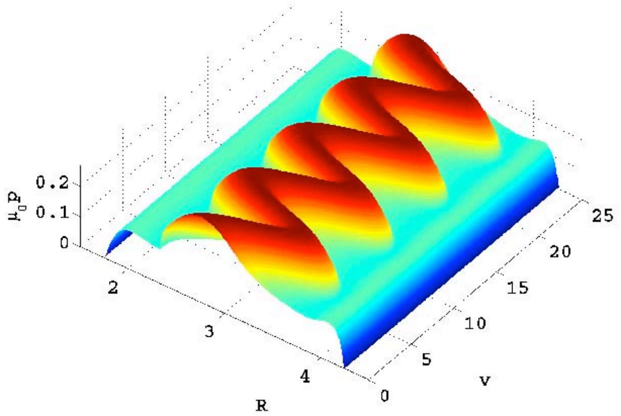

Fig. 2.2.9 *Snakes structure of the pressure at the midplane in a JET equilibrium.*

Free boundary TCV

Preliminary free boundary TCV 3D bifurcated helical core equilibrium states have been computed with the ANIMEC code. For simplicity, the TF and PF coils have been modeled as a single filament. The internal 3D helicoidal structure remains concentrated in the plasma core without noticeably perturbing the plasma-vacuum interface. A sectional cut of the TCV coil system enclosing a 3D helical core equilibrium solution is shown in Fig. 2.2.10.

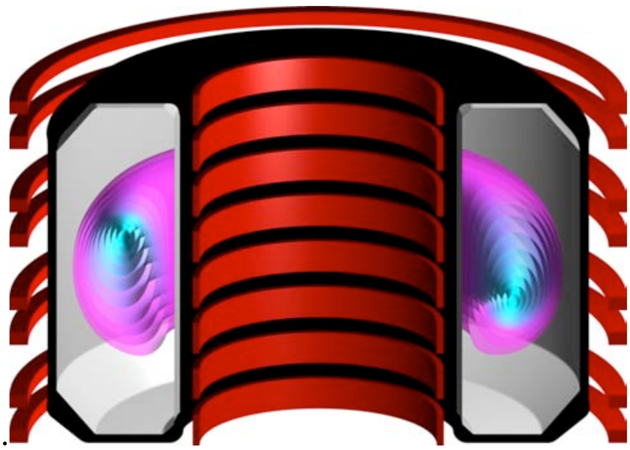

Fig. 2.2.10 *Free-boundary helical core TCV equilibrium with vacuum chamber and PF coils.*

2.2.7 Simulation of plasma edge turbulence

GBS code development

In the course of 2011, we accomplished the implementation of the tokamak-relevant Scrape-Off-Layer (SOL) geometry in the Global Braginskii Solver (GBS) code, initially developed to model plasma turbulence in the TORPEX device. This has allowed us performing the first simulations of SOL plasma turbulence, considering a configuration with a toroidal limiter on the high field side of the device, and focusing on how plasma turbulence is influenced by magnetic shear, electromagnetic effects, plasma shaping, and the boundary conditions at the sheath edge.

Magnetic shear

Magnetic shear is due to the variation in the pitch of the magnetic field lines along the minor radius and is defined by the parameter $s=r/q(\mathrm{d}q/\mathrm{d}r)$. Magnetic field lines twisting tears apart the vortexes and partially destroys the instability structures. In fact, the dominant instabilities present in the SOL, the drift wave and the resistive ballooning mode are stabilized when s reaches value of the order of the unity. For example, in Fig. 2.2.11 we show the growth rate as a function of the safety factor q and the density gradient steepness L_n/R for two different values of the shear parameter. The decrease of the instability growth rate from the s=0 to the s=-1 case is due to the damping effect of the magnetic shear on the instabilities.

We are carrying out a number of nonlinear simulations with the GBS code in order to explore the effect of magnetic shear on the nonlinear turbulent dynamics. Initial results show that, following the linear results, turbulence is suppressed in the case of strong magnetic shear.

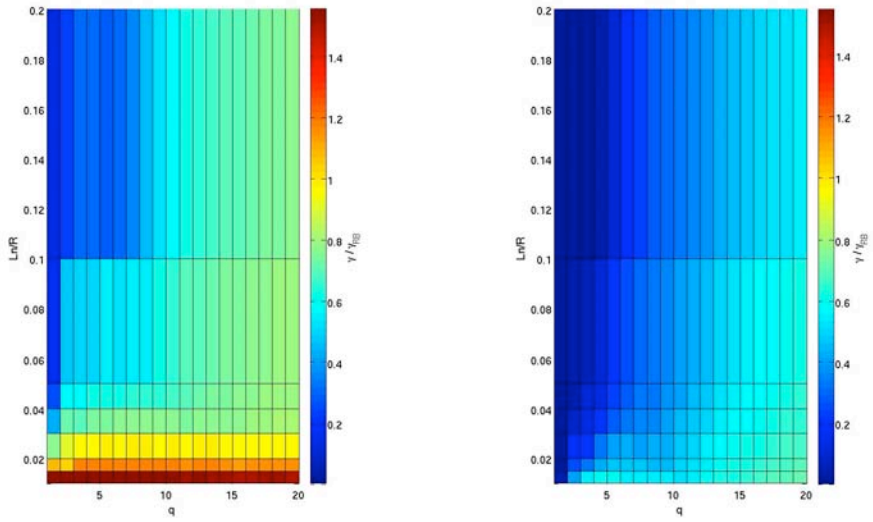

Fig. 2.2.11 *Instability growth rate as a function of the safety factor q and of the density gradient steepness Ln/R for two different values of the magnetic shear.*

Electromagnetic effects

An investigation of electromagnetic effects on SOL turbulence has been carried out. When finite effects are included in a fluid plasma turbulence model, a coupling to the shear Alfven wave is introduced through a magnetic induction term in Ohm's law. In addition, non-linear terms due to the perpendicular displacement of the magnetic field lines must be included to the parallel derivatives of the fluid fields.

The analytical theory indicates that an ideal ballooning mode can be destabilized if the interchange drive from unfavorable curvature exceeds parallel delocalization due to shear Alfvén waves, i.e. when $\alpha = q^2 R/L_p$ 1. The ideal ballooning mode is of a global nature, and it can lead to major MHD events. Linear stability simulations solving the two-fluid equations in SOL configuration with finite roughly confirm this limit.

GBS non-linear simulations are being carried out to investigate electromagnetic effects on SOL turbulence. In low-β case ($\alpha<0.1$) it is found that the electromagnetic effects do not affect the character of the turbulence significantly, and the macroscopic characteristics of the turbulence such as poloidal mode number, radial extension of the structure, and fluctuation amplitude appear to correspond to the previously studied electrostatic case.

However, when is increased such that $\alpha \approx 0.1$, it appears that the amplitude and the radial structure of the fluctuations changes, leading to higher transport. Figure 2.2.12 shows a poloidal slice of the plasma density. The turbulence is stronger than in the electrostatic case, and very large fluctuations are observed in the "driven" region. Although this study is ongoing, the preliminary results are promising because increased transport due to electromagnetic effects is observed at $\alpha \ll 1$, which is observed in the experiment but not predicted by the ideal ballooning mode theory.

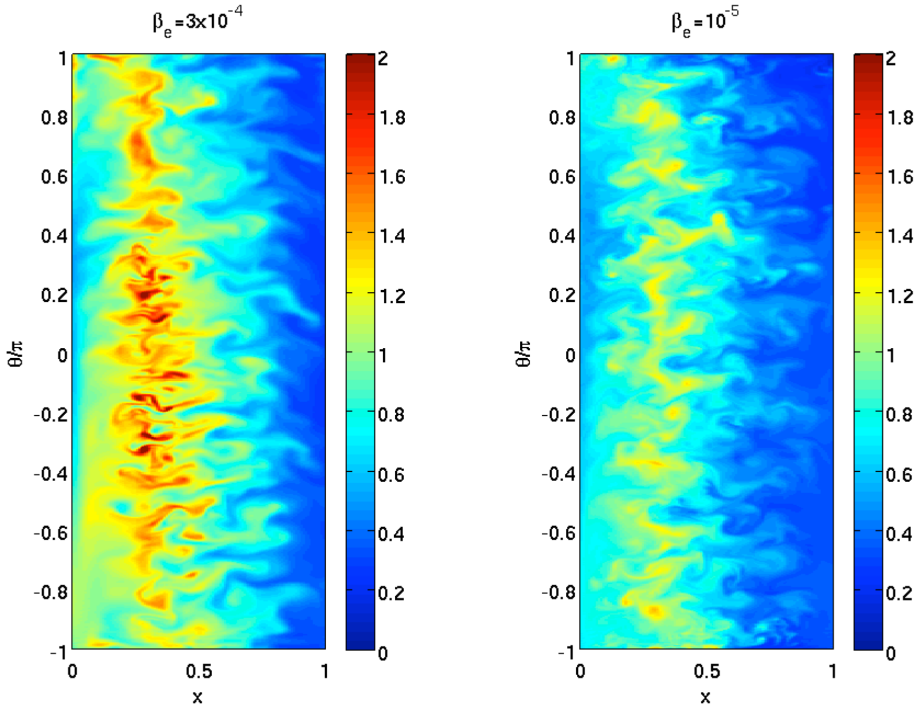

Fig. 2.2.12 *Total plasma density at α≈0.1 (left) and α≈0.03 (right) in GBS electromagnetic non-linear simulations of drift wave turbulence. The low beta case is essentially electrostatic, while the high beta case shows stronger fluctuations."*

Plasma shaping

In the present version of the GBS code, the magnetic equilibrium is approximated to the local s-α model. It is therefore assumed that both the magnetic field amplitude and its curvature are constant; moreover, finite aspect ratio effects are neglected.

We have therefore started a project with the goal of relaxing those approximations. The focus has initally been on implementing finite aspect ratio effects within a local approximation, as a first step towards a general global magnetic equilibrium. The Braginskii equations have been re-derived and now include finite aspect ratio terms related to magnetic trapping. Then, the different operators present in the equations have been rewritten for a general axisymmetric magnetic field. The implemenation of these new operators and of the terms related to finite aspect ratio effects is ongoing.

Sheath boundary conditions

An effort is being put in the improvement of the GBS code, focusing on the physics of the plasma-wall transition (PWT). Indeed, boundary conditions for plasma fluid models are needed at the magnetic presheath entrance, namely the region where the assumptions of the drift-reduced Braginskii model break down and a kinetic model is needed to describe the plasma turbulence. Boundary conditions determine the plasma losses at the vessel, thus strongly affecting the steady state profiles.

For this purposes ODISEE (One-Dimensional Sheath Edge Explorer), a 1D3V fully kinetic particle-in-cell code modeling a plasma bound between two walls, was used to simulate the PWT in the general case of an oblique magnetic field. A combined fluid and kinetic description of the plasma, supported by the numerical results, has been used to derive the position of the magnetic pre-sheath entrance and the relation between the fluid quantities in this location. In particular, the angular dependence of the different potential drops occurring in the different subregions of the PWT has been obtained (see Fig. 2.2.13). The implementation of these boundary conditions in GBS is currently being carried out.

We remark that the ODISEE code has also been upgraded with new tools that allow exploring new interesting features of the PWT. These include, for example, the possibility of setting the wall as either a biased conductor or an insulator, or inserting a biased grid in the system with some given transparency. In particular, this has lead to the discovery of a plasma potential phase transition occurring in a 1D plasma bound between two biased walls when subject to different amounts of charge injection. An experimental verification of this effect is being currently considered in the TORPEX device.

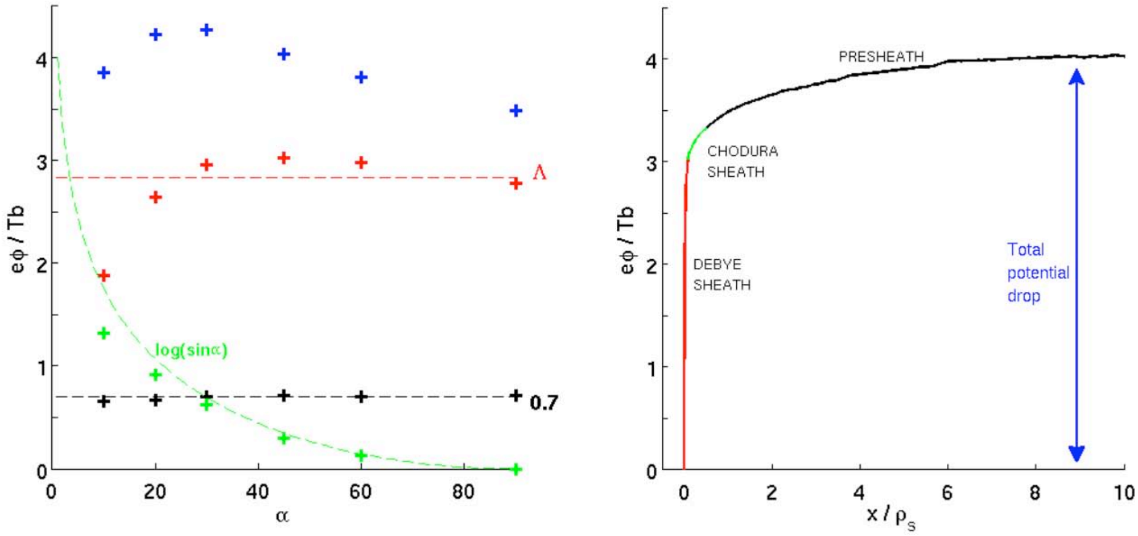

Fig. 2.2.13 *Potential drop as a function of the incidence angle of the magnetic field on the wall (left) and potential profile in the vicinity of the wall (right).*

2.3 Operation of a specialised basic plasma physics device, TORPEX

In magnetically confined fusion plasmas, turbulence is of utmost importance since it causes large particle and energy transport, reducing the effectiveness of the plasma confinement system, hence that of fusion reactors. The role of the CRPP Basic Plasma Physics Group is to contribute to advancing the basic understanding of turbulence in magnetically confined plasmas of direct relevance for fusion devices, and of its effect on the various plasma components, including supra-thermal ions.

The experiments are performed in the TORPEX device, which is characterized by low plasma densities (n_e~10^{16}-$10^{17}m^{-3}$) and temperatures (T_e~5-20eV) and is equipped with an extensive set of diagnostics allowing high-resolution measurements of plasma parameters and wave fields throughout the plasma cross-section. Plasmas of different gases are sustained by microwaves in the electron cyclotron (EC) frequency range, f=2.45GHz. Plasmas are confined by a toroidal magnetic field up to B_T=0.1T, and a smaller vertical component, B_Z≤50mT. This magnetic geometry, known as simple magnetized torus (SMT), incorporates the main ingredients for drift and interchange instabilities and turbulence, namely pressure gradients and magnetic field line curvature. Although it does not possess a rotational transform of the magnetic field lines, the SMT mimics the crucial external region of magnetically confined plasmas for fusion, referred to as the Scrape-Off-Layer (SOL), where magnetic field lines are open and terminate on the vessel wall.

In 2011, the operation of TORPEX has continued to be characterized by a large degree of flexibility, with several short interventions for installation or new or refurbished diagnostic systems, and for modifications to the configuration, e.g. with the insertion of ad hoc metal limiters, and by a significant number of plasma discharges. Such operational flexibility is testified not only by the large number of experimental sessions (with large number of plasma discharges ~10000), following the various modifications to the machine configuration, but also by a continuous involvement of undergraduate and graduate students.

In 2011, significant progress was achieved along several research avenues, from blob physics and control to the interaction between supra-thermal ions and interchange waves and turbulence. Such progress is detailed in the paragraphs here below.

On the technical side, preparations for an upgrade of the TORPEX device have also started. We intend to modify the TORPEX device so that, in addition to the SMT magnetic fields, a poloidal field can be generated by a current driven in a filament running along the toroidal direction or by a current driven in the plasma itself (as in the tokamak configuration). The field lines then wind around the minor axis of the torus with a twist controlled by the toroidal current. Such configuration would increase relevance to magnetic fusion devices, by creating a region of closed field lines and magnetic surfaces.

2.3.1 Blob physics in TORPEX

In virtually all magnetic confinement devices, such as tokamaks, stellarators, reversed field pinches, and linear devices, intermittent cross-field transport of particles and energy are associated, at least in part, with the propagation of plasma blobs. These are poloidally-localized regions extending along the field lines where the plasma pressure is enhanced compared to the surrounding plasma. In recent years, blob physics has been extensively studied in basics plasma physics and fusion devices due to their importance for burning plasma experiments and future thermonuclear reactors.

In previous years, facilitated by the full diagnostics access of the TORPEX device with adequate spatial and temporal resolutions, we have undertaken a throughout investigation of blob physics. First, the blob formation mechanism was identified in scenarios dominated either by two-dimensional (2D) interchange-generated turbulent structures or by fully developed three-dimensional turbulent structures. We have then focused on the propagation properties of blobs once they are formed. The goal was to identify and quantify the different physical effects that determine blob cross-field velocity and, ultimately, develop methods to influence blob motion and cross-field transport. We interpreted blob motion using a 2D, sheath limited blob model, in which parallel currents are determined by sheath boundary conditions. Using this model, we derived a generalized analytical expression for the blob velocity, which takes into account parallel and cross-field currents as well as damping due to the neutral gas background. This new, generalized scaling law shows quantitative agreement with the TORPEX experimental blob size-versus-speed data set. This confirms directly the existence of two regimes, obtained in hydrogen and helium plasmas respectively, in which parallel currents to the sheath do or do not significantly damp charge separation, and thus blob radial velocity.

During the past year, we have further consolidated the previous interpretation of blob motion using magnetic probe measurements of blob current and explored the insights gained from our previous studies to actively influence blob propagation in TORPEX, in particular by testing the two predictions above.

Direct local estimate of the parallel current density is a challenging measurement in thermonuclear oriented plasmas and various attempts are now in progress. In TORPEX, a specially designed current probe, consisting of an L-shaped array of 3 miniaturized three-axial pick up coils (3.5 cm spaced, effective are of $2.3\text{x}10^{-3}\text{m}^{-2}$), was developed in collaboration with Consorzio RFX in Padova (IT). Using this probe, 2D measurements of the parallel current density associated with radially propagating blobs were obtained in TORPEX using conditional sampling techniques. Figure 2.3.1 shows 2D profiles of the parallel current at three times during the blob propagation. An asymmetric dipolar structure of the current density is revealed, which originates from ∇B and curvature induced polarization of the blob and is consistent with sheath boundary conditions. The dipole is strongly asymmetric due to the non-linear dependence of the current density at the sheath edge upon the floating potential. Furthermore, by performing these measurements in hydrogen and helium plasmas we directly demonstrate the existence of the previously observed regimes.

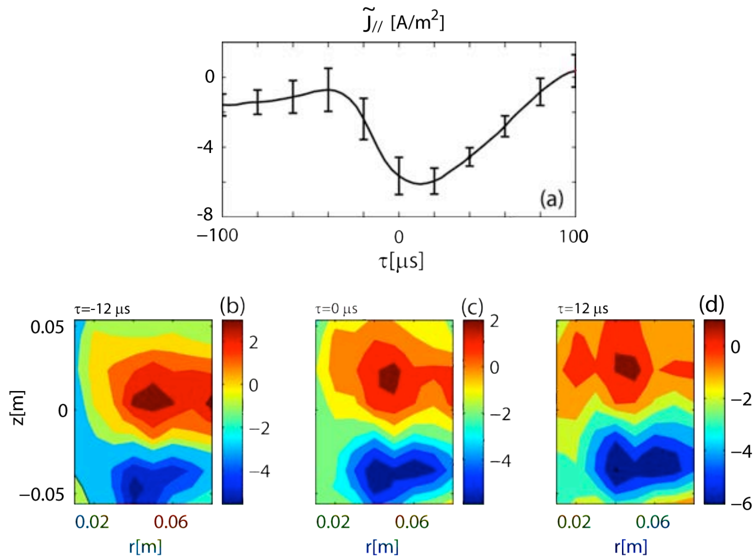

Fig. 2.3.1 *Conditionally sampled data from the current probe measured ~3cm in front of the limiter. Frames (a) shows an example time evolution of the parallel current density at r=6 cm and z=–4cm. Two-dimensional profiles of the parallel current density are shown at three different times during the blob radial propagation in frames (b-d).*

To investigate the effect of the observed asymmetry of the parallel current on the blob motion, we carried out numerical simulations of seeded blobs, using a two-field fluid model, which evolves electron density and vorticity. The simulations span a wide range of blob sizes covering both regimes described above. We used either the complete or a linearized form for the sheath dissipation term in the vorticity equation. The structure of the parallel current density and plasma potential is found to be different in the two cases. Asymmetric profiles are observed in simulations with the complete form, while symmetric profiles are obtained when a linearized form is used. Negligible effects are, however, observed in terms of blob radial velocity.

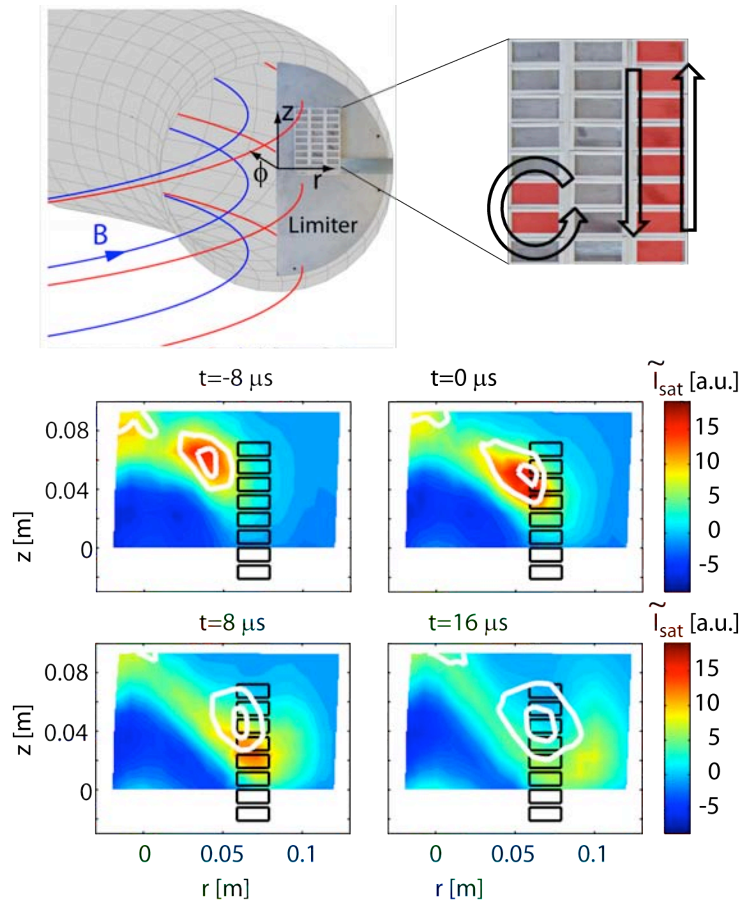

Fig. 2.3.2 *Above: Sketch of the TORPEX vacuum vessel and the electrodes installed on a conducting limiter. Examples of magnetic field lines and the coordinate system are also shown. A zoomed in view of the electrodes is shown at the right. Shaded areas indicate examples of positively biased electrodes and arrows the expected flow pattern. Below: Conditionally averaged blob propagation (Isat fluctuations) for the case where a vertical stripe of electrodes is biased to +40 V (color plots). For comparison, the white contours indicate the results of the same analysis when all electrodes are grounded.*

Based on our understanding of the physics governing blob motion, we have started to develop blob control methods. One of these methods, aimed at inducing radial flows in the edge of tokamak plasmas, is based on the use of biased plates at the edge of the plasma. Basic principles of this idea are being tested in TORPEX. A set of 24 electrodes has been installed on a limiter with the goal to modify the plasma potential and thus the cross-field flows in a controlled way. A sketch of this limiter is shown in Fig. 2.3.2. The set of electrodes provides good flexibility. Different flow patterns can be induced, such as convective cells, radially elongated flows, or vertical flows, as illustrated in Fig. 2.3.2.

Figure 2.3.2 (bottom) presents the effect on blobs, when a bias of +40V is applied to the sets of electrodes indicated by black rectangles in Figs. 2.3.2. Conditional average sampling is applied to obtain the average, 2D evolution of blob propagation. Figure 2.3.2 (bottom) shows successive time frames of blob propagation obtained this way. t=0 corresponds to the time when blobs are detected at the reference probe. In the same figure, the white contours depict the conditional sampled blob in the case without biasing. While early in time, the average blob evolution is very similar, later on, as anticipated, the blob is swept strongly downwards due to the applied bias. The blob vertical velocity in the time window [–8μs, 8μs] is modified from ~700m/s to ~2100m/s due to the biasing, which also results in significant modifications of the time-averaged profiles. Measurements along and across the magnetic field show a fairly good toroidal symmetry of the changes induced by the biasing. Due to a high level of cross-field currents, the magnitude of the achievable potential variations is well below the potential applied to the electrodes. In addition, the strongest potential variations are not induced along the biased flux tube, but at a position shifted in the direction of flows.

2.3.3 Fast ion studies

The complex question of how plasma turbulence influences supra-thermal particles and, in turn, how supra-thermal particles influence turbulence is today receiving much attention in fusion research. In future fusion reactors, to reach the burning regime, additional heating will be needed, which will create strong suprathermal ion components, for example via the injection of energetic neutral beams (NBI). When reached burning conditions, the majority of the heating will come from the fusion-generated, highly energetic α particles. A good confinement of the slowing down α particles and of the NBI-generated fast ions is therefore crucial.

In previous years, we started theoretical and experimental investigations of fast ions-turbulence interaction on TORPEX. The TORPEX device is equipped with a miniaturized Li6+ ion source, which produces fast ions with energies in the range 100eV-1keV. Li-6+ ions at 100eV have a Larmor radius of about 3.5cm for B_T=0.1T, and makes one toroidal turn in 0.11ms. A miniaturized gridded energy is used to measure fast ion energy and current density profiles. Both source and detector can be moved across the plasma cross-section.

In 2011, experiments have been conducted with fast ion energies ranging from 88eV to 290eV. The source was positioned at X=-2.5cm and Y=0cm, with a slight angle downward. Source and detector are separated toroidally by 25°, corresponding to 42cm. The normalized density fluctuations at the injection position are of the order of ~50%. Profiles of the fast ion current density with and without plasma were reconstructed for energies of 88eV, 142eV, 190eV and 290eV (Fig 2.3.3). The vertical shift of the center of the fast ion distribution is due to a combination of the ion Larmor motion and the drifts induced by curvature and gradient of the magnetic field. The profiles are all broadened by the plasma, meaning that the interaction of the fast ions with the plasma is significant. This effect is the most important for ions of 88eV.

To interpret the experimental data, we follow fast ion tracer trajectories using the full Lorentz force, with E and B-fields specified by a numerical model of drift-reduced Braginskii equations (GBS) in two dimensions. This model was previously validated to describe interchange turbulence on TORPEX. Comparisons with the simulations are possible using a synthetic diagnostic, allowing the poloidal cross section of the fast ion current density to be represented (Fig. 2.3.3, right). Comparison of the profiles and FWHM for each case shows relatively good agreement. However, the spread of the beam is extremely sensitive to the distance traveled by the fast ions. Indeed, the effect of the gyromotion of the fast particles is reflected by an oscillation of the beam width. As the energy increases the Larmor radius increases and this effect becomes predominant. Both the experiment and the simulations show that the plasma, i.e. turbulence, effect is the largest for low ion energies. The trend is then similar until the 143eV case. At 300eV the oscillations associated with the gyromotion are more important and it becomes difficult to find a close agreement with 2D measurements.

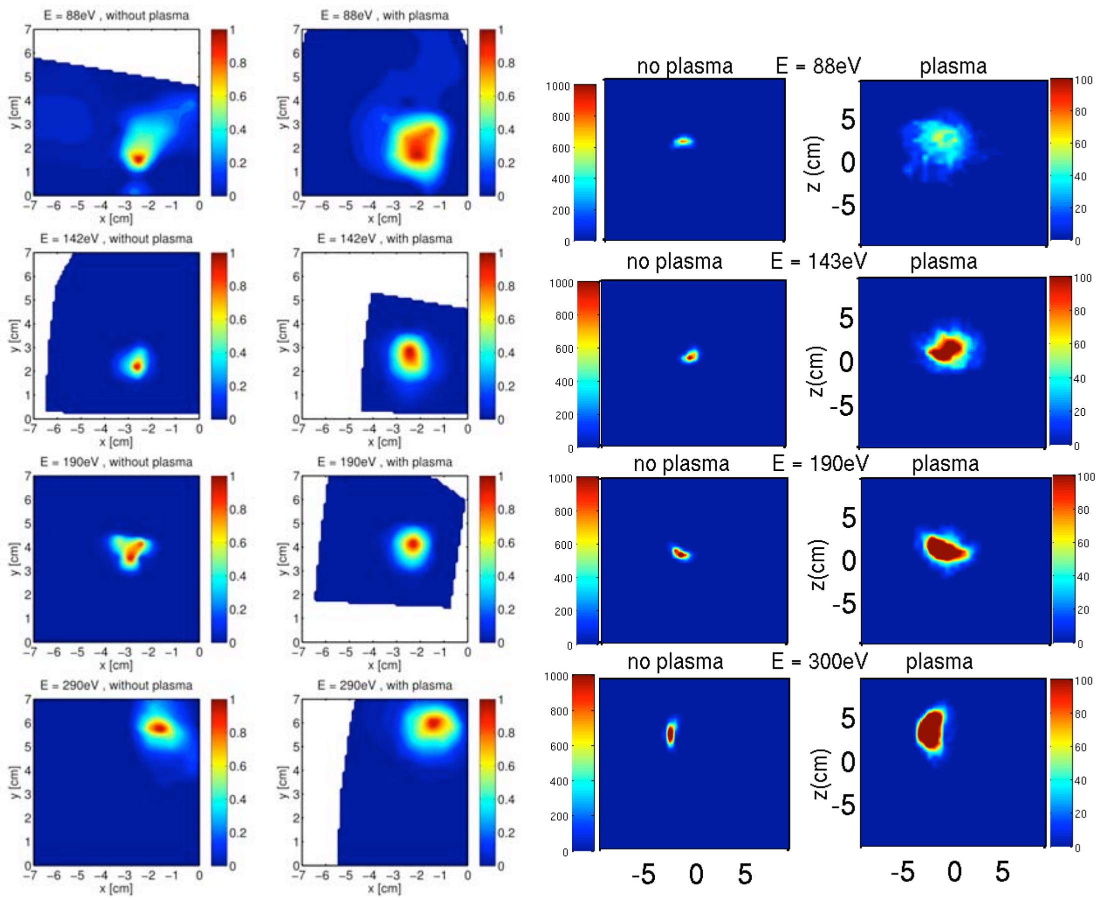

Fig. 2.3.3 *Left: Experimental fast ion current density profiles for different energies, with and without plasma. Right: : Fast ion current profile from the simulations.*

More generally, besides the effort for the experiment-simulation comparison, a comprehensive theoretical study of fast ions transport in turbulence was completed. We focused on characterizing the generalized diffusion power law exponent for the time dependence of fast ion dispersion. In computing the orbits, we studied the effects of a wide range of fast ion injection energies and turbulence fluctuation amplitudes. The results of this parameter scan are shown in the Fig. 2.3.4, where the color of the data-point shows the generally non-diffusive power law exponent for the variance of fast ion radial position. The x-axis gives the injection energy and the y-axis the turbulent fluctuation amplitude. The two curves show the approximate boundaries predicted by analytic expressions based on drift and finite Larmor radius approximations. The dashed red curve shows where the vertical drift-averaging becomes important. The black curve shows where gyro-averaging becomes important. Finally, the horizontal black line at small turbulent fluctuation amplitudes shows where the radial variance becomes very small due to disconnected topology in the velocity field. Some of this parameter space, including the transition region near 100eV, will be accessible to the TORPEX fast ion experiment when the construction of a toroidally moving source will be completed. This system, presently under development, will allow varying continuously the distance between the source and the detector between each discharge to reconstruct the 3D profiles of the fast ions beam.

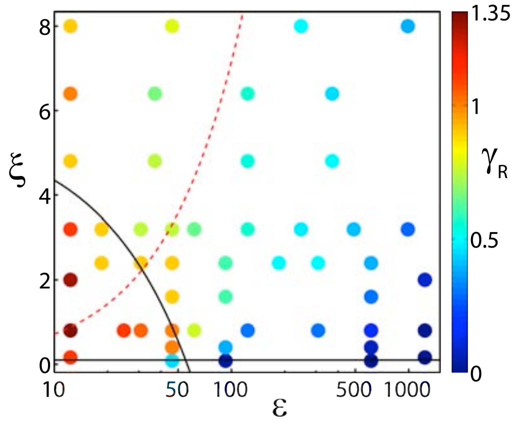

Fig. 2.3.4 *Dispersion exponent γ_R (colored dots) in the interaction phase is displayed in the ξ–ε plane. Regions for γ_R are demarcated by the gyro-averaging condition (solid black curve), by effective drift-averaging condition (dashed red curve), and by the disconnected streamline condition (horizontal line).*

2.3.4 Fast visible imaging of TORPEX plasmas

In basic plasma physics devices, as well as in magnetic confinement fusion experiments, non-perturbative full spatio-temporal imaging of visible light fluctuations with adequate spatial and temporal resolution can be obtained using fast framing cameras. On TORPEX during previous years, a fast imaging system was developed, which includes a Photron Ultima APX-RS fast camera, a Hamamatsu image intensifier unit, and a gas puffing system. The camera together with the intensifier can image TORPEX plasmas up to 200 kframes/s framing rate and with minimum exposure time of 1 micro-second, which results in clear images of plasma wave or turbulent structures. A two-dimensional gas puffing imaging (GPI) system, including a 2D movable gas puff nozzle, has been developed to establish a correlation between the plasma parameters measured by probes and visible light emission. The fast imaging system covers approximately 70% of the TORPEX cross section in a tangential view. To reconstruct the time-resolved poloidal emissivity of visible light from the fast camera data, a pixel method was developed and an optimized reconstruction procedure was applied to the tangentially viewed images. The tomographic problem is formalized by an over-determined set of equations, which is solved in a least-square sense by using a singular value decomposition method, thus providing the time-resolved emissivity profile of TORPEX plasmas. The spatial resolution in the reconstructed emissivity profile is limited only by the plasma pixel size (1cm) to 2cm. This is significantly lower than accessible with probe arrays, and implies no perturbations to the plasma dynamics.

In year 2011, the fast imaging system was used to investigate quasi-coherent interchange modes and intermittent, turbulence-generated blobs under various experimental conditions in TORPEX plasmas. Ideal interchange modes were studied as a function of the vertical magnetic field. We showed that, by increasing the vertical magnetic field, the principal interchange mode is damped and a sharp transition occurs between low-k and high-k spatial harmonics. Conditional sampled images from the fast camera data (an example is shown in Fig. 2.3.4) provide detailed measurements of the vertical and radial sizes of small structures associated with high-wawenumber harmonics. The scaling of the radial width of different interchange harmonics with respect to the vertical wave number is reconstructed and compared with a theoretical scaling law. The results seem to confirm the theoretical predictions for the mode radial extension. Measurements of the radial width of mode structures were used to estimate the saturation levels of the corresponding fluctuations, based on the gradient-removal mechanism. This was tested using experimental data from the visible camera. The saturation level of the interchange instabilities, predicted by the gradient-removal mechanism, is in reasonable agreement with the experimental measurements. These results are important for characterizing the plasma transport due to interchange instabilities, which, similarly to TORPEX, are believed to play an important role in tokamak SOLs.

Tomographically inverted data from the fast camera were used to study the propagation of intermittent blobs. Blob radial speeds and vertical sizes were computed in plasmas of different gases, allowing us to test theory predictions on blob speed-versus-size scaling. The experimental speed-versus-size scaling is found to be in good agreement with both the theoretical scaling law and data from electrostatic probes, as discussed in the previous section. This is clearly shown in Fig. 2.3.6, which displays the joint probability of the normalized blob speed with respect to the normalized blob size together with the scaling expected from theory (red, white, black curves at different neural gas pressures). This reinforces the basis of the theoretical scaling law and confirms the possibility of using fast imaging to reconstruct the blob speed-size scaling law in tokamak plasmas non-perturbatively. This would enable one to identify the mechanism and non-perturbatively estimate the transport levels in the SOL of fusion devices.

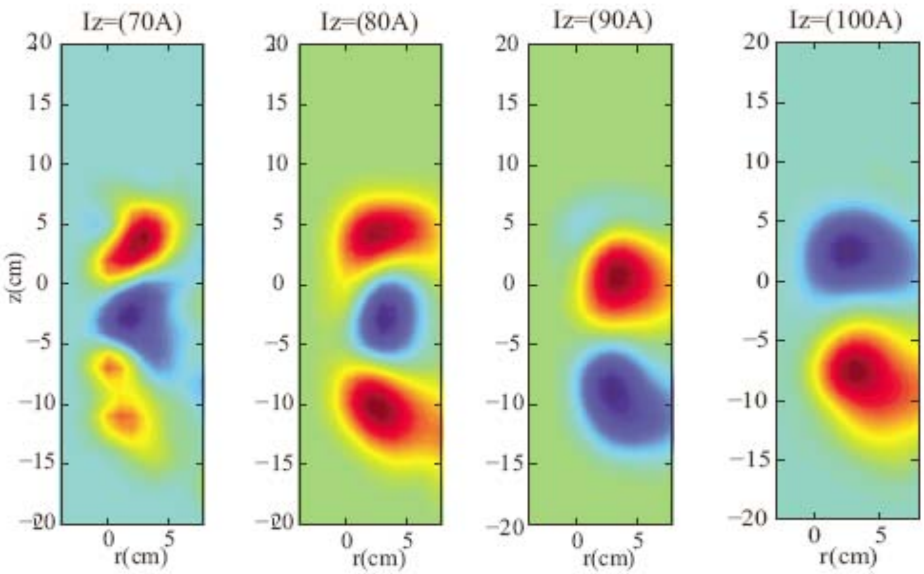

Fig. 2.3.5 *Conditionally sampled 2D profiles of visible light emission from fast camera data at different vertical magnetic fields.*

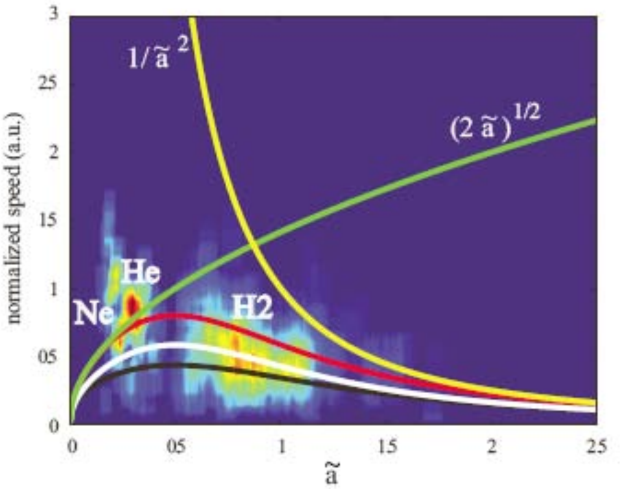

Fig. 2.3.6 *Joint probability of the normalized blob speed with respect to the normalized blob size. Different filling gases (H2, He and Ne) are used to vary the normalized blob size value. High probability peaks correspond to different gases. Theoretical scaling curves are plotted for different neutral gas pressures and values of the plasma background.*

In general, we show that fast imaging technique, a relatively easy to handle diagnostic, can potentially reconstruct turbulent plasma features non-perturbatively in any plasma machine including basic devices and tokamaks, providing high spatio-temporal resolution of measurements in a wide range of plasma parameters. The fast imaging provides the necessary basis to assess theoretical models and to establish detailed comparisons between theoretical predictions and experiments, which will improve our understanding of one of the key factors for the optimization of magnetic confinement fusion.

2.3.5 Technical achievements

In its present setup, TORPEX can produce SMT configurations. To better mimic the SOL-edge magnetic geometry in tokamak, we are planning create twisted field line configurations. To this aim, a poloidal field will be generated by a toroidal current flowing in a copper wire running along the toroidal direction. The twist of the magnetic field line can be easily controlled by the amount of current driven in the wire. A feasibility study has been conducted in 2011. The wire will be suspended inside the vacuum chamber through 4 insulated 1mm diameter stainless steel wires, as schematically shown in Fig. 2.3.7. Heat shrinkable ceramic braidings, which are vacuum and plasma compatible, will be used to avoid direct contact of the metal surfaces with the plasma. The wire will be powered by six 1kA-10V power supplies, which are already available at CRPP. The output dynamics of the power supplies is limited to a maximum slew rate of ~1400A/sec. This will allow reaching a maximum flat top current in approximately 700ms. For simplicity, we are not planning to use water cooling of the wire. Therefore, the flat top current duration is limited by the Ohmic heating of the wire with almost pure radiative cooling in vacuum. We estimate that a maximum current of ~2000A (2 power supplies) will avoid overheating of the wire thus allowing us to make ~100 discharges per day (considering our present repetition rate) with a flat top of approximately 200ms. The latter value will insure a data statistics similar to that in present SMT configurations. The installation of the toroidal wire will allow the production of magnetic geometries with single and double magnetic null-lines. More complex geometries with multiple fully 3D X-points and/or magnetic ergodic/chaotic surfaces will be generated by ad-hoc coils installed inside the TORPEX vessel, and powered by external power supplies.

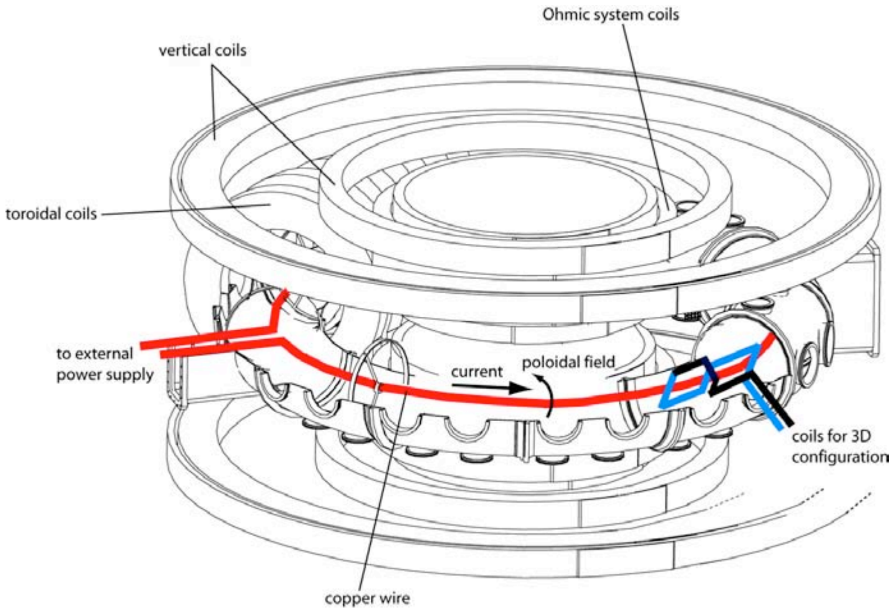

Fig. 2.3.7 *TORPEX schematics showing all major components of the device. The components in the present setup are shown in black. The components in color (toroidal wire in red and an example of internal coils for 3D configurations in blue) are part of the upgrade proposed in this Proposal.*

2.4 Materials research

2.4.1 Emerging technologies

Development of material science and advanced materials for DEMO

Development of ODS ferritics steels

WP11-MAT-ODSFS-01-01/Swiss Confederation/BS: Production and characterization of laboratory-scale batches of nano-structured ODSFS

The goal of this activity is to improve the ductility and high temperature strength of the ODS ferritic steel produced in CRPP Materials Group. To this end, the fabrication conditions must be optimised, including control of the quality of the substrates and selection of powder metallurgical route and thermal-mechanical treatments parameters. In order to reduce oxygen contamination in the milled powder and the consolidated material, prealloyed powders acquired from Alpha-Aesar company were milled with Y2O3 or Fe2Y particles instead of previously used elemental powders. Ball milling times of 8, 24, 48 hours and two BPR ratios were tested using a dynamic hydrogen atmosphere of Ar and H2 were used for flushing the vessel and milling. The prealloyed powders turned out to contain about five times less oxygen and nitrogen than the elemental powders, thus they were selected for production of next small batches and up-scaling of the ODS FS fabrication. The 8 h milling time, as recommended by attritor supplier turned out to be insufficient to uniformly disperse the oxide particles which as indicaded by TEM of a FIB lamella extracted from the powder.

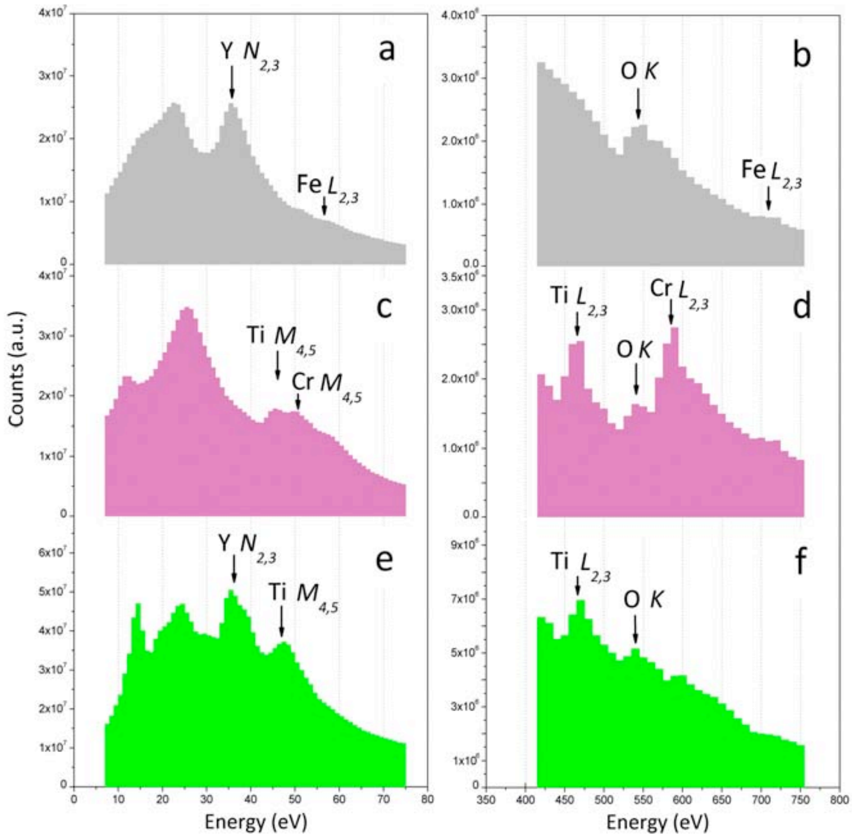

Fig. 2.4.1 *EELS at low loss (a, c, e) and core-loss energy (b, d, f) for three oxides: Y-O (a, b), Cr-Ti-O (c, d) and Y-Ti-O (e, f), by EFTEM (made at CIME EPFL)*

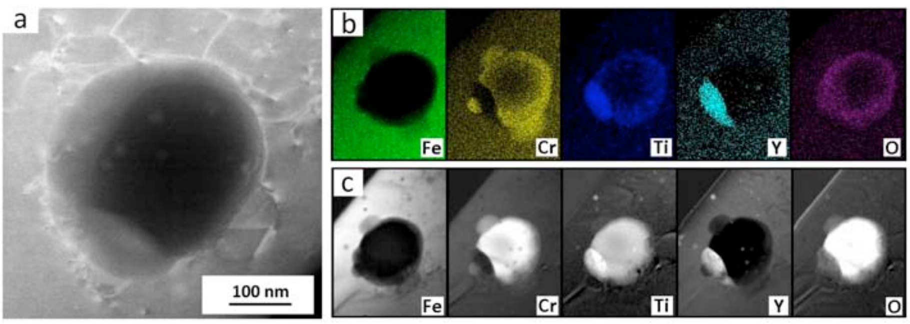

Fig. 2.4.2 *(a) Dark field STEM image of a particle in the Fe-14Cr-2W-0.3Ti-0.3 Y_2O_3 ODS FS (b) X-ray energy dispersive maps in Cs corrected STEM (made at WUT Poland); (c) Electron energy loss maps in EFTEM (made at CIME EPFL) treated by PCA*

The as-HIPped Fe-14Cr-2W-0.3Ti-0.3Y2O3 ODS ferritic steel based on the elemental powders was thoroughly analysed using advanced microscopic and spectroscopic tools to describe the composition and crystal structure of the oxide particles. Various types of nanometric particles in Fe-14Cr-2W-0.3Ti-0.3Y2O3 ferritic steel were identified and quantified by using HR-STEM with EDS (Warsaw University of Technology) and EFTEM with EELS (EPFL-CIME). Principal component analysis (PCA) was applied to the chemical maps obtained by EF-TEM which drastically improved the signal to noise ratio. The problem of sample thickness and related strong signal from Fe(Cr) matrix were overcome by oxide particles extraction on carbon foil. Three types of particles were identified namely Cr-Ti-O, Y-O and Y-Ti-O oxides, as indicated by characteristic EEL edges (Fig. 2.4.1). The EDS and EELS maps indicated a broad size range of the particles from 2 to 300 nm (Fig. 2.4.2) the majority of which (84%) are Y-Ti-O nano-particles. The Cr-Ti-O particles contain Y-Ti-O zones, which were not observed previously. The presence of relatively small amount of Y-O particles indicated a not full dissolution of yttria during mechanical alloying or compaction.

In addition HRTEM (at WUT) was performed to analyse the structure of the oxide particles in the same material. High resolution TEM with EELS (EPFL-CIME) and APT (University of Oxford) analyses were performed to determine composition and crystal structure of complex oxide nanoparticles in ODS ferritic steel after HIP of elemental powders mixture: Fe-14Cr-2W-0.3Ti with 0.3 wt.% Y_2O_3 mechanically alloyed in planetary mill in H_2. The APT of the bulk sample revealed a high number density of fine Y-Ti-O particles with average diameter of only 4 nm and indicated that they are surrounded by Cr-rich zones. The EELS maps of the extracted particles showed that majority of them are composed of Y, Ti and O but there are also large Cr nitrides and Cr-Ti-O oxides. The quantitative analysis of the FFT of HRTEM images oxides and diffraction pattern analysis has led to $YTiO_3$.

Hot Cross-Rolling was performed in collaboration with ENEA at CSM in Rome. The Fe-14Cr-2W-0.3Ti-0.3Y2O3 ODS FS ingots based on elemental powders milled in attritor were subjected to HCR at 850°C preheating temperature, 5% strain per pass and varying reduction of thickness: 50, 65 and 80%. In addition, the Fe-14Cr-2W-0.3Ti-0.3Y2O3 and the Fe-14Cr-2W-0.3Ti-0.5Fe2Y as-HIPped ingots based on prealloyed powders were hot crossed rolled to 65%. The Fe-14Cr-2W-0.3Ti-0.3Y2O3 ODS FS hot cross rolled to 50% and as-HIPed material were investigated to assess the influence of HCR process on the microstructure and mechanical properties of the ODS FS. The XRD analysis indicated similar crystallite size, ca. 250nm like in the case of the as-HIPped steel. The TEM investigation indicates coarsening of the oxide particles and lower dislocation density relative to the as HIPed material. The microhardness tests brought about significant decrease of hardness, from ca. 620 to 330 HV0.1 indentation and tensile tests showed lower Young's modulus and tensile strength strength after HCR, but on the other hand the samples exhibited much higher elongation in two cross-sections compared with the as HIPped steels (Fig. 2.4.3).

The density measurements by Archimedes method showed a decrease of closed porosity from about 2% to 1.2%. Specimens of the two first ingots were sent to ENEA for EBSD analyses. Analysis of the other three other materials will follow.

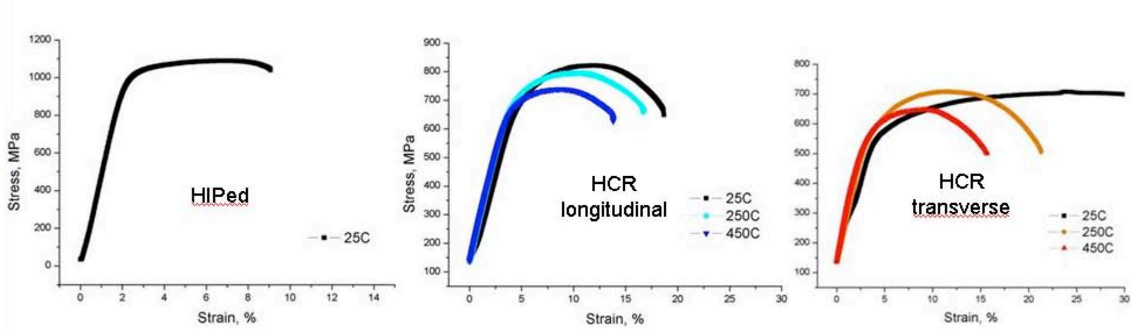

Fig. 2.4.3 *Stress-strain curves of the HIPed and hot-cross rolled samples in longitudinal and transverse directions relative to the rolled plane*

Hot Swaging (uni-axial compression) was applied to six ODS FS samples produced by HIP of elemental powders with either Y_2O_3 or Fe2Y mechanically alloyed in attritor by using Gleeble apparatus at Bergakademie Freiberg (Germany) in order to compare the influence of different thermal-mechanical treatments. Samples were pre-heated to temperature of 850°C or 1150°C and compressed at 850°C to achieve 50 or 75% thickness reduction. Swaging resulted in about 30% reduction of hardness and decrease of porosity to 0.2%. Bend tests on pre-notched samples after swaging will be performed in the future.

WP11-MAT-ODSFS-02-01/Swiss Confederation/PS: Production and characterization of industrial batches of nano-structured ODSFS

Production a 10kg batch of Fe-14Cr-2W-0.3Ti-0.3Y_2O_3 based on the prealloyed powders is an on going task. Several 1 kg batches of prealloyed powder supplied from Alpha Aesar were milled in attritor using BPR of 10:1, speed of 380-750rpm and dynamic hydrogen atmosphere. The canning and HIPping of the powders will be done at ANSTO, Australia. Hot pressing or hot rolling followed by annealing will be subsequently employed.

WP11-MAT-ODSFS-03-01/Swiss Confederation/PS: Irradiation and post-irradiation characterization of produced nano-structured ODSFS

Specimens of Fe-14Cr-2W-0.3Ti-0.3Y2O3 and Fe-14Cr-2W-0.3Ti-0.5Fe2Y were irradiated in 2010 to 5dpa Fe3+ ions 24MeV without He+ ions 2MeV, He:15appm/dpa, to 300°C and 750°C. TEM analysis was performed on FIB lamella extracted from the four samples. It appears that in both materials bubbles, several nanometers in diameter were created which after irradiation at lower temperature are more numerous but finer than at high temperature. The indentation tests indicated about 2% higher hardness in the case of the samples irradiated at 300°C and 6% higher in the case of 750°C.

Further irradiation tests were performed in Saclay in November 2011. The aim is to complete the 2010 irradiations done to 5dpa with a high dose irradiation using Fe3+ ions 24MeV with/without He+ ions 2MeV, ion range 3.5µm, doses: 12dpa, He: 15 appm/dpa and temperatures of 300 and 750°C for the same two materials: ODS Fe-14Cr-2W-0.3Ti-0.3Y2O3 and Fe-14Cr-2W-0.3Ti-0.5Fe2Y and the ones based on the prealloyed powder. Work is in progress to extract FIB lamella for post irradiation analysis by TEM and perform nanoindentation tests to evaluate the mechanical properties.

WP11-MAT-ODSFS-04-01/Swiss Confederation/BS: State of the art of nano-structured ODSFS: Literature review

The literature review was achieved and presented as an invited paper at the ICFRM 15 conference.

Development of tungsten-base materials

WP11-MAT-WWALLOY-02: Structural Materials Development

The W-base materials produced by standard PM methods include mostly pure W and W-Ti, W-V and W-Ta alloys, reinforced or not with either Y_2O_3 or La_2O_3 or TiC particles. For instance, W-(0.3-1.0-2.0)Y, W-(0.3-1.0-2.0)Y_2O_3, and W-(0.3-0.9-1.7)TiC (in weight percent) were produced at the laboratory scale by mechanical alloying in a planetary ball mill, in an argon atmosphere, and HIPping. It was found that all the materials are composed of small grains, with sizes ranging between 20 and 500 nm, and contain a high density (5.4-6.9x10^{22} m^{-3}) of small Y_2O_3 or TiC particles, with sizes between 1 and 50nm. In the case of W-Y materials, all the Y transformed into Y_2O_3 during mechanical alloying, due to the high amount of O (around 1wt.%) present in the milled powders, which is beneficial for reducing the excess O content in the materials. All the materials also contain a residual porosity of a few percents, which is typical of materials compacted by HIPping, and they exhibit high strength and a promising radiation resistance. However, in spite of their small grain sizes, they show no ductility and poor fracture properties at low to moderate temperatures. For instance, the ductile-to-brittle transition temperature of the W-2Y material was found to lie typically in between 1100 and 1200°C.

However, a more prominsing W-2Y_2O_3 material was recently produced by sintering and hot forging in collaboration with the Plansee company (Austria). The relative density of the ingot was found equal to 99.3%. The material appears composed of grains with a mean size around 1µm and also contains Y_2O_3 particles with sizes ranging between 300 and 900nm (Fig. 2.4.4a). The Berkovich hardness was found equal to about 4.9GPa. This value is slighty larger than the typical Vickers microhardness of pure W, of the order of 3.4GPa. Three-point bending tests showed that the material is brittle at 25°C and ductile at 400°C and above, the bending stress at fracture ranging from about 1.3GPa at 25°C down to about 580MPa at 1000°C. This was confirmed by tensile tests that showed that the material is fully ductile in the investigated temperature range of 400-1000°C, the total elongation ranging between 4% and 10% (Figure 2.4.4b).

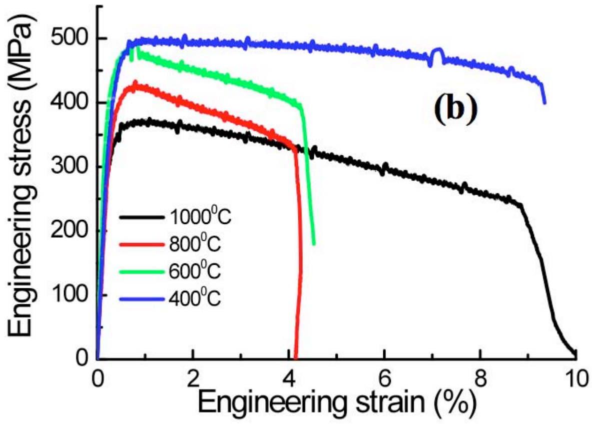

Fig. 2.4.4 *(a) TEM picture of the microstructure of a W-2Y_2O_3 material produced by sintering and hot forging in collaboration with the Plansee company, and (b) tensile stress-strain curves at various temperatures, showing fair ductility.*

WP11-MAT-WWALLOY-04: Irradiation Performance Testing

Specimens of W and W-2Y_2O_3 were irradiated in 2010 to 5dpa Fe^{3+} ions 24MeV without He^+ ions 2MeV with 15appm He/dpa, to 300°C and 750°C. TEM analysis is in progress on FIB lamella extracted from the four samples. Preliminary observations show the presence of helium bubbles and a slight radiation hardening characterized by a Berkovich hardness of about 5.5GPa.

Materials modelling

WP11-MAT-REMEV-02: Radiation damage accumulation and evolution of microstructure

Modelling oriented irradiation experiments in ultra high purity Fe(Cr) model alloys are performed at the French JANNuS platform to understand radiation damage in ferritic steels envisaged for the future fusion reactor. TEM in situ experiments performed at Orsay allow the observation of damage formation during the irradiation in 100 nm thick thin foils. In view of assessing the effect of the proximity of the free surfaces on the ion induced damage, molecular dynamics simulations of highly energetic displacement cascades in thin foils were initiated, in collaboration with the University of Alicante. Energy of the incident ion are chosen to correspond to the experimental conditions for in situ TEM irradiations in JANNuS Orsay, that is to say 300 and 500keV energy for the Fe ion and a foil thickness for the simulation box of 40 and 80nm.

Preliminary results (Fig. 2.4.5) show that number of vacancies exceeds the number of interstitials, as mobile interstitials escape to the free surfaces. Calculations are run on HPC-FF Juropa cluster in Jülich, Germany.

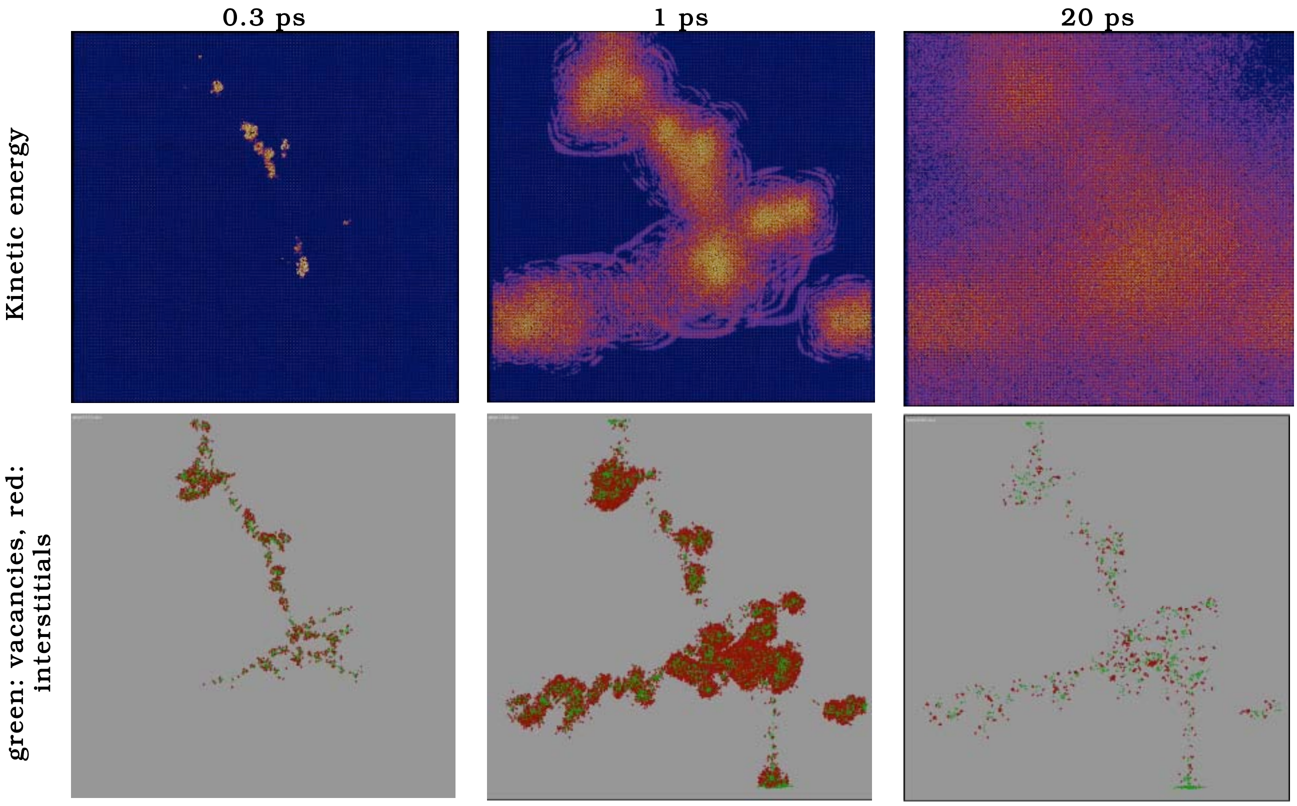

Fig. 2.4.5 *MD simulated time evolution of a 300keV cascade, generated by an Fe atom coming down 22° to the top surface of Fe. Sample is 80x80x80nm^3 with free top and bottom surfaces. It contains 43'904'000 atoms. Top row presents a cross cut of the specimen with a colour code depicting atoms' kinetic energy ; bottom row presents the on-the-fly analysis of generated vacancies and self interstitial atoms. 0.3ps: binary collision phase; 1ps: thermal spike, shock waves; 20ps: cool down.*

WP11-MAT-REMEV-04: Deformation and plasticity

Various empirical interatomic potentials are used in molecular dynamics (MD) simulations to study dislocation-obstacle interactions in pure ferrous materials (Fe, Fe(Cr)) to understand the plasticity of ferritic steels envisaged for the future fusion reactor. The interaction of either an edge or screw dislocation with various obstacles, including voids, He bubbles, secondary phase precipitates (Cr) and dislocation loops, is been extensively studied in the community. These simulations reveal that these particles hinder the dislocation glide to varying degrees, depending on the obstacle type, size and temperature, which leads to material hardening. It appears that the choice of Fe potentials considered for the calculation is critical. We compare here Four Fe interatomic potentials, the so-called Ackland97 (a reference one, 1997), Mendelev03 (2003), Chiesa09 (a follow up of the so-called 'magnetic' potential Dudarev-Derlet 2005, with improved mechanical properties) and Marinica10 (2010). They are compared on the release of an edge dislocation from a 2nm void as a function of temperature. It appears that they all present similar release stress but the much higher from Chiesa09. Comparison at 10K to the obstacle strength derived from elasticity of the continuum indicates that Mendelev03 might be the best potential while Chiesa09 might need revision (Fig. 2.4.6). However, this comparison raises the question of the validity of the elasticity of the continuum at this scale (nm). This work is performed in collaboration with the Max-Planck-Institut für Eisenforschung, Düsseldorf, Germany.

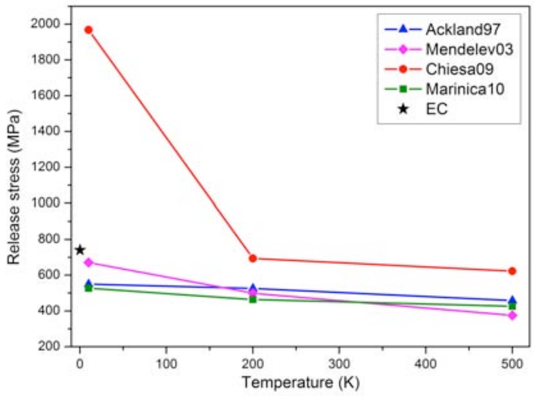

Fig. 2.4.6 *MD simulated release stress of an edge dislocation from a 2nm void as a function of temperature using 4Fe potentials: Ackland97, Mendelev03, Chiesa09 and Marinica10. Star symbol indicates the strength of a 2nm void calculated using elasticity of the continuum (EC)*

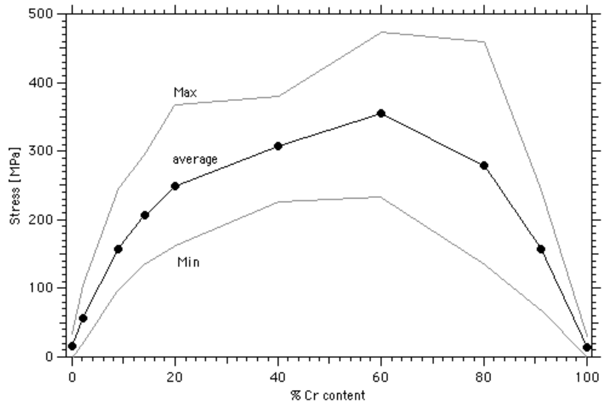

Fig. 2.4.7 *MD simulated shear stress needed to move an edge dislocation in a random solid solution of Fe(Cr) as a function Cr content at 10K. Min and Max bounding lines indicate the scatter in the shear stress due to jerky motion of the dislocation.*

The impact of Cr in Fe on the mobility of a dislocation for contents between 0 and 100at.% was studied. Specimen of Fe containing subtitutional Cr atoms in random locations and one edge dislocation is sheared under a constant strain rate. The stress response is recorded as a function of temperature and Cr content. It appears that the stress to move the edge dislocation increases with Cr content up to about 60at.% , and then decreases (Fig. 2.4.7). This work is performed on HPC-FF Juropa cluster in Jülich, Germany.

In addition, experimental in-situ straining transmission electron microscopy (TEM) coupled to MD simulation was deployed to further analyze the procedure and mechanism of the ½ a_0 <111> screw dipole formation and annihilation in the interaction of an edge dislocation with a nanometric obstacle. These MD studies showed that the obstacle geometry, in our case the void surface curvature, is in direct relation with the critical size and annihilation process of the screw dipole. With increasing void size the critical screw dipole length is increased. Fig. 2.4.8 shows such an experiment performed in our JEOL 2010 operated at 200kV.

Despite the significant difference in the dislocation speed resulting from the applied strain rate in in-situ TEM test, 10^{-7}ms^{-1}, and the MD simulation, 60ms^{-1}, the ½a_0<111> screw dipole is observed in both in-situ staining TEM test and the MD simulations. The length of the dipole that is formed in experimental observations and the MD simulations however differs. Interaction of an edge dislocation with a dislocation loop shows that the dipole size increases with strain rate, hence one may expect much longer <111> screw dipoles in MD simulations than the one of the in-situ straining TEM tests. However, our findings here shows much longer screw dipoles in experiments than in the MD simulation, performed at a local strain rate 8 orders of magnitude higher than in the experiment. This might relate to the type, size and geometry of the obstacle in our experiments that could not be identified during the in-situ straining TEM tests.

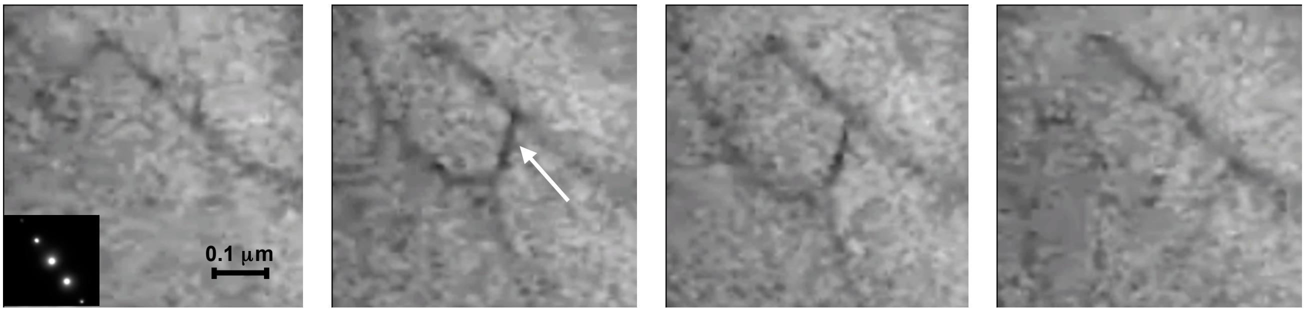

(a) (b) © (d)

Fig. 2.4.8 *Dislocation dipole (shown by arrow) formation and annihilation due to the interaction of a moving dislocation with an immobile dislocation during a TEM in-situ straining at room temperature of UHP Fe, imaging with **g**={011}.*

WP11-MAT-REMEV-05: Experimental validation of models

Modelling oriented irradiation experiments in ultra high purity Fe(Cr) model alloys are performed at the French JANNuS platform to understand radiation damage in ferritic steels envisaged for the future fusion reactor. There is the TEM in situ experiment at Orsay allowing the observation of damage formation during the irradiation in thin foils (100 nm thick) while at Saclay there is ion irradiation allowing irradiation of bulk specimens (few µm thick). In this study we compare thin foil and bulk irradiation, a study that will be used as benchmark for modelling. Ultra high purity iron was irradiated with Fe ions without and in the presence of He. Specimens were irradiated at room temperature to the maximal final dose of 0.8 dpa and ~900 appm He content as thin foil specimens (Fig. 2.4.9) and bulk specimens (Fig. 2.4.10).

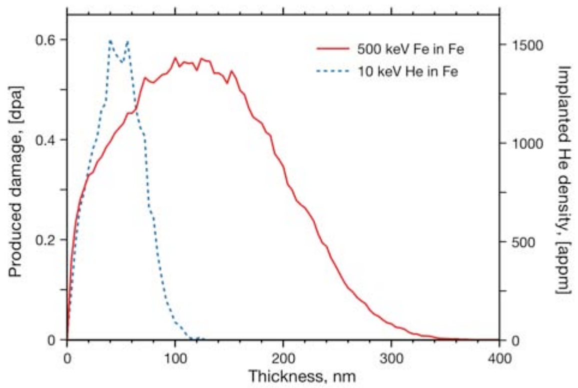

Fig. 2.4.9 *Irradiation/implantation profiles of 500keV Fe^{+} and 10keV He^{+} ions in thin foil UHP Fe*

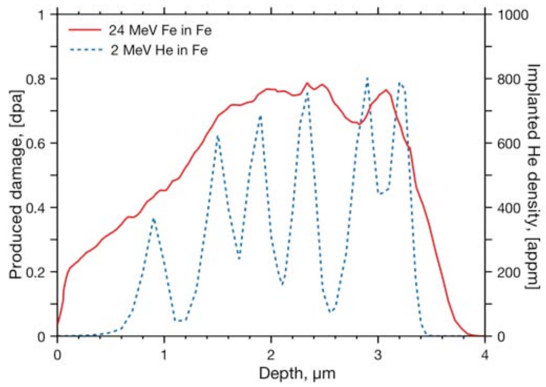

Fig. 2.4.10 *Irradiation/implantation profiles of 24MeV Fe and 2MeV He ions in bulk UHP Fe with a compound degrader of 0µm +0.8µm + 2µm + 3µm + 3.8µm + 5µm Al foils for homogeneization*

In order to observe in TEM the radiation-induced microstructure obtained in bulk specimens, TEM lamellas were extracted from bulk samples using focused ion beam (FIB) at the EML at PSI. Efforts have been devoted to improve preparation of TEM lamella in order to remove FIB (few keV Ga ions) induced damage at the surfaces that interferes in the TEM image with the defects produced during irradiation/implantation. The flash electropolishing method was successfully developed; it allows dissolving in electrolyte the thin surface layers of the lamella. It is found that in irradiated thin foils the a_0 <100> type loops are in absolute majority after irradiation with single beam, while in the presence of He it is the ½ a_0 <111> type loops that prevail. In single beam irradiated bulk samples most of the loops are of ½ a_0 <111> type. In both bulk and thin foils the density of defects visible in TEM (Fig. 2.4.11a) is considerably higher when He is implanted (Fig. 2.4.11b), indicating that He stabilizes small ½ a_0 <111> dislocation loops, as was predicted by MD simulations.

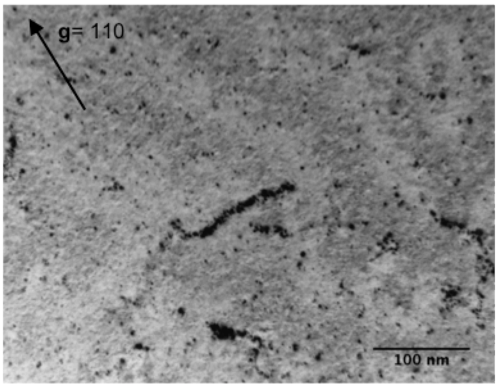

a)

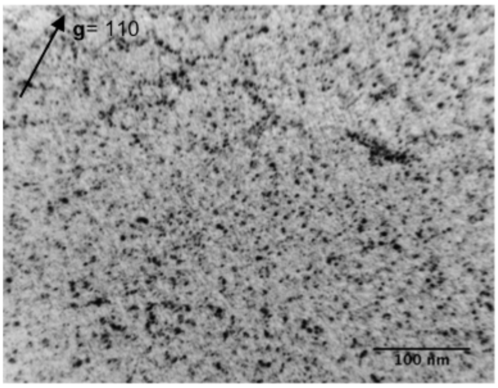

b)

*Fig. 2.4.11 a) Inverted contrast **g(4g)** WBDF image of UHP Fe thin foil irradiated whith 500 keV Fe^+ ions to 0.5 dpa at RT. b) Inverted contrast **g(4g)** WBDF image of UHP Fe thin foil irradiated at RT whith 500 keV Fe^+ and 10 keV He^+ ions to 0.5 dpa and 1000 appm respectively*

Goal oriented training programme

WP10-GOT-FabriCharMe

The kick-off meeting on these activities took place in February 2011 at KIT. The first monitoring meeting took place the 14th and 15th of November 2011 at KIT where the activities between the different partners of the project will be coordinated, in particular, the dates of the working visit at CRPP. The visit is expected in 2012.

Design assessment studies for DEMO

WP11-DAS-MAT-M03-01

The task agreement was signed the 10th of October 2011. The review of the mechanical and physical properties of the ferritic/martensitic and on the ODS ferritic steels has been initiated. Reports and publications have been gathered so far. No delay on this task is expected. The final report will be submitted for the 15th of December 2011.

2.4.2 Collaborative activites

Participation in FEMaS-CA (Fusion Energy Materials Science – Coordination Action)

Participation in the work package 1 (WP1) entitled "Radiation damage: benchmarking experiments"

The aim of our activity in this work package is to understand with simulations the formation and growth of radiation damage in UHP Fe(Cr) induced by TEM in situ dual beam irradiation performed at JANNuS Orsay, F. We perform simulation of those experiments using molecular dynamics simulations (WP1 Activity 7). The aim is the simulation by molecular dynamics (MD) of the displacement cascade in electron transparent thin foil of pure Fe (40~80 nm thick) initiated by a 300keV Fe ion. One collaborator went 2 weeks to Univ. of Alicante for training on the MD calculations and for running preliminary simulations.

These preliminary calculations show the strong impact of the free surfaces on the TEM foil on the displacement cascade. (1) The cascade cooling is slower and (2) there are craters that form at the surfaces where subcascades develop. Calculations are in progress to study the impact of pka energy (100-500keV) and temperature (10-300K) and of the long term evolution of the radiation induced damage after the cascade cooling, probably using object kinetic Monte Carlo method.

Participation in the work package 4 (WP4) entitled "TEM-based methods"

The aim of CRPP activity within WP4 was twofold: 1) perform electron microscopy on fusion relevant materials; we aimed at characterizing ODS ferritic steels and ODS tungsten and tungsten alloys and 2) coordinate WP4.

The aim of this work package was to build a network of TEM competences of interest to fusion material development in order to expand our knowledge on irradiation induced effects on the microstructure, and to improve TEM techniques and related modelling tools for that purpose, in synergy with modelling of related microstructural phenomena in fusion relevant materials.

1. The network consists in transmission electron microscopy facilities and competences of interest to fusion material development.
2. In this work package we collected data using TEM observations on irradiated fusion relevant materials and to synergize TEM experimental observations to modelling of the related micro-structural phenomena.

3. We aimed at developing TEM techniques, including sample preparation techniques, and related modelling tools in collaboration with other diffraction techniques (X-ray and neutron diffraction) to increase spatial and time resolution on irradiation induced defects and related mechanisms.

One collaborator went to Orsay for a group discussion with CEA and Orsay colleagues on the irradiations pursued at JANNuS for materials for fusion. In addition he participated on site to the GUMP meeting ('Groupe des Utilisateurs de Microscopie Philips' http://www.gump-microscopie.fr/ spip.php?article23&calendrier_mois= 03&calendrier_annee=2011) 24-26.12.2010. This GUMP meeting focused on irradiation induced damage. Collaboration with CEA Saclay and CNRS Orsay was strengthened at that occasion.

Two collaborators spent independently time at WUT in Poland with Dr. Plocinski to use the Cs corrected STEM for the investigation of our ODS ferritic model alloy (Fe-14Cr-2W-0.3Y2O3-0.3Ti). We performed detailed analyses of the chemical composition of the oxides present in the ODS ferritic thank to the very fine electron probe achievable with this STEM (0.8 Å). It appears that most of the fine oxides present in this material are made of $YTiO_3$, which has a distorted perovskite structure, in contrast to what other groups around the world have found, that is to say the pyrochlore $Y_2Ti_2O_7$. These results open new investigation routes that are now being pursued.

In this project we have obtained useful results on the chemistry and microstructure of ODS ferritic materials (ODS Fe-14Cr-2W-0.3Y2O3-0.3Ti) and ODS tunsgten materials (W-Y, W-Y2O3 and W-TiC). The benefits of these collaborations, between and CRPP, WUT and CIME, are that we have at our disposal a reliable set of tools, which we put together (such as the Cs corrected STEM) or developed (such as the EFTEM coupled to PCA), that should now be used routinely to establish a statistically significant database on the microstructure of the ODS materials. As WP4 coordinator we have coordinated travels among WP4 partners and promoted advanced electron microscopy for fusion materials, inside and outside of the fusion community.

Participation in the work package 5 (WP5) entitled “Advances mechanical testing and characterization methods”

These activities were undertaken to characterize the strain-rate sensitivity of the tempered martensitic steel Eurofer97 from static to highly dynamic regimes over a range of temperature. The testing and modelling was done in collaboration between SUPSI and EPFL-CRPP. SUPSI performed the tensile tests on the specimens provided by CRPP. The constitutive behaviour of Eurofer97 was analyzed within the framework of a dislocations dynamics model, previously developed at CRPP for static deformation. The model was extended to take into account the strain-rate effects. One collaborator spent two days to SUPSI to discuss the results and to draft a paper. Indeed, results have been elaborated in a regular paper, which has been accepted for publication in the Journal of Nuclear Materials.

The benefits of this collaboration reside in the fact that we have at our disposal a reliable and well documented database on the strain-rate sensitivity of Eurofer97 that is essential to run finite element simulations for specimen configuration where the loading rate is an issue. Typically fracture specimens develop a large strain gradient around their stress concentrators so that neglecting the strain-rate effects is not a well justified assumption. There are many opportunities to pursue the collaboration between CRPP and SUPSI in the field of plasticity and fracture mechanics of structural materials for fusion reactor materials, for which the loading rate in the dynamic regime has not been sufficiently investigated in the past.

2.4.3 EFDA Technology Tasks

TW4-TVM-CUSSPIT : Testing of irradiated CuCrZr/SS joints produced under different blanket manufacturing conditions

Three-point bending small notched bars of two CuCrZr alloys were deformed before and after irradiation. The specimens were irradiated in the BR2 reactor at Mol/Belgium at 150°C and to three different doses: 0.001, 0.01 and 0.1dpa. Theywere tested at room temperature and at 150°C. The load-deflection curves of all specimens, unirradiated and irradiated at all condition, show a great amount of plasticity. There was no evidence of crack initiation around the notch but only the loading induced a significant notch blunting. A significant irradiation-hardening, defined as the increase of the macroscopic yield load, was measured. On one alloy, the dose dependence suggested that irradiation hardening has reached saturation at 0.1dpa. The final report was submitted.

TW6-TTMS-001-D4

The long delay of this task is related to the availability of the hotcell at PSI. An irradiation report of STIP-IV irradiation produced by PSI, showing two severe temperature excursions in the spallation target that affected the specimens, triggered a discussion with F4E on the way how to finalize this task.

2.4.4 Broader approach activities

International Fusion Materials Irradiation Facility – Engineering Validation Engineering Design Activities (IFMIF-EVEDA): Design and manufacturing of a test module for in-situ creep-fatigue tests to be performed in the IFMIF facility

A test module for performing in-situ creep fatigue tests (Called Creep Fatigue Test Module, CFTM) under intense neutron irradiation, to be implemented in the medium flux module of IFMIF, has been designed (Fig. 2.4.12) and manufactured (Fig. 2.4.13). The module consists of three independent actuators. The actuators deliver the force for push-pull testing of the specimens between +12.5kN and -12.5kN. The force ranges for push and pull are selectable. Measurement systems for elongation on the specimens, displacements on the pistons and for the forces are components of the test rig. The motor control system allows for different testing modes. It is possible to push and pull the specimens under force control, under elongation control or even under force control without load cell. The force mode without load cell is a safety option in case of a load cell will be damaged by the neutron irradiation. The system switched automatically in this mode if a load cell is damaged: the control system of the servo motors used the data for voltage and current which are needed to reach the force before the load cell was damaged.

For the measurement systems, attention was paid that the components are irradiation resistant, or that they are shield against the neutrons.

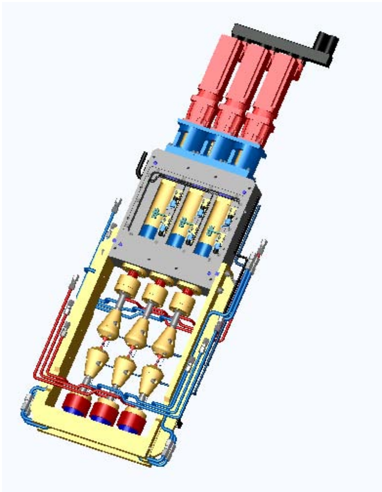

Fig. 2.4.12 Design of the CFTM

Fig. 2.4.13 Manufactured CFTM

In order to make the test as IFMIF-relevant as possible, the entire equipment (Fig. 2.4.14) was designed and manufactured, which consists of: 1) a vacuum vessel , 2) a vacuum control system regulated the vacuum between 95mbar and 100mbar, 3) an eddy current heating system simulated the temperature up to 600°C at the specimens, and 4) a cooling system regulated the free selectable temperature at the specimens between 100°C and 600°C.

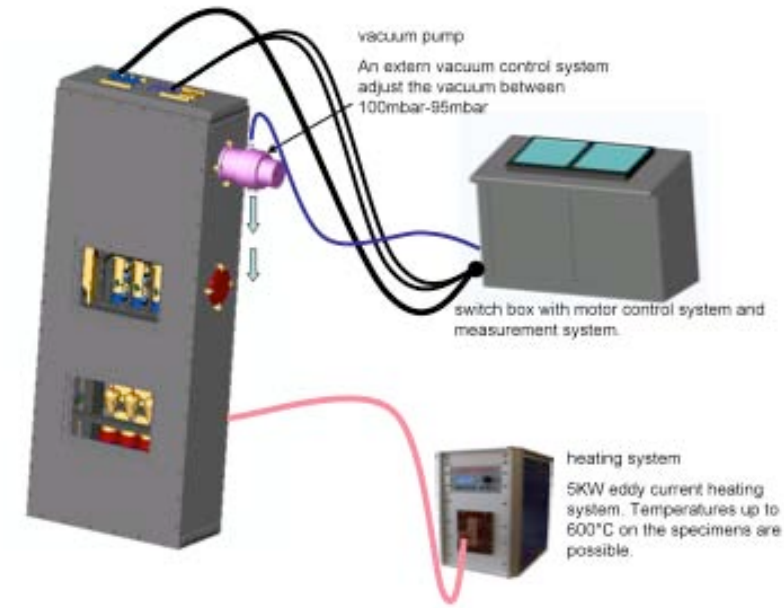

Fig. 2.4.14 Schematic of the equipment of the CFTM

The aim of the first tests without irradiation was to find out, if some parts of the CFTM suffer from abrasion affecting the functionality between the measurement system and the motor control system. The results showed that abrasion on the different mechanical parts does not exist. The data output (Fig. 2.4.15) and the saving procedure of the data were also an issue to address during the testing phase.

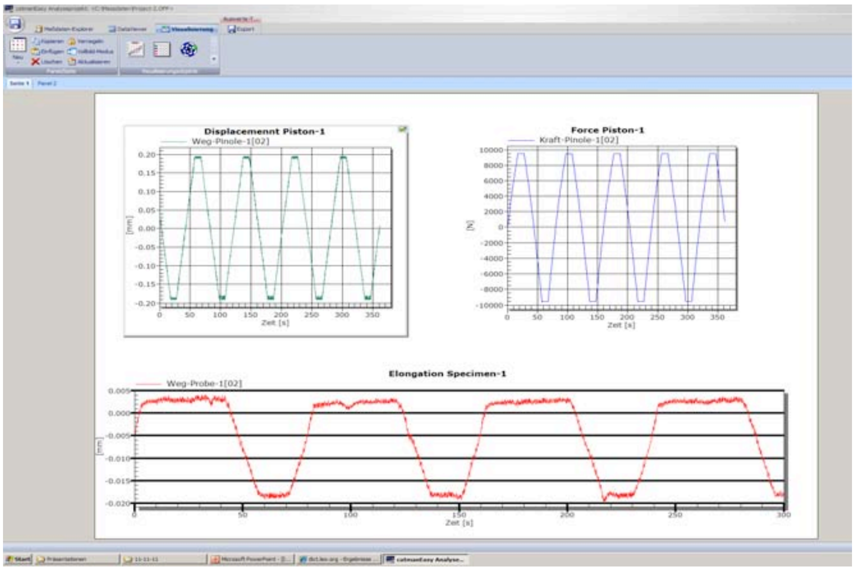

Fig. 2.4.15 *Data output*

Some technical modifications and software updates were found necessary from the result of the first test series. Thus, a new design of the specimen holder and an optimisation of the saving procedure of the measurement data were the most important modifications. A new kind of measurement system for measure the elongation of the specimens was reviewed. It has been suggested that a pneumatic measurement system should be better that a mechanical system, because no electronic measurement amplifier inside of the test cell is necessary.

IFERC: Contribution to the definition of irradiation matrices for IFMIF by means of development of new methods for testing and analyzing sub-sized specimens

Fracture properties of irradiated and cold-deformed Eurofer97

The fracture properties degradation of cold-forged plates of the reduced activation tempered martensitic steel Eurofer97 was determined and compared to the fracture properties behavior following neutron irradiation on the same steel. The cold-forging was done to harden the plate by about 200MPa at the level of the yield stress while reducing the subsequent work-hardening. In order to do so, a reduction of 10% of the plate thickness at room temperature was found to be sufficient. The level of hardening in the cold-forged plate was quantified by Vickers micro-hardness measurements by applying a load of 0.1kg. The Vickers data are given in Table 2.4.1, where results of the hardened Eurofer97 by neutron irradiation are also presented. The irradiation conditions were: irradiation temperature T_{irr}=150°C and irradiation dose =0.33dpa (displacement per atom). We emphasize that the cold-forged and irradiated Eurofer97 have practically the same hardness value while the hardening has been obtained through two different mechanisms, namely cold-forging and neutron irradiation.

	Eurofer97 as received	Eurofer97 cold-forged	Eurofer97 irradiated T_{irr} = 150 °C, 0.33 dpa
Vickers hardness $HV_{0.1}$	220	242	241

Table 2.4.1 *Vickers hardness on Eurofer97 steel in three different conditions.*

We compare hereafter the degradation of the fracture between the cold-forged and irradiated materials. A series of 48 sub-sized compact tension C(T) specimens were cut out of the cold-forged plates. The C(T) specimens were tested according to the recommendations of the ASTM-E1921 standard. The testing was performed in the ductile to brittle transition region, between the so-called lower and upper shelves region characterizing the brittle and ductile fracture modes respectively. The reference temperature T_0, defining the ductile to brittle transition temperature on an absolute temperature scale, is usually taken as that where the median fracture toughness, $K_{Jc(med)}$, is 100MPa $m^{1/2}$. The reference temperature T_0 was then determined for the unirradiated, cold-forged and irradiated materials. In Figures 2.4.16 to 2.4.18, we show the corresponding three data sets with the median toughness temperature curve.

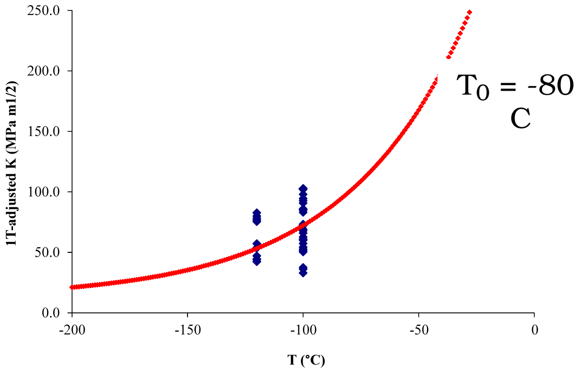

Fig. 2.4.16 *As-received Eurofer97, T_0 determination from 0.18T C(T) data: T_0=-80°C.*

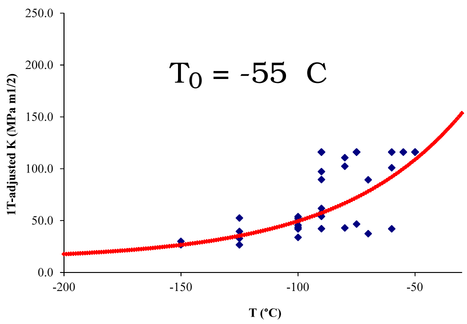

Fig. 2.4.17 *Cold-forged Eurofer97, T_0 determination from 0.18T C(T) data:* T_0 = – 55°C.

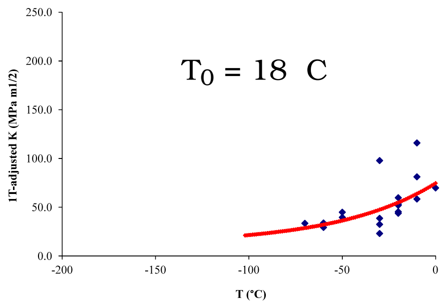

Fig. 2.4.18 *Irradiated Eurofer97, T_0 determination from 0.18T C(T) data:* T_0 = 18°C.

As expected, both the cold-forged and irradiated Eurofer97 are more brittle than the as-received Eurofer97, with higher T_0. However, it has been suggested that the temperature shift of the transition temperature $T_0(\Delta T_0)$ scales with the increase of the Vickers hardness ($\Delta T_0=\alpha\Delta HV$). However, our new results indicate that Vickers hardness increase only is not sufficient to predict the shift of T_0. Indeed we practically measure the same $\Delta HV_{0.1}$ for the cold-forged and irradiated Eurofer97 while a large difference in the corresponding ΔT_0 was evidenced: ΔT_0=98°C for the irradiated Eurofer97 and ΔT_0=25°C for the cold-forged. The increase of the material strength, induced by either cold-forging or by irradiation, results then from two different mechanisms, which are the accumulation of dislocations or the accumulation of small irradiation-induced defects respectively. Even if these two strengthening mechanisms produced the same increase in Vickers hardness, they seem to play a significant role in the micro-mechanisms controlling the initiation and propagation of cracks in the microstructure. Work is now in progress, in particular at the level of modeling, to gain insight into this critical issue.

Small specimen test technique activities

Modelling of load-displacement curve of tensile tests of irradiated Eurofer97

Significant loss of the uniform tensile elongation after irradiation at 150°C (see Fig. 2.4.19) did not allow direct evaluation of true stress true strain curve beyond ≈0.5% plastic strain. Finite element (FE) modeling using ABAQUS 6.10-3 code was performed in order to reconstruct the load-displacement curve of Eurofer97 irradiated at 150°C to 0.33dpa by fitting the constitutive behavior, represented by the true stress-strain curve σ(ε). As an input to the ABAQUS code the Young's modulus (E) and Poisson's ratio (ν) are required as well as the true stress - plastic strain after the yield. The required σ(ε) curve of irradiated material was obtained by iteratively modifying trial σ(ε) input function until the model output reproduced the experimental engineering stress-strain s(e) curve (or in other words the load-displacement curve). Figure 2.4.20 represents the three dimensional (3D) elastic-plastic FE model of small flat tensile specimen used in this study. The specimen instance was meshed with 26796 linear hexahedral elements of the type 8-node linear brick, reduced integration. The contact between the specimen and two pins simulated as analytical rigid bodies was assumed frictionless.

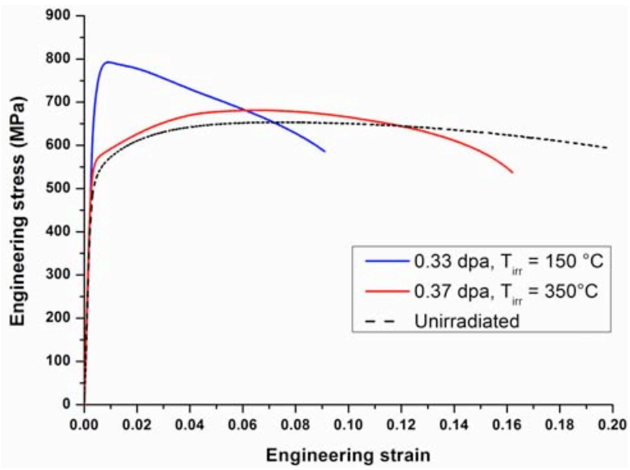

Fig. 2.4.19 *Tensile properties of Eurofer97 measured in the unirradiated and irradiated conditions.*

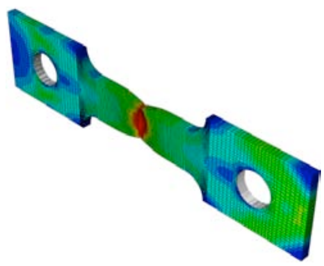

Fig. 2.4.20 *3D finite element model of the flat tensile specimen.*

The trial ( ) input function was modified until the model output reproduced the experimental s(e) curve. In Fig. 2.4.21, we present the experimental engineering stress-strain curve, the fitted true stress-strain curve used to reconstruct the experimental engineering and the calculated engineering stress-strain curve. A very good agreement between the experimental and calculated curves was obtained.

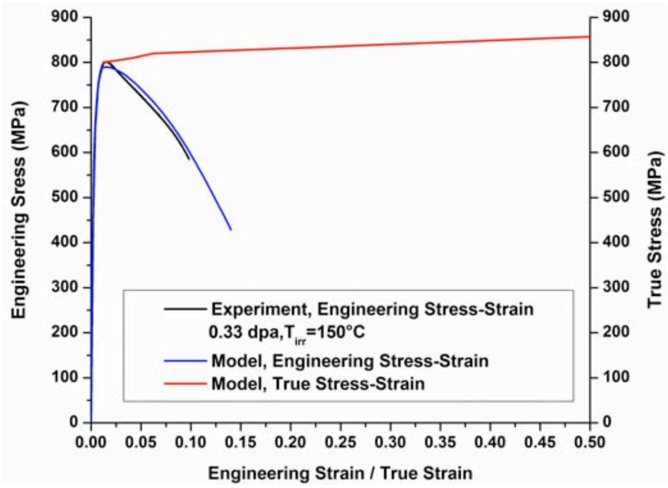

Fig. 2.4.21 *Engineering stress-strain curves (experiment and model) and fitted true stress-strain curve (model input), T_{irr}=150°C.*

Modeling of Vickers indentations

Vickers microhardness test and finite element simulations were undertaken to determine the real contact area of the indenter with the specimen as a function of the indenter penetration depth for tempered martensitic steels. Eurofer97 steel has been selected as the reference material to validate the finite element model. The Vickers indentations were carried out up to a load of 10N with a fully instrumented G200 MTS nanoindenter and the experiments were supplemented with 3D finite element simulations. Two finite element models were built: one with a four-sided pyramid having the Vickers tip geometry and one with an axisymmetric rigid cone tip. The axisymmetric indenter tip with a vertical angle ϕ=70.3° was designed to yield the projected area to depth ratio as that of the Vickers tip. Among the output of the calculations, the load-penetration depth, the profile of the specimen surface and the indenter-specimen contact height were required. Taking advantage of the Vickers tip geometry, only a quarter of the specimen-tip assembly was considered as shown in Fig. 2.4.22. The quarter specimen has the following dimensions: 400·400·400μm (width · length · height). It was meshed with 140000 elements of the type 8-node linear brick, reduced integration. The size of the elements is biased to have a very fine mesh below the indenter tip to catch the strong stress/strain gradient occurring under the tip. The tip itself was meshed with 9638 elements of the type 4-node tetrahedron. The contact between the tip and the specimen was assumed frictionless. The diamond tip deforms elastically and the following values of the Young's modulus and Poisson's ratio were used: E=1141GPa and ν=0.07.

The axisymmetric model was actually developed to save computing time while remaining representative of the Vickers model, at least qualitatively. It is the reason for which the projected area to depth ratio is identical to that of the Vickers. The geometry of the model is shown in Fig. 2.4.23. In this case, the cone is considered as a fully rigid body. The dimensions of the specimens are also 400·400·400μm (width · length · height). The mesh is refined under the tip. For this model, only 10000 elements of the type 4-node axisymmetric quadrilateral, reduced integration were employed.

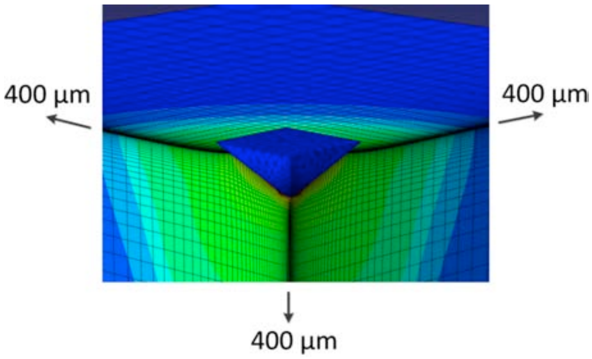

Fig. 2.4.22 *Sketch of the 3D Vickers tip – specimen model.*

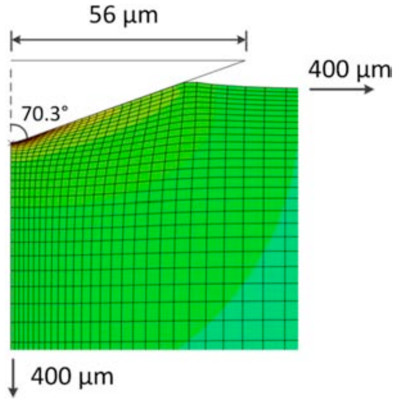

Fig. 2.4.23 *Sketch of the axisymmetric cone tip – specimen model.*

The 3D finite element simulations were shown to reproduce very well the experimental load-displacement curve (Fig. 2.4.24) and axisymmetric simulations with a conical indenter having the same area function as the Vickers were found to be very close to the Vickers 3D simulations in terms of the load-displacement curve.

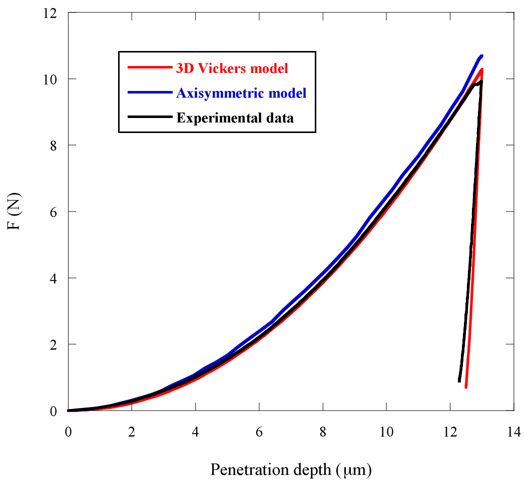

Fig. 2.4.24 *Comparison between the Vickers indentation experimental curve, the 3D and the axisymmetric simulation.*

The specimen surface profile analysis during the simulation shows that a pile-up of material exists in the contact area between the tip and the specimen. In addition, this pile-up forms from the very beginning of the deformation. We emphasize here that such a behavior deviates significantly from the method described by Oliver and Pharr where the contact area is deduced from a model that assumes material sink-in only instead of a pile-up characterizing the tip-specimen contact region and which is used as a default hardness calculation algorithm for the most of instrumented nanoindenters at the moment. In the case, the tip-specimen contact height is evidently greater than the penetration depth, while the opposite is true for the sink-in. To determine the hardness correctly, one has to establish a correlation between the contact height (h_c) and the penetration depth (h_p). Plotting the h_c against h_p for all the simulations done shows that a simple linear relationship holds between these last two quantities. The correlation is shown in Fig. 2.3.25 for the 3D Vickers model. In this Figure, the real contact height dependence on penetration depth obtained from simulations is compared to the contact height dependence on penetration depth calculated according to Oliver-Pharr model using experimental data showing the linear increase of the difference between both.

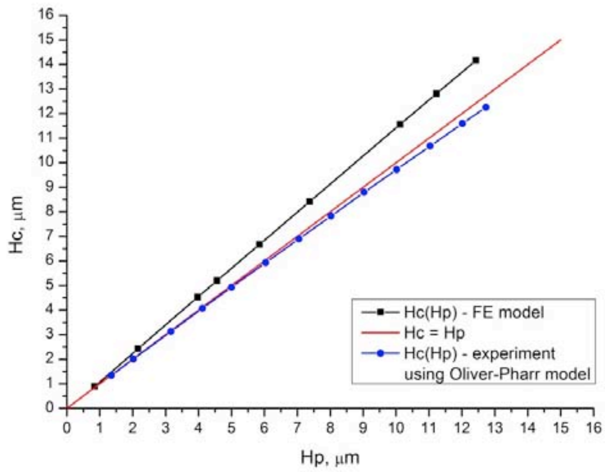

Fig. 2.4.25 *Contact height h_c versus penetration depth h_p for the 3D Vickers model.*

From Fig. 2.4.25 it can be concluded that a correct determination of hardness on the tempered martensitic steel requires either to experimentally measure the height of the pile-up after test to get a reasonable estimate of the contact area or to model it by finite element simulations.

2.4.5 Supporting research

Development of a material resistant to high-pressure aluminium and magnesium die casting*

This project realized in collaboration with CIME EPFL concerns the corrosion of shot sleeves by liquid Al in the die cast of Al. ALLPER, the Swiss company carrying the project, was acquired by CASTOOL, Canada. P. Robbins from CASTOOL gave us confidence that Castool will pursue this project in Switzerland with ALLPER.

The construction of the system for the cyclic diving of the 50mm long, 10mm in diameter specimen in the LMIF is still in progress. This system should mimic the cycle suffered by the shot sleeve in the die casting operation, with a cycle time of 90s (30s in contact, 60s off contact to liquid Al). Evaluation by numerical simulation was performed. It shows that it will be difficult to cool down the specimen when extracted from the liquid aluminium bath at 700°C down to 200°C. Tests were then made manually, consisting of diving an Fe specimen, equipped with a thermocouple, into Al at 700°C. All the installation is in a glove box with an Ar protective atmosphere. The sample reaches after 30s 640-650°C and after retraction it doesn't go lower than 540-570°C after 60s.

The study, conducted along 2 axes (one fundamental, one applied) progresses as planned, on pure Fe (ARMCO) and steels, 1.2343, 1.2344 and C31. Recently, focus was put on 1.2344 (a ferritic steel) by CASTOOL. Standard tests are performed in liquid Al at 700°C for 15, 30, 60 and 90 minutes. Tests performed with industrial Al

* Work not belonging to the EURATOM Association workprogramme.

alloys 'Silafont' and '226' indicated little difference between them in terms of corrosion of pure Fe, 1.2343 and C31. On the metallurgy of the corrosion products, we revealed a new phase, AlFe, which was never observed. This was revealed by TEM performed on lamellas extracted in the 200μm thick intermetallic layer that forms at the interface between liquid Al and the Fe. Lamellas are extracted by FIB at the EML at PSI. The resistance to liquid Al of coatings based on electroless plating of Ni appears to be weak. Other solutions for resistant coatings are sought after in Swiss companies.

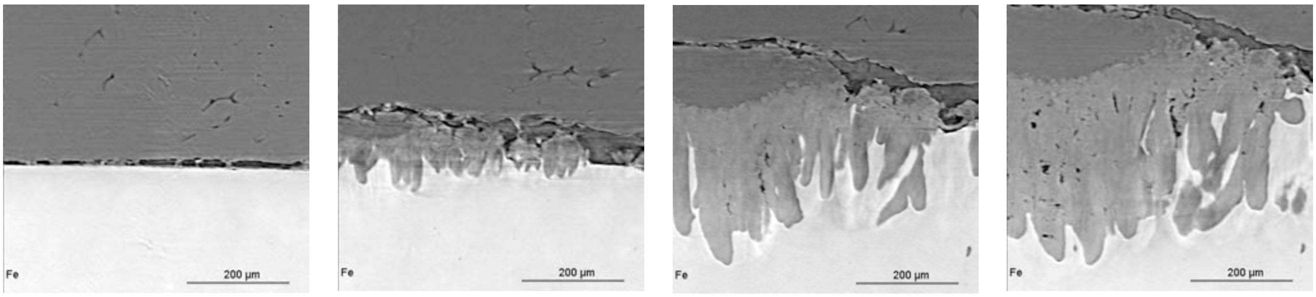

8 min | 24 min | 60 min | 110 min

Fig. 2.4.26 *Time evolution of the intermetallic formation between liquid Al (top) at 700°C and pure Fe (bottom). In situ X-ray 3D tomography performed at ESRF in Grenoble.*

In addition, in situ X-ray 3D tomography was performed at ESRF in Grenoble, to see the time evolution of the intermetallic layer formation in a miniaturized composite specimen of Fe/Al, 3mm in diameter, heated to 700°C. Figure 2.4.26 shows the suprising time sequence realized. Data analysis is in progress, but it shows already clearly the sequence of intermetallic tongue growth in the Fe, the volume expansion due to intermetallic formation and their dissolution in the liquid Al.

The quest for radiation resistant materials
Swiss National Fund – Marie Heim-Vögtlin Programme

Molecular dynamics (MD) simulations are performed in order to understand the reason for the scarcity of stacking fault tetrahedra in austenitic stainless steels following irradiation, despite the extremely favourable conditions for their formation. A literature review on the topic is in progress. For the calculations, a model Ni(Al) system was considered because of the lack of available adequate interatomic potentials for austenitic steels. The MD simulations are performed using the MOLDY-CRPP code. The influence of the Al content, temperature and SFT size on the stability of SFTs is studied. The materials used for simulations are: Ni, Ni-5Al and Ni-10Al. The size of the stacking fault tetrahedra ranges from 6 to 66 vacancies and the temperature from 10 to 800K. Three interatomic potentials – Foiles & Daw, Farkas-1 and Farkas-2 – used to describe the Ni-Ni, Ni-Al, Al-Al interactions have been evaluated. In the case of pure Ni, the platelet of vacancies collapses into an SFT only at sizes greater than 21 vacancies, at all temperatures and for the Farkas-1 potentials, while for Foiles & Daw only at the largest size. Very recently, two independent research groups have released interatomic potential sets reproducing fcc Fe-Ni, a model alloy for austenitic steels (K. Vörtler, N. Juslin, G. Bonny, L. Malerba, K. Nordlund, J. Phys.: Condens. Matter. 23 (2011) 355007, D. Terenthyev, D.J. Bacon, Yu. N. Osetsky, ICFRM-15, 2011). They will be implemented in MOLDY-CRPP. The study is on-going.

2.5 Superconductivity

As in 2010, the bulk of the activities of the Superconductivity section in 2011 are shared between SULTAN (test of ITER conductors) and EDIPO (preparation of the test facility). The test of ITER conductor receives high attention from the fusion community. The absolute priority requested by the ITER Organization (IO) for the conductor tests is hard to be questioned.

Since the restart in August 2010 of the SULTAN test operation after a double failure of the compressor of the cryo-plant, there was no interruption of operation till the end of August 2011, with a record number of test campaigns. As we run out of samples by the end of August, the EDIPO installation work could be moved in the SULTAN hall. However, the work on EDIPO had to be stopped after few weeks in order to resume the ITER conductor preparation and tests.

The coil assembly of EDIPO was received at CRPP on May 13th 2011. The installation work, first in the workshop and later in the SULTAN hall, proceeded slowly due the priority allocation of the technical personnel to the preparation and test of the ITER conductor samples

2.5.1 High Temperature Superconductors for DEMO (Work program 4.4)

CRPP (R. Wesche) contributed to the preparation of the EFDA PPPT Meeting on May 10-11, 2011 in Garching. At this meeting a workgroup was established to assess the status and prospects of high temperature superconducting magnets and their potential use in future fusion reactors. As a member of this working group R. Wesche contributed to the definition of the road map for the development of HTS for use in fusion magnets. The outcome of this work was used by EFDA as an input to define the sub-tasks of the WP11-DAS-HTS Programme, which was allocated in August 2011 among various Associations, coordinated by KIT. The final report is scheduled in February 2012.

The CRPP share of the WP11-DAS-HTS sub-task is about “Assessment of electrical stabilization, quench protection and characterization of samples”. This activity has already started within the former HTS4Fusion task to study the quench behaviour of RE-123 cables using the CryosoftTM code THEA. The first results confirmed that the very slow quench propagation is in fact a critical issue. Within the WP11-DAS-HTS task the effect of a varying copper cross-section in the cable has been studied. In the calculations, the thermal behaviour of HTS cables has been studied with and without direct thermal contact to the helium gas. In principle, the hot spot temperature can be reduced by an enlarged copper cross-section. Preliminary results suggest that a significant reduction of the hot spot temperature would require a copper cross-section that is 50 times larger than that of standard RE-123 tapes. Without helium the hot spot temperature increases within 0.6s from 50K to 100K even for a 50 times enlarged copper cross-section. On the other hand, stability was found to be not a critical issue. Using the critical current data of RE-123 coated conductors as a function of the temperature, field and field angle possible operation conditions have been defined (operation temperature, field, and engineering critical current density in the RE-123 tapes). As soon as the first high current HTS cables will be successfully manufactured, the test as short straight samples in SULTAN would be highly desirable. To be able to test HTS cables at elevated temperatures a large thermal resistance between the HTS under test and the superconducting transformer to be operated at 4.5K would be required. This thermal resistance is in principle the conduction-cooled HTS part of an HTS current lead. The supply of helium gas of up to 50K inlet temperature is a further aspect, which needs to be addressed.

2.5.2 Review Concepts for Nb_3Sn Conductor Construction (DEMO studies WP11-DAS-PLS-P10)

At the EFDA PPPT Meeting on May 10-11, 2011, it was recognized that the cable-in-conduit conductors used by ITER are not suitable for an inductively driven DEMO device, with a number of load cycles in the range of several hundred thousands. In order to prepare a roadmap toward future high current superconductors for DEMO, a sub-task, named “Review Concepts for Nb_3Sn Conductor Construction” has been included in the WP11-DAS.

In August 2011, CRPP has received 0.2ppy with preferential support for WP11-DAS-PLS-P10: Review concepts for Nb3Sn conductor construction. The final report is due in February 2012.

In the scope of this sub-task, the potential advantages of various conductor designs based on Nb_3Sn are assessed. Eventually, two options, both different from the ITER conductors, will be proposed. Based on the R&D experience of the subject (see for examples the Annual Report 2006 and 2007), CRPP recommends the react&wind technology for an effective use of the superconductor and a good performance, stable over hundred thousand cycles. A roadmap for the next four years of DEMO activities will be drafted. To contain the cost in the 2012-2013 period, the hardware expenditure for prototype and testing will be postponed after 2013.

2.5.3 The Preparation of EDIPO Test Facility (EFDA Task 5.1a)

The major milestone of the EDFAC task in 2011 was the delivery of the EDIPO coil assembly to CRPP on May 13th 2011. The coil assembly, in horizontal orientation, has been transported to the workshop area, where the pre-installation work was carried out before moving to the SULTAN hall (coil termination support, soldering, joining and insulating of the series connection of the coils, welding of bushing insulators and cooling lines manifolds, insulation of cooling lines, installation of instrumentation, etc.).

On September 8th, the instrumented coil assembly was put in vertical with the help of a mobile crane and transported to the SULTAN hall. On October 13th the coil assembly was first lowered into the vacuum vessel and on November 2nd the main flange of the vacuum vessel was first placed into position for a trial fitting of the hydraulic and electrical connections, see Fig. 2.5.1.

At a meeting with F4E and IO on April 6th in Barcelona, the schedule for installation of EDIPO was discussed, including the conflicts between EDIPO installation and ITER conductor test in SULTAN. On a meeting on October 26th in Villigen the agreements from April 6th were modified to give highest priority to the ITER conductors preparation and test. Because of the shifted allocation of the technical manpower, the EDIPO installation work cannot be completed in 2011. A firm schedule for the cooldown and commissioning of the EDIPO facility is not yet agreed between IO, CRPP and F4E.

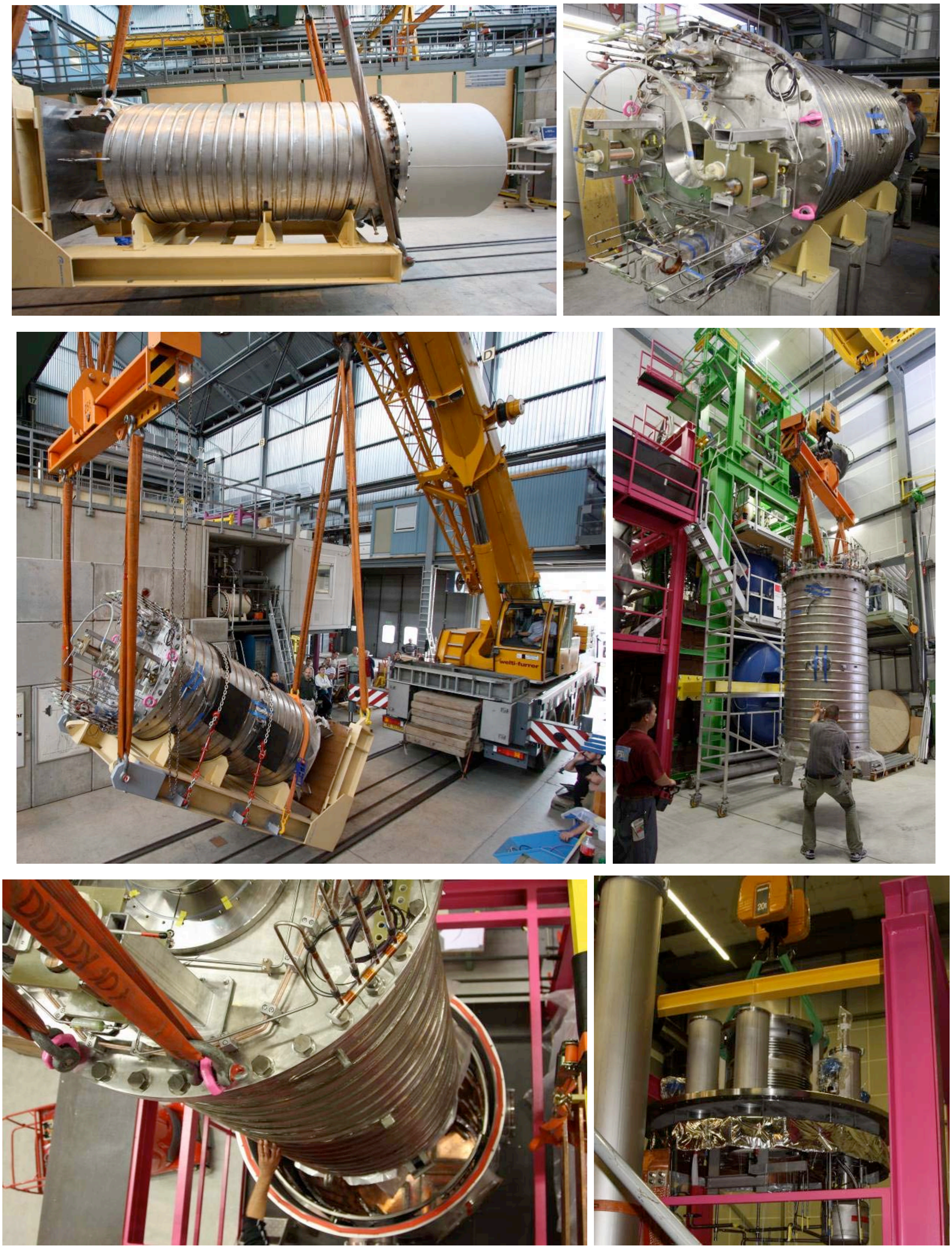

Fig. 2.5.1 *Top-left, unloading of the coil assembly on May 13th. Top-right, pre-installation work completed in the workshop, end of August. Mid-left, put in vertical with two cranes. Mid-right, the EDIPO coil assembly arrives in the SULTAN hall, September 8th. Bottom left, the EDIPO coil assembly is lowered into the vacuum vessel. Bottom right, the top flange lowered on the vacuum vessel.*

In 2009, the EDFAC task was extended (for the second time) to the end of 2011. Do to the actual delivery date of the EDIPO coil assembly and the priority given to the ITER conductors, it is not possible to complete the commissioning of the EDIPO test facility within 2011. A third extension of the EDFAC is necessary and is under way.

During September-October-November 2011, the SULTAN hall was accessible for external companies for regular maintenance (new power distribution cabinet, repairing of the heating system, main switch maintenance, compressor and soft starter repair) and for EDIPO related work (wiring from vacuum vessel to the electronic cabinets, installation of the vacuum equipment and control system, installation of the helium exhaust line and overpressure valves, installation of the hydraulic instrumentation panel).

The contract for the main control system, awarded in January 2011, was terminated in August 2011 because closing of the company. A new vendor was found and a new contract was awarded in October.

*2.6 Industrial process plasmas**

The number of the ongoing project has been strongly reduced during the last year, due to approaching retirement of the Group Leader. The still continuing projects develop new plasma sources for different deposition processes and investigate arcing in processing and equipment. These, for the future important topics, are investigated in the frame of CTI projects in collaboration with Sulzer-Metco, TetraPak, RUAG and Helyssen. Furthermore a CTI project with OC Oerlikon Solar works intensively on a CTI project developing a novel capacitively coupled RF plasma reactor particular designed for the specific demands of the amorphous/microcrystalline deposition for thin film solar cell production.

A new CTI project studying the properties of Nitrogen RF and DC plasmas as sources for the deposition of semiconductor GaN layers in view of the industrial production of LEDs was started during the year. This project is performed in collaboration with Sulzer-Metco and with LASPE (Laboratoire of advanced semiconductors for photonics and electronics) at the EPFL.

Discharge physics remains a key issue in the world of industrial plasmas, in particular the arcing phenomena. The problem of arcing in electronic devices has been investigated in a project in collaboration with RUAG Aerospace funded by ESA. The origin of arcing occurring in so-called slip-rings used in spacecraft is investigated in order to understand the conditions, origins and consequences of arcing within the device. Research and development of Electrical Discharge Machining (EDM) is another point in the research of the industrial plasma group. The finished CTI project studied dry EDM. The work made was grouped around Inspire SA at the ETHZ and Charmilles-Agie Technologies SA.

The industrial plasma group participates in collaboration with the Group de Thermique Applique et de Turbomachines (GTT) and the Laboratoire d'Ingénierie Numérique (LIN) of the Energy Institute (ISE) from the Faculty of Engineering (STI) in the European PLASMAERO project. The main goal of this project is the application of plasma in aerodynamics.

Discharge physics, arcing under various conditions and the development of novel high deposition rate plasma sources and its processing procedures are the main

* Work not belonging to the EURATOM Association workprogramme.

topics during the last year of the industrial plasma group. During the whole year meetings and discussions with various industries on other new plasma processing issues have been made and they might lead to interesting projects for the industrial plasma group of the CRPP in future.

Furthermore the industrial plasma group ensured the education of a master student and of TP students.

2.6.1 A new low ion energy bombardment PECVD reactor for the deposition of thin film silicon for solar cell applications

A novel electrode configuration is being studied for improved plasma-enhanced chemical vapour deposition of films such as amorphous silicon and micro-crystalline silicon. The new electrodes are designed to protect the growing film from damage by plasma ion bombardment, which is crucial for the manufacture of high-performance photovoltaic material. The new plasma reactor concept is optimised in laboratory tests and in a R&D industrial reactor at Oerlikon Solar.

It turned out that the very high breakdown voltage, observed in the newly designed RF reactor, could be considerably reduced by using a suitable structure of the RF electrode. Furthermore the structured RF electrode also reduced considerably the required RF power to achieve a full-area discharge. Low ion energy is a crucial aspect in the new reactor design and therefore the ion energy was measured at the substrate using a custom-built Retarding Field Analyser. The CRPP ion energy analyser was first tested using argon plasma where an ion charge-exchange energy distribution is measured in the parallel-plate RF reactor, showing correct operation of the analyser. At a given plasma potential, the ion energy is lower in the new reactor than for conventional reactors (Fig. 2.6.1); the reduction is almost independent of the geometry (gap distance, hole diameter, grid thickness). The ion energy distribution is well explained for noble gas plasmas, but the interpretation of the ion energies and composition crossing the collisional sheath in reactive hydrogen plasmas is more complex. Understanding of the physical mechanisms responsible for the low-voltage sheath and the cold, dense plasma below the grid will require further work. Suitable diagnostics such as phase-resolved optical emission spectroscopy will be used to elucidate the different mechanism.

Low ion energies (<15eV) were measured at the substrate of the new reactor independently of very high RF electrode voltages, which gave about 80eV ions without the grid. Thus the primary aim of the novel reactor to achieve low ion energy bombardment of the substrate is successfully achieved.

Parameter scans using structured electrodes are interpreted by means of numerical fluid plasma simulation, including the influence of electrode structure on gas breakdown RF voltage. An analytical model and numerical fluid dynamics show the necessary and sufficient properties of a gas showerhead system for uniform plasma processing. The numerical fluid simulation of the argon plasma was upgraded to include electron-molecule collision cross-sections for hydrogen. Comparison with the measured profiles of plasma density suggest that low energy ro-vibrational collisions are the physical mechanism responsible for the different density profiles observed in atomic and molecular gases.

An important point in the present project is the film quality obtained under low ion energy bombardment in the newly designed reactor. The semi-industrial R&D reactor at Oerlikon-Solar in Neuchatel was used to deposit microcrystalline silicon films and even solar cells using the hopping method. The resulting films and solar cells have been characterised by the Oerlikon Solar-Lab in view of potential future application in solar cell industry. The results of the deposited film and solar cells indicate that a material with defect densities comparable to standard material and with high, controllable crystallinity can be obtained. The interesting material properties have triggered activities to prolong the present CTI project for an additional year in order to better quantify the material which can be obtained in this newly designed reactor.

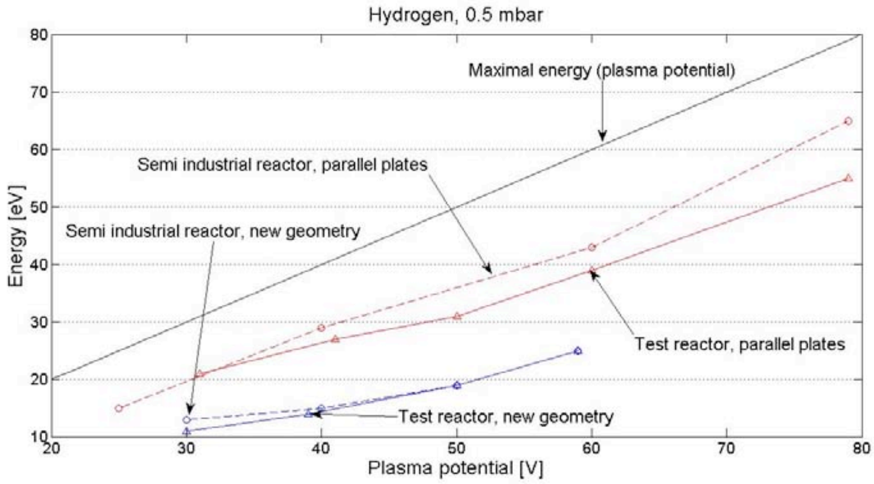

Fig. 2.6.1 *Ion energy versus plasma potential for different capacitively coupled RF reactors*

2.6.2 Plasma diagnostics for dry electrical discharge machining (EDM)

Electrical Discharge Machining (EDM) is a widely used machining technique investigated since several years by the industrial plasma group. The process consists in successively removing small volumes of work piece material, molten or vaporized during a discharge. The sparks are usually created in a flowing dielectric, generally water or oil. Plasma diagnostics in particular optical emission spctroscopy have been developed for electrical discharge machining. In the CTI project, led by Inspire AG (ETHZ), the physical basis of dry EDM was investigated. In dry EDM, oil or water dielectric is replaced by air or by reactive or inert gases. Dry EDM is still a process difficult to control and its industrialization has still to be proven.

This CTI project is in collaboration with Charmilles-Agie Technologies SA, Inspire AG at the ETHZ, Balzer Technik and Carbagas.

2.6.3 Very fast SiOx barrier deposition on polymers by plasma-enhanced chemical vapour (PECVD) process with a helicon plasma source

With regard to the main industrial interests, there is a constant need in plasma source improvements in order to increase the processes rates and to develop new types of products. A first aspect concerns plasma source performances in terms of high dissociation rates and efficient use of the process precursors. A second important aspect lies in the possibility of large area and also large volume plasma generation. This is of main interest to process larger amount of small pieces in a single run or treat larger and larger substrates. A particular example for these demands is the industrial deposition of SiOx barrier coatings on polymers as used in packaging industry.

Last year a cylindrical Helicon RF antenna was shown to be very efficient for plasma generation by means of inductive coupling as well as by helicon waves excitation in presence of a static magnetic field and it was demonstrated that the resulting RF plasma is capable to produce decent barrier coatings.

During this year a planar version RF antenna (Fig. 2.6.2) in an open configuration has been constructed and tested in view of electron density and of plasma uniformity.

The essential characteristic of these novel RF antennas consists in the fact that they are resonant devices. When excited at one of its resonant frequencies the antenna develops very high currents within its structure (Fig. 2.6.3). These resonating current distributions are called the normal modes (Fig. 2.6.4) of the antenna and are characterized by their sinusoidal nature. The planar antenna was designed to operate at a fixed RF frequency of 13.56MHz, which is allocated for industrial purposes. The mode m=6 was chosen for a study on the antenna performance, as this mode is easy to isolate, generates higher RF currents in the antenna legs than lower modes at comparable RF power, and furthermore allows better plasma uniformity. For the antenna under these conditions argon plasmas were ignited and sustained with RF power as low as 10W and up to about 2000W at pressures between $10^{-3}$and 10^{-2}mbar. For plasma diagnostics Langmuir probes, microwave interferometer, optical emission spectroscopy and 2D-B-dot probes were used.

Figure 2.6.5 shows an example of the electron density measured for argon plasma at 1000W along a plane in the middle of the 8cm-gap between the antenna and a floating metallic substrate. The electron density is maximal in the center and decreases rapidly near the sides. The electron density was measured by microwave interferometry to be above 10^{17}m^{-3}. Contour lines shown in Fig. 2.6.5 are plotted each 10% of electron density and show that the electron density is symmetrical in both dimensions and presents a non-uniformity of less than ±5% in the central region Although the antenna is inductively coupled to the plasma, the image of the antenna current distribution is hardly visible in the electron density.

The argon plasmas are easily ignited and are observed to couple capacitively with the antenna at low power (from 10W to 60W) and inductively above a threshold power of about 60W. Working at higher pressure and argon flux shifts the threshold power at which the inductive coupling starts towards lower values.

Besides the fact that the high current distributions generated under resonance are very efficient in terms of plasma generation, a major advantage of these antennas lies in their input impedance properties nearly independent of the geometrical size, which could be used to develop very large area plasma sources with complex shapes. This property is one of the key advantages of this novel type of RF plasma source in comparison with other existing large area sources such as capacitively or conventional inductively coupled devices. The limits in the up scaling of these reactors are due to their very low impedance, which implies high currents and voltages and therefore possible arcing and parasitic discharges.

The planar RF antenna has been installed in a semi-industrial device in order to test the behaviour under industrial conditions and obtain the coating performances of the plasma in view of industrial applications.

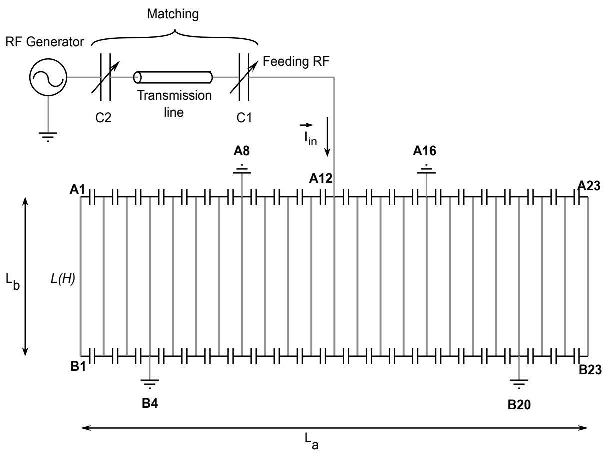

Fig. 2.6.2 *Schematic drawing of the planar antenna*

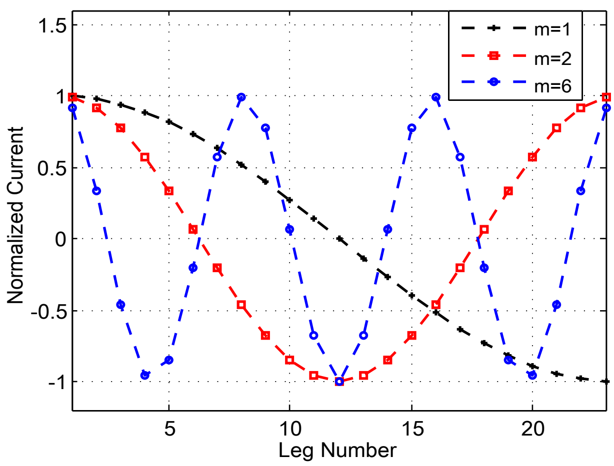

Fig. 2.6.3 *Current distribution in the legs for different modes*

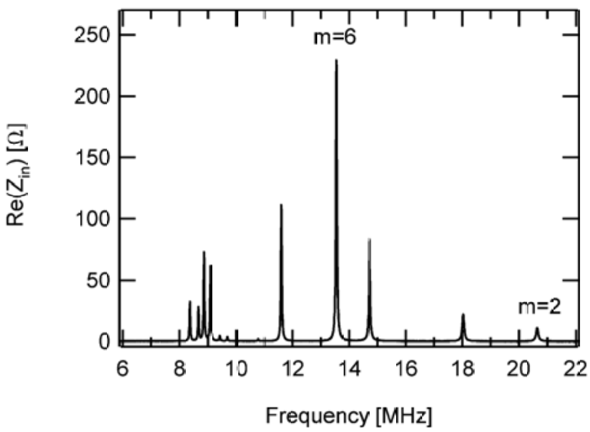

Fig. 2.6.4 *Measured resonance spectrum of the 23-leg planar RF antenna*

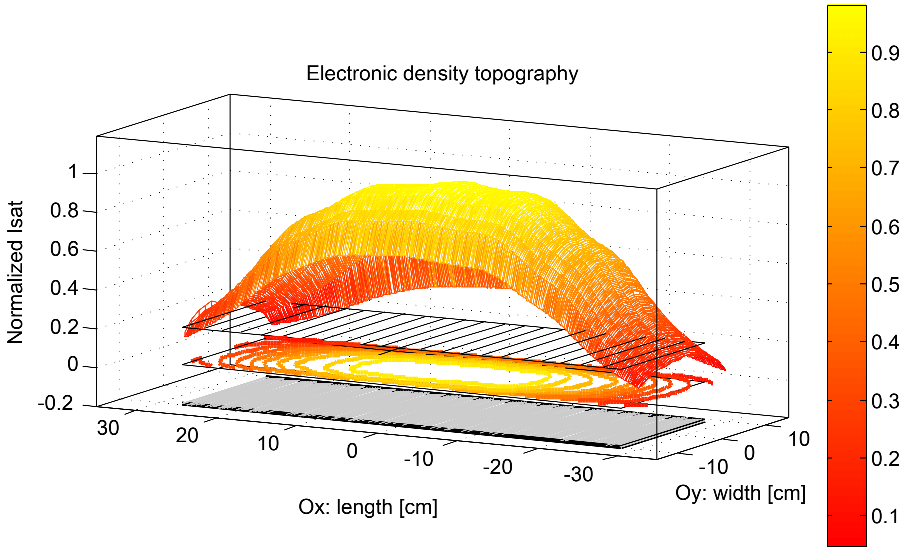

Fig. 2.6.5 *Normalized electron density surface obtained with Langmuir probes at about 4 cm above the antenna and at a power of 1000W. A floating metallic substrate is placed 8 cm above the RF antenna.*

2.6.5 Development of industrial gas-metal plasma sources for the deposition of nanostructured GaN semiconductor layers for lighting applications

Epitaxial coating processes using low-energy gas-metal plasmas offer a promising path to cost-effective manufacturing of highly energy-efficient LED's for power-saving lighting applications and high-efficient third-generation solar cells. The goal of the present CTI project is to move this innovative coating technology a step closer to industrial application and commercial exploitation by developing and optimizing the plasma-processing equipment. In addition better understanding and controlling of the fundamentals of the GaN deposition process will be obtained.

In the frame of the project a commercial RF source and a LEP-DC (low energy plasma source) plasma source shall be compared in view of the deposition of GaN semiconductor layers.

The RF GaN deposition device (Fig. 2.6.6), obtained from Sulzer Metco, using a commercial RF source was installed at the CRPP and first nitrogen (and nitrogen-argon/and hydrogen) plasmas have been produced. In addition, different plasma diagnostics such as Langmuir probes, a Faraday cup and optical emission spectroscopy have been installed on the device. Injection of Gallium into the nitrogen plasma using an effusion cell has also been performed and the device performed the first GaN depositions. First characterization of the Nitrogen-(Argon/Gallium) plasma using the existing diagnostics have been started. These preliminary results for emission spectroscopy are interpreted using available software such as Specair in order to simulate the spectra and to determine the population densities and different species temperatures within the plasma and further investigate the influence of the injection of the neutral Gallium beam. These results will later be correlated with results obtained by deposition characterisation. The characterisation of the obtained semiconductor layers shall be made at the

LASPE (Laboratoire of Advanced Semiconductors for Photonics and Electronics) ofthe EPFL.

The DC plasma equipment already existing at the CRPP had to be modified so that the Nitrogen(-Argon /and Hydrogen) plasma could be produced using either a point electrode or in particular a ring electrode as necessary in view of GaN depositions. For Gallium injection using a effusion cell, the DC plasma source had been changed. In the meantime, the DC device was used to obtain a preliminary characterization of the DC plasma and its composition and in particular also of the stability of the plasma in the presence of a ring electrode. For these experiments optical emission spectroscopy and a moveable Langmuir probe have been applied and the very first results indicate a large difference between the RF nitrogen plasma and the DC nitrogen plasma.

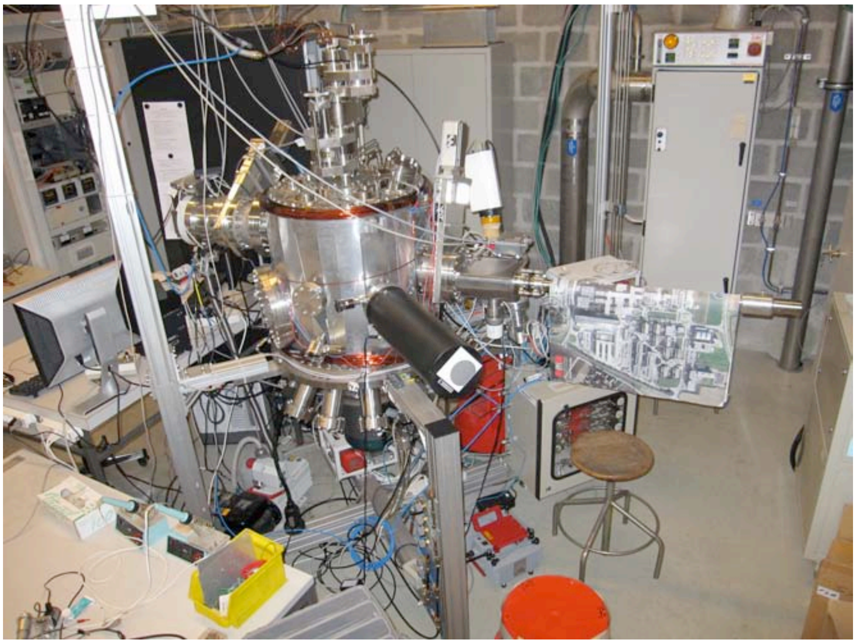

Fig. 2.6.6 Plasma reactor for the deposition of GaN semiconductor layers

2.6.6 European FP7 project: PLASMAERO

The consortium of the FP7 project PLASMAERO is composed of 12 partners from 8 countries (Arttic (F), ONERA (F), CNRS(F), EPFL(CH), CIRA(I), Technische Universitaet Darmstadt (D), University of Nottingham(GB), NLR(NL), University of Southampton(GB), TRINITI(RU), SNECMA(F) IMP(PL)). It gathers the key players from the plasma and aerodynamic scientific community of Europe. The PLASMAERO project was officially started at the end of 2009 and will last three years.

The CRPP participates together with the Groupe de Thermique Appliquée et de Turbomachines (GTT) and the Laboratoire d'Ingénierie Numérique (LIN) of the Energy Institute (ISE) from the Faculty of Engineering (STI) in this project. In addition the CRPP is work-package 1 leader ("Plasma devices, investigation, development and improvement") and task leader 3.5 (Shock/Boundary layer interaction).

The different partners at the EPFL perform experiments at transonic flow speed in their research wind tunnel facility on basic configurations of a flat surface dielectric discharge barrier (DBD) and on 2D profiles with curved DBD in order to obtain results on the modifications of flow and plasma characteristics. One part of the wind tunnel testing will be performed in the large wind tunnel of CIRA.

The CRPP developed a power supply to drive fast nanosecond pulsed DBD's. The power supply is based on the use of a MOS-FET switch, which handles voltages up to 10kV and discharge currents up to 40A. Rise and fall time of a few tens of nanoseconds could be obtained. The circuit design used allows the construction of a low weight version of this nanosecond pulse power supply, which can be incorporated into the UVA planned to fly during activities later in the PLASMAERO project. Other nanosecond pulse producing power supplies used in PLASMAERO are too large and heavy to be loaded into the UAV.

A modified CRPP power supply is also considered to drive PSJ actuators during the UAV flights, since the power supply used by ONERA are based on a different design and turns out to be too big and heavy. Different tests under various occasions showed that perturbations of the fast nanosecond pulsed DBD are small and should not influence their application in the mentioned tests and experiments. This is in contrast to the other power supplies used in the project, where severe disturbances can be observed. The difference of the electro-magnetic disturbances induced by different power supplies might be explained by the different design.

Optical plasma diagnostics were used to characterise the actuator plasmas in particular also the nanosecond pulsed discharges. The temporal and spatial discharge development created by the FRP discharges was investigated using ICCD cameras as was already done in the previous period. The mechanism due to which pulsed DBDs are expected to achieve control authority in transonic flows relies on instantaneous energy deposition in the region close to the discharge, thus generating a micro shockwave. Besides these experiments, time-resolved emission spectrometry gives interesting insight into the heat creating mechanism (this is investigated in an additional SNF project). The method of fast imaging was also applied to a Schlieren diagnostic in order to visualize the dynamic and propagation of fast compression wave fronts triggered by nanosecond discharges. Classical Schlieren techniques have been used to visualize the flow interaction and are interesting methods characterizing the discharge-airflow interaction. In particular this method has been applied in order to further understand the interaction between the discharge and flow.

Plasma imaging is a very widely used plasma diagnostic to visualise the actuator discharge. Also, the CRPP applied imaging diagnostic to the classic DBD discharges and in particular to the nanosecond DBD discharges. Fast imaging was used for the visualisation of the discharge of the compressive wave induced by the nanosecond pulsed DBD. The compressive wave, its origin and propagation can be investigated using Schlieren. It has to be mentioned that up till now, with the exception of the CRPP, no interaction between the fast DBD produced compression wave with the airflow has been studied. Such experiments are extremely important to understand the interaction of the plasma actuator with airflow and to interpret the results from the experiments.

Time-resolved optical emission spectroscopy has been used as plasma diagnostics in a SNF project (Fig. 2.6.7) in collaboration with GTT. Emission spectroscopy is used to determine the different population of the plasma and the different temperatures. These results are importantto elucidate the time development of a nanosecond pulsed DBD discharge. Such measurements are of importance also to obtain more detailed understanding of the interaction of the DBD plasma with the airflow and of the phenomena leading to the compressive wave.

First results using a NACA 3506 show that the compression wave is also existent in transonic flow (Fig. 2.6.8) and propagates downstream. These experiments were made in preparation for the experiments to be performed on a BAC1-11 profile (Fig. 2.6.9) in order to investigate buffeting at elevated airflow velocities. The use of the fast nanosecond power supply is also foreseen for these tests at CIRA.The air foil used will be BAC1-11, a supercritical air foil with the 11% of maximum thickness designed by the British Aircraft Corporation, which shows buffeting conditions at low Mach numbers (M=0.7-0.76) at low angles of attack (0-5°) and Reynolds number about 2-3 million.

a)

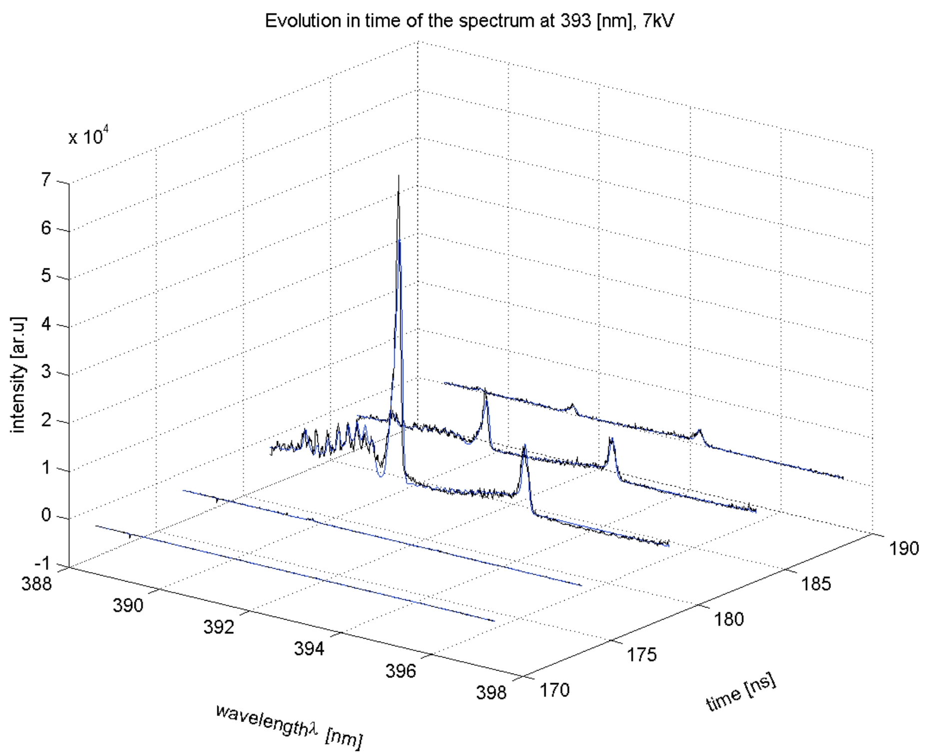

b)

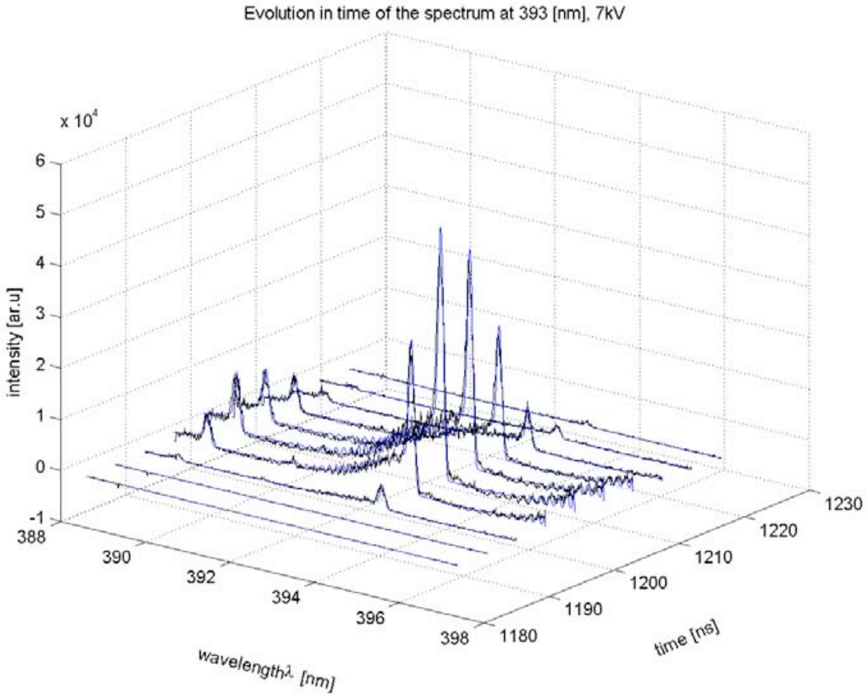

Fig. 2.6.7 *Time resolved emission spectroscopy a) at voltage rise and b) at voltage decay*

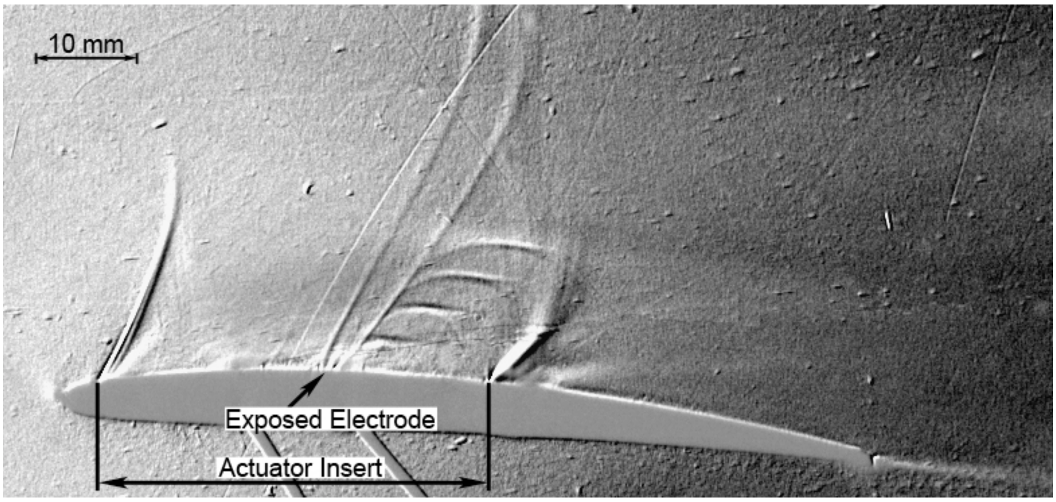

Fig. 2.6.8 *Schlieren visualisation of the interaction of the airflow shock on an airfoil (NACA 3506) and discharge produced micro-shocks*

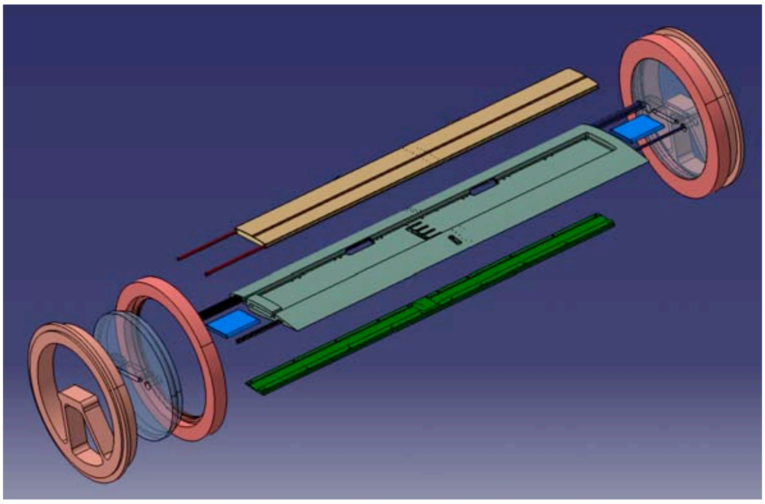

Fig. 2.6.9 *Schematic of the wind tunnel model designed by the EPFL and to be used at CIRA. The model chord is 0.12m.*

2.6.6 Arc Phenomena in Space Environment and Equipment (Project RETS)

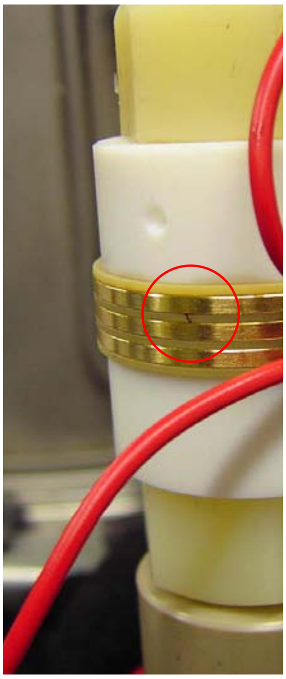

Fig. 2.6.10 *Test arrangement, simulating a part of a slip-ring, for arcing limit testing*

In the present work for the space agency ESA in collaboration with RUAG Aerospace in Nyon and the Haute Ecole d'Ingénierie et de Gestion du Canton de Vaud (HEIG/VD-IESE) laboratory, the necessary fundamentals of the arcing in slip-ring or similar geometries shall be established and be applied to space equipment in order to reduce or suppress arcing in space environment.

Arcing is considered by the Industrial Plasma Group as an essential key issue in the application of plasma in industry and also, as in the present case, in space environment and space equipment. Modern satellites, in particular transmission satellites, are being equipped with larger and larger power systems. Since also the weight aspect is very important the dimensions of the conducting paths for instance, in slip rings, are small. Therefore arcing is also considered to be a limiting factor in several other applications of plasmas, thus triggering intense research and development on this topic.

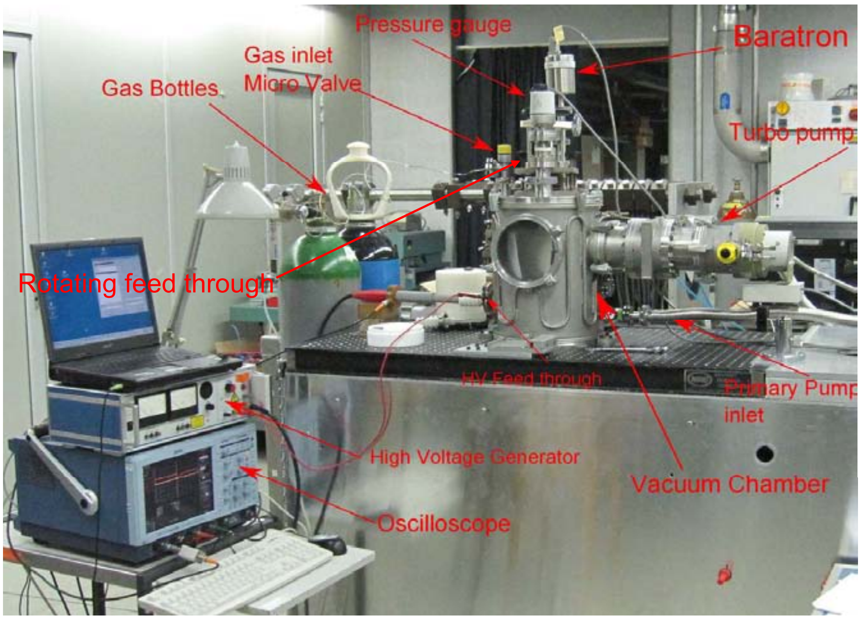

Fig. 2.6.11 *Experimental set up for arc-testing of slip-ring assemblies under space conditions*

In the frame of this project funded by the ESA the arc ignition, propagation and stability experiments in space environment are studied. Slip rings are an important part in the power supply chain of a satellite. For this reason, electrical simulations of the whole solar cell circuit were conducted by the HEIG/VD-IESE laboratory in order to obtain realistic voltage and current limits for the operation of the slip rings.

The test facilities proposed at the present time consist of metal and insulator rings arranged as in a real slip-ring device (Fig. 2.6.10) connected to a high power DC (high voltage) power supply under space conditions. The breakdown measurements performed determine the extreme operation limits of a test ring assembly as a function of the environment gas pressure and different gases (Fig. 2.6.11). The main phenomena when a DC high voltage up to 30kV has been applied were vacuum arcs, corona and glow. Two different zones depending on the applied high voltage are observed: The high-pressure side where the breakdown voltage is clearly dominated by gas effect, whereas on the low pressure side breakdown leads to vacuum arcing.

The obtained results lead clearly to define limits of operation of the present slip ring and also to new clues in order to increase the performances of this important piece of spacecraft equipment and also contributed essentially to new testing procedures.

2.6.7 Collaboration with the start up company Helyssen SARL

Helyssen SARL (www.helyssen.com), a start-up company, has now for several years used a test bed at the laboratories of the industrial plasma group to evaluate the performance of novel RF antennae for high deposition rate processes. The necessary equipment for benchmarking and infrastructure have been lent to Helyssen SARL by the CRPP. This includes equipment also for plasma diagnostics and know-how in order to test the performance of high power RF plasma sources.

In particular, Helyssen SARL, in collaboration with TetraPak Romont and the CRPP, is developing a novel planar high power RF Plasma source in the frame of CTI project for application in packaging industry.

2.7 Gyrotron physics and simulations of mm-wave rf systems

In support to the different research programs for which gyrotrons are used (TCV ECRH system, TCV X3-upgrade, W7-X EC-system, ITER EC-system, DNP-gyrotron), a significant effort has been devoted in 2010 to the extension of the simulating capabilities for this class of high-power coherent sources by intense electron beams.

This effort was mainly motivated by three complementary aspects, with the first one devoted to gain a deeper physics understanding on the complicated non-linear wave-particle interaction occurring in these devices. In particular the research effort has been focused to the basic physics understanding of the so-called “spurious effects” such as beam-duct instabilities, static and dynamic after cavity interaction (ACI), dynamics of trapped secondary electrons in the electron gun. These effects have been somehow disregarded in the past but have recently appeared to be a potential limiting factor for reliable operation in these devices. The second important aspect, complementary to the one outline above, is to be more efficient in simulating real experiment carried out at CRPP. Depending on the experimental results and having developed the simulating tools it is significantly easier to exploit the codes and add new physics when needed. The third aspect has a pedagogic connotation in the sense that with the available simulations tools and maintaining a deep knowledge on the underlying physics, it allows to captivate young scientists which will eventually be trained in this very challenging research domain.

In support to the theory on gyrotron physics and the modeling of overmoded electromagnetic (EM) systems, an important effort has been devoted in modeling these EM-systems using commercially available software packages such as COMSOL-multiphysics[1] and/or HFSS[2] based on a finite element discretization of Maxwell’s equations. The usage of these softwares for monomode systems is well-established, but the modeling of highly-overmoded and/or quasi-optical systems is still at the level of R&D.

The spin-off activity on gyrotron physics, aimed at developing gyrotrons for Dynamic Nuclear Polarization enhanced NMR spectroscopy, is also summarized. From this spin-off activity and thanks to the expertise developed at CRPP in simulating, developing and exploiting mm and sub-mm wave systems, a start-up company, Swissto12, has been recently founded.

[1] http://www.ch.comsol.com/

[2] http://www.ansoft.com/products/hf/hfss/

2.7.1 Gyrotron physics and simulations

TWANG code

The time-dependent monomode-code TWANG is an extension of the existing steady-state code TWA. TWANG is based on the slow-time scale formulation of the electron equation of motion for any cyclotron harmonics. For any given TE transverse mode, the equation of motion for the three cartesian components of the electron momentum include the interaction with both the electric and magnetic rf-fields. The longitudinal dependence of the electron beam properties (velocities, guiding center) associated to the inhomogeneous DC magnetic field is included. The equation of motion of an ensemble of N_p electrons is solved using a forth-order Runge-Kutta method. Beam velocities and guiding center spreads effects can be studied.

The time-dependent wave equation for the longitudinal profile of the rf field is solved using a finite element method (FEM) based on B-splines of any order. The radiation boundary conditions at the input and output of the interaction space are introduced as natural boundary conditions in the FEM formulation. Ohmic losses are included in the wave-equation via the DC wall conductivity. The time integration of the wave equation is performed by using a 2^{nd} order predictor-corrector scheme.

From the FEM discretized wave-equation, a global power balance equation can be derived which is used as a diagnostic for verifying the convergence of the time dependent simulations. Other diagnostics such as the Fourier analysis of both the complex RF-wave electric field and/or the wave reflection coefficient along of the interaction space have been implemented.

An extended benchmarking with the codes EURIDICE (Hellas) and SELFT (KIT) has been performed. It has to be underlined that in these two codes, both the particle equation of motion and the wave-equation are solved using different numerical schemes than for TWANG. In particular, the wave-equation is solved in EURIDICE using a finite-difference numerical technique and the numerical integration of the particle trajectory uses a predictor-corrector scheme which is equivalent to 2^{nd} order Runge-Kutta.

The FEM together with the possibility of varying the order of the B-splines has allowed to verify the sensitivity on the B-spline order of the radiation boundary conditions defined at the boundaries of the interaction space. As an example, for the case of the 118GHz gyrotron cavity operated on TCV, the simulated radiation spectrum, the spectrum of the complex reflection coefficient is shown in Fig. 2.7.1 below for linear and cubic B-splines.

For studying spurious effects such as beam-duct instabilities or static and dynamic after cavity interactions it is essential to insure that the radiation boundary conditions are accurately satisfied for avoiding misleading results associated to a possible numerically generated reflection.

The TWANG code has been extensively used for the preliminary design and detailed design of the X3 1MW-gyrotrons planned for the upgrade of the TCV EC-system. It will be used to analyse the monomode behavior of the present experimental campaign on the ITER 2MW coaxial-cavity gyrotron. In addition it is being used for all others gyrotron R&D activities carried out at CRPP and within the European collaboration on gyrotrons.

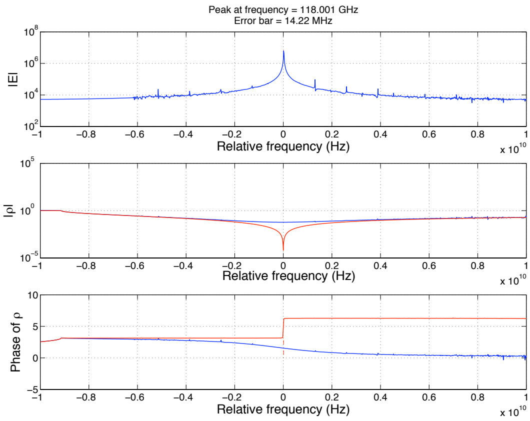

Fig. 2.7.1 *TWANG simulations of the 118GHz gyrotron cavity used on TCV. Top figure: spectrum of the rf E-field amplitude. The 'relative frequency' is relative to the reference frequency of 118GHz. The comparison of linear (blue lines) and cubic B-splines (red lines) of the complex reflection coefficient (amplitude and phase) shows the enhanced numerical accuracy of the third-order B-splines close to the required matched condition (zero reflection) at zero relative frequency.*

Gyrotron beam-duct instabilities

In MW-level gyrotrons for fusion applications, instabilities developing in the beam-duct preceding the gyrotron cavity, if excited, have a deleterious effect since they generate electron-beam energy-spread hence significantly degrade the interaction efficiency. This research topic is recently very active and different schemes of damping structures have been proposed. A recently proposed structure, successfully tested in the 140-GHz gyrotron for W7-X, consists of a ring loaded structure where copper and dielectric rings are alternated. The particularity of the proposed structure consists in indenting the copper rings azimuthally with a random orientations of the indentations when going from one copper ring to the next one (see Fig. 2.7.2b). Intuitively the role of the indentation was believed to be associated to the elimination of surface currents supported by azimuthally symmetric $TE_{0,m}$ modes which were identified to be the most unstable modes in non-indented beam-duct damping structures. However, EM simulations carried out within a collaboration with L. Thorndahl from CERN, it has been shown that the main effect of the indentations results in mode coupling such to generate a very weak coupling between the electron beam and the resulting transverse EM-field structure. This effect is the actual mechanism responsible for avoiding beam-duct instabilities.

To complete this study, other damping structures currently used by other high-power gyrotrons developers have been studied. In particular, it has been shown that the structure used in the Japanese gyrotrons developed for ITER and consisting of a smooth conical section of a doped Silicon Carbide (SiC-B), might again destabilize beam-duct modes for electron beam-current exceeding the present nominal levels required for 1MW operation. In fact, for these smooth dielectric electromagnetic structures, the damping term only depends on the imaginary part of the surface impedance associated to the dielectric. Detailed measurement at 170GHz of the imaginary dielectric constant of SiC-B has shown that the level of surface impedance is too low for insuring parasitic-mode stabilization at higher current than the one presently used in the 1MW-gyrotron. CRPP has procured a complete SiC-B beam-duct structure which will be tested at KIT on the 2MW/170GHz coaxial-cavity short-pulse gyrotron.

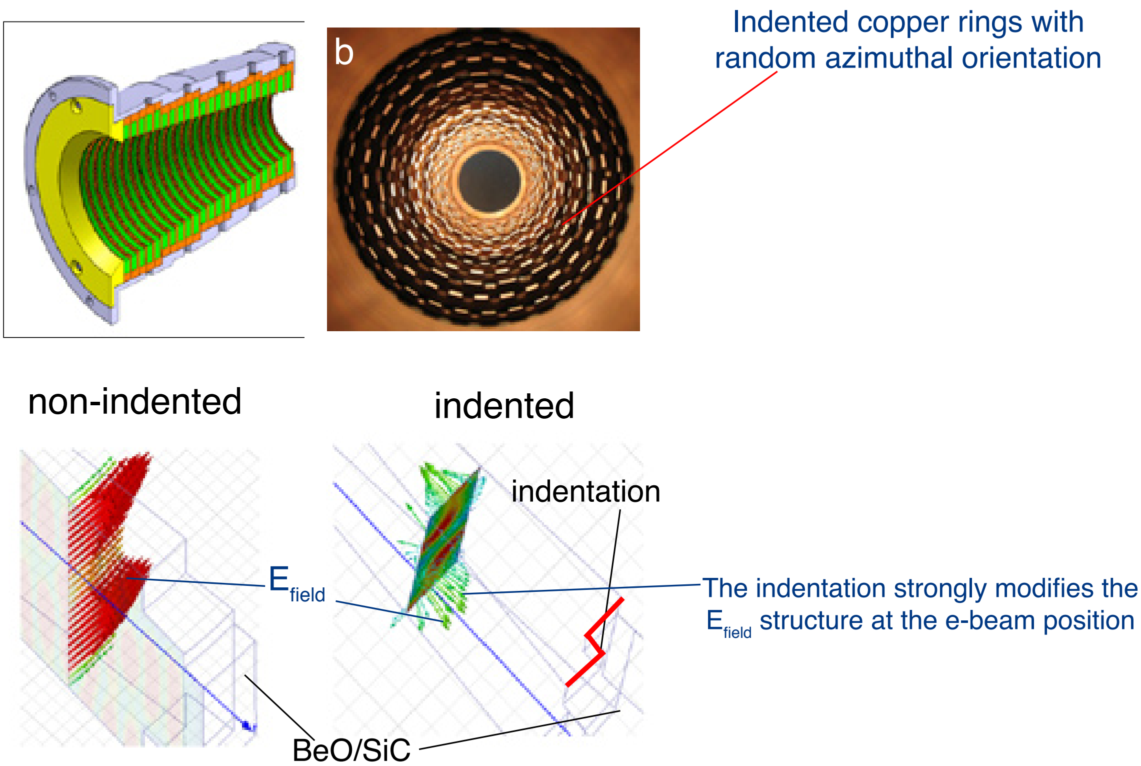

Fig. 2.7.1 *Top left and right figures: dielectric loaded beam duct structure composed by a stack of alternating dielectric and copper rings. On the top-right figure the copper ring indentations are shown. Bottom left and right figures: results of the EM simulations using the software HFSS and considering a small angular wedge of a unit cell representing the dielctric ring and the indentation on the copper rings on each side. The arrows represent the calculated rf E-field at the electron beam radial postion and one clearly observes that for the indented case, the E-field is strongly perturbed.*

Gyrotron after cavity interaction (ACI)

The theory of static after cavity interaction is presently well understood and has been recently validated by experiments. This spurious effect occurs after the main extraction cavity, in the launcher section, where, under some conditions essentially depending on the DC magnetic field profile, the spent beam undergoes a second interaction at the same frequency as the extraction cavity frequency and with the same transverse EM-mode. Often, the interaction is such to have a significant amount of EM-energy transferred back to kinetic energy of the spent electron beam. Using TWANG it has been shown that the presently used 118GHz gyrotron suffers of static-ACI and approximately 50kW of rf power (10% of the nominal power) is lost by this mechanism.

A second type of ACI, so called dynamic-ACI, is presently investigated in a collaborative effort between KIT, Hellas and CRPP. Dynamic-ACI differs from static-ACI in the fact that the second interaction after the cavity occurs at the same transverse mode as the cavity-mode, but at a different frequency close to cut-off in the launcher section. The launcher radius being larger than the cavity radius the dynamic-ACI frequency is always lower than the cavity-frequency with a frequency difference as high as 8-10GHz.

For the case of the 140GHz gyrotron for W7-X, dynamic ACI is observed using TWANG with a predicted frequency of 132.3GHz. The simulated spectrum of the radiation rf field together with the complex spectrum of the reflection coefficient are shown in Fig. 2.7.3. It is clearly visible on the top figure that in addition to the main frequency of 140GHz (corresponding to zero relative frequency on the plot) a second peak appears at a downshifted frequency of 7.7GHz corresponding to 132.3GHz. This oscillation is the dynamic-ACI which is excited in the launcher section.

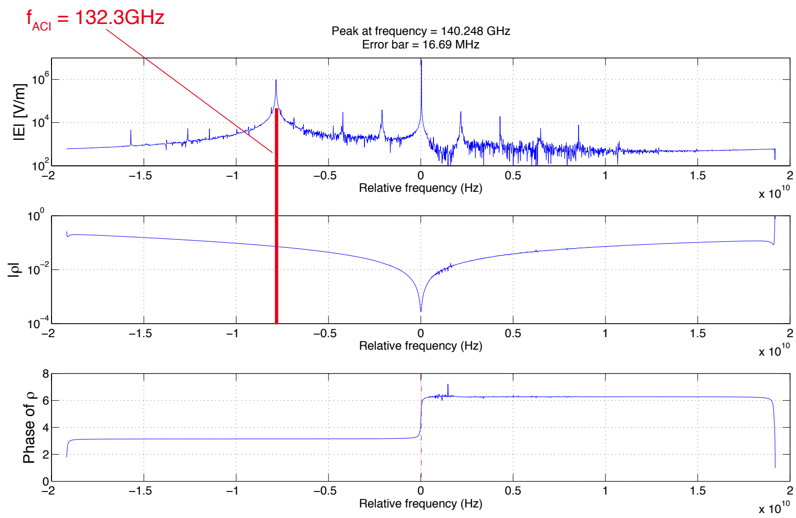

Fig. 2.7.3 *TWANG simulations of the 140GHz gyrotron cavity-launcher system for W7-X. Top figure: spectrum of the rf E-field amplitude. It is clearly visible the excitation of a spurious frequency occuring at 132.3GHz. The lower curves are the amplitude and phase of the frequency dependent reflection coefficient, respectively.*

In the last series tube (SN4R) manufactured by Thales Electron Devices (TED) and tested at KIT and Greifswald a very detailed measurement of parasitic oscillations have been performed by A. Schlaich (KIT). This gyrotron has implemented the indented dielectric beam-duct structure mentioned above and it has been experimentally verified that no spurious oscillations occur in the beam-duct. Any measured spurious frequency are believed to be associated to dynamic ACI. In Figure 2.7.4, the spectrum of experiementally measured spurious frequencies is shown were two sets of experiments have been performed: in short-pulse regime (blue points) and long-pulse regime (green point). The y-axis gives the relative frequency of occurrence of any measured spurious frequency. The dynamic-ACI frequency predicted by TWANG is in excellent agreement with the most frequent frequency measured in short pulse regime. The global frequency shift occuring in long-pulse is believed to be associated with the radius increase due to rf heating.

The excitation of this instability strongly depends on the magnetic field profile in the launcher section. A detailed study on the dependence of this excitation on the gyrotron system parameters will be part of future work. Benchmark studies between the TWANG results on dynamic ACI and the ones given by other codes such as SELFT and EURIDICE are presently ongoing.

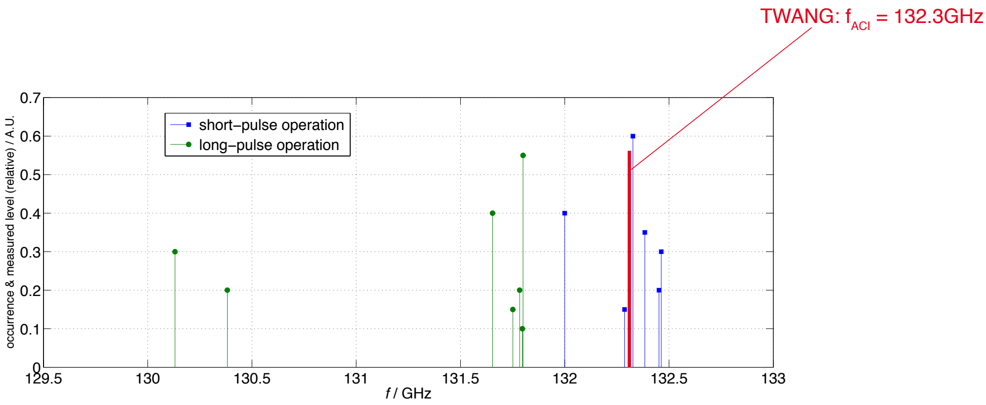

Fig. 2.7.4 *Comparison between theory and experiment on dynamic-ACI measured on the 140GHz gyrotron for W7-X.*

Trapped secondary electrons dynamics in Magnetron Injection Guns (MIG)

The study on the possible formation of secondary trapped electrons in the gyrotron MIG has been pursued during 2011. As a reminder, trapped secondary electrons exist when the topology of equipotential lines and magnetic field lines is as schematically shown in Fig. 2.7.5 were the parallel components of the electric field, relative to the B-field, are such to confine electrons. The formation of this trapped electrons have been identified as responsible of lowering the voltage standoff of the MIG as experimentally observed on a first prototype of the gun for the 170GHz coaxial cavity gyrotron for ITER.

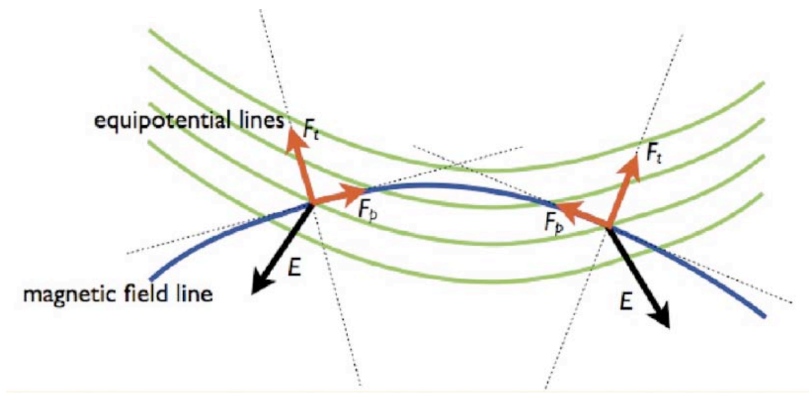

Fig. 2.7.5 *Equipotential lines and magnetic field lines configuration giving rise to the formation of secondary electron trapping.*

Based on the identification of this mechanism, an extensive redesign of the gun has been performed and an accompanying experimental study has been carried out on a dummy-gun for which no formation of trapped regions was possible at the gyrotron nominal parameters. However, by imposing different magnetic field configurations such to form trapped region it has been possible to experimentally validate the model. The results of the experimental study confirming the theoretical prediction is shown in Fig. 2.7.6, were the control parameter for the formation of trapped electron is one of the current (Bucking coil current) feeding the superconducting coils needed to operate the gyrotron.

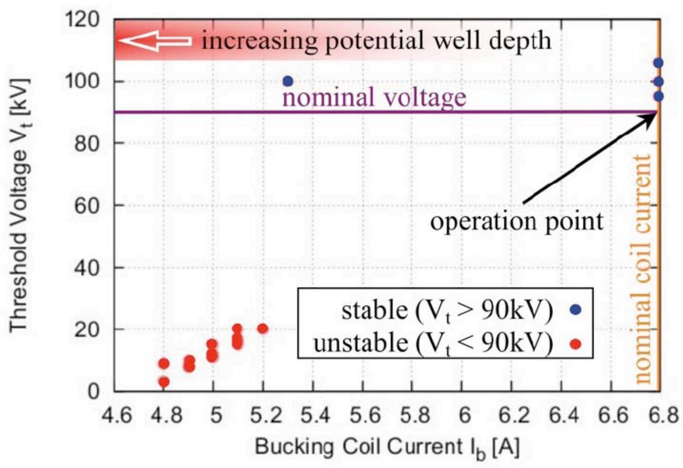

Fig. 2.7.6 *Experimental results on the voltage standoff capability of the MIG used on the 170GHz 2MW coaxial cavity gyrotron. The control parameter for the formation of trapped electrons is the bucking coil current. It is clearly visible that for currents below 5.3A, the voltage standoff capability is strongly degraded (red points) and this threshold corresponds to the situation in which a trapped electron population is predicted by modeling. At the nominal parameter the reached stnadoff voltage higher than 90kV meets our expectations.*

In 2011, this activity was pursued in the frame of a PhD thesis aimed at studying the full dynamics of the secondary electron population. For studying this effect, the ionization processes as well as the self-consistent space charge effects associated to the formation of the trapped electron population need to be included in the model. A preliminary model has been developed and has given a significant physical insight. In parallel, the experiment on the dummy-gun has been continued with a major improvement in the diagnostics were visible spectroscopy and fast imaging systems were used. The experimental data collected are still to be analysed and will be part of a future PhD project after the unexpected departure of the PhD candidate.

*2.7.2 A spin-off activity: Gyrotron for Dynamic Nuclear Polarisation**

This project has started in 2008 and is presently ongoing with a delivery and commissioning of the designed gyrotron foreseen by the end of 2011. Detailed results on this activity are given in section 3.7 of the present annual report.

Regardless of the application of this gyrotron for this domain somewhat outside the main stream activities of CRPP, the part associated to the theory and simulation of gyrotron has allowed to further extend our understanding of these coherent sources and is certainly also profitable for the R&D of gyrotron for fusion applications.

Within the DNP project, future extensions of our studies using TWANG will be aimed on one side at designing a gyrotron operating at the 2nd cyclotron harmonic operation (527GHz) and on the other side investigating pulsed-regimes based on non-stationary equilibrium points.

---

* Work not belonging to the Euratom Association Workprogramme

2.7.3 Simulations of overmoded mm-wave systems

As pointed out earlier with regard to the study of beam-duct dumping structures, the highly inhomogeneous EM structures used are such that an analytic or semi-analytic approach for characterizing their properties is not possible without imposing strong assumptions such that key physics is possibly missed. Numerical simulations is an alternative, with the main difficulty that, with the overmoded nature of the systems of interest, the numerical constraint of having a meshing with at least 5 to 10 mesh points per wavelength makes the treatment of real problem difficult. With computer platforms having large RAM (up to 160GB), the numerical issue is alleviated, but still requires to impose assumptions for rendering the problem numerically treatable. An example of the possible volumes treatable with these codes was given above with the simulation of beam-ducts using HFSS.

At CRPP one takes advantage of a site license of EPFL for the COMSOL multi-physics package and the availability of a large RAM (160GB) high performance platform financed by the gyrotron-DNP program. Using this computing capability a variety of designs for passive components to be used in domains such as ECE radiometry on TCV, quasi-optical components for testing the 170GHz transmission line and EC-launcher system, DNP related instrumentation have been initiated. As an example, in Fig. 2.7.7, the simulation using COMSOL of an optimized horn for a TCV EC-radiometer is shown in part b).

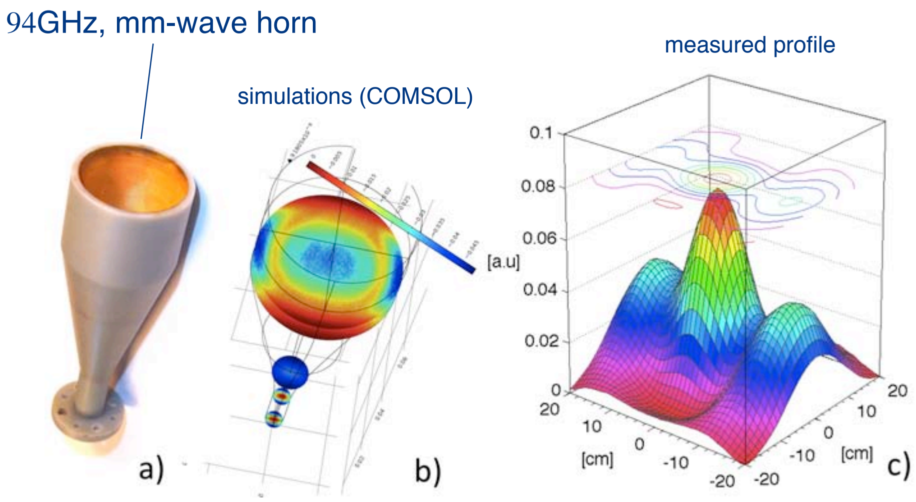

Fig. 2.7.7 *Development of an optimized horn for one of the TCV ECE radiometers. Figure a) the horn manufactured with a new technique based on a stereolithography (SL) technique on plastic epoxy followed by an etchingless electroless gold-plating (EEGP). This technique has been developed by the newly founded Swissto12 start-up company. On part b) is shown the simulation using the COMSOL multiphysics code and on part c) the measured transverse rf-power profile.*

2.7.4 Swissto12 a new start-up company*

Swissto12 (www.swissto12.ch) is a newly funded company which is a spin-off of both the DNP-gyrotron project and the CRPP activity in R&D of rf instrumentation for EC systems. Swissto12 is specialized in the development of passive components ranging from mm to sub-mm wavelength. A variety of novel techniques have been developed for manufacturing these components which includes the above mentioned technique of SL-EEGP, but also a different technique more suitable for higher rf-powers based on a stacked-ring assembly. Details on these developments are given in the section 3.7 of the present annual report. An example of a fusion related applications of the SL-EGGP technique, in Fig. 2.7.8 are shown the experimental results on an astigmatic phase-correcting mirror used in the matching optics unit of the 170GHz gyrotron. The SL-EGGP can only be used so far for low power components, but its manufacturing simplicity and rapidity allows to validate by experiment novel complicated optical components which would need significant longer times and being significantly more expensive if manufactured by standard techniques. In addition it opens the possibility to manufacture components with geometries impossible to manufacture with standard machining techniques.

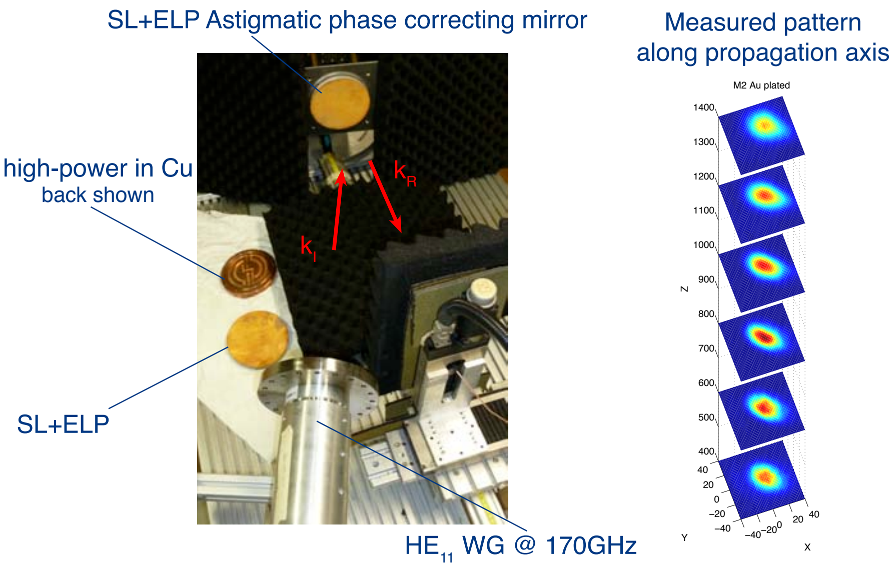

Fig. 2.7.8 *Left figure: setup used to characterize the optical properties of an astigmatic phase correcting mirror manufactured using the SL-EEGP technique. In the left part of the setup are shown a SL-EEGP mirror and the same in copper manufactured by standard milling machining. On the right part, for the SL-EGGP mirror, are shown the transfer rf-power profiles measured along the propagation axis.*

* Work not belonging to the Euratom Association Workprogramme

3 TECHNICAL ACHIEVEMENTS

3.1 TCV operation

The TCV tokamak facility was operated almost continuously in 2011 from the beginning of February, with a regular one-week for every three weeks of operation and an additional 5-week break in August, resulting in 220 experimental sessions (half-days) as of 10 November. Machine availability was at a record high, with close to 80% of the sessions labelled as successful.

The short summer break was occupied by a vessel vacuum break to perform minor repairs and diagnostic installation.

3.2 TCV ECH systems

During 2011 the X2 system continued with a successful operation using 5 gyrotrons. The non-working gyrotron magnet has been repaired and the factory acceptance test has been successfully performed in October 2011. The repaired magnet is presently at CRPP and is being prepared for carrying out the on-site acceptance tests. Among the 5 remaining superconducting magnets one of them is showing some weaknesses since it recently quenched on several occasions, and its evolution is closely followed.

The X3 system was still limited to a total power of ~1MW (2 gyrotrons). A contract has been placed with Thales for repairing the 3rd gyrotron with the faulty window. After inspection by Thales, additional issues in other gyrotron sub-systems have been identified on the cavity, internal launcher and collector. A complementary repair contract has been placed and the delivery of the repaired gyrotron is foreseen for the second quarter of 2012.

The preparation work for the upgrade of the X3 electron cyclotron heating system with three additional 1 MW gyrotrons in top-launch configuration has been continued focusing more on technology points of view and is described in this report in the section devoted to the TCV upgrades (Section 3.5.3)

3.2.1 ECH security

The existing EC protection system constrains EC current drive operation to small toroidal launch angle and in its present form has only limited machine coverage.

A new EC protection system, that will allow a more flexible operation of the EC installation and in particular operation with large toroidal injection angle, is being put in place. This system has automatic detection of high stray power and automatically stops gyrotron operation when it might compromise TCV machine integrity. It also has observers on all TCV ports. The new protection system is being commissioned at this time.

3.2.2 ECH Real-time control

The new distributed real-time control system has been successfully integrated and commissioned into the EC system. It is routinely, extensively and very successfully exploited for the scientific program of TCV. The results obtained with this system are described in this report in the section devoted to the research achievements.

3.3 TCV Diagnostics

3.3.1 Thomson Scattering and Interferometry

The Thomson scattering diagnostic hardware has changed little over recent years. As a cost saving measure, 10 of the spectrometers we transferred from CRPP's previous TCA Tokamak device and only have 3 spectral channels that are insufficient to cover TCV's wider temperature range. Furthermore, some of the APD detector modules have failed in recent years and are no longer available.

The diagnostic principles used in TCV's system are still used in systems designed today, and we are considering our options to a) ensure operations of existing spectrometers and b) replace the weaker spectrometers with an up-to-date design using modern components. In collaboration with the MAST group in the UK that have recently built a large Thomson system, we are considering the following approach.

1) Develop a new APD detector module that can be retro-fitted to our existing spectrometer and used in the design for the new spectrometer

2) Conceive the design of a new spectrometer module most probably similar to the MAST design that would save on design costs and, possibly, construction costs allowing us to obtain more spectral channels within our budget.

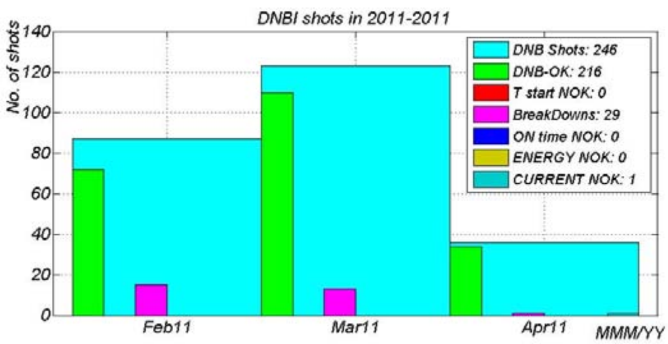

Fig. 3.3.1 Statistics of DNBI-TCV operation in February-April 2011

A channel of the MAST system is presently on loan at the CRPP where we are considering the use of APD devices with or without on-chip Peltier cooling and with or without on-board pre-amplifiers. Since each spectrometer requires at least 4 detector systems requiring a total of ~100 detector systems, this choice is financially important.

During 2011, the 1mm interferometer was successfully operated providing a backup for the more complex FIR measurement and lower noise at low densities. In contrast, the mechanical wobble of the FIR spectrometer, that has plagued low density operation over recent years, was considerably improved by re-tightening some of the optical alignment elements. During the early 2012 opening, the system must be dismounted from TCV for access purposes and special care will be taken when rebuilding the diagnostic to reduce the vibrations further.

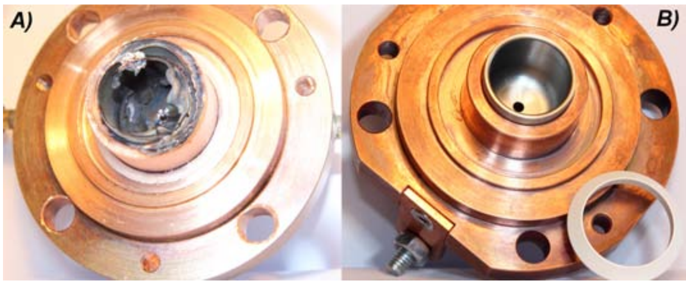

Fig. 3.3.2 *"Old" (A) and "re-fabricated" (B) cathodes of arc-discharge plasma source*

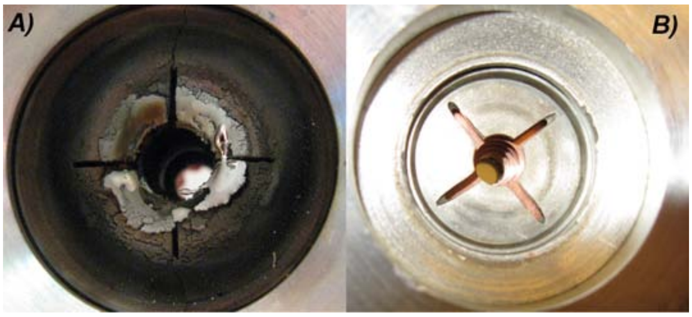

Fig. 3.3.3 *"Old" (A) and "re-fabricated" (B) arc-discharge channel with discs (diaphragms)*

3.3.2 Diagnostic Neutral Beam (DNB)

The Diagnostic Neutral Beam Injector (DNBI) was operated in February-April 2011 and used for active CXRS measurement of the plasma ion temperature, impurity (C^{VI}) density, toroidal and poloidal ion velocity profiles. Beam operation was suspended by the damage of the arc-discharge plasma source due to the source key elements resource life time limitation. The beam was operated for 173 plasma Tokamak discharges with a beam availability ~90%. The main faults were electrical breakdowns (11.8% of beam shots) in the injector ion optical system; the statistics of the DNB faults is shown in Fig. 3.3.1.

The arc-discharge plasma source operates since February 2010 after delivery in a contract with Budker Institute (Novosibirsk, Russia), integral operation time of about 2500 sec (1500 beam shots). Inspection shows critical damage of the cathode molybdenum insert (Fig. 3.3.2.A), floating electrode and channel disks (washers, Fig. 3.3.3.A). A long delivery period, procurement difficulties and quality control issues triggered a decision to manufacture a source at the CRPP. The fabrication technology and re-assembly procedure were developed and implemented (Fig. 3.3.4). Most parts were manufactured by CRPP workshop, with a few (molybdenum, tungsten, ceramics and elastomer) components were ordered from

Swiss and European industrial companies. The re-installation of the plasma source on the DNBI-TCV and continuation of the beam utilisation in TCV experiments is scheduled for the end of 2011. The developed in situ repairing/re-fabrication of the plasma source should make the annual source replacement requirement simpler and efficient, providing the potential for a strong improvement in DNBI availability for TCV experiments.

3.3.3 Charge Exchange Recombination Spectroscopy (CXRS)

The two new high speed Andor CCD cameras are now fully integrated into the TCV shot cycle. Considerable time was spent in tracking the passage of light from the Tokamak to the spectrometer's detector as we investigate the possibilities of improving the CXRS sensitivity. A full error reduction analysis was performed that concluded that a 50% increase in the spectrometer entrance slit widths would result in a small increase in the error in the ion temperature measurement with a linear increase in the system sensitivity.

A third, potentially high throughput, spectrometer, is used to observe the high field side toroidal rotation that has recently been requested for rotation symmetry experiments. Due to beam attenuation, this system is particularly challenged by a reduced signal level. Before a third high-sensitivity camera is purchased, the spectrometer is being stripped down to attempt to correct its present poor focussing performance. This should be completed by the end of TCV's 2012 machine opening for operations in 2012.

It is to be noted that the new cameras installed in 2010, now provide reliable high spatial and temporal ion parameter profiles for a wide range of TCV discharges. The increasing demand for this data for many TCV missions requires that this system operate reliably and as automatically as possible, putting quite severe constraints on a somewhat complex system.

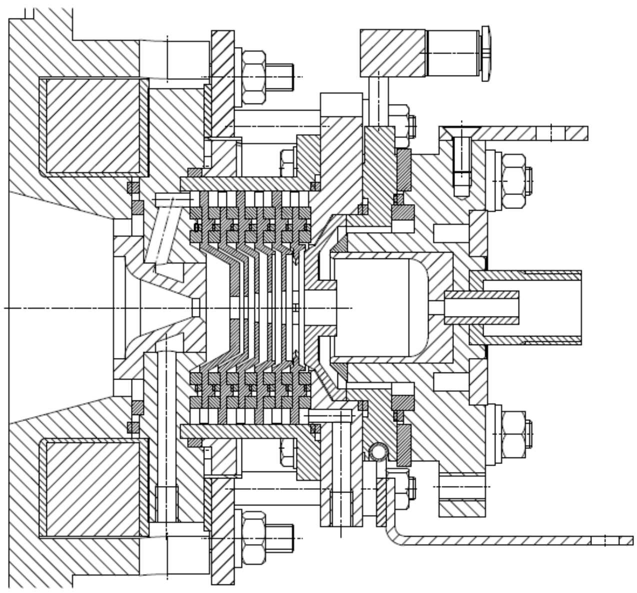

Fig. 3.3.4 *Arc-discharge plasma source re-fabrication design.*

3.3.4 AXUV and Foil Bolometer Tomography

Refurbishment of the 7 AXUV cameras was completed in September 2011. Following aging problems and poor filter transmission, the two diode array cameras were equipped with remotely controlled shutters to shield the diode arrays during cleaning, boronisation and other non-research orientated plasma operations. Furthermore, one diode array was intended for regular plasma operations and the second was kept shuttered from the plasma and used sparingly to monitor any sensitivity changes of the first array.

This, somewhat complicated, arrangement has immediately proved necessary when a sensitivity change of up to 60% in some detectors was discovered after only observing 60 TCV plasma discharges. The physical reason for this fast sensitivity loss is, as yet, unclear but seems mainly due to strong illumination from the plasma boundary (UV and VUV photons).

By limiting the diode's plasma exposure, preliminary cross-comparisons can be made between the Golf Foil bolometer array and the AXUV diode array

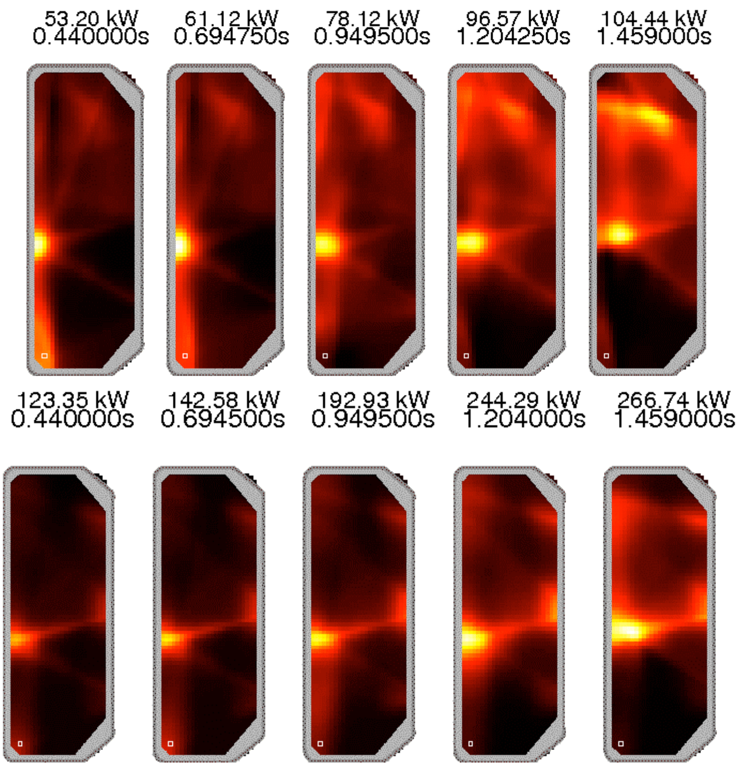

Fig. 3.3.4 *Preliminary bolometric inversions at five times during discharge #44697 (density increases with time) top: AXUV bottom:Foil-Bolometers. In this single-null-divertor configuration, there is a radiative mantle with a strong radiation region near the X-point*

3.3.5 Upgrading of the TCV ECE diagnostic suite

The suite of electron cyclotron emission (ECE) diagnostics on TCV was installed in the years 2000 to 2002. Some components are outdated and others are aging badly. There has been a sufficient degradation in the signal quality from a number of channels in the ECE diagnostic suite to merit an upgrade of the entire system. The TCV group decided to dedicate a large proportion of the available 2011 diagnostic resources for this upgrade and purchase of components has begun and some components have been already delivered and construction of the new radiometers has begun.

There are three ECE heterodyne radiometers installed on TCV. One radiometer has a line of sight viewing from the low field side (LFS) of the Tokamak and covers the radio frequency (RF) range 65GHz to 93GHz. A second ECE radiometer views the plasma from the high field side (HFS) and covers the RF range 86 GHz to 114GHz. Both radiometers have 24 channels working in the intermediate frequency (IF) range 2GHz to 20GHz, each channel having a bandwidth of 750MHz. The third device is a correlation ECE (CECE) radiometer designed to measure electron temperature fluctuations. The CECE radiometer shares RF signal with the LFS radiometer and comprises two tuneable narrow band YIG filters working in the intermediate frequency (IF) range 6GHz to 18GHz.

Upgrades to the LFS and HFS radiometers and to the CECE radiometer are now described.

HFS & LFS radiometer upgrade

It has been decided to build an image of the existing HFS and LFS ECE radiometers as their spectral coverage was optimised for TCV. The front end RF electronics will remain as is but the IF section will be renewed wholesale.

It has been decided to avoid use of multiple heterodyne sections replacing them with cavity filters and Schottky barrier detector diodes. It is hoped to this simplify greatly the IF sections to the upgraded radiometers.

48 cavity filters, imaging the same spectral coverage as the original radiometers, covering the range 2 GHz to 20 GHz have been purchased, along with 48 detector diodes. The filters are specified to have a rejection of greater than 50 dB with an insertion loss of less than 2.0dB. The detector diodes will have a sensitivity of 1000 mV/mW. The IF gain of each branch has been increased by the addition of four new amplifiers with 40dB gain and this will assure sufficient signal for most TCV plasmas.

It is planned to use the same model of video amplifier as developed for the CECE diagnostic (see below) with a bandwidth reduced to 100 kHz. IF components have been ordered for this upgrade and it is expected that they will be delivered before the end of the 2011. The upgrade should be ready for installation on TCV by June 2012.

CECE radiometer upgrade

The present CECE radiometer is a two channel device. Each channel comprises a 100 MHz bandwidth tuneable YIG filter, IF amplifier and detector diode. Following the detector diode is a video amplifier and finally data acquisition.

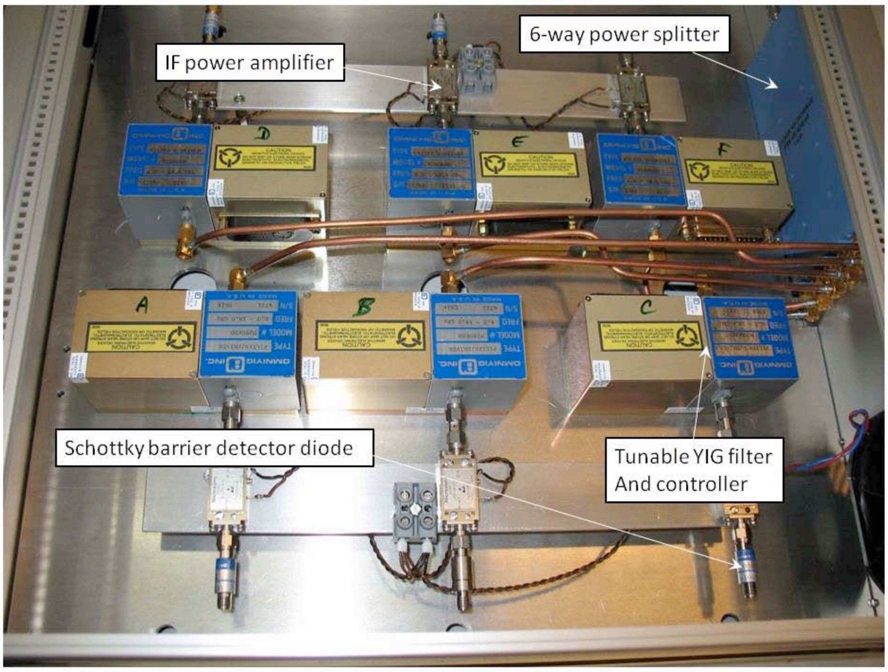

Fig. 3.3.5 *The IF section of the upgraded CECE radiometer which is now under construction. One the extreme right we see a blue six-way power splitter which is preceded by a 20 dB gain amplifier (not seen in this view). Six semi-rigid cables transport the RF power to six more 20 dB amplifiers that have high compression power level (> 20 dBm) and high harmonic distortion power level. After each of the power amplifiers we find the tunable YIG filters followed by the unbiased Schottky barrier detector diodes.*

The upgraded CECE radiometer will be a six channel device reducing by a factor 4 the number of pulses required to obtain estimates of radial correlation length of electron temperature fluctuations. IF amplification has been increased and care has been taken to choose amplifiers with low gain compression and minimal harmonic distortion. Figure 3.3.5 shows a picture of the CECE upgrade under construction. The new YIG filters are identical to the original filters having a bandwidth of 100 MHz and being tuneable over the frequency range 6 GHz to 18 GHz. The Schottky detector diodes are full band diodes (2-20 GHz) with a sensitivity of 100 mV/mW.
The video amplifiers, connected directly to the output of the Schottky detectors, will have programmable gain between 300 and 3000 with a fixed bandwidth of 450kHz (-50 dB at 600 kHz). The video stage electronic will be powered using true DC power supplies to prevent spurious spectral peaks appearing in power spectra of measured fluctuations from power supply modulation. The digitisers will be clocked at 1.7MHz precisely using new in-house built clocks ensuring no Nyquist limited effects in the acquired data.

The upgraded CECE radiometer will be tested during the months of December 2011 and January 2012 and for installation and commissioning on TCV during the late winter and Spring 2012.

3.3.6 TCV Protection System

As previously reported, following machine damage from EC power on TCV ports, (particularly those with windows), a pyroelectric detector assembly with a large gain range was developed and 30 such detectors mounted behind TCV diagnostic windows. One of the main reasons for EC power misdirection is an increased density refracting the EC power away from the plasma or the EC power being maintained even when the plasma density was lower than expected. A switching box integrates the 30 pyroelectric detector signals with individual thresholds to create an "error signal". The same box accepts a density measurement from one of the FIR interferometer channels which is compared to a maximum and minimum reference that are programmed before the plasma discharge such that if any of the detectors, or the measured density is outside the programmed range, the EC power is shut off.

An extensive series of test EC pulses over the whole range of EC angles was used to set the maximum signal thresholds for all the pyroelectric detectors. The system is now complete and will imminently be integrated into the TCV control and EC security

3.3.7 Hard X-ray tomography

Significant progress has been made in the development of a spectroscopic hard X-ray tomography diagnostic. In particular, the first of four eventual cameras (Fig. SC.1) was installed on TCV and is now fully operational after initial debugging. This instrument, and the three that will follow, are comprised of 24 CdTe detectors, plus an additional "blind" monitoring detector situated behind heavy tungsten shielding to discriminate against non-collimated γ rays. The primary goal of the diagnostic is to study for the first time the full 2D distribution of bremsstrahlung emission from suprathermal electrons, and compare its poloidal dependence with theoretical predictions. Two of the cameras, including that already installed, are rotatable by 90 degrees, to view the plasma tangentially when desired and thus allow analysis of the electron distribution function in 2D velocity space, both parallel and perpendicular to the magnetic field.

The first instrument has delivered the design performance, with ~7-8keV resolution in the 5-200keV energy range and a spatial resolution in the vessel of approximately 7% of the minor radius. A fast, low-noise electronic card built in-house has proven crucial in the success of the apparatus. Full digital acquisition of the entire pulse history, at a rate of 12 MSamples/s, provides for the first time complete flexibility in the details of spectroscopic analysis and statistical averaging. Pulse detection algorithms have been developed and tested for this purpose and are continuously being adapted and improved.

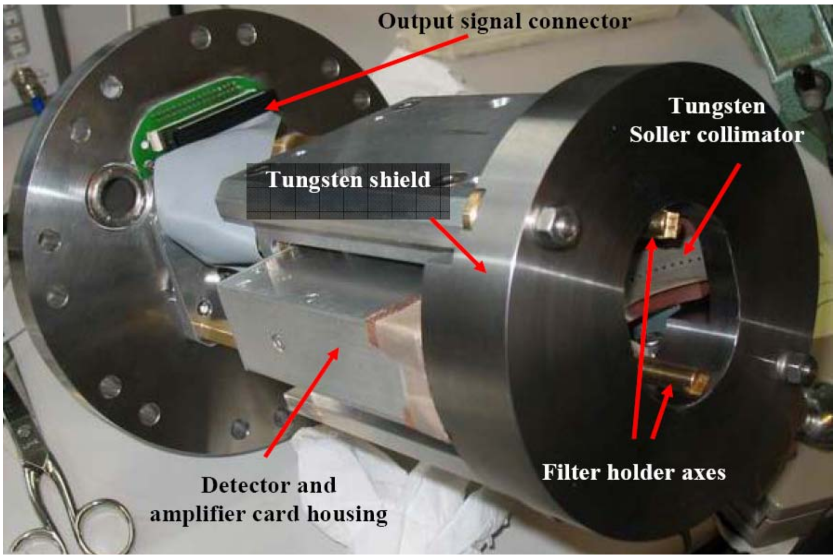

Fig. 3.3.6 *First hard-X-ray camera of the HXRS system prior to installation in the TCV tokamak*

Most procurements have been made for the remainder of the diagnostic and the primary vacuum interfaces for two of the remaining three cameras are already installed on the torus. The design and fabrication of the diagnostic is expected to be completed by mid-2012, with full operation beginning shortly thereafter.

3.3.8 Vertical Pulse Height Analyser

This system, consisting of a single silicon drift detector viewing the plasma through a collimator, measures line radiation from heavy impurity ions in the soft X-ray range with high energy resolution (200 eV). The diagnostic was reactivated on TCV in 2011 after a two year interruption due to manpower limitations. A spectral calibration was performed and a new, fully automatic, acquisition system was developed and integrated into the TCV shot cycle.

3.3.9 Reflectometry

In addition to an existing homodyne reflectometer (switchable between 78 and 92 GHz) on loan from IPP-Greifswald and the University of Stuttgart, two additional reflectometers have been transferred temporarily to TCV from collaborating institutions. A V-band, sweepable system covering the frequency range from 50 to 76 GHz is on loan from CEA-Cadarache and the Ecole Polytechnique Palaiseau in France; a U-band, 40-GHz system is on loan from FZJ Jülich in Germany. Both instruments are heterodyne. The coupling to the steerable launcher/receiver used for reflectometry on TCV has been made possible by fabrication of a dedicated horn by FZJ Jülich. The main waveguide used is in U-band, and the V-band instrument is coupled to it through a taper and a hybrid coupler. A linear polariser/splitter is employed to separate X- and O-mode radiation, with the 78-GHz reflectometer usually employed in X-mode and the lower-frequency systems in O-mode.

As these are single-channel instruments, their envisioned primary application for Doppler reflectometry (more accurately termed back-scattering) measurements, with the goal of studying plasma flows and especially their fluctuating components, which include the zonal flows and geodesic acoustic modes that are believed to play a crucial role in regulating turbulence and transport.

This reflectometer set has been installed on TCV recently and first tests are currently taking place. These instruments are expected to remain on TCV for the rest of the 2011 and part of the 2012 campaigns.

3.3.10 Tangential phase contrast imaging

A laser imaging apparatus has been installed on TCV to study core density fluctuations with extremely high spatial localization (down to 1% of the minor radius), thanks to a tangential arrangement. Work has resumed on this diagnostic after a one-year hiatus due to a lack of manpower. All subsystems have been tested and various initial problems solved. Final debugging is currently taking place and first data are expected imminently.

3.3.11 Edge diagnostics upgrade

Recent investigations, reported above, on the snowflake divertor has motivated an upgrade of the Langmuir probes system on TCV. At the present time, three arrays of probes are installed in TCV: 26 probes cover the machine floor, 34 are mounted on the central column of the torus and 19 on the upper part of the TCV outer wall. A new array of 19 probes will be installed in the lower part of the TCV outer wall. This new array is a replication of the existing LFS system but in the lower half of the machine and will be mounted in sector 16. This new array of probes will improve the diagnostic coverage, in particular, for the snowflake diverted plasmas, where simultaneous heat load measurements around the four strike points will now be possible (see Fig. 3.3.7). This will significantly improve our diagnosis of the snowflake divertor properties and its possible advantages compared to the single-null divertor. This new array of probes will be also useful in the characterisation of diverted plasma at negative triangularity.

A new heated tile will be installed on the central column of the TCV vessel in front of the port where an IR camera can be installed for calibration and alignment purposes. These upgrades will be accomplished during the early-2012 TCV vacuum opening.

In order to better diagnose the plasma boundary, a new reciprocating probe is under study in collaboration with colleagues from Consorzio RFX, Padova (Italy). This will be a multi-head probe and will feature several reciprocations during a single TCV discharge. It is also hoped that the availability of a Real-Time plasma reconstruction can be used to get closer to the plasma boundary without burning the probe tips.

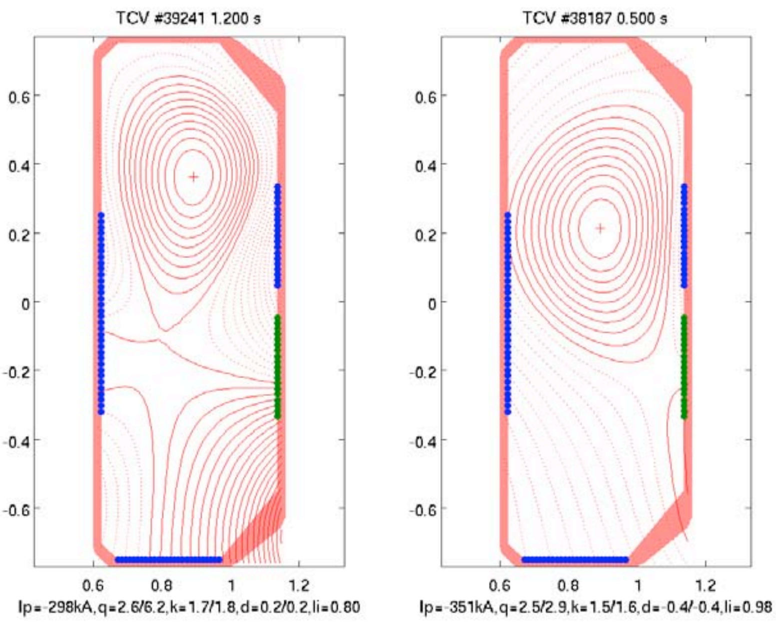

Fig. 3.3.7 *Reconstructed plasma equilibrium for a snowflake divertor plasma (left) and a single null diverted plasma at negative triangulariy (right). The blue dots represent the existing Langmuir probes. The new array of probes is shown with the green dots.*

3.3.12 Vertical InfraRed Camera

The core of the Vertical InfraRed (VIR) camera system is a Thermosensorik CMT256M HS, a camera using a 256x256 pixel semiconductor detector with CMT (Cadmium Mercury Telluride) technology with sensibility in the infrared range 1.5-5.1 m. The photons emitted from the vessel's tiles surfaces in the short to medium wavelength infrared (SWIR-MWIR) pass through a relay optic, consisting of a folding mirror and a number of lenses (6 made of Si, 1 from Ge), and are detected by the CMT chip, amplified and then subsequently digitised to 14 bit resolution. The main task of the diagnostic is to observe the heat deposition at the strike point located on the floor tiles of TCV on a fast time-scale (up to 25kHz) enabling ELM- and disruption-related studies, as well steady-state divertor behaviour. Assuming a given tile surface emissivity, each pixel's signal may be converted into a surface temperature providing information about the spatial and temporal temperature distribution on the surface of those tiles. Once the tile surface temperature profiles have been calculated, can codes (e.g. THEODOR - Thermal Energy Onto DivertOR) can estimate the tile incident heat fluxes impinging the strike points.

During 2011 the system has been revised to reduce image vibration seen during plasma operation and thermal data acquired for the snowflake and single-null divertor configurations.

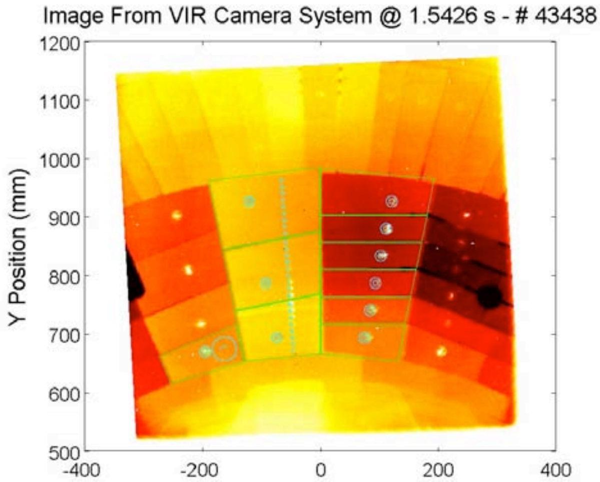

Fig. 3.3.8 *Example image of the TCV vessel floor tiles using the Infra-Red camera. The brighter floor tiles (slightly left of centre) have a thin surface layer that requires modified emissivity coefficients to obtain valid temperatures but reacts faster to temperature changes.*

3.3.13 Oblique ECE

A Matlab interface for controlling the fast-polarizers in real-time has been written and successfully tested. The integration of this interface into the TCV control system is ongoing.

3.4 TCV control

Over the past year the TCV control system SCD (Système de Contrôle Distribué), installed in its present form and commissioned in 2010, was employed in a multitude of new applications. This not only provides access to new operational modes and plasma parameters but also makes achieving the parameters of previous experiments more robust resulting in a more efficient use of the limited TCV pulse operations time.

The basic philosophy underlying the architecture of the system is its modularity and expandability. A set of independent nodes, each with their local real-time (RT) program running on their CPUs, is interconnected across a shared memory system, where each node writes to its reserved space in this memory while retaining read access to the data written by other nodes. This naturally allows each node to have a different clock rate and/or to interact with different diagnostics and/or perform different tasks. Thus, as needs increase and more diagnostic information is available in a form useable for RT control, extra modules can be introduced without requiring major changes in the system topology.

At present, two of the nodes are connected to complementary sets of diagnostics and actuators. One node is connected to X-ray (DMPX, XTe) and interferometer (FIR) channels and has the capability of controlling the ECH system including launcher mirror angles and power. A second node is connected to the main TCV magnetic diagnostics set including flux loops and magnetic probes, as well as photodiodes. This node can control the full set of 16 independent PF coils and the 2

Ohmic coil circuits, gas valves, as well as control the ECH system. In effect, this node was designed to replace the functionality of the TCV hybrid control system with the exception of control of TCV's fast internal vertical coil.

Of the other two nodes available, one is a dedicated computational node and is not equipped with analog input/output hardware. The final node is, at present, spare and available for other applications but could be quickly equipped to incorporate more diagnostic data into the control system.

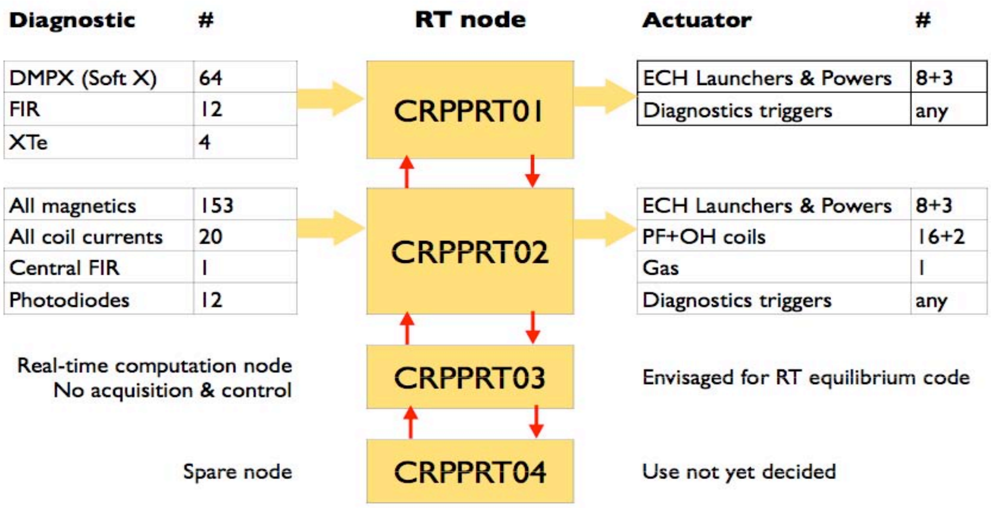

Fig. 3.4.1 *Overview of SCD nodes with connected diagnostics and actuators. Each node can run at a different clock rate and run different algorithms as each node hosts its own CPU.*

One new possibility, available with the new control system, is to react on events on the plasma as they occur in real-time, rather than relying on pre-programming that will only function if the plasma pulse develops as expected. Particular examples of this include real-time diagnostic triggering, in which the acquisition by certain diagnostics is triggered by the detection of an event of interest, such as sawteeth. More recently, this concept has been expanded in to that of "pacing", a promising new method for MHD instability control in which the instability is triggered by an appropriate actuator (usually ECH) based on the time of occurrence of the *previous* event. Application of this technique to the sawtooth instability is shown in Section 2.1.6 and application to ELMs is discussed in Sections 2.1.2 and 2.1.6. On the control side, these algorithms rely simply on a resetable software counter which triggers a command (diagnostic trigger, EC power command...) when the counter value reaches a given value. Implementation of such algorithms is greatly facilitated by the Matlab-Simulink interface, which allows the user to build and test block diagrams in an intuitive and straightforward manner.

Control methods for neoclassical tearing modes (NTMs) have further been explored by developing the capability of (full or partial power) modulation of the gyrotron power based on a PLL (phase locked loop) signal locked to a magnetic probe signal. This will enable future studies of NTM stabilisation physics using modulated power in the O or X point of a magnetic island, compared to the phase of the gyrotron power modulation.

Other algorithms which have recently been developed include enhancements to the operation in so-called IOH control mode. In this mode, the Ohmic coil current is controlled in feedback, rather than being adjusted to maintain a desired plasma current. The limitations of the hybrid control system meant that transients in the coil currents could occasionally occur which would lead to plasma disruptions. Using adjustments in the digital system, this problem is now resolved such that independently of the previous plasma evolution, the plasma current transition from fed-back to constant is always smooth.

Many other systems that previously required the physics operators to “out-guess” the machine conditioning evolution are being encoded into RT control loops. Work is, for instance, underway to commission an enhanced plasma density controller, exploiting the nonlinear control capabilities to produce a controller taking into account the asymmetric nature of the control problem due to gas valve saturations. This should allow for more robust density control over the, sometimes large, variation in TCV plasma wall gas recycling behaviour.

The development of the new RAPTOR code has been discussed in the previous report, but has been further validated and tested more recently. The RAPTOR approach of “real-time simulation”, simulating the plasma poloidal flux profile evolution in real-time, allows each diagnostic to provide the information it has available to further constrain the real-time estimate of the plasma state. In all, each element of the control system works in concert to provide an accurate and consistent picture of the plasma conditions at any given time with the available measurements. Loss of a particular diagnostic, or degradation of its accuracy, leads to degraded accuracy of the overall system but not of loss of the plasma state information. Control decisions based on this enhanced situational awareness are by therefore more robust than control decisions directly based on diagnostic data.

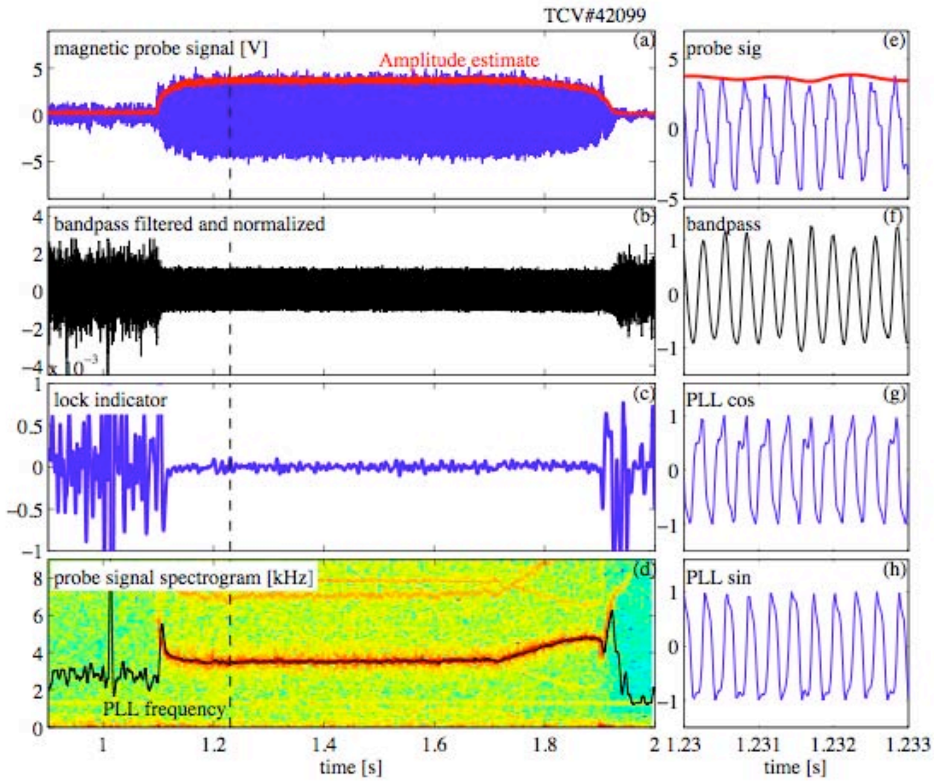

Fig. 3.4.2 *Example of real-time PLL (phase-locked-loop) processing of magnetics data to yield information about NTM frequency, amplitude, as well as to provide reference signals for gyrotron power modulation. For this application, the SCD node runs at a clock rate of 50kHz.*

In the future, it is planned to expand this paradigm to include real-time reconstruction of the plasma shape by a real-time version of the in-house TCV Grad-Shafranov equlibrium reconstruction code LIUQE. In this framework, the real-time 1D poloidal flux profile is combined with knowledge of the 2D poloidal flux map to yield a complete map of the TCV plasma state during the discharge.

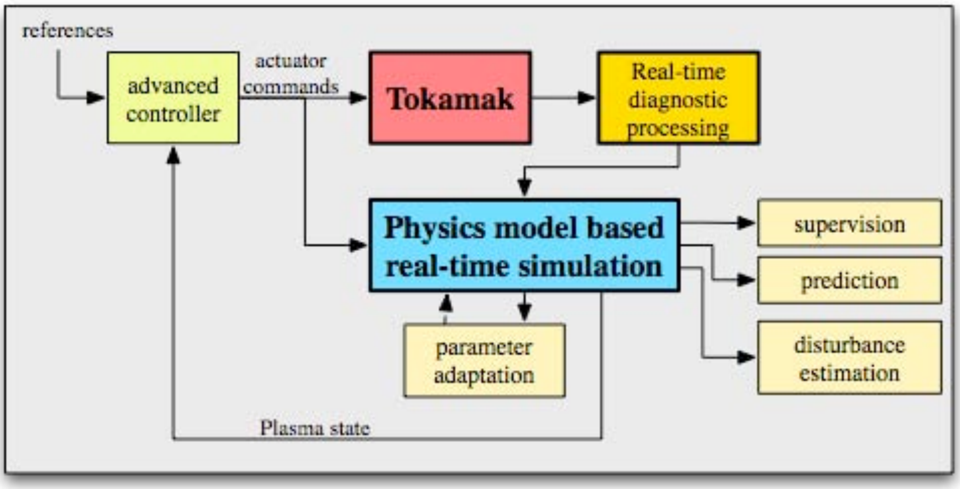

Fig. 3.4.3 *Overview of the real-time simulation paradigm at the basis of the RAPTOR concept. Diagnostics feed into a physics-based simulation, enhancing its accuracy and reliability. This physics-based estimate is then used for various applications in stead of relying purely on diagnostic data.*

3.5 TCV upgrades

3.5.1 Introduction

A number of upgrades should be implemented on TCV to extend its operational domain towards the burning plasma regime and enhance the reactor relevance of its results. This implies heating high-density plasmas with variable ion and electron temperature ratio, and exploring new plasma shapes.

Although financial support for the upgrades still needs to be secured, feasibility studies and preparation work have already started since a few years ago. The preliminary design of the ELM control coil system was previously completed.

As detailed below, activities in 2011 focused on the minimal set of upgrades that was endorsed in a recent audit, encompassing the installation of a ~1MW neutral beam heating system and an increase of the microwave plasma heating power at the third harmonic (2MW). These, together with the modifications of in-vessel components (low-field-side tiles) necessary to combine shape capabilities with increased heating power, will put TCV in a unique position to contribute to ITER and DEMO physics basis. In fact, TCV will become able to desentangle effects of electron-ion coupling, rotation, q_{95}, edge density control and shape, in L- and H-modes and study heat, particle and momentum transport in dominantly electron heated discharges with varying T_e/T_i and keeping shape flexibility.

3.5.2 Neutral beam heating

Numerical simulations of TCV scenarios of relevance for neutral beam heating have been undertaken using the ASTRA code. The injection of 1-2MW Deuterium or Hydrogen beams (up to 1MW per injector) with energy below 35keV would allow to access T_i/T_e ratio >1 and higher plasma pressure (β) in both L- and H-mode, in high density plasmas (>$4\times10^{19}m^{-3}$) compatible with third harmonic (X3) EC heating. The lower power (0.5-1 MW) 20-25keV deuterium NBI at intermediate ($1\text{-}3\times10^{19}m^{-3}$) plasma densities is suitable for experiments at lower plasma current (100-250kA) with X2 ECH and ECCD. The tangential double path NB alignment is considered to decrease the shine-through losses and avoid strong first orbit losses, especially at low plasma current. The possibility of gradually varying the injected into tokamak power (in the range of 30-100%) during the plasma discharge of about 2 sec is essential for the TCV. Two balanced NBIs (one in Co- and another in Counter-current direction) would allow us to investigate the effects of NB induced plasma rotation, fast ion behaviour and MHD physics in scenarios such as stationary ELM free H-modes and fully non-inductive electron internal transport barriers. The effect of fast ion orbit losses has been numerically studied using the VENUS code and confirms earlier results on good confinement of 25-35keV ions injected in Co-current direction and strong losses in the case of Counter-current injection at plasma currents below 100-150kA.

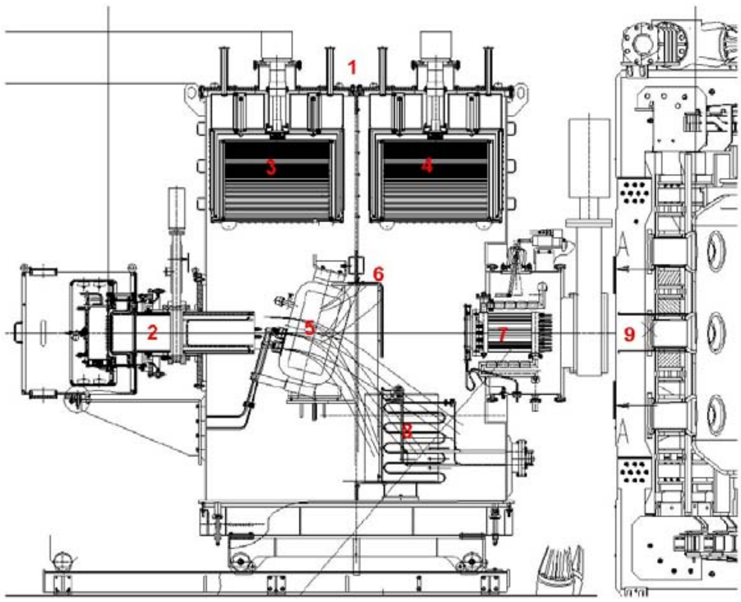

Fig. 3.5.1 *Proposed NBI-TCV layout: 1 – injector vacuum tank, 2 – neutralizer tube, 3,4 – cryo-pumps, 5 – bending magnet, 6 – central diaphragm, 7 – V-target, 8 – ion dump, 9 – beam outlet.*

A preliminary study of the NB injector(s) design suitable for the TCV has been completed by the Budker Institute of Nuclear Physics, Novosibirsk and approved by the CRPP. The mandate covered the design of the NBI layout, the optimisation of the ion optical system and plasma source, an assessment of vacuum conditions in the injector duct, and the optimisation of the TCV port extension for tangential injection of the beam. A geometrically focused ion beam is formed in the ion source section of the injector using a multi-slit triode ion optical system from a RF plasma emitter. The injector is equipped with a neutralizer, a bending magnet, a residual ion dump and a moveable calorimeter (Fig. 3.5.2). The implementation of such injector layout for the TCV required the distance between the injector Ion Optical

System (IOS) and the beam entrance to the TCV vacuum vessel to be about 3300mm. This permits to install the movable calorimeter (V-target) suitable for full duration (2sec) beam conditioning, tests and measurements. The existing design of the triode IOS with round (about 5mm diameter) elementary cell and angular divergence of 30mrad is not suitable for TCV due to access restrictions. A multi-slit triode IOS with a divergence of 8×18mrad is proposed as a basic variant for the NBI-TCV. The port of 200×220×480mm with the 190mm diameter circular diaphragm permits to transmit 1MW beam in TCV without significant losses on limiters (about 2%) and beam blocking. Two helium cryopumps are used for differential pumping of the injector tank, which is divided into two parts by a diaphragm to reduce the gas pressure on the beam entrance in the tokamak. In the chosen layout the power load from the beam at the surface of the tokamak central column does not exceed 1.7MW/m^2, which is well below the limit of 7.6MW/m^2 for the existing TCV first wall. On the other hand, the maximal possible power load (without plasma attenuation) on the beam dump on low field side tokamak wall, about 10MW/m^2, requires a modification of the VV beam facing components. The neutral beam power during a pulse can be controlled using a simultaneous adjustment of beam energy and ion beam current. The energy and current should correspond to the Child–Langmuir low for keeping of optimal beam formation with minimal beam angular divergence.

Fig. 3.5.2 *Stresses in the outer shell of the TCV vacuum vessel, with plasma disruption loads and atmospheric static pressure applied.*

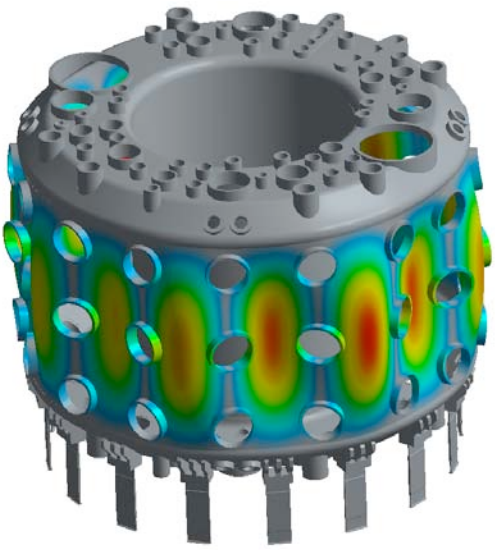

Fig. 3.5.3 *Fundamental buckling mode in the outer shell of the TCV vacuum vessel.*

To implement the tangential NB alignment on TCV, a modification of the tokamak vacuum vessel to create new ports, specially designed for NBIs and fitted between magnetic field coils, for which modification is not feasible, is considered. CRPP has contacted the vessel manufacturer De Pretto Industrie S.r.l., Schio, Italy, concerning in situ modifications of the TCV vacuum vessel to provide access for two neutral beams. A contract on the technological feasibility of the in situ vacuum vessel modification should be established to define the sequence of activities and the boundary conditions for the installation of the two new tangential NBI ports on TCV. The 3-D complete models (drawings) of the TCV vacuum vessel and structural elements have been developed as background for the existing VV and will be completed this year to accommodate the tangential port design. The preliminary structural ANSYS FEM analysis of TCV VV has been completed in order to assess the structural margins against pressure and electromagnetic loads, as shown in Fig.3.5.3, and various cases of buckling (structural instabilities), see Fig.3.5.3. Among the many technical challenges facing the in-situ upgrade of the vacuum vessel, highest priority is given to the accurate prediction of structural stresses and buckling margins after machining and re-welding, without the possibility of thermal annealing.

3.5.3 TCV/EC-system upgrade

X3-1MW/2s gyrotron

During 2011, the main effort with regard to the X3-upgrade project on TCV has been devoted to the detailed gyrotron design by including new physical phenomena (beam duct instabilities, after cavity interaction, trapped secondary electrons in the electron-gun, see section 2.4) and technological constraints aimed at taking maximum advantage of the industrialization process carried out by Thales Electron Devices (TED) on the 140GHz gyrotron for W7-X.

The foreseen X3-upgraded gyrotron should radiate at a frequencies between 115 and 129GHz, with an output power of 1MW and 2s pulse length. In view of not only satisfying the needs of TCV, but also those of other experiments needing ECRH, the gyrotron design has been carried out with the aim of having a dual frequency gyrotron of MW-class, with CW capabilities and operating at a second frequency close to 170GHz, which is the ITER frequency.

Starting form the preliminary design carried out in 2010 (126.2GHz on $TE_{26,7}$ mode and 168.45GHz on the $TE_{35,9}$ mode), the detailed gyrotron design is being developed by exactly satisfying the ITER frequency of 170GHz and allowing the lower-frequency to be in the range suitable for TCV X3 top-launch heating. Moreover, compared to the preliminary design, the design strategy has been refocused to use the largest possible fraction of the sub-systems that are already in place for the 140GHz gyrotron.

The final design will require further iterations with TED and verifications by our collaborating partners within the EGYC consortium (KIT, Germany; HELLAS, Greece), but the present status of the design is advanced enough that TED should be able to provide a quotation by the end of 2011.

The main features of the detailed design are highlighted below:

Electron-gun: as already determined during the preliminary design phase, for a dual-frequency gyrotron based on the W7-X/140GHz gyrotron design a triode Magnetron Injection Gun (MIG) is necessary. In the detailed design phase the additional constraint of having exactly the same cathode stock geometry and only shaping the control anode for optimizing the electron-beam parameters has been imposed. The electron-optics gun-design was initiated at CRPP in 2010 using the ARIADNE code developed by Dr. I. Pagonakis and is presently continued at KIT since Dr. Pagonakis has moved there.

Beam-duct: the beam duct will have the exact same damping structure as the last version presently implemented in the W7-X series gyrotron, for which it has successfully solved the issues related to beam-duct instabilities. Extended electromagnetic simulations of this structure have been performed during 2011 in collaboration with CERN and have allowed us to gain a significant physical understanding on the wave-particle interaction occurring in this complex damping structure.

Cavity-launcher: the cavity-launcher geometry will be nearly identical to the one of the 140GHz gyrotron, with the only difference of adapting the cavity radius in order to exactly match the 170GHz frequency. Using the TWANG code, the optimization of the DC magnetic field profile in the launcher section in order to prevent static and dynamic After Cavity Interaction is ongoing.

Quasi-optical converter: further verifications performed at KIT will be done to assess whether the present design of the QO-converter implemented in the W/-X gyrotron can be used as is.

Collector: the collector geometry will be the same as for the present W7-X gyrotron with the transverse magnetic field sweeping system, which has recently demonstrated to generate the most homogeneous longitudinal power deposition profile. For the operation of the gyrotron on TCV where 1MW/2s are required, it is very likely that no beam-depression will be necessary since the collector equilibration time is of the order of 7-8s. If this operational feature on TCV is confirmed by TED it will allow to avoid using an additional HV power supply normally used in the depressed collector configuration.

Global vacuum chamber: the external gyrotron geometry will be exactly the same as the one of the W7-X gyrotron.

X3 top-launcher

In view of using the present X3-top launcher, further studies on the electromagnetic and thermo-mechanical propoerties have given rise to the following conclusions:

a) Thermal calculations using the present X3 top-mirror geometry and assuming an injected power of 1MW/2s, corresponding to the rf-beam of one gyrotron, show that the peak temperature rise after 2s is as high as 60^{o}C. The ballistic equilibration time (neglecting heat conduction and radiation) is of the order of 70s with an equilibrium temperature rise of 7^{o}C. Knowing that this is a pessimistic value and that the typical TCV intra-shot time is larger than 10min this result allows us to avoid any active cooling on the mirror, which significantly simplifies the launcher design.

b) The present X3 top-mirror geometry is such that 3 rf-beams are converging on the mirror surface and are reflected vertically-down towards the TCV-plasma. In this configuration, the central rf-beam has a normal incidence on the X3 mirror. Therefore the injected rf-beams have also a normal incidence on the bottom part of the TCV vacuum chamber. The reflected power from the bottom part of the vacuum vessel has in the past generated stray radiation levels problematic for different plasma diagnostic located in the same TCV toroidal sector. In order to avoid direct reflection from the bottom part of the vacuum vessel a redesign of the X3-mirror supporting structure is presently being carried out.

3.6 Superconductivity

The 25 years old power distribution cabinet in the SULTAN hall and all the related cables has been replaced under the responsibility of PSI, see Fig. 3.6.1.

Under bilateral service contract with the ITER Organization, one spare electric motor for the compressor of the SULTAN refrigerator and one vacuum furnace for the heat treatment of the Nb3Sn SULTAN samples have been procured in 2011, see Fig. 3.6.2. The spare motor, equipped to fit the mechanical and electrical interfaces as the existing one, has been delivered in September 2011 and stored at PSI. The vacuum furnace has been delivered in July 2011 and put in operation in November 2011 with the dedicated vacuum pumps and control system.

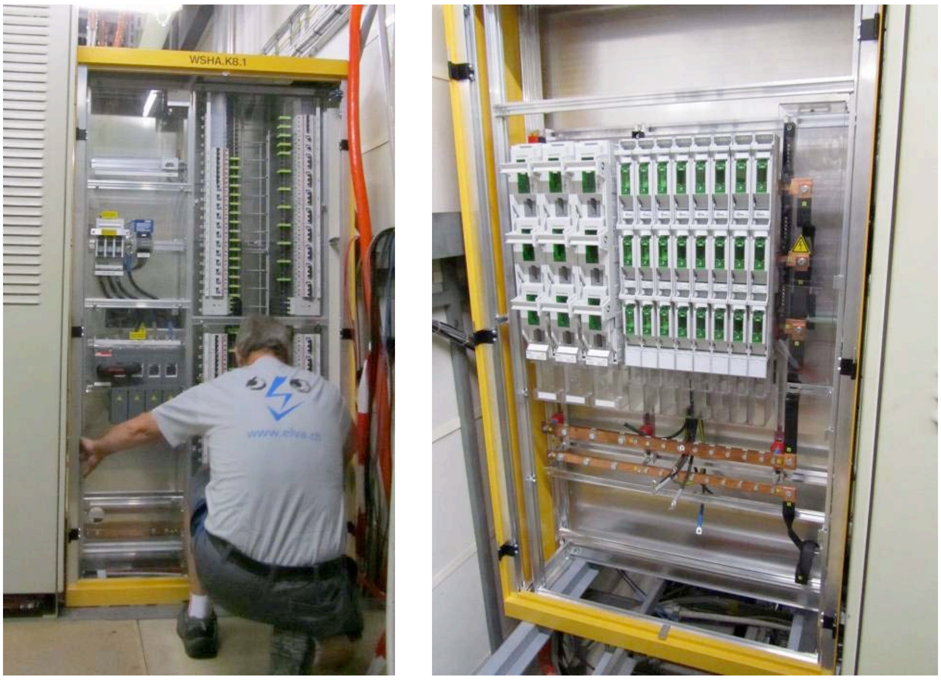

Fig. 3.6.1 *Front and rear view of the new power distribution cabinet*

Fig. 3.6.2 *The spare motor for the Sultan compressor (left) and the furnace during installation (right).*

4 ACTIVITIES IN SUPPORT OF ITER

4.1 Introduction

Most of the research programme of CRPP is related to fusion development in general and to ITER in particular. In this chapter we assemble the more specific activities directly linked to the ITER project. They are covered by IO, F4E or Domestic Agencies grants and contracts.

4.2 ITER 170GHZ gyrotron

OPE-094 Supply of Mirrors for the RF-Conditioning Unit (RFCU)

A supply contract between F4E and CRPP was signed for the procurement of new mirrors for the RFCU. This is necessary because of the updated, and hopefully improved radiation pattern of the refurbished tube.

Three new mirrors were fabricated and installed in the RFCU. The new design uses one flat mirror (now allowing better matching of the optical axis of the gyrotron beam to the optical axis of the waveguide) and two focusing mirrors. The latter were designed using a new optimization code based on the results of S. Jawlas PhD thesis (see AR 2010 section 4.1.7). Their surfaces are elliptic paraboloids so that the phase changes introduced upon reflections optimize the power transmission to the waveguide as well as the matching of the complex electric field to the desired HE_{11} mode in the waveguide. The power transmission from the window to the waveguide is >95% and the coupling into the HE11 mode is >95%. The losses in the insert are ~0.05% and the total ohmic losses on the mirrors are ~1.1%. The expected beam pattern transverse to the direction of propagation is shown at several positions in the RFCU in Fig. 4.2.1 on a linear scale. The peak power density at each cross-section is listed below the frames and the size of the mirrors (or apertures) is indicated by red circles (note the change in scale of each frame).

One mirror is shown, being measured for mechanical certification, in Fig. 4.2.2 and the insert is show in Fig. 4.2.3. Following water and vacuum leak-tightness testing (presently on-going), the contract will be closed.

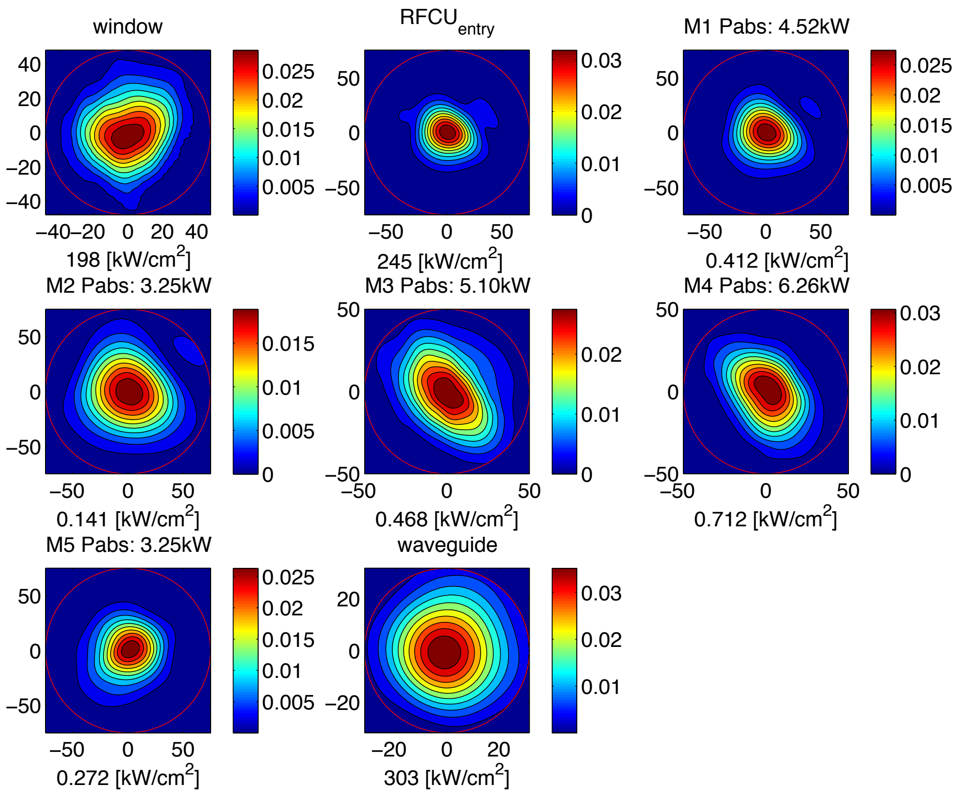

Fig. 4.2.1 *Electric field amplitude pattern in linear scale, at various locations, with an indication of the peak circulating power density (at the window, RFCU entry and at the waveguide), or the peak ohmic loading (M1, M2, M3, M4 and M5).*

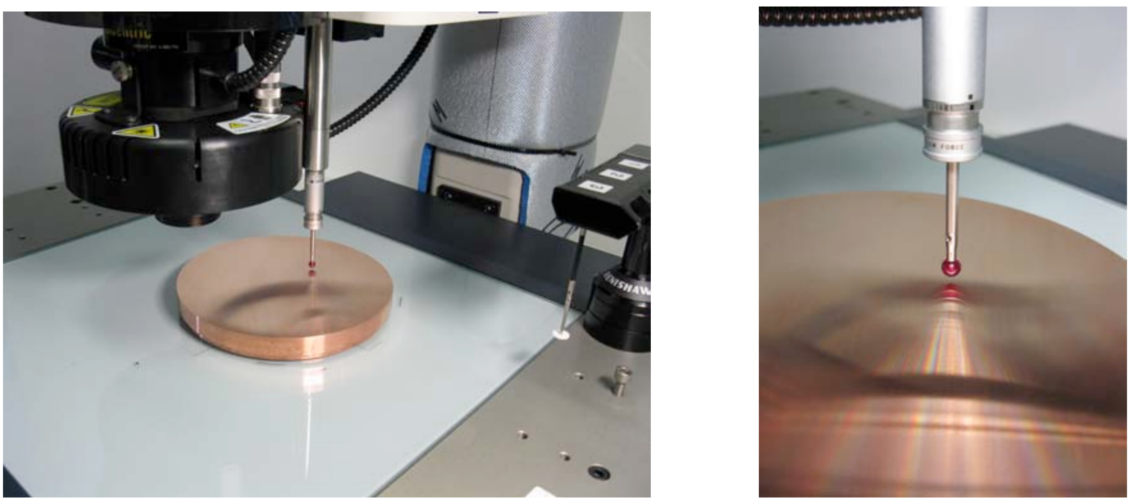

Fig. 4.2.2 *Work zone of the 3D measuring machine, using optical and mechanical probes (left), and enlargement of the ruby tip above the mirror surface (right).*

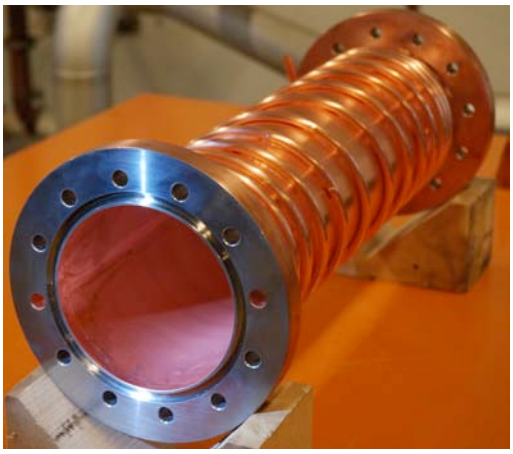

Fig. 4.2.3 *Finished insert with copper coating (nominally 5–10µm, skin depth 0.2µm at 170GHz) ready for installation.*

4.3 The ITER Upper Launcher for Electron Cyclotron Waves

Preparation of the ITER Upper Launcher Consortium

In anticipation of grants and contracts from F4E for work on the ITER electron cyclotron (EC) upper launcher (UL), negotiations were undertaken to establish a consortium of associates possessing between them the requisite manpower and expertise to cover the scope of the expected work. This resulted in the creation of ECHUL-CA (electron cyclotron heating upper launcher - consortium of associates) who successfully bid for and received a first grant for the finalization of the design of the ITER EC UL.

F4E-GRT-161

The first grant for the finalization of the ITER UL has been given to ECHUL-CA. The work is concentrated on the first confinement system (FCS) but requires an update of the quasi-optical portions of the launcher system as well, taking into account the various modifications to the ITER vessel, issues raised by the expert panel, etc. since the time of the preliminary design review (PDR) in November 2009.

A very significant effort has been made to establish, with our partners, a baseline and proper work plan to ensure a timely efficient and traceable execution of the works. Additionally, closer ties and new methodologies have been established amongst the associates to ease the inevitable transfer of information and enhance our collaboration.

Prototype testing of machine springs for the ITER EC Upper Launcher

Prototype testing of the springs, a critical element of the UL, was continued in the test facility at CRPP. After a complete revision of the test device, with all worn parts replaced, a set of prototype springs was cycled at the limits of the load specifications, nearing $4x10^6$ cycles. The cycling will continue until failure occurs. Figure 4.3.1 shows the test jig for the springs.

Fig. 4.3.1 *The machine springs are held is a special refurbished jig to permit cyclic testing to failure in a heated vacuum chamber mimicking ITER conditions.*

4.4 Superconductivity ITER studies

4.4.1 Tests in SULTAN

The activities in support of ITER are focused on the test in SULTAN of the ITER conductors, carried out under bilateral contracts with the Domestic Agencies and the ITER Organization. In 2011, following samples have been tested:

1. JATF5 and JATF6, Japanese qualification and process qualification samples for the toroidal field conductors, under contract with JAERI. The sample assembly was done in 2010, the test in SULTAN was carried out in January/February and March. A re-test of JATF5, funded under contract with IO was carried out in April.
2. CNPF2, Chinese qualification sample for the poloidal field conductor of coil PF5, under contract with ASIPP, in March.
3. CNTF3, Chinese TF conductor sample (bronze strand). Re-test campaign after thermal cycles under contract with IO, in May.
4. Trasek, CRPP conductor sample for the secondary winding of the EDIPO transformer, under contract with F4E, second test campaign with solder filled termination, April.
5. JACS2, second Japanese qualification sample for the Central Solenoid conductor, under contract with JAERI, May-June-July. Two re-test campaigns funded under contract with IO were carried out in August and in December.
6. CNCC2, Chinese qualification sample for the Correction Coil conductor using NbTi strand, under contract with ASIPP. The test campaign was split between July and December.
7. CNMB1, Chinese qualification sample for the Main Busbar conductor using NbTi strand, under contract with ASIPP, July-August.

For each test in SULTAN, a detailed report including results assessment is handed to the respective funding agency.

4.5 The development of the ITER magnetic diagnostics

Development of magnetic sensors (Grant F4E 012)

This year saw the end of the development work on this F4E Grant and the results were presented in June this year. The work involved CEA, RFX and CRPP. The qualification tests of the sensors procured during the Grant were excellent with the exception of the vacuum tests of prototype Rogowski coils. CRPP contributions to the large inductive sensors to be placed outside the vacuum vessel included the frequency response and also the precision of the geometric and magnetic axes.

Fig. 4.5.1 *Layout of the magnetic axis qualification test inside a Helmholtz coil pair*

Contributions to the Rogowski cable included the tolerance to mechanical and thermal abuse, and a measurement of the thermal expansion at liquid nitrogen temperature.

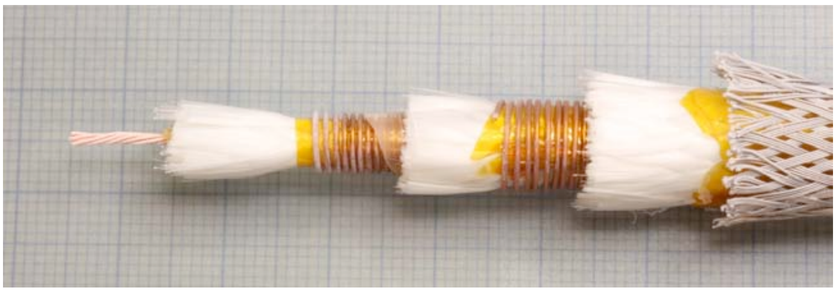

Fig. 4.5.2 *Sample of the Rogowski cable during expansion tests.*

Another qualification was to look for hysteresis of the sensitivity when cooling to liquid nitrogen temperatures.

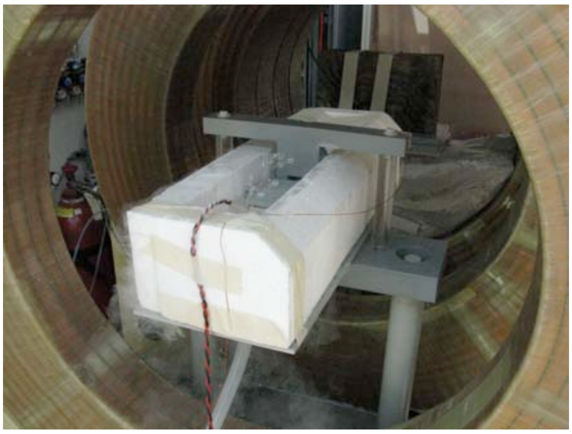

Fig. 4.5.3 *Rogowski cable at LN2 temperature inside a Helmholtz coil configuration*

4.6 ITER discharge simulation

Self-consistent simulations of ITER scenarios (Grant F4E 255)

This year saw the first half of an F4E Grant combining CCFE, TU Vienna, CREATE, CEA and CRPP. CEA and CRPP worked together on two specific scenarios, namely the 12.2 MA hybrid scenario and the 10MA steady state scenario. The tool used was CRONOS in standalone, performed by CEA, and DINA-CH&CRONOS performed by CRPP. Several enhancements to DINA-CH were made before the Grant started to align the simulator with current ITER thinking. The first part of the Grant was to set up a new simulation environment with the new ITER geometry and with the internal VS3 coils. A number of technical improvements had to be made to the DINA-CH code and to the CRONOS code due to the high edge pressure gradients in these scenarios and to the presence of the VS3 coils. An initial submission of the results was encouraging and led to an extension of the Grant. Final simulation results will be reported in 2012.

4.7 Support for Plasma Control and CODAC

CRPP continues to support the evolution of Plasma Control and CODAC for ITER, chairing a Conceptual Design Review and as a member of a Preliminary Design Review for CODAC. There remains a strong link between the ITERIS modelling activity, reported elsewhere, and CODAC. Plasma Control was a voluntary activity inside the Plasma Control Working Group during 2011.

4.8 ITERIS

The ITER integrated simulation (ITERIS) consortium-team is under contract with IO to provide the services for the Design and Implementation of an Integrated Modelling Infrastructure. The first Task, carried out in 2011 with a final report accepted in March 2012, was dedicated to the conceptual design of an integrated modelling infrastructure.

The global strategic functionalities have been laid out in a document discussed between the I IO and the IMEG group ("The ITER Integrated Modelling Programme" IDM reference 2EFR4K). The ITERIS team first analysed this document, proposed some amendments to better take into account the activities in support to plasma operations and in support to the physics research, which are the two main areas of the integrated modelling activities.

In the initial phase of this work, several use cases have been identified and studied in details, in order to make sure to cover the main modelling activities expected, both at the ITER site and at the DAs sites. This lead to the first report, D1.1, on *Use Cases and Strategic Requirements for the ITER Integrated Modelling Infrastructure*). This document deals with the relation with data (the need for a simple and well-defined data model, the data reference, the data storage and access), with the ITER modelling infrastructure itself (access to advanced computing resources, interactivity, external access to the IM infrastructure, lifecycle management, supported software, ...), with the link to the plant operating zone (data flow, Pulse schedule, pulse validation and influence of inter-pulse analysis, ...) and the links to the plasma control systems.

Integrated modelling shall not only be used to perform physics research related to the experimental results, as on present machines, but shall also be an integral part of the pulse validation, pulse schedule and pulse design. In addition, given the slower characteristics timescale of ITER and the increased CPU capabilities expected in ten years, real-time control shall also be linked to developments in the integrated modelling research studies. This is why the ITER integrated modelling infrastructure has interfaces with many, if not all, of the physics and technical aspects of ITER. In addition, many of the integrated modelling activities are expected to take place off-site, leading to additional constraints. This is why it was important to define well the strategic requirements. The detailed requirements have then been presented in the D1.2 document. Finally the global conceptual design has been presented in the D2 report, where a timeline for the implementation of the infrastructure has been provided as well as coding standards. In addition, the ITERIS team has organised a technology workshop to review the technologies available for the implementation of the IM infrastructure. The results of this workshop are also provided in the D2 document.

The work performed has always been organised such as to interact as much as possible with the ITER team and colleagues of various DAs, in order to make sure the solutions proposed would be useful and supportive of the various ITER integrated modelling activities in the next 20 years or so. This is also why the various reports have been presented in Autumn 2011 to the IMEG group, for their evaluation. Our proposals have been very well received and we have incorporated IMEG remarks/proposals in our final report.

4.9 Participation in ITER committees

Members of the CRPP continued to contribute on various ITER committees (ITER STAC, review panel) as in the past.

5 INTERNATIONAL AND NATIONAL COLLABORATIONS

5.1 *Exploitation of the JET facilities*

5.1.1 *Control of MHD instabilities*

JET experiments have been undertaken in which sawteeth have been controlled and neoclassical tearing modes (NTMs) avoided in high confinement mode. This is the first known clear demonstration of sawtooth control in H-mode using ICRH. It has been shown that NTMs would have been triggered in this environment if the sawteeth had not been controlled (shortened). The scenario employed He3 minority at low concentration with resonance on the high field side. The He3 minority is relevant to the primary scheme for ICRH in ITER. However, sawtooth control in ITER will probably be limited to having resonance on the low field side. Consequently, future JET experiments have been planned, and are expected to take place next year, in which sawteeth will be controlled with hydrogen resonance on the low field side of the device. It will not be possible to use He3 minority in forthcoming JET campaigns.

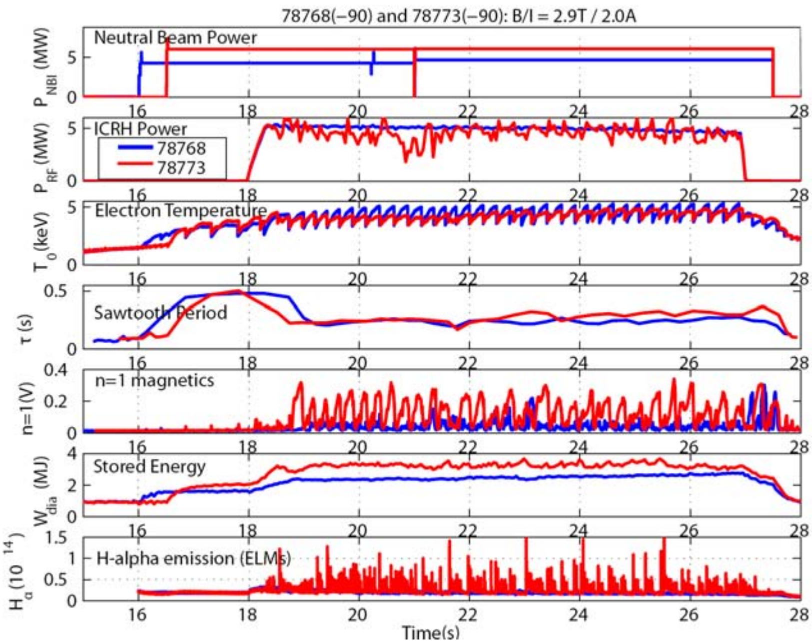

Fig. 5.1.1 *Showing JET pulse 78768 (in blue) with 4.8MW of NBI, and JET pulse 78773 (in red) with 6.4MW of NBI, where both employed low concentration He3 minority ICRH at around 5MW. In both, the -90 degree antenna phasing produces counter current propagating waves which shorten the sawtooth period. Also shown is the central electron temperatures in the core, the stored energy Wdia, the n=1 magnetic perturbation amplitude, and H-alpha emission, which indicates that JET pulse 78773 is in high confinement.*

5.1.2 Collaboration on Alfvén waves and fast particles studies

The study of Alfvén Eigenmodes (AE) and their interaction with fast particles is an important topic in the JET programme. Following the shutdown for the installation of the ITER-Like Wall (ILW), we have pursued the analysis of the data collected during the C20-C27 experimental campaigns, as AE experiments have not yet been run on JET with the new ILW. The main focus of our work has been the analysis of the dependence of the damping rate of Toroidal Alfvén Eigenmodes (TAEs) with toroidal mode numbers $|n|\leq 15$ as a function of the plasma effective isotope ratio A_{EFF}, which was varied throughout a dedicated D-H-He4 gas scan in C27. In ITER the optimization of the fuel ratio constitutes an important parameter towards achieving a high energy gain, whereas the destabilization of AEs with intermediate toroidal mode numbers may prevent such goal from being reached. It then becomes important to determine whether an optimum fuel mixture, hence an optimum A_{EFF}, can be defined. Furthermore, it is important to assess the diagnostic potential of AEs in determining A_{EFF} in real-time, as no dedicated diagnostic is foreseen in ITER for this measurement.

The analysis of the recent data acquired during C27 suggests that the effect of A_{EFF} on the damping rate of medium-n TAEs is not as clear as that observed for low-n modes (the damping rate of n=1 TAEs decreases with increasing A_{EFF}), most likely because of the different spatial structure of the modes. An example of these measurements is shown for n=7 TAEs in Fig. 5.1.2. For modes whose frequency is close to the centre of the gap, γ/ω increases with increasing A_{EFF}. This experimental trend is qualitatively consistent with previous calculations predicting that electron Landau damping $\gamma/\omega_{EL}\propto\sqrt{A_{EFF}}$ and the radiative damping $\gamma/\omega_{RAD}\propto\exp(-1/\rho_i)\propto\exp(-1/\sqrt{A_{EFF}})$, are the dominant damping mechanisms for modes with intermediate mode numbers. For modes whose frequency sits closer to the top and/or bottom continuum, we have in general that $\gamma/\omega\sim A_{EFF}$. In these low magnetic shear configurations, the turning point for the γ/ω vs. A_{EFF} dependence, i.e. from a damping rate that decreases to a damping rate that increases with increasing A_{EFF} irrespective of the mode position inside the corresponding gap, is found for medium-n modes with n=3.

Analysis of the “anomalous” ion heating during the JET DTE1 experiment

In the “alpha-heating” experiment performed on the JET tokamak during the deuterium-tritium (DTE1) campaign of 1997, the ion temperature was found to be exceeding, and with a shorter rise time, the level that could have been expected from direct collisional heating by the fusion-born alpha particles and energy equipartition with the electrons. To date, no explanation has been put forward for this long standing puzzle, despite much work having been performed on this subject in the early 2000s.

Two analysis methods that have recently become available have been employed to re-analyse these observations of an anomalous ion heating. First, an algorithm based on the Sparse Representation of Signals has been used to analyse magnetic, reflectometry and electron cyclotron emission measurements of the turbulence spectra in the drift-wave range of frequencies. This analysis has then been complemented with turbulence simulations performed with the GENE code.

We have found, both experimentally and in the simulations, that the presence of a minority, but sufficiently large, population of fusion-born alpha particles that have not yet fully thermalized stabilizes the turbulence in the ion drift direction, but practically does not affect the turbulence in the electron drift direction. We conjecture that such stabilization of the ion drift wave turbulence is responsible for the increase in the ion temperature above the level achieved in similar discharges that did not have alpha particles. When the fusion-born alpha particles have fully thermalized, the turbulence spectrum in the ion drift direction reappears at somewhat larger amplitudes, which we conjecture is the cause of the ensuing ion temperature decrease. A typical dynamical evolution is shown in Fig. 5.1.3. By taking into account an effect of the alpha particles that had not been previously considered, our new analysis finally presents a phenomenological explanation for the so-far unexplained anomalous ion heating observed in the JET alpha-heating experiment of 1997.

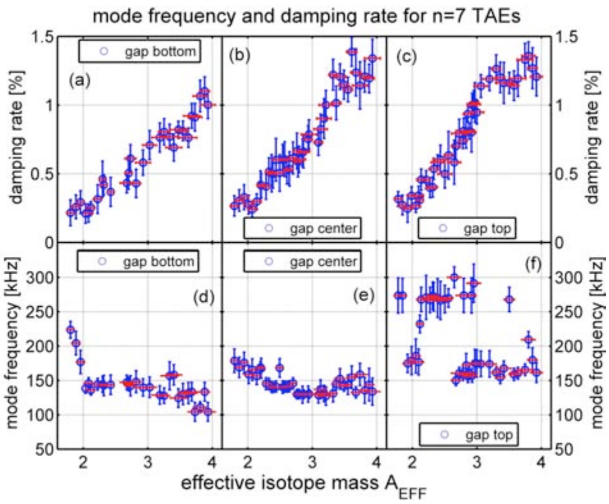

Fig. 5.1.2 *Measurement of the A_{EFF} dependence of the mode frequency and damping rate for n=7 TAEs as function of their position within the gap.*

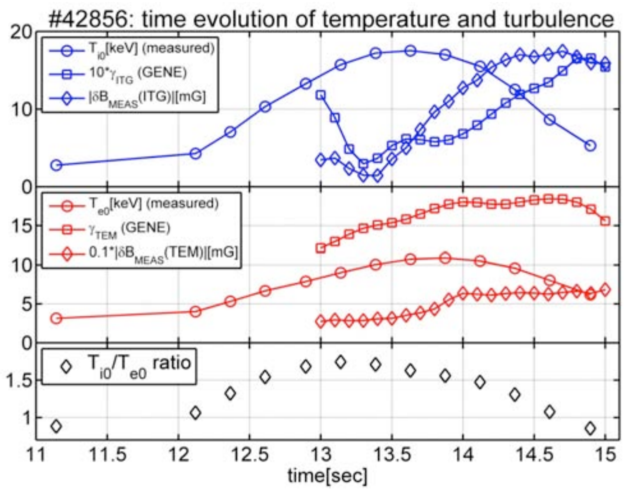

Fig. 5.1.3 *Reconstructed time evolution of the Trapped Electron Modes (TEM) and Ion Temperature Gradient (ITG) turbulence amplitude and growth rates for a representative DTE1 discharge (#42856), where the anomalous ion heating was observed. The data are plotted as function of the background ion and electron temperatures in the plasma core, and their ratio T_{i0}/T_{e0}.*

Through the formulation of an empirical criterion for ion-drift-wave turbulence stabilization by fusion-born alpha particles, we also show why similar observations were not made in the other deuterium-tritium experiments run so far in JET and TFTR. This allows us to assess the operational domain for this stabilization mechanism for ion drift wave turbulence in future burning plasma experiments such as ITER (Fig. 5.1.4), which may open a new path towards the sustainment of a high energy gain in such forthcoming devices.

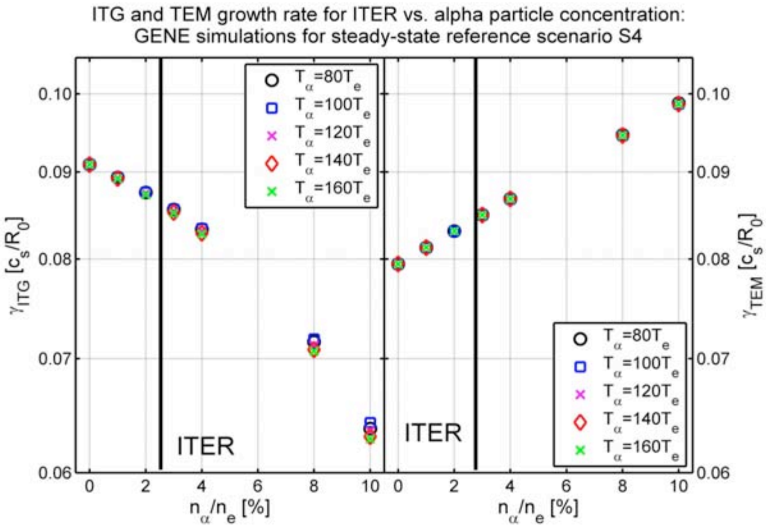

Fig. 5.1.4 *Predicted ITG (left) and TEM (right) growth rates for the ITER reference steady state scenario S4, as calculated by GENE as function of n_α/n_e for different values of T_α. The black vertical line at the n_α/n_e=2.5% value represents the expected operational point for ITER S4 plasmas.*

TAE Amplifier and Control Upgrade

The JET diagnostic enhancement project "TAE Amplifier and Control Upgrade" was launched in May 2011. The project is supported by the Task Agreement JW11-TA-SED-TAU-02 and involves international collaborations with MIT (US) and the University of Sao Paulo (IFUSP-Brazil). CRPP is leading this project and is providing scientific and technical expertise throughout. The main project objectives are to install a new generation of RF amplifiers and a new digital control system to the JET- Toroidal Alfvén Eigenmode (TAE) diagnostic aiming at increasing the antenna current and setting arbitrary phasing between each of the in-vessel antennas. In 2011, the main project activities were the development at IFUSP of a solid state RF amplifier prototype and the conceptual design of the digital control system.

5.1.3 General diagnostic support for JET operation

In 2011, CRPP staff was detached to JET as a diagnostic specialist and worked in the Thomson Scattering group. Both of the currently functioning JET Thomson scattering diagnostics were upgraded during his secondment period and considerable improvement of the data quality was demonstrated during the ITER-like Wall campaigns. High Resolution Thomson Scattering (HRTS) had its spectrometers refurbished and a new alignment procedure was implemented. As a result, HRTS produced independently calibrated Te measurements for the first time.

The core LIDAR diagnostics has undergone a major maintenance which included modification of the spectrometer optics and replacement of the light detectors by those which are proposed for the ITER LIDAR project.

Electron temperature measurements on JET during the recent plasma experiments have shown an unprecedented agreement between the results provided from three independent sources (Fig. 5.1.5).

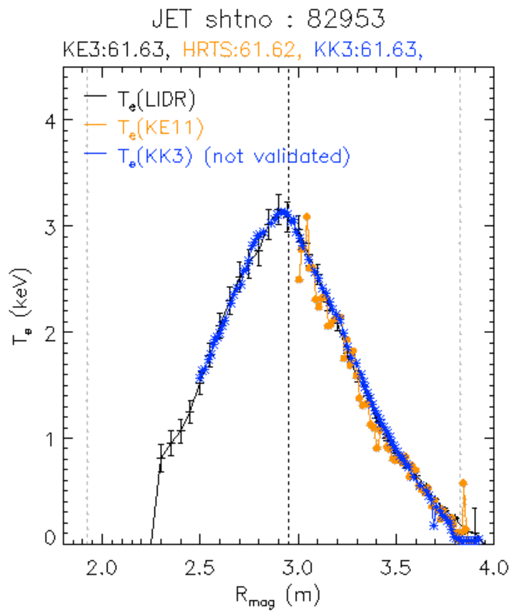

Fig. 5.1.5 *Example of Te profile as measured on JET by 3 diagnostics: LIDAR (black), ECE (blue), HRTS (orange). Shot #82953, t=61.63s, low density ICRH heated plasma.*

*5.2 Plasma surface interactions (University of Basel)**

Most of ITER optical diagnostics will be equipped with in-vessel metallic mirrors as plasma viewing components. These mirrors will be exposed to severe plasma environment which implies important research and developments on their design and manufacturing. As a consequence, investigations on engineering and manufacturing have been carried out on diagnostic mirrors towards the development of full-scale stainless steel and TZM (Mo-based alloy) ITER mirrors, with several micrometers in thickness of rhodium and molybdenum reflective coating layers, which is needed to insure long-lasting of the mirrors exposed to an environment that could be dominated by neutral charge-exchange flux.

First, investigations have been performed on the design and manufacturing of the mirror integrated cooling system, so that the optical surface deformation due to radiations from the plasma and nuclear heating is limited, which is of importance to insure reliability and precision of the optical diagnostics in ITER operational mode. For the thermo-mechanical design of the mock-ups, plasma radiation flux of 0.5MW/m and neutron head load of 7MW/m^3 have been considered.

Secondly, the polishing capability of full-scale (109mm in diameter) metallic mirrors has been demonstrated: the mock-ups Surface Front Error is lower than 0,06μm Root Mean Square, and the mirrors exhibit low roughness (Ra<2nm) and low surface defects (scratch width lower than 0,02mm) after polishing.

---

* Work performed in the frame of the Association. For information.

Thirdly, the manufacturing feasibility of molybdenum and rhodium thick coating layers deposited by magnetron sputtering has been evaluated. The objective of depositing layers up to 3µm to 5µm thick has been achieved on the mock-ups, with spectral performances reaching the theoretical values and showing high reflectivity over a large spectral range (from 400nm to 11µm).

Finally the tests campaign of the manufactured mirrors, which is being prepared in several European facilities to expose the mirrors to deuterium plasma, ELMs, neutrons, erosion and deposition conditions, is ongoing.

Fig.5.3.1 *Prototype of ITER first mirror: rhodium or molybdenum thick reflective coating layers on stainless steel or TZM cooled blank*

EFDA Technology Tasks

WP11-PWI-01-01-01: Fuel retention in Mixed tungsten/boron layers
WP11-PWI-01-01-02: Fuel retention in Mixed tungsten/carbon/aluminium layers
WP11-PWI-04-01-01: Effect of transient heat/particle loads on helium induced nano-structure
WP11-PWI-04-01-02: Tungsten nitrogen and carbon interaction
WP11-PWI-06-05-01: Material damage during ELM-like heat loads in Pilot-PSI

5.3 Collaborations with other EURATOM Associations

J-F. Artaud, V. Basiuk, Association EURATOM-CEA, France, *"Coupling of the DINA-CH and CRONOS codes to simulate the ITER hybrid scenario"*

K. Avramides, Association Euratom Hellenic Republic, Greece, *"Studies of high-power gyrotrons for ITER"*

A. Bottino, IPP-Garching, Germany, *"Global PIC gyrokinetic simulations of turbulence and code development"*

S. Bremont, Tore Supra, CEA-Cadarache, F, *"Real-time control of TCV and Tore Supra"*

I.T. Chapman, CCFE, UKAEA, U.K., "*Collaboration with MAST on the accessibility* *of bifurcated helical core equilibrium states in the presence of external perturbed n=3 coils used for ELM control"*

C. Cianfarani, O. Tudisco, ENEA, Frascati, *Italy, "Collaboration on high-frequency magnetic sensors based on the Low-Temperature Co-fired Ceramic technology for FTU"*

A. dellaCorte, Association EURATOM-ENEA, Italy, *"Review of superconductors for DEMO"*

G. Conway, IPP-Garching, Germany, *"Turbulence and flow measurements on TCV"*

D. Coster, IPP-Garching, Germany, *"SOLPS simulations of scrape-off layer in TCV and JET elmy-H discharges"*

G. Cunningham, CCFE, U.K., *"Experiments on H-modes and transformerless tokamak operation in TCV"*

C. Cianfarani, ENEA-Frascati, Italy, *"Development of low-temperature co-fired ceramic magnetic pick-up coils for the measurement of high-frequency instabilities in the FTU tokamak"*

J. Decker, Y. Peysson, CEA-Cadarache, France, "*Quasilinear Fokker-Planck simulations and modelling of hard X-ray emission in TCV*"

J. Decker, Y. Peysson, CEA-Cadarache, France, *"Quasilinear Fokker-Planck simulations with the LUKE code for Electron Cyclotron and Electron Bernstein Wave Heating and Current Drive in TCV"*

T. Eich, IPP-Garching, Germany, *"Parallel transport dynamics of type-I ELMs in JET and comparison to PIC modelling"*

V. Erckmann, H.P. Laqua, IPP-Greifswald, Germany, **M. Thumm, G. Gantenbein,** KIT, Karlsruhe, Germany, *"Collaboration with W-7X"*

W. Fietz, KIT Karlsruhe, Germany, *"Planning of High Temperature Superconductivity activities for EFDA and Demo"*

X. Garbet, Ph. Ghendrih, V. Grandgirard, G. Falchetto. Y. Sarrazin, Association EURATOM-CEA, France, *"Gyrokinetic global turbulence simulations"*

G. Granucci, A. Tuccillo and F. Crisanti, ENEA, Frascati, Italy, *"Collaboration on EC systems with FAST and FTU"*

P. Hennequin, L. Vermare, Ecole Polytechnique Palaiseau and CEA-Cadarache, France, "*Measurements of edge turbulence and flows in TCV by reflectometry"*

P. Hill, S. Saarelma, CCFE-Culham, UK, *"Global PIC gyrokinetic simulations of turbulence with flows"*

M. Hirsch, IPP-Greifswald and **E. Holzhauer**, University of Stuttgart, Germany, *"Loan of a reflectometer and participation in data analysis and interpretation*"

F. Jenko, T. Goerler, F. Merz, IPP-Garching, Germany, *"Development and application of the gyrokinetic code GENE"*

T. Johnson, EURATOM-VR Association, Stockholm Univ., Sweden *"Ion cyclotron current drive, heating, and sawteeth"*

A. Koenies, V. Kornilov, A. Mishchenko, S. Sorge, IPP Greifswald, Germany, **A. Bottino, A. Peeters**, IPP Garching, Germany, **R. Hatzky**, Rechenzentrum MPG Garching, Germany *"Linear and nonlinear gyrokinetic code developments and simulations"*

A. Krämer-Flecken, S. Soldatov, FZJ, Jülich, Germany, "*Measurements of edge turbulence and flows in TEXTOR and TCV by reflectometry"*

P. Lauber, IPP-Garching, Germany, *"Damping rates of Alfvén Eigenmodes: theory-experiment comparison"*

E. Lazzaro, S. Nowak, CNR-Milano, I, *"Study of the rôle of rotation on the onset of triggerless NTM/TMs"*

M. Lewandowska, EURATOM-Poland Association, Univ. of Stectin, *"Hydraulic experiments and modeling of CICC"*

Y. Liu, CCFE, UKAEA, U.K., "*Resistive wall modes and interaction with energetic ions"*

M. Lontano, **G. Grosso**, EURATOM-ENEA-CNR Association, Italy, *"Development of a linear plasma device for basic wave-particle interactions studies"*

N. Mellet, Association EURATOM-CEA, Cadarache, France, *"Application of the LEMAN code for heating and stability"*

P. McDermott, IPP-Garching, Germany, *"Intrinsic rotation measurement comparison AUG & TCV"*

C. Michael, CCFE, U.K., *"Collaboration on the design of a phase contrast imaging diagnostic for MAST"*

F. Nave, JET/IST Abingdon, UK, *"Plasma rotation measurement comparison between JET and TCV plasmas"*

M. Spolaore, N. Vianello, Consorzio RFX, Padova, Italy *"Collaboration on the investigation of current filaments in magnetized plasmas with RFX"*

D. Ricci, G. Granucci and M. Lontano CNR-Milano, Italy, *"Collaboration with the linear basic plasma device GyM"*

A. Rodrigues, N. Cruz, C. Varandas, CFN Lisbon, Portugal, *"Advanced plasma control for TCV"*

J. Romero, CIEMAT and **M.G.S. Berasategui, I. Garrido,** EHU, Spain, *"Real-time control of the current profile in TCV"*

O. Schmitz, KFZ Juelich and the DIII-D team, *"Collaboration with DIII-D, General Atomics, USA on bifurcated helical equilibria and ELM control coils"*

G. Temmerman, FOM, the Netherlands, *"Inner-outer divertor power assymetries on TCV"*

D. Terranova, P. Martin, L. Marrelli, M. Gobbin, EURATOM-ENEA-CNR Association, Italy, "RFX-Mod Shax equilibrium and MHD stability"

I. Tigelis, G. Latsas, Association Euratom Hellenic Republic, Greece, *"Instability calculations in the 170GHz coaxial-cavity-gyrotron beam-duct"*

J. Urban, J. Preinhaelter, IPP Prague, Czech Republic, *"Ray-tracing simulations with the AMR code for the Electron Bernstein Wave mode conversion, propagation and linear absorption in TCV"*

M. Valisa, L. Carraro, A. Scaggion, Consorzio RFX, Padova, Italy, *"H-mode studies in TCV"*

G. Veres, B. Tal, S. Zoletnik, D. Nagy, Association EURATOM-HAS, KFKI Reasearch Inst. For Particle & Nuclear Physics, Budapest, Hungary, *"Plasma imaging and tomography" and "Mitigation disruption studies, particle transport studies in the SOL, high temporal resolution radiation measurements for ELMs"*

L. Vermare, P. Hennequin, Ecole Polytechnique, Palaiseau + CEA, France, *"Reflectrometry measurements on TCV"*

C. Wahlberg, EURATOM-VR Association, Uppsala University, Sweden, *"MHD aspects of the sawtooth instability, Kelvin Helmholz and infernal modes"*

W. Witrant, Univ. Joseph Fourier, GAPSI-Lab, Grenoble, F, *"Real time current profile control"*

Collaboration with KIT, NTUA and CNR in the frame of the gyrotron consortium EGYC

Collaboration with KIT, FOM, CNR, IPP, NTUA in the frame of the Upper Launcher Consortium ECHUL

Collaboration with CEA and RFX in the frame of the Magnetic Diagnostics Consortium

5.4 Other international collaborations

G. Annino, Istituto per i Processi Chimico-Fisici, CNR, via G. Moruzzi 1, 56124 Pisa, Italy, *"Development of THz-waves Instrumentation for DNP-NMR spectroscopy"*

A. Bortolon, PPPL, Princeton, USA, *"Rotation comparison between NSTX and TCV"*

R. Buttery, L. Lao, A.D. Turnbull, General Atomics, San Diego, USA, *"Quasiaxisymmetric field in DIII-D for enhanced élongation"*

Y. Camenen, Univ. Marseille, France, *"Modelling of plasma rotation and momentum transport on the TCV tokamak"*

H. Carfantan, Laboratoire d'Astrophysique de Toulouse - Tarbes, Université de Toulouse - CNRS, Toulouse, FR, *"Development of the Sparse Signal Representation method for real-time and post-pulse decomposition and analysis of a frequency-degenerate spectrum"*

P.K. Chattopadhyay, IPR, Bhat, Gujarat, India, *"Detection and analysis of Lower Hybrid Parametric Decay Instability (LHPI) during Electron Bernstein Wave Heating in the TCV tokamak"*

P.K. Chattopadhyay, IPR, Bhat, Gujarat, India, *"Collaboration on the limits of operation and of operational domain in the ADITYA tokamak"*

W. Choe, Korea Advanced Institute of Science and Technology, Daejeon, Korea, "*Collaboration on multi-wire soft X-ray diagnostics*"

B. Décamps, Centre de Spectrométrie Nucléaire et de Spectrométrie de Masse, Université Paris-Sud, "*In-situ irradiations with JANNUS facility at Orsay*".

M. Frei, M. Bader, Thomson Broadcast&Multimedia AG, Turgi, Switzerland, **S. Moriyama,** JT-60 RF Heating Group, JAEA, Japan, "*Participation of Switzerland to the Broader Approach (BA) through the JT60-SA project"*

R. Galvao, Univ. of Sao Paulo, Brazil, *"Upgrade of the TET Alfvén Eigenmode Exciter"*

R. Ganesh, J. Chowdury, Inst. For Plasma Research, Bhat, Gandhinagar, India, *"Effects of non-adiabatic electron dynamics in gyrokinetic simulations of microinstabilities"*

R. Gruber, EPF-Lausanne, Switzerland, **S.P. Hirshman**, **Y. Suzuki**, **Y. Asahi, S. Ohdachi, R. Seki**, ORNL, USA, **K.Y. Watanabe, H. Yamada, S. Okamura, Y. Narushima**, NIFS, Japan, **K. Yamazaki**, Nagoya Univ., Japan, *"3D anisotropic pressure equilibrium and fluid magnetohydrodynamic stability"*

E. Gusakov, A. Popov, A. Saveliev, Ioffe Institute, St. Petersburg, Russian Federation, *"Modelling of parametric decay from EC wave in TCV"*

R.W. Harvey, A.P. Smirnov, Comp-X, San Diego, CA, USA, *"Modelling of electron cyclotron heating and emission in TCV"*

W. Heidbrink, H. Boehmer, UC Irvine, USA, *"Sources for energetic ions for a simple magnetized torus"*

S.P. Hirshman, Oak Ridge National Laboratory, USA, *"Three-dimensional anisotropic pressure free boundary equilibria: the ANIMEC code"*

J. Hittinger, R. Berger, Lawrence Livermore National Laboratory, USA, **E. Valeo**, Princeton University, USA, and *"Development of numerical methods for Vlasov simulations"*

Y. Idomura, JAEA, Japan, *"Global gyrokinetic simulations of turbulence with grid-based and particle-based methods"*

M.Yu. Isaev, Russian Research Centre Kurchatov Institute, Moscow, Russia, **A. Konies**, IPP-Greifswald, D, *"Development of the VENUS-df Code for Bootstrap Current and Neoclassical Transport and Alfvén mode stability in Stellarators"*

JT60-SA research team, JAEA, Japan, "*Participation to the definition of the JT60-SA research project"*

N. Kirneva, RRC Kurchatov Institute, Moscow, Russia, *"Investigation of turbulent tokamak plasma self-organization and influence of the tokamak cross-section geometry on the plasma-pressure self-consistant radial profile"*

N. Kirneva, KIAE, RRC Kurchatov Institute, Moscow, Russian Federation, *"Tokamak performance improvement by tailoring the electron heating deposition"*

T. Kruml, Institute of Physics of Materials, Brno. Czech Republic, *"Low-cycle fatigue of ODS-steels"*

L. Lao, A.D. Turnbull, T.E. Evans, Genaral Atomics, San Diego, USA, *"Torkil Jensers Award experiment on Helical core structures in DIII-D"*

V.E. Lukash, Kurchatov Inst. Moscow, Russia, **R.R. Khayrutdinov**, TRINITI, Russia, *"Development of the DINA-CH simulator"*

B. McMillan, Univ. of Warwick, UK, *"Global gyrokinteic simulations of turbulent flows and momentum transport"*

A. Marinoni, C. Rost, M. Porkolab, PSFC, MIT, MA, USA, *"Turbulence measurements by phase contrast imaging in TCV, C-Mod, DIII-D"*

S.Yu. Medvedev, A.A. Martynov, A.A. Ivanov, Yu.Yu. Poshekhonov, Keldysh Institute of Applied Mathematics, Moscow, Russia, **M.Yu. Isaev, V.D.Shafranov, A.A. Subbotin**, RRC Kurchatov Institute, Moscow, Russia, *"Equilibrium and Stability of 2D and 3D plasma configurations"*

M. Mikhailov, A. Subbotin, V.D. Shafranov, M.Yu. Isaev, M. Samitov, Russian Research Centre Kurchatov Institute, Moscow, Russia; **J. Nuehrenberg**, Max Planck Institut fuer Plasma Physik, Greifswald *"Optimisation of Advanced Stellarator Systems"*

N. Mitchell, **A. Devred**, **M. Jewell**, ITER Organisation, *"In-situ measurements of Tc for SULTAN samples", "Protective investments for SULTAN", "Thermal cycles at liquid nitrogen of SULTAN samples", "Preliminary development of a thermal-hydraulic code", "CSI01 and TFI01 SULTAN sample manufacture and test"*

G.R. Odette, Univ. California Santa Barbara (UCSB), Santa Barbara, CA, USA, *"Fracture mechanics and small specimen test technology"*

Z. Oksiuta, Bialystok Technical University, Poland, *"Development of ODS-steels".*

K. Okuno, **Y. Takahashi**, JAEA, Japan, *"Assembly and test in SULTAN of the Japanese ITER conductors JATF5, JATF6, JACS2"*

A. ten Ouden, Radbaud University, Nijmegen, The Netherland, *"Assembly and test in SULTAN of a prototype conductor for a high field magnet"*

M. Porkolab, P. Woskov, PFSC, MIT, USA, *"Fast particle physics, Alfven waves, and active MHD mode excitation on the Alcator C-Mod tokamak plasma"*

J. Rice, C-MOD, Boston, USA, *"Intrinsic rotation comparison between CMOD & TCV"*

B. Rogers, Dartmouth College, USA, *"Theoretical characterization of turbulence in TORPEX plasmas".*

D. Ryutov, **T. Rognlien, M. Umansky**, LLNL, USA, *"Snowflake divertor generation and characterization in TCV"*

P. Savrukhin, A. Sushkov, E. Shestakov, RRC Kurchatov Institute, Russian Federation, *"Suprathermal electron physics on T-10 and TCV"* (SC)

M.J. Schaffer, General Atomics and the TBM task force on DIII-D, San Diego, Ca, USA, *"Collaboration on the effect of test blanket modules (TBMs) in ITER on H-mode energy, particle and momentum confinement"*

Dr. T.Shimozuma, National Institute of Fusion Science, Japan, *"Real-time control of ECH polarization"*

P. Smeibidl, HZB, Berlin, Germany, *"Design and construction of a SC Cable-in-Conduit coil for a horizontal series-connected hybrid magnet system within the framework of the high field magnet project (HFM) at HZB"*

A. Sushkov, KIAE, RRC Kurchatov Institute, Russian Federation, "*Collaboration on multi-wire DMPX soft X-ray diagnostics during ECRH*"

A.D. Turnbull, General Atomics, San Diego, USA, *"Stability studies of ARIES stellarator configurations"*

K.Y. Watanabe, NIFS, Japan, *"Collaboration on LHD MHD equilibrium and stability"*

Y. Wu, ASIPP, P.R. China, *"Assembly and test in SULTAN of the ITER conductors CNPF2 and CNMB1 and CNCC1"*

5.4.1 International Tokamak Physics Activity (ITPA)

The following staff members were involved in ITPA activities in 2011:

ITPA Diagnostics Topical Group: H. Weisen (member), R. Behn (expert), L. Marot (expert)

ITPA Energetic Particle Physics Topical Group: A. Fasoli (member), D. Testa (expert)

ITPA MHD, Disruptions & Control Topical Group: O. Sauter (expert), J.B. Lister (expert), A. Fasoli (expert)

ITPA Pedestal & Edge Physics Topical Group: Y. Martin (member)

ITPA Transport & Confinement Topical Group: Y. Martin (expert), H. Weisen (expert), O. Sauter (expert

5.5 Other collaborations within Switzerland

J.-Ph. Ansermet, EPFL/SB/LPMN; **A. Comment**, EPFL/SB/IPSB/LIFMET; **G. Bodenhausen**, EPFL/SB/ISIC/LRMB, **G. Boero**, EPFL/STI/IMT/LMIS1, *"Development of THz-waves Instrumentation for DNP-NMR spectroscopy"*

E. Cadoni, University of Applied Sciences of Southern Switzerland, Canobbio, *“High strain rate tensile testing of the EUROFER 97 RAFM steel”*

C. Hébert, CIME-EPFL, *“TEM analysis of nanoscale oxide particles in ODS steels and Cr in Fe(Cr) in model alloys”*

F. Holdener, WEKA, Bäretswil, *"Technology transfer for HTS current leads manufacture"*

G. Lucas, CIME-EPFL, *“Advanced statistical analysis methods in TEM spectroscopy“*

A. Macor, E. de Rijk, Swissto12, *"Development of passive THz-waves components"*

R. Wepf, EMEZ-ETHZ, *“Advanced TEM techniques and TAP for ODS steels and Fe(Cr)“*

R. Spolenak, LNM-ETHZ, *“Radiation induced mechanisms of selective grain growth in metals”*

Besides the activities in the field of plasma wall interaction with the University of Basel, the CRPP also collaborates with the PSI in the field of materials under irradiation.

6 THE EDUCATIONAL ROLE OF THE CRPP

The CRPP plays a role in the education of undergraduate and postgraduate students, particularly in the Faculté des Sciences de Base (FSB) of the EPFL. Advanced education and training in fusion physics and technology and plasma physics topics is carried out as part of the research activities of the Association. Section 6.1 presents the 9 courses given to physics undergraduates and to engineering undergraduates. In their fourth and final year, physics undergraduates spend time with a research group at the EPFL, typically 12 hours per week for the whole year. During this period, they perform experimental or theoretical studies alongside research staff, discovering the differences between formal laboratory experiments and the “real” world of research. After successful completion of the first year of the Master Programme (4th year of studies), physics students are required to complete a “master project” with a research group, lasting a full semester. This master project is written up and defended in front of external experts. The CRPP plays a role in all of these phases of an undergraduate’s education, detailed in Sections 6.2 and 6.3.

As an academic institution, the CRPP supervises many Ph.D. theses, also in the frame of the Physics Section of the EPFL. 7 PhDs were awarded in 2010. At the end of 2010 we had 33 PhD students supervised by CRPP members of staff, in Lausanne and at the PSI site in Villigen. Their work is summarised in Section 6.4.

6.1 Undergraduate courses given by CRPP staff

S. Alberti, *MER – “Plasma Physics I”*
This course is an introduction to plasma physics aimed at giving an overall view of the essential properties of a plasma and at presenting the approaches commonly used to describe its behaviour. We study single particle motion, the fluid description and the kinetic model. The relation between plasma physics and developing a thermonuclear reactor is presented and illustrated with examples.

R. Schäublin - Maître d'Enseignement et Recherche, **P. Spätig** - Maître d'Enseignement et Recherche: *"Fundamentals of radiation damage and effects"*
This 28-hours course is part of the EPFL’s Minor in Space Technologies. The objective of this course is to provide a detailed description of fundamental interaction mechanisms between particles and matter, radiation damage and its characterization methods, and radiation effects with emphasis on the relationships between microstructure and mechanical properties. Various types of materials are being considered as well as various examples of applications related to nuclear, semi-conductor and aerospace industries.

R. Schäublin, Maître d'Enseignement et Recherche, *"Materials for fusion reactors"* and *"Multiscale modelling"*
The aim of these courses are to provide a basic introduction to candidate materials for fusion reactors, the status of their characterization, their advantages and key issues for use in fusion reactors, and to the numerical and analytic tools used for modelling radiation damage and effects. These courses were given within the frame of the Master in Nuclear Engineerings.

P. Ricci, Assistant Professor – *"Plasma physics II"*
One semester option course presented to 4th year Physics students, introducing the theory of hot plasmas via the foundations of kinetic and magnetohydrodynamic theories and using them to describe simple collective phenomena. Coulomb collisions and elementary transport theory are also treated. The students also learn to use various theoretical techniques like perturbation theory, complex analysis, integral transforms and solutions of differential equations.

A. Fasoli, Professor – *"General Physics II"*
This course completes the introduction to mechanics provided in the first semester with the basic concepts of statics, oscillations and special relativity. It also covers the whole of thermodynamics, from the introduction to heat, temperature and kinetic theory to the first and second principles, including entropy and thermal engines, ending with a treatment of transport and non-equilibrium phenomena in open systems.

A. Fasoli, Professor and **M.Q. Tran**, Professor - *"Nuclear fusion and plasma physics"*
The aim of this course is to provide a basic understanding of plasma physics concepts of fusion energy, and of the basic principles of fusion reactors, including the main technological aspects. This course was given within the frame of the Master in Nuclear Engineering.

J.B. Lister, *Maître d'Enseignement et Recherche (MER) – "Plasma Physics III"*
An introduction to controlled fusion, presented as a one semester option to 4th year Physics students. The course covers the basics of controlled fusion energy research. Inertial confinement is summarily treated and the course concentrates on magnetic confinement from the earliest linear experiments through to tokamaks and stellarators, leading to the open questions related to future large scale fusion experiments.

M.Q. Tran, *Professor - "General Physics II and III"*
This course, given to the Mathematics Section, covers mechanics and thermodynamics (General Physics II) and hydrostatic, hydrodynamics waves and electromagnetism (General Physics III).

L. Villard, *Professeur Titulaire – "Computational Physics I-II"*
Full year course given to students in their 2nd year in Physics. The course covers various time and space integration techniques for ordinary and partial differential equations, and is applied to various physics problems ranging from particle dynamics, hydrodynamical equilibrium, electromagnetism, waves and quantum mechanics. It includes a strong practical work aspect.

6.2 Undergraduate work performed at the CRPP

EPFL Master students (4th year)

During the Spring semester of 2011, CRPP staff members have supervised 6 students performing their Advanced Physics Laboratory work. During the Automn semester of 2011, we had 6 students.

6.3 EPFL Master degrees awarded in 2011

D. Barmaz, *"High-n stability of a pressure discontinuity in a three-dimensional plasma"*

G. Induni, *"Simulation du transport électronique dans des plasmas à haut confinement"*

F. Moix, *"Characterization of a large area planar RF source"*

6.4 Postgraduate studies

Postgraduate courses given in 2011

R. Schäublin, Maître d'Enseignement et de Recherche, *'Transmission Electron Microscopy Imaging of Crystal Defects'*, Doctoral School, EPFL

R. Schäublin, Maître d'Enseignement et de Recherche, **P. Spätig**, Maître d'Enseignement et de Recherche, **'Effects of Radiation on Materials'**, Doctoral School, EPFL

J.P. Graves and **S. Brunner**, *"Advanced theory of plasmas"*. This advanced plasma physics course covers MHD Equilibrium and Instabilities in Tokamak Plasmas, kinetic Theory of Microinstabilities, an introduction to Non-linear Phenomena, and kinetic Theory of Macroscopic Instabilities.

Doctorate degrees awarded during 2011

Mattia ALBERGANTE: *"Interaction Between Fast Ions and Microturbulence in Thermonuclear Devices: Theory and Modelling"*, EPFL Thesis 5164 (2011)
The work carried out in this thesis focuses on the interaction between fast ions and turbulence. The aim of the project is to explore this phenomenon and develop the numerical framework required for investigations on present day machines and predictions for burning plasmas. The analysis of the background plasma turbu- lence and the resulting fast ion diffusivities is carried out with the gyrokinetic code GENE. A set of kinetic transport quantities are defined in order to discriminate the transport of ions with different energies. Gyroaveraging effects are studied. It is observed that only at large values of the E/T_e ratio is the particle transport efficiently suppressed (E is the energy of a fast particle and T_e the electron tem- perature). For smaller values, $E/T_e<15$, larger fast ion transport is observed due to resonant interactions between the particle motion and the phase velocity of the underlying turbulent waves. The transport of fusion generated alpha particles induced by electrostatic fluctuations is lower than collisional expectations, due to their large energies. Magnetic turbulence has an even smaller effect.
To verify whether similar conclusions can be drawn for neutral beam ions, substantial upgrades to the VENUS code have been implemented. The results of numerical simulations of the beam ion transport in ITER, DEMO and TCV, with the inclusion of collisional and turbulent effects, are discussed. It is demonstrated that the transport of the 1MeV ions generated by the neutral beam

injector of ITER is only marginally affected by microturbulence and it is concluded that fast ion confinement is not compromised. Given the large plasma temperatures foreseen for DEMO, anomalous transport of beam ions is significant, and in par- ticular collisional models fail to estimate the correct heat deposited on the ions and the electrons. Given the low energy of the planned TCV NBI injector, even stronger anomalies are expected. The effect, however, can be regulated with aux- iliary ECRH heating, which would allow for new studies of the fast ion turbulent transport.

Loïc CURCHOD: *"Heating of High Density Plasmas in the TCV Tokamak"* EPFL Thesis 5012(2011)

The *Tokamak à Configuration Variable* (TCV) is a medium size magnetic confinement thermonuclear fusion experiment designed for the study of the plasma performances as a function of its shape. It is equipped with a high power and highly flexible electron cyclotron heating (ECH) and current drive (ECCD) system. Up to 3 MW of 2nd harmonic EC power in ordinary (O2) or extraordinary (X2) polarization can be injected from TCV low-field side via six independently steerable launchers. In addition, up to 1.5 MW of 3rd harmonic EC power (X3) can be launched along the EC resonance from the top of TCV vacuum vessel.

At high density, standard ECH and ECCD are prevented by the appearance of a cutoff layer screening the access to the EC resonance at the plasma center. As a consequence, less than 50% of TCV density operational domain is accessible to X2 and X3 ECH. The electron Bernstein waves (EBW) have been proposed to overcome this limitation. EBW is an electrostatic mode propagating beyond the plasma cutoff without upper density limit. Since it cannot propagate in vacuum, it has to be excited by mode conversion of EC waves in the plasma.

Efficient electron Bernstein waves heating (EBH) and current drive (EBCD) were previously performed in several fusion devices, in particular in the W7-AS stellarator and in the MAST spherical tokamak. In TCV, the conditions for an efficient O-X-B mode conversion (i.e. a steep density gradient at the O2 plasma cutoff) are met at the edge of high confinement (H-mode) plasmas characterized by the appearance of a pedestal in the electron temperature and density profiles. TCV experiments have demonstrated the first EBW coupling to overdense plasmas in a medium aspect-ratio tokamak via O-X-B mode conversion.

This thesis work focuses on several aspects of ECH and EBH in low and high density plasmas. Firstly, the experimental optimum angles for the O-X-B mode conversion is successfully compared to the full-wave mode conversion calculation of the AMR code. The implementation of TCV ECH system geometry in AMR and the coupling of AMR to the LUKE quasi-linear Fokker-Planck solver for the TCV environment were part of this work.

The power deposition location of modulated EBH is then detected inside the O2 plasma cutoff by oscillation analysis of the soft X-ray emission profile using the break-in-slope (BIS) analysis and a harmonic response identification method (HRIM), which is the demonstration of resonant EBH in TCV. The BIS and HRIM methods are also used to successfully detect and track the time-varying deposition locations of one and then two X2 power beams simultaneously. All experimental results are in good agreement within 10% of the normalized plasma radius with numerical results of the AMR and C3PO ray-tracing codes coupled to LUKE.

The global power absorption coefficient of modulated ECH (MECH) is studied by HRIM analysis of the plasma toroidal flux response measured by TCV diamagnetic loop (DML). Analysis of earlier X3 MECH and new X2 MECH experiments reveals a major perturbation of the method by the sawtooth magnetohydrodynamic activity in the plasma center. Indeed, an asymmetric improvement of the X3 power absorption (up to 100%) with respect to the sign of the X2 ECCD pre-heating was observed in previous TCV experiments and remained unexplained by Fokker-Planck simulations until now. The present work allows us to attribute this asymmetry to a

sawtooth activity strongly destabilized by the central X2 co-ECCD locking to the X3 power modulation.
The performances of EBW current drive (EBCD) in TCV are studied with the AMR-LUKE codes for several poloidal positions of the EBW injection. The maximum EBCD efficiency is obtained when the EBW are injected close the plasma midplane such that the wave parallel refractive index upshift is moderate and the absorption takes place at the plasma center where the electron temperature is the highest. However, the absolute driven current remains small (i.e. ≲1% of the Ohmic current).
Finally, a new loop-antenna for the detection of the lower-hybrid (LH) waves generated by a parametric instability (PI) at the X-B mode conversion was designed, built and installed in TCV torus. Fast monitoring of the LHPI spectrum allows to show for the first time the correlation of the amplitude of the detected waves with the local LHPI threshold power at the mode conversion region, estimated from the experimental profiles data. In an EBW power scan, the LHPI threshold power is estimated to be ≲50 kW in good agreement with the value predicted from the experimental profiles data. The LHPI energy cascade from the low to the high LH frequency bands with increasing EBH power is shown for the first time in TCV.

Federico FELICI: *"Real-time control of tokamak plasmas: from control of physics to physics-based control"* EPFL Thesis No. 5203(2011)
Stable, high-performance operation of a tokamak requires several plasma control problems to be handled simultaneously. Moreover, the complex physics which governs the tokamak plasma evolution must be studied and understood to make correct choices in controller design. In this thesis, the two subjects have been merged, using control solutions as experimental tool for physics studies, and using physics knowledge for developing new advanced control solutions.
The TCV tokamak at CRPP-EPFL is ideally placed to explore issues at the interface between plasma physics and plasma control, by combining a state-of-the-art digital real-time control system with a flexible and powerful set of actuators, in particular the electron cyclotron heating and current drive system (ECRH/ECCD). This unique experimental platform has been used to develop and test new control strategies for three important and reactor-relevant tokamak plasma physics instabilities, including the sawtooth, the edge localized mode (ELM) and the neoclassical tearing mode (NTM). These control strategies offer new possibilities for fusion plasma control and at the same time facilitate studies of the physics of the instabilities with greater precision and detail in a controlled environment.

The period of the sawtooth crash, a periodic MHD instability in the core of a tokamak plasma, can be varied by localized deposition of ECRH/ECCD near the q=1 surface, where q is the safety factor. Exploiting this known physical phenomenon, a sawtooth pacing controller was developed which is able to precisely control the time of appearance of the next sawtooth crash. It was also shown that each individual sawtooth period can be controlled in real-time. A similar scheme is applied to H-mode plasmas with type-I ELMs, where it is shown that pacing regularizes the ELM period.
The regular, reproducible and therefore predictable sawtooth crashes obtained by the sawtooth pacing controller have been used to study the relationship between sawteeth and NTMs . It is known that post-crash MHD activity can provide the ``seed'' island for an NTM, which then grows under its neoclassical bootstrap drive. Experiments are shown which demonstrate that the seeding of 3/2 NTMs by long sawtooth crashes can be avoided by preemptive, crash-synchronized EC power injection pulses at the q=3/2 rational surface location. NTM stabilization experiments in which the ECRH deposition location is moved in real-time with steerable mirrors have shown effective stabilization of both 3/2 and 2/1 NTMs, and have precisely localized the deposition location that is most effective.

Studies of current-profile driven destabilization of tearing modes in TCV plasmas with significant amounts of ECCD show a great sensitivity to details of the current profile, but failed to identify a stationary region in the parameter space in which NTMs are always destabilized. This suggests that transient effects intrinsically play a role.
Next to instability control, the simultaneous control of magnetic and kinetic plasma profiles is another key requirement for advanced tokamak operation. While control of kinetic plasma profiles around an operating point can be handled using standard linear control techniques, the strongly nonlinear physics of the coupled profiles complicates the problem significantly. Even more, since internal magnetic quantities are difficult to measure with sufficient spatial and temporal resolution - even after years of diagnostic development - routine control of tokamak plasma profiles remains a daunting and extremely challenging task.
In this thesis, a model-based approach is used in which physics understanding of plasma current and energy transport is embedded in the control solution. To this aim, a new lightweight transport code has been derived focusing on simplicity and speed of simulation, which is compatible with the demands for real-time control. This code has been named RAPTOR (RApid Plasma Transport simulatOR).
In a first-of-its-kind application, the partial differential equation for current diffusion is solved in real-time during a plasma shot in the TCV control system using RAPTOR. This concept is known in control terms as a state observer, and it is applied experimentally to the tokamak current density profile problem for the first time. The real-time simulation gives a physics-model-based estimate of key plasma quantities, to be controlled or monitored in real-time by different control systems. Any available diagnostics can be naturally included into the real-time simulation providing additional constraints and removing measurement uncertainties. The real-time simulation approach holds the advantage that knowledge of the plasma profiles is no longer restricted to those points in space and time where they are measured by a diagnostic, but that an estimate for any quantity can be computed at any time. This includes estimates of otherwise unmeasurable quantities such as the loop voltage profile or the bootstrap current distribution. In a first closed-loop experiment, an estimate of the internal inductance resulting from the real-time simulation is feedback controlled, independently from the plasma central temperature, by an appropriate mix of co- and counter- ECCD.
As a tokamak plasma evolves from one state to another during plasma ramp-up or ramp-down, the profile trajectories must stay within a prescribed operational envelope delimited by physics instabilities and engineering constraints. Determining the appropriate actuator command sequence to navigate this operational space has traditionally been a trial-and-error procedure based on experience of tokamak physics operators. A computational technique is developed based on the RAPTOR code which can calculate these trajectories based on the profile transport physics model, by solving an open-loop optimal control problem.
The solution of this problem is greatly aided by the fact that the code returns the plasma state trajectory sensitivities to input trajectory parameters, a functionality which is unique to RAPTOR. This information can also be used to construct linearized models around the optimal trajectory, and to determine the active constraint, which can be used for time-varying closed-loop controller design.
This physics-model-based approach has shown excellent results and holds great potential for application in other tokamaks worldwide as well as in future devices.

Silvano GNESIN: *"Electron Cyclotron Heating and Suprathermal Electron Dynamics in the TCV tokamak"* EPFL thesis No. 5181(2011)
This thesis is concerned with the physics of suprathermal electrons in thermonuclear, magnetically confined plasmas. Under a variety of conditions, in laboratory as well as space plasmas, the electron velocity distribution function is not in thermodynamic equilibrium owing to internal or external drives. Accordingly,

the distribution function departs from the equilibrium Maxwellian, and in particular generally develops a high-energy tail. In tokamak plasmas, this occurs especially as a result of injection of high-power electromagnetic waves, used for heating and current drive, as well as a result of internal magnetohydrodynamic (MHD) instabilities. The physics of these phenomena is intimately tied to the properties and dynamics of this suprathermal electron population. This motivates the development of instrumental apparatus to measure its properties as well as of numerical codes to simulate their dynamics. Both aspects are reflected in this thesis work, which features advanced instrumental development and experimental measurements as well as numerical modeling.

The instrumental development consisted of the complete design of a spectroscopic and tomographic system of four multi-detector hard X-ray (HXR) cameras for the TCV tokamak. The goal is to measure bremsstrahlung emission from suprathermal electrons with energies in the 10-300 keV range, with the ultimate aim of providing the first full tomographic reconstruction at these energies in a noncircular plasma. In particular, suprathermal electrons are generated in TCV by a high-power electron cyclotron heating (ECH) system and are also observed in the presence of MHD events, such as sawtooth oscillations and disruptive instabilities. This diagnostic employs state-of-the-art solid-state detectors and is optimized for the tight space requirements of the TCV ports. It features a novel collimator concept that combines compactness and flexibility as well as full digital acquisition of the photon pulses, greatly enhancing its potential for full spectral analysis in high-fluency scenarios. Additional flexibility is afforded by the possibility to rotate the orientation of two of the cameras, permitting the crucial comparison of radiation emitted perpendicular and parallel to the primary magnetic field.

The design of the HXR system was optimized through an extensive iterative simulation process with the aid of tomographic reconstruction codes as well as quasilinear Fokker-Planck modeling of ECH-driven TCV plasmas. In parallel, the selection of the detectors for this system was performed through comprehensive laboratory testing of several candidate detectors available on the market. While the design was completed in the course of the thesis work, commissioning of the system has only commenced recently with one of the four cameras installed on TCV. The first preliminary results, discussed in the last part of this thesis, include basic parameter scans of ECH wave-plasma interaction and the investigation of the dynamic response of suprathermal electrons to modulated ECH. In addition, the cameras possess the novel ability to discriminate against very high-energy γ-ray radiation that cannot be collimated and must thus be excluded from spatial distribution analysis. A basic study of the conditions for γ-ray suppression was conducted in preparation for future experiments.

The Fokker-Planck modeling tool used in this diagnostic development was acquired through a collaboration with CEA-Cadarache, initially with the primary motivation of studying the simultaneous plasma heating by 2nd and 3rd harmonic electron cyclotron waves that is uniquely possible on TCV. This motivated a dedicated study, both theoretical and experimental, of one particular instance of this combined heating, which became a second primary subject of this thesis work. The particular scenario studied here is one in which a single ECH frequency is resonant at both harmonics in the same plasma. The primary objective of this study was to determine whether a synergy effect existed, permitting an enhancement of the intrinsically weak 3rd harmonic absorption by the suprathermal electrons generated at the 2nd harmonic resonance. An associated question was whether this effect, if it existed, was experimentally measurable or was in fact observed in TCV. The simulations performed in the course of this study indeed predict the existence of such a synergy, although the answer to the second question was ultimately negative, at least within the current technical limitations. This study has proven nevertheless highly valuable in providing new insight into the complex velocity-space dynamics that govern ECH wave-particle interaction and suprathermal electron dynamics.

Davoud IRAJI: *"Fast Imaging of turubulent plasmas in the TORPEX device"* EPFL Thesis 5073(2011)

This thesis addresses the issue of turbulence generated modes and intermittent structures using a fast visible imaging system on TORPEX. The plasma radiation mechanisms and experimental setup of the imaging system are discussed together with an optimized tomographic reconstruction method. In TORPEX typical plasmas, radiative ionization is the dominant radiation mechanism. A Photron Ultima APX-RS fast visible camera was used to acquire the light emission of TORPEX plasmas. The camera equipped with the image intensifier is able to image TORPEX plasmas up to 200 kframes/s of framing rate and down to 1 s of exposure time, which results in clear images of plasma structures. The time-resolved poloidal emissivity of TORPEX plasma emission are tomographically reconstructed from tangentially viewed images using a pixel method and singular value decomposition approach. The spatial resolution in the reconstructed emissivity profiles, is 2cm.

The plasma emissivity and ion saturation current profiles are compared using the conditional average sampling (CAS) technique and statistical analysis of fluctuations. The CAS is performed to visualize the mode structures and to estimate their sizes. The resulting fast imaging of the plasma, non-perturbative and high spatio-temporal resolution diagnostics, can visualize small scale turbulent plasma structures, well beyond the typical spatial resolution of probe arrays.

A two-dimensional gas puff (2D-GPI) imaging system, including a 2D movable gas puff nozzle and a fast framing camera, has been developed in the TORPEX device. Direct local measurements from a large number of probes, distributed across the plasma column, are used to establish a correlation between the plasma parameters and the locally measured visible light emission. GPI and ion saturation current signals are well correlated, with correlation coefficients higher than 0.75. Fourier analysis of the GPI and internal probes show that the GPI can detect the dominant interchange mode. Quasi-coherent interchange modes and intermittent, turbulence generated blobs can be detected and studied using fast visible imaging in TORPEX. For an increasing vertical magnetic field, the principal interchange mode is damped and a sharp transition occurs between low-k and high-k harmonics. The scaling of the radial width of different interchange harmonics with respect to the vertical wave-number k_z shows good agreement between the experimental and theoretical radial-width-k_z scaling in TORPEX plasmas. The gradient-removal mechanism, describing the level of turbulent fluctuations, was tested using experimental data from the visible camera. The saturation level of the interchange instabilities predicted by the gradient-removal mechanism is in reasonable agreement with the experimental measurements. Tomographically inverted data from the fast camera were used to study the propagation of intermittent blobs. The experimental speed-versus-size scaling of blobs in the camera data is in good agreement with theoretical predictions.

This thesis confirms the possibility of using fast imaging to estimate saturation level of fluctuations associated with ideal interchange instability and to reconstruct the blob speed-size scaling law in tokamak plasmas non-perturbatively. This can be used to non-perturbatively estimate the transport levels in the SOL of fusion devices.

Boris LEGRADIC: *"Arcing in Very Large Area Plasma-Enhanced Chemical Vapour Deposition Reactors"* EPFL Thesis 5040(2011)

This thesis presents an investigation into arcing and parasitic plasmas in large area plasma enhanced chemical vapour deposi- tion reactors. Two types were investigated: RF breakdown in millimetric gaps in absence of plasma (e.g. dark space shielding), in a millibar pressure range, and RF hollow cathodes in glow discharges. RF breakdown curves (voltage vs. pressure) for parallel plate electrodes generally show a steep left-hand branch at low pressures and a flatter right hand branch at higher pressures. Introducing protrusions or holes in parallel plate electrodes will lower the breakdown voltage in certain conditions. This is, however, not due to the increased electric field at sharp edges or ridges. Instead, both experiments and simulation show that breakdown at high pressure will occur at the protrusion providing the smallest gap, while breakdown at low pressure will occur in the aperture providing the largest gap. This holds true as long as the feature in question is wide enough: Features that are too narrow will lose too many electrons due to diffusion, either to the walls of the apertures or to the surroundings of the protrusion, which negates the effect on the breakdown voltage. An analytical approximation of breakdown in parallel plates with cylindrical protrusions supports this argument. The simulation developed to study breakdown in structured parallel plate elec- trodes also presents a tool to aid the design of complex RF parts for dark-space shielding. A method was developed to measure the pressure-limits of ignition for RF hollow cathodes, and it could be shown that these limits not only depend on gas type, diameter and depth of the hollow cathode, but also on the presence and/or absence of other hollow cathodes in the vicinity. It could also be conclusively shown that hollow cathodes damage the electrode by sputtering and/or evaporation.

Francesco PIRAS: *"Extremely Shaped Plasmas to Improve the Tokamak Concept"*
EPFL Thesis 5015(2011)

Energy is essential for human existence and our future depends on plentiful and accessible sources of energy. The world population is fast growing and the average energy used per capita increases. One of the greatest challenges for human beings is that of meeting the growing demand for energy in a responsible, equitable and sustainable way.

The possibility to obtain energy by “fusing” light atoms addresses these needs. Nuclear fusion reactions are clean, safe and the amount of fuel present on Earth (hydrogen isotopes) is practically inexhaustible and well distributed. Nuclear fusion is a natural process that occurs in all active stars like our Sun. Since the first demonstration of a deuterium fusion reaction (Rutherford 1933), researchers worldwide have tried to replicate this process on Earth by building a thermonuclear fusion reactor. Nevertheless, the challenge posed by the construction of a nuclear fusion reactor is greater than the one presented earlier by the development of a fission reactor. During the IAEA Conference in Geneva in the early 1958, L.A.Artsimovich declared: “Plasma physics is very difficult. Worldwide collaboration is needed for progress” and E.Teller, at the same conference: “Fusion technology is very complex. It is almost impossible to build a fusion reactor in this century”. They were right. The extremely high temperature and density necessary to fuse hydrogen isotopes makes it difficult indeed to create a successful fusion reactor. Even though the physics of the fusion reaction appears clear, we are still facing problems on the road towards building the “box” that can efficiently confine the hot gas in the state of plasma.

The best results so far have been obtained confining a plasma with strong magnetic fields in a toroidal configuration (“tokamak”). The Centre de Recherches en Physique des Plasmas in Switzerland actively studies this promising configuration towards the development of a nuclear fusion reactor. The experimental activity of the Tokamak à Configuration Variable (TCV) mainly focuses on the research of optimized plasma shapes capable of improving the global performance and solve the technological challenges of a tokamak reactor. Several theoretical and experimental results show the importance of the plasma shape in tokamaks. The maximum value of β (an indicator of the confinement efficiency) is for example related to the ratio between the height and the width of the plasma. The plasma shape can also affect the power necessary to access improved confinement regimes, as well as the plasma stability.

This thesis reports on a contribution towards the optimization of the tokamak plasma shape. In particular, it describes the theoretical and experimental studies carried out in the TCV tokamak on two innovative plasma shapes: the doublet shaped plasma and the snowflake divertor. Doublet shaped plasmas have been studied in the past by the General Atomics group. Since then, the development of new plasma diagnostics and the discovery of new confinement regimes have given new reasons for interest in this unusual configuration. TCV is the only tokamak worldwide theoretically able to establish and control this configuration. This thesis illustrates new motivations for creating doublet plasmas. The vertical stability of the configuration is studied using a rigid model and the results are compared with those obtained with the KINX MHD stability code. The best strategy for controlling a doublet on TCV is also investigated, and a possible setup of the TCV control system is suggested for the doublet configuration. Analyzing the possible scenarios for doublet creation, the most promising scenario consists of the creation of two independent plasmas, which are subsequently merged to establish a doublet. For this reason, particular attention needs to be devoted to the problem of the plasma start-up. In this thesis, a general analysis of the TCV ohmic and assisted with ECH plasma start-up is presented, and recent attempts to create a doublet plasma are reported. Since the magnetic field reconstruction at the breakdown time is important to better diagnose these plasmas, the entire magnetic system of TCV has been calibrated with an original technique, also described in the manuscript. The last part of this thesis is devoted to the snowflake divertor configuration. This innovative plasma shape has been proposed and theoretically studied by Dr. D.D.Ryutov from the Lawrence Livermore National Laboratory. In Ryutov's articles, this configuration was proposed to alleviate the problems of the plasma-wall interaction and possibly affect the plasma edge stability. The TCV tokamak was the first to report the creation and control of a snowflake configuration, and the candidate was the principal investigator of this work. These results are accordingly discussed in this thesis. Details are provided in particular on the strategy used to establish the configuration. An edge-localized mode (ELM) H-mode regime, supported by electron cyclotron heating, has been successfully established in a snowflake. This regime exhibits 2 to 3 times lower ELM frequency but only a 20%-30% increase in normalized ELM energy (W_{ELM}/W_P) compared to an identically-shaped, conventional, single-null, diverted H-mode. Enhanced stability of mid- to high-toroidal-mode-number ideal modes is consistent with the different snowflake ELM phenomenology. Finally, the capability of the snowflake to redistribute the edge power on the additional strike points has been confirmed experimentally and is also reported in this thesis.

Marina RICCI: *"On the powder formation in the plasma enhanced chemical vapor deposition process for the deposition of SiOx barrier coatings"* EPFL Thesis 4991(2011)

Nowadays thin films play an important role in everyday life and in industries. Thin film technology has been developed primarily for the growing demand for development of smaller and smaller devices that require advanced materials and new processing tech- niques suitable for micro and nano technology. One of the methods of producing thin films is by means of plasma technology. This is a technique by which plasma, also known as 'the fourth state of matter', is used to generate ions, electrons and radicals which deposit at a surface where they will form a thin film. The source of these depositing species could be either gaseous, liquid or solid in origin. Most of the time a plasma is generated by means of an electrical discharge. Plasma technologies are used for various applications. One of these is Plasma Enhanced Chemical Vapor Deposition (PECVD). PECVD systems have widespread applications in the electronic sector, because of their flexibility in depositing different films such as silicon oxide thin films (SiO_x). These films,

currently deposited by organosilicon compounds, such as hexamethyldisiloxane (HMDSO), have dielectric and good barrier properties.
The aim of the work at CRPP consists in optimizing PECVD processes for the deposition of these films on polymers. In this study, the species in gaseous phase and the powder produced in oxygen-diluted HMDSO plasmas were experimentally characterized in a radiofrequency (RF) capacitively-coupled reactor at 13.56MHz. The gaseous phase of these plasmas and the particle formation were studied by in-situ infrared absorption spectroscopy and optical emission spectroscopy. The study of the powder formation is important because the particle deposition imposes an upper limit on the deposition rate.
Particle formation was firstly studied as a function of HMDSO/O_2 ratio. Analysis of the time evolution of the infrared absorption spectra gives the development of the size, the number density, the structure and the particle composition. At high oxygen dilution the formation of large particles is observed. The analysis of HMDSO/O_2 plasma at low O_2 content suggests that at the beginning of the process very small particles are formed by polymerization; the same particles do not grow much and keep sizes around 50 nm. The admixture of inert or non-reactant gases, such as Ar or N_2, into the plasma promotes polymerization of the monomer; a high value of one of these inert or non-reactant gases leads to small powder particle size, since only polymerization takes place in this case. Particle size around 50nm is also found in this case. At the same time we see a decrease of the carbon content and a weak reduction of the stoichiometry in SiO_x indicated by the shift of the SiOSi asymmetric stretching vibration. This reduction also influences the deposited layers, less oxidized and, thus, quite far from a stoichiometric character.
Hexamethyldisilazane (HMDSN) and tetramethylsilane (TMS) are other reagents that have been identified as alternatives to HMDSO. The in-situ infrared absorption spectra show that HMDSO/O_2 and HMDSN/O_2 plasmas are quite similar, but in the second case a lower SiOSi stretching peak intensity, due to NH and SiN peaks, is seen. TMS/O_2 and HMDSN/O_2 plasma spectra show a low SiOSi bending and stretching peak intensity, due also to the oxygen atom absence in their chemical structure.
Two separate chapters are respectively devoted to the silicon nitride thin films (SiN_x) and plasma crystal formation. SiN_x layers are deposited by three different organosilicon compounds, such as HMDSN, TMS and bis(dimethylamino)dimethylsilane (BDMADMS). No powder formation is visualized in this contest. The ex-situ infrared absorption spectra show the difficulty to produce stable SiN_x films; they present a low SiN peak intensity and are quite hygroscopic. Furthermore, in HMDSO/O_2 plasmas at high oxygen dilution and high pressure, later in time into the discharge, accretion leads to larger and larger particles which can finish up in particles forming a plasma crystal. The study of RF harmonics shows the presence of instabilities, clear indications of the passage from small particulate to plasma crystal structure.

Christian THEILER: *"Basic investigations of turbulent structures and blobs of relevance for magnetic fusion plasmas",* EPFL Thesis 5228 (2011)
Similarly to neutral fluids, plasmas often exhibit turbulent behavior. Turbulence in plasmas is usually more complex than in neutral fluids due to long range interactions via electric and magnetic fields, and kinetic effects. It gives rise to many interesting phenomena such as self-generated magnetic fields (dynamos), zonal-flows, transport barriers, or particle pinches. Plasma turbulence plays a crucial role for the success of nuclear fusion as a potentially clean, safe, and long-term source for electric power production.
Turbulent processes in the edge and scrape-off layer (SOL) of magnetic fusion plasmas determine, to a large extent, the overall confinement properties. They also influence the life time of plasma facing components, impurity production and influx, main chamber recycling, tritium retention, and helium ash removal. Edge

turbulence is often dominated by blobs or filaments, magnetic-field-aligned plasma structures observed in the edge of virtually all magnetized plasmas.
This thesis investigates basic aspects of edge turbulence and blobs in simple magnetized toroidal TORPEX plasmas. TORPEX includes important ingredients of SOL physics, such as pressure gradients, grad-B and curvature of the magnetic field, together with open field lines. A relatively simple magnetic geometry, full diagnostics access and the possibility of controlled parameter scans allow isolating and studying instabilities and turbulence effects that occur in more complicated forms in fusion and astrophysical plasmas.
Using a number of optimized probe diagnostic methods, the mechanisms for the generation of blobs from ideal interchange waves and for their subsequent propagation are elucidated. A blob velocity scaling law is introduced that takes into account several damping effects of blob cross-field velocity. This scaling law is in good agreement both with blob simulations and experiments on TORPEX. Studies on blob parallel dynamics shed light on blob induced parallel currents and the transport of parallel momentum. Based on this understanding of blob motion, several tools to influence blobs and turbulence as a whole are developed. A methodology for plasma turbulence code validation is established. Using a large set of observables, the agreement between experiments and both 2D and global 3D two-fluid simulations is quantified.

Lyubomira VELEVA, *"Contribution to the Production and Characterization of W-Y, W-Y2O3 and W-TiC Materials for Fusion Reactors"*, EPFL Thesis 4995 (2011)
This PhD Thesis work was aimed at investigating the potentiality of tungsten-base materials as *structural materials* for the future thermonuclear fusion reactors in attempting to develop reduced activation tungsten-base materials with high strength and sufficient ductility, especially in terms of fracture toughness and ductile-to-brittle transition temperature, on the basis of the following ideas: (1) nanograined materials are expected to show an improved ductility with respect to normal grain-sized materials, and (2) nano-grained materials and materials reinforced with either oxide or carbide particles are expected to show improved strength and radiation resistance, as (i) the particles should act as obstacles for the propagation of mobile dislocations, (ii) the numerous grain boundaries and interfaces between the matrix and the particles should act as sinks for the irradiationinduced defects, and (iii) the particles should also help stabilizing the numerous grain boundaries upon thermal annealing and/or irradiation. A variety of W-base materials, namely W-(0.3-1.0-2.0)Y2O3, W-(0.3-1.0- 2.0)Y and W-(0.3-0.9-1.7)TiC materials (in weight percent), have been successfully produced at the laboratory scale by powder metallurgy techniques including mechanical alloying followed by either cold pressing and sintering or hot isostatic pressing (HIPping). X-ray diffractometry and scanning and transmission electron microscopy observations combined with density and microhardness measurements as well as with tensile, Charpy impact, fracture toughness and nonstandard three point bending tests allowed the identification of optimal chemical compositions and manufacturing conditions, among those investigated and on the basis of the experimental devices at disposal. Microscopic investigations showed that the materials produced at the laboratory scale are composed of small grains, with sizes between a few tens and a few hundreds nanometers, and contain a high density of small Y2O3 or TiC particles, with sizes between 1 and 50nm. In the case of W-Y materials, all the Y transformed into Y2O3 during mechanical alloying, due to the high amount of O (around 1wt.%) present in the milled powders, which is beneficial for reducing the excess O content in the materials. All materials also contain a residual porosity of a few percents, which is typical of materials compacted by HIPping. Macroscopic investigations showed that the HIPed materials exhibit high strength values and a promising resistance to irradiation but poor fracture properties up to a very high temperature of about 1100°C, due mostly to air contamination of the mechanically

alloyed powders and to residual porosity of the compacted materials. The materials produced entirely at the laboratory scale by mechanical alloying and HIPping are of better quality than a W-2Y material that was produced by mechanical alloying at the laboratory scale and compacted by sintering and forging at the Plansee company (Austria). Further studies should focus on reducing the O content in the mechanically alloyed powders and the residual porosity of the compacted materials. The grain size should be also optimized as well as the size distribution, number density and crystallographic features of the oxide and carbide particles.

Ph.D. Theses supervised by CRPP staff at the end of 2011

Fabio AVINO: *"Study of the design of the TORPEX in-vessel toroidal wire"*
The TORPEX device has been used in previous years to study Scrape-Off Layer relevant physics and plasma instabilities in magnetic configurations with open field lines. These are generated by a toroidal magnetic field together with a small vertical magnetic field component. In order to obtain a magnetic field configuration closer to a tokamak, an in-vessel toroidal copper wire will be installed. A dedicated power supply will provide a current flowing inside the wire of the order of 1 kA during the flat-top phase, for a time interval of about 0.2s. This will produce a poloidal magnetic field resulting in magnetic configurations with closed field lines. Furthermore, the plasma production will be decoupled from the source of the magnetic field.
During the last year my work has been focused on the optimization of the design of this new system, including the computation of the mechanical forces that will act on the different parts of it, as well as the Ohmic heating of the wire; this last point was carefully studied to avoid any active in-vacuum cooling of the wire. The first simulations of the magnetic field configurations that will be accessible have also been performed, showing that Single NULL or Double NULL X-point configurations will be achievable using the vertical magnetic field coils already available.

Karim BESSEGHIR: *"On-line re-optimisation of ITER scenario trajectories and full tokamak simulations for ITER"*
The research work performed this year is twofold, both topics being linked to the specific features and requirements of ITER operation:
1) On-line re-optimisation of ITER scenario trajectories
One of the major challenges in ITER operation is to perform plasma pulses close to ITER optimal performance, while avoiding exceeding the tokamak operating limits or reaching regimes that may lead to plasma disruptions, to which ITER has a very low tolerance. ITER operators will therefore need to compromise between optimal performance and acceptable risk during a plasma pulse, and some degree of automation in ITER operation is necessary for performing such a task quickly and reliably. Moreover, re-optimising the scenario trajectories mid-pulse, according to the state of the tokamak, presents a considerable added value in that it guarantees close-to-optimal performance.
Keeping that goal in mind, a simple approach has been tested and implemented, in order to assess the performance of optimal control algorithms to tokamak operation. Thus, an open-loop optimal control algorithm has been developed, tested, and implemented on the full tokamak simulator DINA-CH. The implementation of this algorithm demonstrated the validity of the optimal control algorithm, as well as demonstrating that a measurable increase in performance was made – at least according to our definition of optimal operation. This work was presented at the 2011 European Physical Society conference in Strasbourg, France.
2) Full tokamak simulations for ITER

In the framework of a grant partially funded by Fusion for Energy (F4E), simulation of an ITER hybrid scenario and an ITER steady-state scenario was undertaken. This work aimed at demonstrating the feasibility of performing such scenarios using the present ITER tokamak design. The outcome of this work was the simulation of a full length hybrid scenario simulation and of a half-length steady-state scenario simulation. These results were reported to F4E, and the strengths and weaknesses of our approach were discussed. Work under this grant is still ongoing and will involve the design of a simple kinetic controller that should enable us to address the remaining issues.

Alexandre BOVET: *" Investigation of fast ion transport in the TORPEX experiment"*
Basic aspects of fast ion transport in ideal interchange turbulent plasmas are investigated in the simple toroidal plasma device TORPEX. Fast ions are injected in the plasma by a miniaturized lithium 6+ ion source with energies up to 1keV, and are detected using a double-gridded energy analyzer (GEA) mounted on a two-dimensional movable system. The signal to noise ratio is enhanced by applying to the fast ion source a modulated biasing voltage and using a synchronous detection scheme. An analog lock-in amplifier has been developed, which allows removing the capacitive noise associated with the voltage modulation.
A first set of experiments is conducted using four different fast ion energies ranging from 88eV to 290eV. The GEA is placed at 40cm away in the toroidal direction from the fast ion source and the fast ion current density profiles are reconstructed in the poloidal cross section. The profiles are broadened by the plasma for all energies, demonstrating that the interaction of the fast ions with the turbulence is important.
To interpret the experimental data, fast ion tracer trajectories are followed using the full Lorentz force, with turbulent electric fields, which are numerical computed by solving the drift-reduced Braginskii equations in two dimensions. Comparisons with simulations are performed using a synthetic diagnostic, allowing the poloidal cross section of the fast ion current density to be reconstructed. Both the experiments and the simulations show that the turbulent spreading is the largest for low ion energies.
The construction of a toroidally moving system for the fast ion source is under way. This system will allow reconstructing the fast ion beam in the three spatial dimensions.

Danielle BRUNETTI: *"A study of internal kink modes in ITER hybrid scenarios"*
Numerical simulations for ITER like equilibria, with hollow *q* profiles which have an off axis minimum close to unity, were carried out using the 3D equilibrium code ANIMEC, which showed the presence of 3D helical cores in these particular configurations; it has been shown that these three dimensional structures have the characteristics of a saturated internal kink mode. Given this surprisingly result, we choose to examine the problem in a more conventio- nal manner, by investigating the internal kink perturbation non-linearly using the XTOR code, initially in the ideal frame. We start from a given 2D ITER like equilibrium ($\beta \approx 3\%$, $0.96 < q_{min} < 1.01$, with the same profiles which give rise to the 3D helical cores, an interface between ANIMEC and CHEASE code was built, providing the required equilibrium files for XTOR. A convenient value for the viscosity was chosen, in order to avoid numerical instabilities in the core region; a scan in the current was done, ranging from 13.2 to 13.8MA, showing a good agreement in the helical distorsion with ANIMEC when the minimum of q is above the unity (low currents), but a significant deviation when $q_{min} < 1$: while the helical distorsion predicted by ANIMEC decreases to 0 when $q_{min} \approx 0.96$, XTOR gives a residual tail in this region accordingly with the linear stability calculations performed with TERPSICHORE code. This difference between the equilibrium state calculated with ANIMEC and the saturated XTOR results are

not presently understood, but will be investigated as part of future studies in this area.

Ciro CALZOLAIO: *"Irreversible degradation in Nb_3Sn CICC"*
Conductors made by Nb3Sn material are characterized by high critical temperature (T_c), for Low Temperature Superconductors, and high upper critical field (B_{c2}) but these significant advantages are tempered by the propensity of the superconducting filaments to fracture. Nb_3Sn is a brittle material that has a limited maximum elongation and as such is characterized by its very strain sensitive superconducting performance.
A novel technique to measure the temperature dependence of the magnetic susceptibility of a large cable in conduit conductor (CICC) has been developed. From these measurements it is possible to evaluate the critical temperature (T_c) of the CICC and to monitor the T_c behaviour during the electromagnetic cyclic loading tests in the SULTAN facility. Comparing the T_c of the CICC with the one of the filaments used for the cable manufacture it is possible to estimate the thermal strain distribution in the CICC cross section.
The derivation of the cable cross section strain state has been performed using a deconvolution algorithm. The main idea behind the deconvolution algorithm is that the CICC susceptibility is the sum of all the susceptibilities (χ) of the Nb_3Sn filaments present in the cable. Each filament is characterized by a certain strain state, therefore by a certain T_c value. The goal of the algorithm is to find a probability distribution function (pdf) able to describe the probability that the T_c of a filament falls inside a certain T_c range. Therefore it is necessary to divide the T_c range into a limited number of intervals, the largest possible T_c being the one of the free standing filaments. The result of this discretization process is a susceptibility matrix X_M. From a numerical standpoint the deconvolution algorithm consists in solving an over-determined least square problem for which the Moore-Penrose pseudo-inverse of the susceptibility matrix has to be calculated.
The procedure has been applied to both a toroidal field and a central solenoid conductor showing a broad distribution of thermal strain, peaked at negative strain.

Gustavo CANAL: *"Sawtooth Generated Magnetic Islands and properties of New Divertor Configurations"*
It has been observed that the performance in long-pulse tokamak plasmas has been limited by tearing modes, which are usually found to be linearly stable. A sufficiently large seed island flattens the pressure profile across the island and, thereby, perturbs the neoclassical bootstrap current, which can result in a further growth of the island. Hence, these instabilities are called Neoclassical Tearing Modes (NTMs). NTMs degrade the energy confinement and may lead to disruptions and must be avoided in a future reactor. This part of the work aims to improve the understanding of the coupling between sawteeth and tearing modes, which could indicate ways to avoid the coupling and safely operate at higher plasma pressures where NTMs are meta-stable.
Energy and particle losses across the separatrix are directed into the divertor region. The power flux on the divertor plates may cause overheating and destructive erosion. The problem is aggravated by edge localized modes (ELMs) which occur in the high-confinement H-mode and cause periodic bursts of energy and particles leading to even higher peak of heat fluxes onto the divertor surfaces. In order to maintain steady state operation in a reactor, the power exhaust and plasma–wall interaction must be kept at a level compatible with the properties of the wall materials. Different solutions have been proposed to reduce the plasma–wall interaction. This part of the work seeks to evaluate the advantages of a so-called Snowflake (SF) divertor. While in a standard X-point configuration (Single Null

configuration), the poloidal magnetic field vanishes at the null point, in a SF the first derivative of the poloidal magnetic field vanishes too.

Michael CHESAUX: *"A new low ion energy bombardment PECVD reactor for the deposition of thin film silicon for solar cell applications"*
The deposition of thin film silicon solar cells done with PECVD using a CCP at VHF lead to a deposition rate of few Å/s and the film thickness is in the range of 0.2 to 3 m. To obtain higher deposition rates more power is often used but this causes an increase of the ion bombardment intensity thus creating higher defects density of the produced films. It is thus necessary to reduce this bombardment in order to increase solar cells efficiencies and satisfy industry demand in term of production yield. This research aims to reduce this ion bombardment by changing the reactor design.
During 2011, a retarding field analyser was built and tested. It shows that the new reactor design successfully reduces the ion energy. To understand the physical mechanism underling this lower ion energy, other reactor designs are being tested and a phase resolved optical emission spectroscopy will be installed.
The work on numerical simulations is continued. It provided useful numerical data to understand the mechanism underling this lower ion and to understand better the influence on the plasma of atomic and molecular gas.

Cornelis DE MEIJERE: *"Experimental study of turbulence in TCV plasmas"*
A phase-contrast imaging diagnostic for measuring turbulent density fluctuations on TCV has been commissioned and operated for the first time. The unique and novel asset of this CO2 laser based imaging system is its viewing direction, which is tangential to the magnetic field: this allows localization of the measurement by appropriate spatial filtering in a focal plane. Several technical issues were encountered during the commissioning, including the loss of 21 of the 30 detector elements, and excessive vibration of the vessel-mounted optics, which were also found to introduce severe optical aberrations. These problems could be solved only partially so that the performance of the diagnostic is not yet optimal. Nevertheless, several dedicated experiments were performed in December to measure for the first time the suppression of turbulence in plasmas with an electron internal transport barrier. A scan of triangularity has also been performed, to address the long standing issue of the associated improved confinement variation. The data are currently being analyzed.
In early 2011, the analysis of previously performed reflectometer measurements on the TEXTOR tokamak was finalized, revealing for the first time in TEXTOR the presence of a so called fishbone mode. This mode triggers ELMs and it also interacts with beam driven Alfvén waves. Several other, distinct ELM precursor modes were also characterized. These results were presented at the EPS plasma physics conference in June 2011.

Wondwossen Wubie ESHETU: *"Electron cyclotron emission (ECE) diagnostic on TCV"*
A vertical electron cyclotron emission (V-ECE) diagnostic was installed on TCV for the study of non-thermal electrons. The transmission line of the V-ECE system was laser-aligned. A technique has been developed for the calibration of the V-ECE system using the plasma as a known source. This involves developing of analysis code for the calculation of the radiation temperature using radiation transfer equations, and the existing analysis codes of TCV.
First measurements were taken for the calibration of the V-ECE system. Some of the radiometers channels were calibrated to demonstrate the technique. Analysis

techniques for the calculation of the distribution function of non-thermal electrons from the calibrated V-ECE signals has been developed.
In addition to V-ECE, TCV has previously installed horizontal ECE diagnostics. The horizontal ECE diagnostics are used to measure ECE along a horizontal sight from both the high field side and the low field side of TCV. In order to interpret the measurements, the signals have to be calibrated. For this purpose, a code has been developed that allows the calibration of horizontal ECE-signals against Thomson diagnostic. The code includes the effect of harmonic overlap and wall radiation and is being used for post shot analysis of the TCV experiments.

Lucia FEDERSPIEL: *"CXRS diagnostic update and momentum transport in TCV across sawteeth events"*
During this year an analysis of the complete CXRS optical path covered by the photons emitted from the CX reactions in TCV to the CXRS cameras was performed. The largest system losses (at the spectrometer's entrance slit and first mirror) were determined and it was seen that the total efficiency of the Toroidal and Poloidal Low Field Side systems (TLFS and PLFS) is only of about 1-2%.
In the second half of 2011 considerable effort was employed in reviving the Toroidal High Field Side (THFS) system by installing the previous TLFS camera (Xcam Ltd with an e2V CCD57 detector) on a ACTON AM-506 spectrometer. Unfortunately, the spectrometer mirrors have important defects reduced by partially masking the first mirror. Moreover, the THFS acquisition was synchronized with the TLFS and PLFS systems and integrated into the TCV plant control system.
The evolution of the toroidal plasma rotation across ST events was remeasured with the new CXRS diagnostics using a real-time triggering sequence on ST crashes measured using a soft X-ray detector, together with ECH partially stabilised ST. Preliminary rotation profiles obtained with the Andor cameras (allowing a better radial resolution for a 2ms acquisition) appear to confirm our previous results and show a strong co-current acceleration of the plasma core at the ST crash followed by a smaller counter-current acceleration outside the ST inversion radius.
The formation and sustainment of eITBs was the main focus of experiments this year. The aim was to assess the role of rotation and E×B shearing rate in TCV's eITBs using the present CXRS cameras set up in standard and fast acquisition allowing measurements of stationary and pre-barrier formation rotation profiles. The effect of EC power on the barrier strength and rotation profiles was examined by applying 730kW central ECH or counter-ECCD (giving a central eITB). When applying a central cnt-CD power the peaked counter current rotation sustained in the core and the p_e profiles have doubled values compared with the ECH case, indicating a confinement improvement in the central region. In addition, two eITBs targets at z=2-5 cm have been developed on TCV, by applying off-axis co-ECCD with central ECH or just using counter-ECCD applied on axis. The development of these targets has proved to be extremely challenging due to unfavorable EC power depositi
on regions around z=0cm and a density too elevated to obtain strong barriers. The effect of central ECH power and inductive current density perturbations on the barrier strength and rotation profiles has been partially examined on both targets using the new CXRS configuration and the data will be analysed next year.

Natalia GLOWA: *"Quench characterization of a small solenoidal insert coil"*
High Temperature Superconductors (HTS) have been widely studied because of their merits, which include low cooling cost and high critical current density for high magnetic fields.
Thanks to the superconducting and excellent mechanical properties of the substrate used in the second generation YBCO coated conductor, the potential of

using it as insert coils in order to upgrade the existing low temperature superconductors (LTS) is significant.
The stability of the HTS is much higher than for LTS, thus HTS magnets hardly quench both during current charging and operating conditions. However, with the quench propagation velocity along the wire being very low, it is difficult to detect a hot spot and protect the HTS from overheating.
Therefore, it is of great importance to address the challenges associated with quench detection and protection. This will require an understanding of quench behaviour of HTS materials which could be the starting point of my PhD thesis.

Nazar ILCHUK: *"Characterization and modeling of neutron irradiation, pre-deformation and warm prestressing effects on the fracture behavior of the tempered martensitic steel Eurofer97"*
The fracture toughness behavior of cold-forged tempered martensitic steel Eurofer97 was investigated. Sub-sized pre-cracked compact tension fracture specimens were machined from cold-forged plate and tested in the lower transition temperature region accordingly to the ASTM-E1820 standard of the Master-Curve. The cold-forged material has shown similar behavior to the irradiated one in terms of fracture properties degradation, i.e. a shift of the reference temperature T_0 to the higher temperature values. In order to supplement our previous fracture toughness database on irradiated Eurofer97, experimental activities were undertaken to investigate the tensile behavior after irradiations to 0.35dpa at two different temperatures, 150°C and 350°C, respectively. The tests were carried out on small flat tensile specimens with a shielded machine in the hotlab at Paul Scherrer Institute. A finite element (FE) model of that tensile specimen geometry was successfully developed in order to extract the constitutive behavior of irradiated material using an inverse methodology to reconstruct the experimental load-displacement data. The microhardness characterization by instrumented nanoindentation undertaken in the past revealed the importance of a precise determination of the indenter-specimen contact area for the tempered martensitic steels. Thus, 3D and axisymmetric FE models of Vickers indenter were developed and experimentally validated to properly take into account and quantify the effect of a pile-up in the hardness measurements of Eurofer97. The effect of warm prestressing treatment and residual stresses on the fracture and notch toughness was also studied using notched tensile fracture specimens of the tempered martensitic steel F82H pre-loaded at room temperature to different loads to create a region with residual stresses around the notch. The triaxial stress state of residual stresses in prestressed notched tensile fracture specimens was measured by the time-of-flight neutron diffraction method using POLDI-SINQ instrument at PSI. While the stress distribution around the notch is in relative good agreement with FEM results, the absolute values of the stress components show some discrepancy; work is in progress to clarify that issue.

Josef KAMLEITNER: *"Suprathermal electron studies in Tokamak plasmas by means of diagnostic measurements and modeling"*
The main objective of this work is to improve the current understanding and develop new insight into the physics involving electrons at suprathermal energies in tokamak plasmas. These electrons represent an important channel of energy release from magnetic reconnection during the evolution of the sawtooth instability, and runaway bursts are also observed during major disruptions. Their dynamics in both physical and velocity space are also crucial for the understanding of electron cyclotron resonance heating and current drive (ECRH and ECCD).
During collisions these electrons emit hard x-ray bremsstrahlung radiation in the range of several to hundreds of keV. This emission is measured using the new hard x-ray tomographic spectrometer (HXRS) diagnostic of which the first of four

cameras, comprising 25 CdTe detectors and a digital data acquisition system, was fabricated, tested, calibrated and subsequently installed and successfully commissioned on TCV. Other diagnostics were improved: for the tangential x-ray detector array (TXDA), which measures hard x-ray flux to investigate fast events such as sawteeth, an automated remote control system was implemented. Furthermore the vertical pulse height analyzer (PHAV) was re-installed and equipped with an automated data acquisition connected to the TCV database.
Several codes for both basic and advanced data analysis have been developed. The general tomographic inversion (GTI) code unifies the data analysis of several multichord and tomographic diagnostics. It offers an exhaustive set of options regarding inversion method, discretization and data pre- and post-processing.
To model ECRH/ECCD as well as the suprathermal electron dynamics, quasilinear Fokker-Planck codes like CQL3D and LUKE used, which are also coupled to bremsstrahlung calculators linking modeled to measured data. Work in 2011 has focused on the LUKE code.
The following are the main physics results obtained within the first year of the thesis:
During sawtooth crashes in low density plasmas (typically n_e<2 $10^{-19}m^{-3}$) electrons are accelerated to relativistic energies (runaway electrons) emitting bursts of gamma radiation that is practically impossible to stop or collimate.
Above this density limit, however, the uncollimated hard x-ray radiation reaching the HXRS and TXDA detectors becomes negligible. Conditional averaging techniques permit resolving on a fast time scale the spatial and temporal evolution of hard x-ray emission from ECR heated electrons at different energies before, during and after sawtooth crashes. By using ECCD modulation and coherent averaging it is also possible to follow the suprathermal electron dynamics at high time resolution in response to ECCD.
Tangential hard x-ray measurements of strongly ECCD heated plasmas show, as theoretically expected, a clear asymmetry between hard x-ray emission in the co- and counter- plasma current directions at suprathermal energies.

Doohyun KIM: *"Experimental analysis and simulation of the pacing and locking of sawteeth in the TCV tokamak"*
As a first step of studying sawtooth pacing and locking, I have studied the change, due to reconnection, of magnetic flux surfaces before and after a sawtooth crash. By following Kadomtsev(full) and Porcelli(partial) reconnection model, I made a module which can describe the change of plasma properties during a sawtooth crash. I also have studied the effect of ECH on sawtooth period with ASTRA simulations. First, I have looked into the effect of heating position and power level. By radially sweeping the ECH position at fixed power, I was able to show the change of sawtooth period and find the best position to stabilise sawtooth. Alternately, I changed the heating power level at fixed heating position. The position of q=1 surface is affected by the heating power value therefore the relative heating position changes resulting in a change of sawteeth period. By careful simulation, I was able to see the change of sawteeth period corresponded by the heating power and position, seperately. Second, I simulated pacing and locking of sawtooth periods. In this case the simulation was done by changing free parameters to make the sawteeth period match a reference experimental result. Sawtooth pacing is a real-time control method. After detecting the sawtooth crash, ECH is turned on during a time interval (τ_{set}) and then turned off. The shear at the q=1 surface increases more slowly when ECH is on than when it is off, and using this phenomenon, the sawtooth crash can be induced by choosing τ_{set}; that is removal of the power induces a rapid rise in the shear above the critical value that triggers the crash. This expectation was verified by the simulation. It showed comparable sawtooth periods to experimental results that are successfully paced by ECH modulation. In contrast, sawtooth locking, while basically similar to pacing, is not

based on real-time control. Disregarding the sawtooth crash, ECH can be applied with a desired period and duty cycle. Under certain conditions, the sawtooth period matches the modulated ECH period. As in the pacing simulation, the locking simulation also agreed with experimental results. By changing the duty cycle of ECH, I was able to find the range in which the sawtooth period was locked to the modulated ECH period. During this year, with these simulations, I have been able to understand how magnetic surfaces are reconnected during a sawtooth crash and how the sawteeth period is affected by the position and power of ECH. In addition, I also have an idea how to control sawteeth periods with modulated ECH and can now plan to apply this control method to other tokamaks.

Joaquim LOIZU: *"Simulation of plasma turbulence in the TORPEX basic plasma physics experiment"*
An effort is being put in the improvement of the GBS code, focusing on the physics of the plasma-wall transition (PWT). Indeed, boundary conditions for plasma fluid models are needed at the magnetic presheath entrance, namely the region where the assumptions of the model breakdown. Boundary conditions determine the plasma losses at the vessel, thus strongly affecting the steady state profiles. A kinetic approach is needed in order to describe the PWT, since the drift-reduced approximation breaks (magnetic presheath), followed by a breaking of quasi-neutrality (electrostatic sheath). For this purposes ODISEE (One-Dimensional Sheath Edge Explorer), a 1D3V fully kinetic particle-in-cell code modeling a plasma bound between two walls [Physical Review E, 83, 016406, 2011], was used to simulate the PWT in the general case of an oblique magnetic field. A combined fluid and kinetic description of the plasma, supported by the numerical results, has been used to derive the position of the magnetic presheath entrance and to understand how the fluid quantities are related at this point. In particular, the angular dependence of the different potential drops ocurring in the different subregions of the PWT has been obtained. The implementation of these boundary conditions in the GBS is currently being carried out. The ODISEE code has also been upgraded with new tools that allow for exploring new interesting features of the PWT. These include for example the possibility of seting the wall as either a biased conductor or an insulator, or inserting a biased grid in the system with some given transparency. This has in particular lead to the discovery of a plasma potential phase transition ocurring in a 1D plasma bound between two biased walls when subject to different amounts of charge injection. An experimental verification of this effect is being currently considered.

David MARTINET: *"Development of industrial gas-metal plasma sources for the deposition of nanostructured GaN semiconductor layers for lighting applications"*
This CTI project (No. 11548.1 PFIW-IW), in collaboration with Sulzer METCO and the Laboratory of Advanced Semiconductors for Photonics and Electronics (LASPE) at the EPFL, will try to modify the existing RF and DC plasma sources in order to grow GaN films on SiC or sapphire substrates, by evaporating Ga in nitrogen plasma.
The RF plasma source has fully characterized by optical emission spectroscopy (OES), Langmuir probe and Faraday cup (FC), in two different configurations: with and without an extraction grid. The major effect of this grid is to create an ion beam. Different gas mixtures have also been tested: pure nitrogen, nitrogen-hydrogen and nitrogen-argon. OES measurements with Ga at different fluxes have been made too. In this reactor, the first GaN layers have been grown on silicon substrates.
The DC plasma source with the circular anode has also been characterized with OES and Langmuir measurements, with pure nitrogen, to check the uniformity across the reactor. This device had to be prepared to the Ga evaporation too,

leading to major changes. Different anode positions and gas mixtures will be tested, in order to find an optimal deposition design. The wall effects on the plasma composition will also be tested in this reactor.
Beside laboratory experiments, modelling has been started, using OOPIC (particle-in-cell simulations) and COMSOL Multiphysics. The main goals of the simulations are first to find the plasma composition in the source, then to find it on the substrate by transport, and finally to test different reactor geometries. To verify the simulations results, spectra from the plasma composition are made and compared with the measured ones.

Annamaria MOSETTO: *"Linear and non-linear modelling of scrape off layer instabilities"*
Along this year, in the frame of my PhD, I continued the studies on the SOL physics by means of the GBS non-linear code and a linear code, in parallel. Both of them have been developed and maintained by prof. Paolo Ricci and his research group. In particular I concentrated on the analysis of the influ- ence of the magnetic shear on the main SOL electrostatic instabilities, the drift wave (DW) and the resistive ballooning (RB) instabilities. The magnetic shear defines the variation in the pitch of the magnetic field lines along the minor radius. Their twisting tears apart the vortexes and partially destroys the insta- bility structures. I explored linearly the dependence of each instability on the shear parameter. Both the DW and the RB are expected to be damped, but for different values of the shear parameter, due to the different physical mech- anisms involved. Hence I identified the limits in which they are significantly damped. I chose a linear case in which the instability groth rate was clearly decreased and I set the input parameters for a series of non-linear simulations in order to compare the linear and the non-linear response. Through the linear studies, the system appeared to be much more sensitive to the magnetic shear in the absence of electron mass, consequently we decided to modify the GBS code, including the possibility of evolving the system without electron inertia effects. This modification required the introduction of an algebraic equation for the evolution of the parallel electron velocity. The runs including the newly implemented option will allow us to better understand the non linear saturation mechanism in the presence of magnetic shear.

David PFEFFERLE: "*Energetic ion dynamics and interaction with MHD in 3D anisotropic plasmas*"
Making progress in guiding-centre drift theory, a generalisation of the equations of motions including full 3D electromagnetic fields with anisotropic pressure and relativistic effects has been found. Instead of the standard hamiltonian approach, the non-canonical phase-space Lagrangian has been explored and the derived equations of motion have been written in a form which is independent of coordinate choice. It has also been verified that they express the same conservation properties as in the canonical formalism. These features are essential for numerical implementation of guiding-centre motion.
Recently, the VENUS code has been rewritten from scratch to match performance, modularity and clarity criteria. Its new structure is thought to simplify future development and its maintenance. The identification and separation of the "objects" entering in the simulation steps allow greater flexibility and lower risk of bug spread. Benchmarks have encouragingly shown the new version, VENUS-LEVIS, to be faster and more precise. Finally, the guiding-centre equations of motion cited above have been implemented successfully, permitting the use of any type of magnetic coordinates (currently Boozer, VMEC or ANIMEC). This opens a whole new area of investigation, such as transport of hot particles in Stellarators or helical core configurations, runaway electrons, etc.

Anna PROKHODTSEVA: *"Primary Radiation Damage in Ultra High Purity Iron and Model Iron Cromium Alloys"*
Irradiations of bulk ultra high purity Fe, Fe -5, -10, 14Cr specimens were performed in JANNuS facility in Saclay with 24MeV Fe^{8+} and 2MeV He^{+} ions at room temperature to 0.8dpa without and in the presence of ~800 appm He. Nanoindentation of the implanted samples was performed in order to evaluate effects of Cr concentration and presence of He on radiation induced hardening of the investigated materials. It was found that hardness increases linearly with Cr content in not irradiated as well as in single and dual beam irradiated specimens. Also, it appears that He enhances radiation induced hardening.
In order to compare the radiation-induced microstructure obtained in bulk specimens relative to TEM specimens, TEM lamellas were extracted from bulk samples using focused ion beam (FIB) at PSI. Efforts have been made to improve preparation of TEM lamella in order to remove FIB induced damage that interferes with the defects produced during irradiation/implantation. Flash electropolishing method was developed after which thin surface layer of a lamella damaged by FIB is dissolved in the electrolyte. Investigations revealed that the number density of defects visible in TEM was lower in bulk samples. In the single beam case defects of type a_0<100> and 1 2 a_0<111> are in majority in thin foil and bulk specimens, respectively. ½ a_0<111> defects produced in thin foils partially may escape to free surfaces or transform into a_0<100> loops. Comparing the experimental and calculated irradiation profiles in bulk specimens and **g•b** data for single and dual beam irradiation of thin foils it appears that He stabilizes produced defects and 1⁄2 a_0<111> loops is the most probable configuration in the presence of He. In view of assessing the effect of free surfaces molecular dynamics simulations of highly energetic displacement cascades in thin foils were launched. Energy of the incident ion was chosen 300 and 500keV and thickness of the simulation box 40 and 80nm, which corresponds to the experimental conditions for in situ TEM irradiations in JANNuS Orsay. Preliminary results show that number of vacancies exceeds the number of interstitials as mobile interstitials escape to the free surface.
TEM in situ single and dual beam irradiations/implantations were performed in JANNuS facility in Orsay in order to study the effect of crystallographic orientation of the samples on the accumulation of damage. Analyses of the results is in progress.

Jonathan ROSSEL: *"Edge localized mode control in TCV"*
Experiments have been designed and performed in TCV to study the effects of X2 ECRH power deposition in the edge of a type I ELMing H-mode plasma. These experiments included power scans, power deposition location scans and power modulation experiments. Among the power modulation experiments, various heating schemes have been used, in particular feed-forward power modulation and power modulation synchronized in real-time with the ELM cycle. While the power scans have confirmed the ELM type, the deposition location scans have revealed a new technique of ELM amplitude control. The power modulation experiments have also yielded important results concerning the ELM cycle dynamics, ELM pacing being successfully obtained when the ELMs are triggered during the high power phase of the power modulation. A significant part of the year has also been dedicated to the writing of articles and thesis.

Ralf SCHNYDER: *"Discharge ignition phenomena in a complex electrode configuration for space applications"*
Arcing is again a key issue in the application of plasma in industry and also, as in the present case, in space environment and space equipment. Modern satellites, in particular transmission satellites, are being equipped with larger and larger power

systems. Since also the weight aspect is very important the dimensions of the conducting paths for instance, in slide rings are small. Moreover arcing is also considered to be a limiting factor in several other applications of plasmas, thus triggering intense research and development on this topic.

In the present work for ESA (European Space Agency), the collaboration with RUAG Aerospace led to an understanding of fundamentals of the arcing and this knowledge should to be applied to reduce or suppress arcing in space environment and equipment.

The aim of the work at CRPP is to conduct arc ignition, propagation and stability experiments in space environment and to define and conduct elementary experiments. This year optical spectroscopy with different gases confirmed the two main discharge zones for a simplified ring assembly: metal lines for vacuum arc zone (low pressure) ignited by field emission and gas lines for gas discharge zone (high pressure) determined by Paschen law.

Simulation was also started with a parallel plate configuration based on simple Paschen law. Once the simple model was correct according to analytic solution, the model was stepwise extended to the complex ring assembly.

Thibaud VERNAY: *"Collision operators in the gyrokinetic code ORB5: neoclassical transport and turbulence studies"*

In addition to further developments brought to the collision algorithms in the gyrokinetic code ORB5, my main activity was related to the study of collisional ITG turbulence with the code ORB5. The complex interplay between collisions and turbulence in ITG regimes has been studied in detail. Non-linear collisional simulations were made possible thanks to a coarse-graining procedure, written by Dr. Ben McMillan in ORB5, which is able to reduce the numerical noise of a Particle-In-Cell simulation. It has turned out that the collision algorithms in ORB5 are robust and allow relevant studies of the collisional physics in turbulent regimes, confirming the earlier success of neoclassical simulations. Different approximations related to collision operators have been tested as well. The results from the collisional turbulence investigations have been gathered in a paper submitted to *Physics of Plasmas*. Additionaly, the merge between the collisional version of ORB5 and the new electromagnetic version of the code NEMORB has been completed.

David WAGNER: *"Experimental and theoretical study of Impurity Transport on TCV"*

The collisionality dependence of the local logarithmic electron density gradient was investigated in ohmic and electron cyclotron resonance heated H-mode plasmas on TCV. The density profile was seen to flatten when ECH power is added. The dependence of density peakedness on the collisionality is rather unusual: the density peaking increases with increasing collisionality.

With local quasi-linear gyrokinetic simulations it was concluded that the change in collisionality alone cannot reproduce the observed experimental behaviour. The simulation results show that the most important parameter is the ion temperature gradient which was, unfortunately, not available in these experiments. If a rather low ion temperature gradient ($R/LT_i=4$) is assumed the experimental trends can be qualitatively explained. Simulations of H-mode plasmas with ohmic heating only give a moderately peaked density profile, with a significant contribution of the neoclassical Ware-pinch. For cases with ECH, flatter profiles are found and the Ware-pinch contribution is negligible. It is also found that, though the dependence of the peakedness on various parameters (temperature gradients, electron to ion temperature ratio, collisionality) may seem to be very different, the real mode frequency orders the simulation results remarkably. The maximum of the peaking is found where the real mode frequency is close to zero, near the ITG-TEM transition region, and the peakedness decreases moving away from zero to both

directions. This behaviour was also found in the analysis of TCV L-mode plasmas and eITBs, as well as in various AUG studies.
During the last year a series of gas injection experiments has been performed on the TCV tokamak. An extensive dataset was collected mainly on L-mode plasmas and plasmas with internal electron transport barrier. Mainly argon and neon were used as impurity. Argon injection is usually detected as a fast increase (~10ms) followed by a slow decay (~300ms) of the photon emission in the soft X-ray range. Time traces of the soft X-ray diagnostics show very similar pattern and these time scales do not appear to change significantly with, for instance, the addition of central ECH or changing the plasma triangularity from positive to negative. Neon is observed to behave differently in all situations. The decay time is at least one order of magnitude larger than for argon injections.

7 PUBLIC RELATION ACTIVITIES IN 2011

The largest fraction of the CRPP effort in public relation was devoted to the presentation of our research activities to the public through visits of our experimental devices: TCV, TORPEX, GT170 and the reactors for Plasma Processing. In total, more than 1300 persons were introduced to plasma physics, fusion, tokamak, turbulence and industrial process. Most groups were classes of students aged from 10 to 25. Other visitors were groups of politicians, collaborators of technical industries and members scientific organisations. Guided tours were given in French, English, Italian, German, Polish and Hungarian. The biggest event was the 'Journée des Classes': 100 classes of about 20 children (~12 years old) from the french speaking part of Switzerland visited EPFL and among them 15 stopped at the CRPP.

2011 was also marked by the begining of regular publication of news on the web site.

8 FUSION & INDUSTRY RELATION

Swiss Industry benefits from the services of a Industry Liaison Officer. Calls for Tender are issued by the European Domestic Agency (i.e.: Fusion for Energy, in short "F4E", seated in Barcelona) as well as by the ITER Organization (IO) itself, located in Cadarache, France.

The Industrial Liaison Officer (ILO) forwards the Calls issued either by F4E or the IO to firms and individuals deemed capable of fulfilling the contracts. A follow-up on these actions enables to gain a feed-back on how industry responded to the Calls. The success rate of Swiss Industry with Calls issued by the IO is higher than with Calls issued by F4E. Indeed, Swiss Industry is more responsive to fulfilling specialized tasks as called for by the IO.

In 2011, invitations were sent to Swiss Industry to 2 events in particular. Such events are meant to increase the awareness of industry towards ITER:

- March 30, 2011: Conference on "Industry, Services and R&D for ITER", an information day organized in Berne for Swiss and European Industry (84 participants)

- December 7 and 8, 2011: IBF/11 (International Business Forum 2011) in Manosque (F), bringing together representatives from mainly European industry (575 participants). The Swiss Desk at IBF/11 housed brochures and information leaflets from over 20 Swiss companies.

Attendance to similar events in the future can only be encouraged in order for Swiss firms to network with prime contractors in Europe.

The potential of Swiss Industry to contribute to ITER is not negligible. It will be ever more valued in upcoming Calls, asking for more demanding, specialized and high precision components and services rather than for large mechanical components or buildings. Many capable, high-tech firms have been identified; these will be encouraged to participate in tender calls.

APPENDICES

APPENDIX A Members of the Steering committee

Members of the Steering Committee of the Association Euratom – Confédération Suisse are:

for the European Commission, Euratom
Ruggero Giannella
Alexis Loncke,
Vito Marchese

for the Swiss Confederation:
Prof. Ambrogio Fasoli, CRPP-EPFL
Prof. Giorgio Margaritondo, EPFL
Prof. Minh Quang Tran, CRPP-EPFL, Head of Research Unit
Andreas Werthmueller, Secrétariat d'Etat à l'éducation et à la recherche - SER

APPENDIX B Articles published in Refereed Scientific Reviews during 2011

(see CRPP archives at http://crppwww.epfl.ch/archives)

M. Albergante, J.P. Graves, A. Fasoli, M. Jucker, X. Lapillonne, W.A. Cooper, *Numerical Modelling of Electromagnetic Turbulent Transport of Energetic Ions in Burning Plasmas,* Plasma Physics and Controlled Fusion **53**, 054002 (2011).

Y. Andrèbe, R. Behn, B.P. Duval, P. Etienne, A. Pitzschke, *Use of Webcams as Tools for Alignment and Supervision of a Thomson Scattering System in the near Infrared,* Fusion Engineering and Design **86**, 1273-1276 (2011).

N. Baluc, J.L. Boutard, S.L. Dudarev, M. Rieth, J.B. Correia, B. Fournier, J. Henry, F. Legendre, T. Leguey, M. Lewandowska, R. Lindau, E. Marquis, A. Munoz, B. Radiguet, Z. Oksiuta, *Review on the EFDA Work Programme on Nano-Structured ODS RAF Steels,* Journal Of Nuclear Materials **417**, 149-153 (2011).

N. Baluc, R. Schaeublin, P. Spaetig, N. Ilchuk, L. Veleva, Z. Oksiuta, J.R. Theile, M.Q. Tran, *From Materials Development to Their Test in Ifmif: An Overview,* Nuclear Fusion **51**, 113006 (2011).

J.W. Banks, R.L. Berger, S. Brunner, B.I. Cohen, J.a.F. Hittinger, *Two-Dimensional Vlasov Simulation of Electron Plasma Wave Trapping, Wavefront Bowing, Self-Focusing, and Sideloss,* Physics of Plasmas **18**, - (2011).

A. Bottino, T. Vernay, B. Scott, S. Brunner, R. Hatzky, S. Jolliet, B.F. Mcmillan, T.M. Tran, L. Villard, *Global Simulations of Tokamak Microturbulence: Finite Beta Effects and Collisions,* Plasma Physics and Controlled Fusion **53**, 124027 (2011).

P. Bruzzone, *Review of Design Aspects for High Current Nb3Sn Conductors,* IEEE Transactions on Applied Superconductivity **21**, 2036-2041 (2011).

P. Bruzzone, B. Stepanov, R. Wesche, R. Herzog, C. Calzolaio, M. Vogel, *Test of ITER Conductors in Sultan: An Update,* Fusion Engineering and Design **86**, 1406-1409 (2011).

R.J. Buttery, S. Gerhardt, R.J. La Haye, Y.Q. Liu, H. Reimerdes, S. Sabbagh, M.S. Chu, T.H. Osborne, J.K. Park, R.I. Pinsker, E.J. Strait, J.H. Yu, The DIII-D Team, The NSTX Team, *The Impact of 3D Fields on Tearing Mode Stability of H-Modes,* Nuclear Fusion **51**, 073016 (2011).

E. Cadoni, M. Dotta, D. Forni, P. Spaetig, *Strain-Rate Behavior in Tension of the Tempered Martensitic Reduced Activation Steel Eurofer97,* Journal Of Nuclear Materials **414**, 360-366 (2011).

I.T. Chapman, R.J. Akers, W.A. Cooper, A.R. Field, J.P. Graves, M.P. Gryaznevich, R.J. Hastie, T.C. Hender, D.F. Howell, H.D. Hua, G.T. Huysmans, Y.Q. Liu, H.F. Meyer, C.A. Michael, G. Naylor, S.D. Pinches, S. Saarelma, R. Scannell, S.A. Sabbagh, *Macroscopic Stability of High Beta MAST Plasmas,* Nuclear Fusion **51**, 073040 (2011).

I.T. Chapman, J.P. Graves, T. Johnson, O. Asunta, P. Bonoli, M. Choi, E.F. Jaeger, M. Jucker, O. Sauter, *Sawtooth Control in ITER Using Ion Cyclotron Resonance Heating,* Plasma Physics and Controlled Fusion **53**, 124003 (2011).

I.T. Chapman, N.R. Walkden, J.P. Graves, C. Wahlberg, *The Effects of*

Sheared Toroidal Rotation on Stability Limits in Tokamak Plasmas, Plasma Physics and Controlled Fusion **53**, 125002 (2011).

M.S. Chu, L.L. Lao, M.J. Schaffer, T.E. Evans, E.J. Strait, Y.Q. Liu, M.J. Lanctot, H. Reimerdes, Y. Liu, T.A. Casper, Y. Gribov, *Response of a Resistive and Rotating Tokamak to External Magnetic Perturbations Below the Alfvén Frequency,* Nuclear Fusion **51**, 073036 (2011).

S. Coda, and the TCV Team, *Progress and Scientific Results in the TCV Tokamak,* Nuclear Fusion **51**, 094017 (2011).

A.J. Cole, J.D. Callen, W.M. Solomon, A.M. Garofalo, C.C. Hegna, M.J. Lanctot, H. Reimerdes, *Peak Neoclassical Toroidal Viscosity at Low Toroidal Rotation in the DIII-D Tokamak,* Physics of Plasmas **18**, 055711 (2011).

A.J. Cole, J.D. Callen, W.M. Solomon, A.M. Garofalo, C.C. Hegna, M.J. Lanctot, H. Reimerdes, The DIII-Team, *Observation of Peak Neoclassical Toroidal Viscous Force in the DIII-D Tokamak,* Physical Review Letters **106**, 225002 (2011).

W.A. Cooper, G.A. Cooper, J.P. Graves, M.Y. Isaev, *Full-Field Drift Hamiltonian Particle Orbits in Axisymmetric Tokamak Geometry,* Physics of Plasmas **18**, 052507 (2011).

W.A. Cooper, J.P. Graves, S. Brunner, M.Y. Isaev, *Full-Field Drift Hamiltonian Particle Orbits in 3D Geometry,* Plasma Physics and Controlled Fusion **53**, 024001 (2011).

W.A. Cooper, J.P. Graves, O. Sauter, *Helical ITER Hybrid Scenario Equilibria,* Plasma Physics and Controlled Fusion **53**, 024002 (2011).

W.A. Cooper, J.P. Graves, O. Sauter, *JET Snake Magnetohydrodynamic Equilibria,* Nuclear Fusion **51**, 072002 (2011).

W.A. Cooper, J.P. Graves, O. Sauter, I.T. Chapman, M. Gobbin, L. Marrelli, P. Martin, I. Predebon, D. Terranova, *Magnetohydrodynamic Properties of Nominally Axisymmetric Systems with 3D Helical Core,* Plasma Physics and Controlled Fusion **53**, - (2011).

W.A. Cooper, J.P. Graves, O. Sauter, J. Rossel, M. Albergante, S. Coda, B.P. Duval, B. Labit, A. Pochelon, H. Reimerdes, The TCV Team, *Helical Core Tokamak MHD Equilibrium States,* Plasma Physics Controlled Fusion **53**, 124005 (2011).

W.A. Cooper, J.P. Graves, O. Sauter, D. Terranova, M. Gobbin, L. Marrelli, P. Martin, I. Predebon, R. Dendy, *MHD Equilibrium and Stability of Tokamaks and RFP Systems with 3D Helical Cores,* Plasma Physics and Controlled Fusion **53**, 084001 (2011).

N. Cruz, J.M. Moret, S. Coda, J.I. Paley, B.P. Duval, A.P. Rodrigues, F. Piras, F. Felici, C.M.B.A. Correia, C.A.F. Varandas, *Using APCS for Plasma Vertical Control at TCV,* IEEE Transactions on Nuclear Science **58**, 1570-1575 (2011).

L. Curchod, F. Felici, A. Pochelon, J. Decker, T.P. Goodman, J.M. Moret, J.I. Paley, Y. Peysson, *Multiple Electron Cyclotron Power Deposition Location Tracking by Break-in-Slope Analysis in TCV Plasmas,* Plasma Physics and Controlled Fusion **53**, 115005 (2011).

E. De Rijk, A. Macor, J.P. Hogge, S. Alberti, J.P. Ansermet, *Note: Stacked Rings for Terahertz Wave-Guiding,* Review of Scientific Instruments **82**, 66105 (2011).

R.O. Dendy, W.A. Cooper, J.P. Graves, O. Sauter, I.T. Chapman, M. Gobbin, L. Marrelli, P. Martin, I. Predebon, D. Terranova,

Magentohydrodynamic Properties of Nominally Axisymmetric Systems with 3D Helical Core, 15th International Congress on Plasma Physics **53**, 074008 (2011).

D. Fasel, F. Albajar, T. Bonicelli, A. Perez, L. Rinaldi, U. Siravo, L. Sita, G. Taddia, *5MW CW Supply System for the ITER Gyrotrons Test Facility,* Fusion Engineering and Design **86**, 872-875 (2011).

F. Felici, O. Sauter, S. Coda, B.P. Duval, T.P. Goodman, J.M. Moret, J.I. Paley, *Real-Time Physics-Model-Based Simulation of the Current Density Profile in Tokamak Plasmas,* Nuclear Fusion **51**, 083052 (2011).

J.R. Ferron, C.T. Holcomb, T.C. Luce, P.A. Politzer, F. Turco, J.C. Deboo, E.J. Doyle, Y. In, R.J. La Haye, M. Murakami, M. Okabayashi, J.M. Park, T.W. Petrie, C.C. Petty, H. Reimerdes, *Balancing Current Drive and Heating in DIII-D High Noninductive Current Fraction Discharges through Choice of the Toroidal Field,* Nuclear Fusion **51**, 113007 (2011).

I. Furno, M. Spolaore, C. Theiler, N. Vianello, N. Cavazzana, A. Fasoli, *Direct Two-Dimensional Measurements of the Eld-Aligned Current Associated with Plasma Blobs,* Physical Review Letters (2011).

I. Furno, C. Theiler, A. Fasoli, B. Labit, *Three-Dimensional Imaging of a Radially Propagating Plasma Blob Using Conditional Sampling Techniques,* IEEE Transactions on Plasma Science **39**, 3018-3019 (2011).

I. Furno, C. Theiler, D. Lan Son, A. Fasoli, D. Iraji, P. Ricci, M. Spolaore, N. Vianello, *Blob Current Structures in TORPEX Plasmas: Experimental Measurements and Numerical Simulations,* Plasma Physics and Controlled Fusion **53**, 124016 (2011).

A.M. Garofalo, W.M. Solomon, J.K. Park, K.H. Burrell, J.C. Deboo, M.J. Lanctot, G.R. Mckee, H. Reimerdes, L. Schmitz, M.J. Schaffer, P.B. Snyder, *Advances Towards QH-Mode Viability for ELM-Stable Operation in ITER,* Nuclear Fusion **51**, 083018 (2011).

M. Gindrat, H.M. Hoehle, K. Von Niessen, P. Guittienne, D. Grange, C. Hollenstein, *Plasma Spray-CVD: A New Thermal Spray Process to Produce Thin Films from Liquid or Gaseous Precursors,* Journal Of Thermal Spray Technology **20**, 882-887 (2011).

M. Gobbin, D. Bonfiglio, A.H. Boozer, A.W. Cooper, D.F. Escande, S.P. Hirshman, J. Lore, R. Lorenzini, L. Marrelli, P. Martin, E. Martines, B. Momo, N. Pomphrey, I. Predebon, M.E. Puiatti, R. Sanchez, G. Spizzo, D.A. Spong, D. Terranova, *Three-Dimensional Equilibria and Transport in Rfx-Mod: A Description Using Stellarator Tools,* Physics of Plasmas **18**, - (2011).

T. Goerler, X. Lapillonne, S. Brunner, T. Dannert, F. Jenko, S.K. Aghdam, P. Marcus, B.F. Mcmillan, F. Merz, O. Sauter, D. Told, L. Villard, *Flux- and Gradient-Driven Global Gyrokinetic Simulation of Tokamak Turbulence,* Physics of Plasmas **18**, 056103 (2011).

T. Goerler, X. Lapillonne, S. Brunner, T. Dannert, F. Jenko, F. Merz, D. Told, *The Global Version of the Gyrokinetic Turbulence Code Gene,* Journal of Computational Physics **230**, 7053-7071 (2011).

T.P. Goodman, F. Felici, O. Sauter, J.P.T.C.V.T. Graves, *Sawtooth Pacing by Real-Time Auxiliary Power Control in a Tokamak,* Physical Review Letters **106**, 245002 (2011).

J.P. Graves, S. Coda, O. Sauter, J.I. Paley, T. Johnson, I.T. Chapman, M. Lennholm, *Recent Advances in Sawtooth Control,* Fusion Science and Technology **59**, 539 (2011).

B. Gulejova, R. Pitts, D. Tskhakaya, D. Coster, *Benchmark of Fluid and Kinetic Simulations of Type III Elming H-Mode on TCV,* Fusion Science and Technology **60**, 48-55 (2011).

S.M. Hafez Haghighat, D. Terentyev, R. Schaeublin, *Atomistic Simulation of the Influence of Cr on the Mobility of the Edge Dislocation in Fe(Cr) Alloys,* Journal Of Nuclear Materials **417**, 1094-1097 (2011).

F.D. Halpern, H. Lütjens, J.-F.O. Luciani, *Diamagnetic Thresholds for Sawtooth Cycling in Tokamak Plasmas,* Physics of Plasmas **18**, 102501 (2011).

D. Iraji, I. Furno, A. Fasoli, *Fast Imaging of Blob Motion in TORPEX Plasmas,* IEEE Transactions on Plasma Science **39**, 3010-3011 (2011).

M. Jucker, W.A. Cooper, J.P. Graves, *Integrated Modelling of ICRH in a Quasi-Axisymmetric Stellarator,* Nuclear Fusion **52**, 013015 (2011).

M. Jucker, W.A. Cooper, J.P. Graves, T. Johnson, *Ion Cyclotron Resonance Heating with Consistent Finite Orbit Widths and Anisotropic Equilibria,* Plasma Physics and Controlled Fusion **53**, 054010 (2011).

M. Jucker, J.P. Graves, W.A. Cooper, N. Mellet, T. Johnson, S. Brunner, *Integrated Modelling of Ion Cyclotron Resonant Heating in Toroidal System,* Computer Physics Communications **182**, 912 (2011).

A. Karpushov, B.P. Duval, R. Chavan, E. Fable, J.M. Mayor, O. Sauter, H. Weisen, *A Scoping Study of the Application of Neutral Beam Heating on the TCV Tokamak,* Fusion Engineering and Design **86**, 868-871 (2011).

B. Labit, C. Theiler, A. Fasoli, I. Furno, P. Ricci, *Blob-Induced Toroidal Momentum Transport in Simple Magnetized Plasmas,* Physics of Plasmas 18, 3, 32308 (2011).

C.C. Lalescu, B. Teaca, D. Carati, *Influence of Numerical Schemes on Statistical Properties of Computed Charged Particle Trajectories in Turbulent Electromagnetic Fields,* Journal Of Computational Physics (2011).

M.J. Lanctot, H. Reimerdes, A.M. Garofalo, M.S. Chu, J.M. Hanson, Y.Q. Liu, G.A. Navratil, I.N. Bogatu, Y. In, G.L. Jackson, R.J. La Haye, M. Okayabashi, J.K. Park, M.J. Schaffer, O. Schmitz, E.J. Strait, A.D. Turnbull, *Measurement and Modeling of Three-Dimensional Equilibria in DIII-D,* Physics of Plasmas **18**, 056121 (2011).

X. Lapillonne, S. Brunner, O. Sauter, L. Villard, E. Fable, T. Goerler, F. Jenko, F. Merz, *Non-Linear Gyrokinetic Simulations of Microturbulence in TCV Electron Internal Transport Barriers,* Plasma Physics and Controlled Fusion **53**, 054011 (2011).

M. Lennholm, M.T. Blackman, I.T. Chapman, L.G. Eriksson, J.P. Graves, D.F. Howell, M.D. Baar, G. Calabro, R. Dumont, M. Graham, S. Jachmich, M.L. Mayoral, C. Sozzi, M. Stamp, M. Tsalas, P. Vries, *Feedback Control of the Sawtooth Period through Real Time Control of the Ion Cyclotron Resonance Frequency,* Nuclear Fusion **51**, 073032 (2011).

M. Lewandowska, M. Bagnasco, *Thermo-Hydraulic Analysis of the Cool-Down of the EDIPO Test Facility,* Cryogenics **51**, 485-493 (2011).

M. Lewandowska, M. Bagnasco, *Modified Friction Factor Correlation for CICC's Based on a Porous Media Analogy,* Cryogenics **51**, 541-545 (2011).

M. Lewandowska, R. Herzog, *Transverse Heat Transfer Coefficient in the Dual Channel ITER TF CICC's Part I: Analysis of Steady State Temperature Profiles Resulting from Annular Heating,* Cryogenics **51**, 598-608 (2011).

B. Li, B. Rogers, P. Ricci, K. Gentle, A. Bhattacharjee, *Turbulence and*

Bias-Induced Flows in Simple Magnetized Toroidal Plasmas, Physical Review E **83**, (2011).

B. Liu, Y. Wu, P. Bruzzone, *The Results of the Second Chinese TF Conductor Sample,* Fusion Engineering and Design **86**, 369-372 (2011).

A. Loarte, V. Riccardo, J.R. Martin-Solis, J. Paley, A. Huber, M. Lehnen, *Magnetic Energy Flows During the Current Quench and Termination of Disruptions with Runaway Current Plateau Formation in JET and Implications for ITER,* Nuclear Fusion **51**, - (2011).

J. Loizu, P. Ricci, C. Theiler, *Existence of Subsonic Plasma Sheaths,* Physical Review E **83**, (2011).

A. Macor, E. De Rijk, G. Annino, S. Alberti, J.P. Ansermet, *Thz-Waves Channeling in a Monolithic Saddle-Coil for Dynamic Nuclear Polarization Enhanced NMR,* Journal Of Magnetic Resonance **212**, 440-449 (2011).

C. Marinucci, L. Bottura, M. Calvi, R. Wesche, *Quench Analysis of a High-Current Forced-Flow Hts Conductor Model for Fusion Magnets,* IEEE Transactions on Applied Superconductivity **21**, 2445-2448 (2011).

P. Martin, J. Adamek, P. Agostinetti, et al., W.A. Cooper, *Overview of the RFX Fusion Science Program,* Nuclear Fusion **51**, 94023 (2011).

B.F. McMillan, P. Hill, A. Bottino, S. Jolliet, T. Vernay, L. Villard, *Interaction of Large Scale Flow Structures with Gyrokinetic Turbulence,* Physics of Plasmas **18**, 112503 (2011).

N. Mellet, W.A. Cooper, P. Popovich, L. Villard, S. Brunner, *Convolution and Iterative Methods Applied to Low Frequency Waves in 3D Configurations,* Computer Physics Communications **182**, 570 (2011).

D. Moseev, F. Meo, S.B. Korsholm, T. Koskela, M. Albergante, O. Asunta, H. Bindslev, A. Buerger, V. Furtula, M.Y. Kantor, F. Leipold, P.K. Michelsen, S.K. Nielsen, M. Salewski, O. Schmitz, M. Stejner, E. Westerhof, *Comparison of Measured and Simulated Fast Ion Velocity Distributions in the TEXTOR Tokamak,* Plasma Physics and Controlled Fusion **53**, - (2011).

M. Muzyk, D. Nguyen-Manh, K.J. Kurzydlowski, N.L. Baluc, S.L. Dudarev, *Phase Stability, Point Defects, and Elastic Properties of W-V and W-Ta Alloys,* Physical Review B **84**, 104115 (2011).

R. Narkowicz, M.R. Siegrist, P. Moreau, J.P. Hogge, R. Raguotis, R. Brazis, *Third-Order Susceptibility of Silicon Crystals Measured with Millimeter-Wave Gyrotron,* Acta Physica Polonica A **119**, 509-513 (2011).

T. Nishitani, H. Tanigawa, T. Nozawa, S. Jitsukawa, M. Nakamichi, T. Hoshino, T. Yamanishi, N. Baluc, A. M Slang, R. Lindou, S. Tosti, E.R. Hodgson, S. Clement Lorenzo, A. Kohyama, A. Kimura, T. Shikama, K. Hayashi, M. Araki, *Recent Progress in Blanket Materials Development in the Broader Approach Activities,* Journal Of Nuclear Materials **417**, 1331-1335 (2011).

Y. Nunoya, Y. Nabara, M. Yoshikawa, K. Matsui, T. Hemmi, Y. Takahashi, T. Isono, N. Koizumi, H. Nakajima, B. Stepanov, P. Bruzzone, *Test Result of a Full-Size Nb3Sn Conductor Developed for the ITER TF Coils,* IEEE Transactions on Applied Superconductivity **21**, 1982-1986 (2011).

M. Okabayashi, G. Matsunaga, J.S. Degrassie, W.W. Heidbrink, Y. In, Y.Q. Liu, H. Reimerdes, W.M. Solomon, E.J. Strait, M. Takechi, N. Asakura, R.V. Budny, G.L. Jackson, J.M. Hanson, R.J. La Haye, M.J. Lanctot, J. Manickam, K. Shinohara, Y.B. Zhu, *Off-Axis Fishbone-Like Instability and Excitation of Resistive Wall Modes in JT-60U and DIII-D,* Physics of

Plasmas **18**, 056112 (2011).

Z. Oksiuta, M. Lewandowska, K.J. Kurzydlowski, N. Baluc, *Influence of Hot Rolling and High Speed Hydrostatic Extrusion on the Microstructure and Mechanical Properties of an ODS RAF Steel,* Journal Of Nuclear Materials **409**, 86-93 (2011).

Z. Oksiuta, M. Lewandowska, P. Unifantowicz, N. Baluc, K.J. Kurzydlowski, *Influence of Y2o3 and Fe2y Additions on the Formation of Nano-Scale Oxide Particles and the Mechanical Properties of an ODS RAF Steel,* Fusion Engineering and Design **86**, 2417-2420 (2011).

Z. Oksiuta, P. Mueller, P. Spaetig, N. Baluc, *Effect of Thermo-Mechanical Treatments on the Microstructure and Mechanical Properties of an ODS Ferritic Steel,* Journal Of Nuclear Materials **412**, 221-226 (2011).

T. Omori, M.A. Henderson, F. Albajar, et al., S. Alberti, R. Chavan, A. Collazos, T.P. Goodman, J.P. Hogge, L. Porte, F. Sanchez, O. Sauter, M.Q. Tran, *Overview of the ITER EC H&CD System and Its Capabilities,* Fusion Engineering and Design **86**, 951-954 (2011).

A.G. Peeters, C. Angioni, A. Bortolon, Y. Camenen, F.J. Casson, B. Duval, L. Fiederspiel, W.A. Hornsby, Y. Idomura, T. Hein, N. Kluy, P. Mantica, F.I. Parra, A.P. Snodin, G. Szepesi, D. Strintzi, T. Tala, G. Tardini, P. De Vries, J. Weiland, *Overview of Toroidal Momentum Transport,* Nuclear Fusion **51**, 094027 (2011).

L. Peng, Y. Dai, *Helium-Induced Hardening Effect in Ferritic/Martensitic Steels F82h and Optimax-a Irradiated in a Mixed Spectrum of High Energy Protons and Spallation Neutrons,* Journal Of Nuclear Materials **417**, 996-1000 (2011).

A. Perez, D. Fasel, J. Lister, B. Marletaz, P. Marmillod, U. Siravo, *ITER - Earthing,* Fusion Engineering and Design **86**, 2694-2697 (2011).

Y. Peysson, J. Decker, L. Morini, S. Coda, *RF Current Drive and Plasma Fluctuations,* Plasma Physics and Controlled Fusion **53**, 124028 (2011).

L. Piron, J.M. Hanson, Y. In, G. Marchiori, L. Marrelli, P. Martin, M. Okabayashi, P. Piovesan, H. Reimerdes, A. Soppelsa, E.J. Strait, *Improved Dynamic Response of Magnetic Feedback in RFX-Mod and DIII-D,* Plasma Physics and Controlled Fusion **53**, 084004 (2011).

A. Portone, M. Bagnasco, B. Baker, P. Bruzzone, F. Cau, E. Fernandez-Cano, E. Salpietro, P. Testoni, E. Theisen, M. Vogel, R. Wesche, *Status Report of the EDIPO Project,* IEEE Transactions on Applied Superconductivity **21**, 1953-1959 (2011).

R. Raman, J.W. Ahn, J.P. Allain, et al., H. Reimerdes, *Overview of Physics Results from NSTX,* Nuclear Fusion **51**, 094011 (2011).

H. Reimerdes, J. Berkery, M. Lanctot, A. Garofalo, J. Hanson, Y. In, M. Okabayashi, S. Sabbagh, E. Strait, *Evidence for the Importance of Trapped Particle Resonances for Resistive Wall Mode Stability in High Beta Tokamak Plasmas,* Physical Review Letters **106**, (2011).

H. Reimerdes, A.J. Buttery, A. Garofalo, Y. In, R.J. La Haye, M.J. Lanctot, M. Okabayashi, J.K. Park, M.J. Schaffer, E.J. Strait, F.A. Volpe, *Error Field Tolerance and Error Field Correction Strategies and Their Applicability to ITER,* Fusion Science and Technology **59**, 572-585 (2011).

M. Ricci, J.-L. Dorier, C. Hollenstein, P. Fayet, *Influence of Argon and Nitrogen Admixture in Hmdso/O-2 Plasmas onto Powder Formation,* Plasma Processes And Polymers **8**, 108-117 (2011).

P. Ricci, C. Theiler, A. Fasoli, I. Furno, K. Gustafson, D. Iraji, J. Loizu,

Methodology for Turbulence Code Validation: Quantification of Simulation-Experiment Agreement and Application to the TORPEX Experiment, Physics of Plasmas **18**, 032109 (2011).

J. Rice, I. Cziegler, P. Diamond, B. Duval, Y. Podpaly, M. Reinke, P. Ennever, M. Greenwald, J. Hughes, Y. Ma, E. Marmar, M. Porkolab, N. Tsujii, S. Wolfe, *Rotation Reversal Bifurcation and Energy Confinement Saturation in Tokamak Ohmic L-Mode Plasmas,* Physical Review Letters **107**, 265001 (2011).

J.E. Rice, B.P. Duval, M.L. Reinke, Y.A. Podpaly, A. Bortolon, R.M. Churchill, I. Cziegler, P.H. Diamond, A. Dominguez, P.C. Ennever, C.L. Fiore, R.S. Granetz, M.J. Greenwald, A.E. Hubbard, J.W. Hughes, J.H. Irby, Y. Ma, E.S. Marmar, R.M. Mcdermott, M. Porkolab, N. Tsujii, S.M. Wolfe, *Observations of Core Toroidal Rotation Reversals in Alcator C-Mod Ohmic L-Mode Plasmas,* Nuclear Fusion **51**, Q83005 (2011).

M. Rieth, J.L. Boutard, S.L. Dudarev, et al., N. Baluc, J. Fikar, R. Schaeublin, L. Veleva, *Review on the EFDA Programme on Tungsten Materials Technology and Science,* Journal Of Nuclear Materials **417**, 463-467 (2011).

B.N. Rogers, S. Kobayashi, P. Ricci, W. Dorland, J. Drake, T. Tatsuno, *Gyrokinetic Simulations of Collisionless Magnetic Reconnection (Vol 14, 092110, 2007),* Physics of Plasmas **18**, - (2011).

D.M.S. Ronden, M. De Baar, R. Chavan, B.S.Q. Elzendoorn, T. Goodman, C.J.M. Heemskerk, M.A. Henderson, J.F. Koning, G. Saibene, P. Spaeh, D. Strauss, *The ITER EC H&CD Upper Launcher: Analysis of Remote Handling Compatibility,* Fusion Engineering and Design **86**, 963-966 (2011).

J.X. Rossel, J.M. Moret, Y. Martin, G.T.C.V.T. Pochon, *Physics Design of a Saddle Coil System for TCV,* Fusion Engineering and Design **86**, 2843-2864 (2011).

Y. Sarazin, V. Grandgirard, J. Abiteboul, S. Allfrey, X. Garbet, P. Ghendrih, G. Latu, A. Strugarek, G. Dif-Pradalier, P.H. Diamond, S. Ku, C.S. Chang, B.F. Mcmillan, T.M. Tran, L. Villard, S. Jolliet, A. Bottino, P. Angelino, *Predictions on Heat Transport and Plasma Rotation from Global Gyrokinetic Simulations,* Nuclear Fusion **51**, 103023 (2011).

M.J. Schaffer, J.A. Snipes, P. Gohil, et al. H. Reimerdes, *ITER Test Blanket Module Error Field Simulation Experiments at DIII-D,* Nuclear Fusion **51**, 103028 (2011).

H. Schulenburg, B. Schwanitz, J. Krbanjevic, N. Linse, G.G. Scherer, A. Wokaun, *Quantification of Platinum Deposition in Polymer Electrolyte Fuel Cell Membranes,* Electrochemistry Communications **13**, 921-923 (2011).

H. Schulenburg, B. Schwanitz, N. Linse, G.G. Scherer, A. Wokaun, J. Krbanjevic, R. Grothausmann, I. Manke, *3D Imaging of Catalyst Support Corrosion in Polymer Electrolyte Fuel Cells,* Journal Of Physical Chemistry C **115**, 14236-14243 (2011).

M. Silva, T. Goodman, F. Felici, L. Porte, *Fast Polarizers Installation for ECRH and ECE in TCV,* Fusion Engineering and Design **86**, 1256-1259 (2011).

U. Siravo, J. Alex, M. Bader, M. Carpita, D. Fasel, S. Gavin, A. Perez, *Magy: An Innovative High Voltage - Low Current Power Supply for Gyrotron,* Fusion Engineering and Design **86**, 880 (2011).

S. Soare, N. Balshaw, P. Blanchard, T. Craciunescu, D. Croft, M. Curuia, T. Edlington, V. Kiptily, A. Murari, P. Prior, S. Sanders, B. Syme, V. Zoita, *Tandem Collimators for the JET Tangential Gamma-Ray*

Spectrometer, Fusion Engineering and Design **86**, 1359-1364 (2011).

W.M. Solomon, K.H. Burrell, J.S. Degrassie, J.A. Boedo, A.M. Garofalo, R.A. Moyer, S.H. Muller, C.C. Petty, H. Reimerdes, *Characterization of Intrinsic Rotation Drive on DIII-D,* Nuclear Fusion **51**, 073010 (2011).

P. Spaeh, G. Aiello, M. De Baar, R. Chavan, B. Elzendoorn, T. Goodman, M. Henderson, K. Kleefeldt, J.D. Landis, A. Meier, D. Ronden, G. Saibene, T. Scherer, S. Schreck, A. Serikov, D. Strauss, A. Vaccaro, *The ITER EC H&CD Upper Launcher: Structural Design,* Fusion Engineering and Design **86**, 724-727 (2011).

M. Tardocchi, M. Nocente, I. Proverbio, V.G. Kiptily, P. Blanchard, S. Conroy, M. Fontanesi, G. Grosso, K. Kneupner, E. Lerche, A. Murari, E.P. Cippo, A. Pietropaolo, B. Syme, D. Van Eester, G. Gorini, *Spectral Broadening of Characteristic Gamma-Ray Emission Peaks from C-12(He-3, P Gamma)N-14 Reactions in Fusion Plasmas,* Physical Review Letters **107**, - (2011).

B. Teaca, D. Carati, J.A. Domaradzki, *On the Locality of MHD Turbulence Scale Fluxes,* Physics of Plasmas **18**, 112307 (2011)

D. Testa, H. Carfantan, M. Toussaint, R. Chavan, Y. Fournier, J. Guterl, J.B. Lister, T. Maeder, J.M. Moret, A. Perez, F. Sanchez, B. Schaller, C. Slater, M. Stoeck, G. Tonetti, *Assessment of the ITER High-Frequency Magnetic Diagnostic Set,* Fusion Engineering and Design **86**, 1248 (2011).

D. Testa, A. Fasoli, A. Goodyear, Q. King, P. Blanchard, H. Carfantan, A. Klein, P. Lavanchy, T. Panis, J.-E. Contributors, *The JET Alfven Eigenmode Local Manager for the Real-Time Detection and Tracking of a Frequency-Degenerate Spectrum of MHD Instabilities,* Fusion Engineering and Design **86**, 381 (2011).

D. Testa, Y. Fournier, T. Maeder, M. Toussaint, R. Chavan, J. Guterl, J.B. Lister, J.M. Moret, B. Schaller, G. Tonetti, *Prototyping the ITER High Frequency Magnetic Sensor Using the Non-Conventional, Low Temperature Co-Fired Ceramic Technology,* Fusion Science and Technology **59**, 376 (2011).

D. Testa, D. Spong, P. Blanchard, A. Fasoli, T. Panis, JET Contributors, *Recent JET Experiments on Alfvén Eigenmodes with Intermediate Toroidal Mode Numbers: Measurements and Modelling with the Taefl Code,* Nuclear Fusion **51**, 043009 (2011).

C. Theiler, I. Furno, A. Fasoli, P. Ricci, B. Labit, D. Iraji, *Blob Motion and Control in Simple Magnetized Plasmas,* Physics of Plasmas **18**, 055901 (2011).

C. Theiler, I. Furno, A. Kuenlin, P. Marmillod, A. Fasoli, *Practical Solutions for Reliable Triple Probe Measurements in Magnetized Plasmas,* Review Of Scientific Instruments **82**, 013504 (2011).

M. Toussaint, D. Testa, N. Baluc, R. Chavan, Y. Fournier, J.B. Lister, T. Maeder, P. Marmillod, F. Sanchez, M. Stoeck, *Design of the ITER High-Frequency Magnetic Diagnostic Coils,* Fusion Engineering and Design **86**, 1248-1251 (2011).

A.D. Turnbull, W.A. Cooper, L.L. Lao, L.-P. Ku, *Ideal MHD Spectrum Calculations for the Aries-CS Configuration,* Nuclear Fusion **51**, 123011 (2011).

P. Unifantowicz, Z. Oksiuta, P. Olier, Y. De Carlan, N. Baluc, *Microstructure and Mechanical Properties of an ODS RAF Steel Fabricated by Hot Extrusion or Hot Isostatic Pressing,* Fusion Engineering and Design **86**, 2413-2416 (2011).

G. Vayakis, L. Bertalot, A. Encheva, C. Walker, B. Brichard,

M.S. Cheon, G. Chitarin, E. Hodgson, C. Ingesson, M. Ishikawa, T. Kondoh, H. Meister, P. Moreau, S. Peruzzo, S. Pak, G.N. Perez-Pichel, R. Reichle, D. Testa, M. Toussaint, L. Vermeeren, V. Vershkov, *Nuclear Technology Aspects of ITER Vessel-Mounted Diagnostics,* Journal Of Nuclear Materials **417**, 780-786 (2011).

L. Veleva, R. Schaeublin, T. Plocinski, M. Walter, N. Baluc, *Processing and Characterization of a W-2Y Material for Fusion Power Reactors,* Fusion Engineering and Design **86**, 2450-2453 (2011).

H. Weisen, A.V. Melnikov, S. Perfilov, S. Lysenko, *On the Possibility of Using a Heavy Ion Beam Probe for Local Poloidal Flux Measurements in a Tokamak,* Fusion Science and Technology **59**, 418-426 (2011).

R. Wesche, M. Bagnasco, P. Bruzzone, R. Felder, M. Guetg, M. Holenstein, M. Jenni, S. March, F. Roth, M. Vogel, *Test Results of the 18kA EDIPO HTS Current Leads,* Fusion Engineering and Design **86**, 1414-1417 (2011).

APPENDIX C Conferences and Seminars

(see CRPP archives at http://crppwww.epfl.ch/archives)

C.1 Conference and conference proceedings published in 2011

S. Alberti, T.M. Tran, K.A. Avramides, F. Li, J.P. Hogge, *Gyrotron Parasitic-Effects Studies Using the Time-Dependent Self-Consistent Monomode Code Twang,* 36th International Conference on Infrared, Millimeter, and Terahertz Waves (IRMMW THz 2011), Houston, TX, USA, 2-7 October 2011, 2011 International Conference on Infrared, Millimeter, and Terahertz Waves, 1-2 (2011).

Y. Asashi, Y. Suzuki, K.Y. Watanabe, W.A. Cooper, *MHD Equilibrium Analysis with Anisotropic Pressure in LHD,* Plasma Physics Controlled Fusion, Strasbourg, F, June 27 - July 1, 2011, ECA **35G**, P1.076 (2011).

K. Besseghir, J.B. Lister, *Scenario Optimisation for ITER,* Plasma Physics Controlled Fusion, Strasbourg, F, June 27 - July 1, 2011, ECA **35G**, P1.104 (2011).

J.A. Boedo, O. Schmitz, H. Reimerdes, A. Etemad-Sajadi, *Plasma Response to Applied Resonant Magnetic Perturbations in DIII-D,* Plasma Physics Controlled Fusion, Strasbourg, F, June 27 - July 1, 2011, ECA **35G**, P1.122 (2011).

C. Calzolaio, P. Bruzzone, D. Uglietti, *Measurement of Tc Distribution in Nbsn CICC,* Mem 11, Okinawa, Japan, November 2011, Superconductor Science & Technology **25**, - (2011).

C. Calzolaio, P. Bruzzone, D. Uglietti, B. Stepanov, D. Bessette, M. Jewell, *In Situ Tc Measurements of Cable in Conduit Conductors Via an Inductive Method,* MT 22, International Conference on Magnet Technology, Marseille, France, September 11-16, 2011 (2011).

G.P. Canal, B. Duval, F.a.A. Felici, T. Goodman, J. Graves, A. Pochelon, H. Reimerdes, O. Sauter, D. Testa, T.C.V. Team, *Coupling between Sawteeth and Tearing Modes in TCV,* Plasma Physics Controlled Fusion, Strasbourg, F, June 27 - July 1, 2011, ECA **35G**, P1.080 (2011).

G. Croari, P. Bruzzone, C. Marinucci, S.A. March, R. Felder, *EDIPO Quench Detection System: Concept and Development,* MT 22, International Conference on Magnet Technology, Marseille, France, September 11-16, 2011 (2011).

C.A. De Mejeire, S. Coda, A. Kraemer-Flecken, S. Soldatov, M. Albergante, *Observations on Turbulence Dynamics and Beam-Ion Driven Modes on the TEXTOR Tokamak,* Plasma Physics Controlled Fusion, Strasbourg, F, June 27 - July 1, 2011, ECA **35G**, P1.137 (2011).

E. De Rijk, A. Macor, S. Alberti, J.P. Hogge, J.P. Ansermet, *Innovative Corrugated Transmission Line for Terahertz Wave-Guiding,* 36th International Conference on Infrared, Millimeter, and Terahertz Waves (IRMMW THz 2011), Houston, TX, USA, 2-7 October 2011, 2011 International Conference on Infrared, Millimeter, and Terahertz Waves, 1-2 (2011).

J. Decker, Y. Peysson, J.F. Artaud, V. Basiuk, S. Coda, A. Ekedahl, S. Gnesin, M. Gonich, D. Mazon, P.K. Sharma, *Bremsstrahlung Emission Modelling and Application to Fast Electron Physics,* AIP Conf. Proc. (USA), Newport, RI, USA, June 1-3, 2011, AIP Conf. Proc. (USA) **1406**, 447-450 (2011).

A. Fasoli, A. Bovet, I. Furno, K. Gustafson, D. Iraji, B. Labit, D. Lancon, J. Loizu, P. Ricci, C.G. Theiler, M. Spolaore, N. Vianello,

R. Cavazzana, *Overview of Turbulence and Transport Studies in the TORPEX Simple Magnetized Plasmas,* Plasma Physics Controlled Fusion, Strasbourg, F, June 27 - July 1, 2011, ECA **35G**, P1.003 (2011).

L. Federspiel, B. Duval, A. Karpushov, Y. Andrebe, F.a.A. Felici, T. Goodman, O. Sauter, *Cxrs Acquisition Optimisation for Rotation Studies of Fast Events on TCV (Rotation Studies in Transport Barriers on TCV),* Plasma Physics Controlled Fusion, Strasbourg, F, June 27 - July 1, 2011, ECA **35G**, P2.117 (2011).

F.A.A. Felici, O. Sauter, S. Coda, B. Duval, T. Goodman, J.-M. Moret, T.C.V. Team, *Optimization, Real-Time Simulation and Feedback Control of Tokamak Plasma Profiles on TCV,* Plasma Physics Controlled Fusion, Strasbourg, F, June 27 - July 1, 2011, ECA **35G**, O5.420 (2011).

J.R. Ferron, C.T. Holcombe, T.C. Luce, H. Reimerdes, *Design Parameters for DIII-D Steady-State Scenario Discharges,* Plasma Physics Controlled Fusion, Strasbourg, F, June 27 - July 1, 2011, ECA **35G** (P1.089) (2011).

T. Goodman, F.a.A. Felici, G. Canal, B. Duval, J. Graves, H. Reimerdes, O. Sauter, D. Testa, *Individual Sawtooth Pacing by Synchronized ECCD in TCV,* 19th Topical Conference on Radio Frequency Power in Plasmas, US Japan Workshop on RF Physics, Newport, USA, June 1-3, 2011, Radio Frequency Power in Plasmas: Proceedings of the 19th Topical Conference **1406** (2011).

T.P. Goodman, E. Fable, F. Felici, A. Pochelon, L. Porte, M. Rancic, O. Sauter, C. Schlatter, V.S. Udintsev, C. Zucca, P.K. Chattopadyay, R. Prater, *Oblique and Correlation ECE in TCV,* EC 16, Joint Workshop on Electron Cyclotron Emission and Electron Cyclotron Resonance Heating, Sanya, China, 12-15 April 2010, Electron Cyclotron Emission and Electron Cyclotron Resonance Heating (EC-16): Proceedings of the 16th Joint Workshop, 174 (2011).

K. Gustafson, A. Bovet, A. Fasoli, I. Furno, P. Ricci, *Fast Ion Transport in TORPEX: Framework for Comparison between Theory and Experiment,* Plasma Physics Controlled Fusion, Strasbourg, F, June 27 - July 1, 2011, ECA **35G**, O5.418 (2011).

T. Hellsten, A. Hannan, T. Johnson, L.G. Eriksson, J. Hook, L. Villard, *Self-Consistent ICRH Modelling,* AIP Conf. Proc. (USA), Newport, RI, USA, June 1-3, 2011, AIP Conf. Proc. (USA) **1406**, 365-370 (2011).

K. Kim, F.a.A. Felici, O. Sauter, L. Terzolo, Y.S. Na, *Time-Dependent Simulations of Neoclassical Tearing Mode Stabilization in TCV,* Plasma Physics Controlled Fusion, Strasbourg, F, June 27 - July 1, 2011, ECA **35G**, P2.086 (2011).

B. Labit, I. Furno, H. Reimerdes, W. Vijvers, S. Coda, *Scrape-Off Layer Properties of Single-Null and Snowflake Diverted Plasmas in TCV,* Plasma Physics Controlled Fusion, Strasbourg, France, June 27-July 1, 2011, ECA **35G**, P2.076 (2011).

M. Lewandowska, R. Wesche, *Parametric Study for the Cooling of High Temperature Superconductor (Hts) Current Leads,* CHATS on Applied Superconductivity 2011, Geneva, Switzerland, October 12-14, 2011 (2011).

F. Li, S. Alberti, J.P. Hogge, I.G. Pagonakis, *Calculation of Stray Magnetic Field Effects on the Operation of the ITER Electron Cyclotron System,* 2011 Ieee/Npss 24Th Symposium On Fusion Engineering (Sofe), Chicago, IL, Jun 26-30, 2011, 2011 IEEE/NPSS 24Th Symposium On Fusion Engineering (Sofe), - (2011).

J.B. Lister, K. Besseghir, J.F. Artaud, R.R. Khayrutdinov, S.H. Kim, V.E. Lukash, *Development of the DINA-Ch Full Tokamak Simulator,* Plasma Physics Controlled Fusion, Strasbourg, F, June 27 - July 1, 2011, ECA **35G**, P1.105 (2011).

A. Macor, E. De Rijk, S. Alberti, A. Comment, J.P. Ansermet, *Universal Polarizer at 140 for DNP-Enhanced NMR Experiments,* 2011 36th International Conference on Infrared, Millimeter, and Terahertz Waves (IRMMW THz 2011), Houston, TX, USA, 2-7 October 2011, International Conference on Infrared, Millimeter, and Terahertz Waves, 1-2 (2011).

S.A. March, P. Bruzzone, B. Stepanov, D. Bessette, M. Jewell, *Effect of Thermal Loading on Nb3Sn CICC Performance,* MT 22, International Conference on Magnet Technology, Marseille, France, September 11-16, 2011 (2011).

C. Marinucci, L. Bottura, M. Calvi, *Integrated Analysis of Quench Propagation in a System of Magnetically Coupled Superconducting Coils,* Chats as Xi, Geneva, Switzerland, October 12-14, 2011 (2011).

C. Marinucci, L. Bottura, M. Calvi, R. Wesche, *Quench Analysis of a High-Current Forced-Flow Hts Conductor Model for Fusion Magnets,* Asc, Washington, DC, USA, August 1-6, 2010, Ieee Transactions On Applied Superconductivity **21**, 2445-2448 (2011).

A.A. Martynov, S.Y. Medvedev, L. Villard, *Helically Symmetric Magnetic Islands: Equilibrium and Stability,* Plasma Physics Controlled Fusion, Strasbourg, F, June 27 - July 1, 2011, ECA **35G**, PD2.07 (2011).

S.Y. Medvedev, A.A. Ivanov, A.A. Martynov, Y.Y. Poshekhonov, Y. Martin, J.-M. Moret, F. Piras, A. Pitzschke, A. Pochelon, H. Reimerdes, O. Sauter, L. Villard, *Advanced Shaping and Stability Limits in the TCV Tokamak,* Plasma Physics Controlled Fusion, Strasbourg, F, June 27 - July 1, 2011, ECA **35G**, P2.093 (2011).

M. Muzyk, D. Nguyen-Manh, K.J. Kurzydlowski, N.L. Baluc, S.L. Dudarev, *Modeling W-V and W-Ta Alloys for Fusion Applications: Phase Stability, Short-Range Order and Point Defect Properties*, Materials Research Society Symposium Proceedings **1298**, 49-54 (2011).

S. Nowak, E. Lazzaro, D. Brunetti, B. Esposito, G. Granucci, M. Maraschek, H. Zohm, *Analysis of Ntm (De)Stabilization by ECH in Asdex Upgrade,* Plasma Physics Controlled Fusion, Strasbourg, F, June 27 - July 1, 2011, ECA **35G**, P1.088 (2011).

M. Okabayashi, J.S. Degrassie, W.W. Heidbrink, H. Reimerdes, *Off-Axis Fishbone Modes and Excitation of Rwm in DIII-D,* Plasma Physics Controlled Fusion, Strasbourg, F, June 27 - July 1, 2011, ECA **35G**, P4.087 (2011).

A.G. Peeters, C. Angioni, A. Bortolon, Y. Camenen, F.J. Casson, B. Duval, L. Federspiel, W.A. Hornsby, Y. Idomura, T. Hein, N. Kluy, P. Mantica, F.I. Parra, A.P. Snodin, G. Szepesi, D. Strintzi, T. Tala, G. Tardini, P. De Vries, J. Weiland, *Overview of Toroidal Momentum Transport*, Nuclear Fusion **51** (9), 094027 (2011).

P. Peschke, S. Goekce, C. Hollenstein, P.N.L. Leyland, P. Ott, *Interaction between Nanosecond Pulse Dbd Actuators and Transonic Flow,* 41st AIAA Fluid Dynamics Conference and Exhibit, Honolulu, HI, USA, June 27-40, 2011 (2011).

A. Pitzschke, R. Behn, B. Duval, G.L. Induni, S.Y. Medvedev, L. Porte, O. Sauter, T.C.V. Team, *Dynamics of Pedestal Profiles in ELMy H-Mode Plasmas in TCV at Different Collisionalities,* Plasma Physics Controlled Fusion, Strasbourg, F, June 27 - July 1, 2011, ECA **35G**, P1.077 (2011).

A.R. Polevoi, R. Bilato, T. Casper, O. Sauter, *Operational Limits of ITER Helium-4 Plasmas with ELM Pace-Making,* Plasma Physics Controlled Fusion, Strasbourg, F, June 27 - July 1, 2011, ECA **35G**, P4.109 (2011).

H. Reimerdes, G.P. Canal, S. Coda, B.P. Duval, B. Labit, F. Piras, W. Vijvers, G. De Temmerman, J. Zielinski, B. Tal, S.Y. Medvedev,

T.D. Rognlien, D.D. Ryutov, M.V. Umansky, *Transport Studies in the Snowflake Divertor in TCV,* Bulletin of the American Physical Society, Salt Lake City, Utah, USA, November 14-18, 2011, Bulletin of the American Physical Society **56** (16), JP9.110 (2011).

M.G. Sevillano, I. Garrido, A.J. Garrido, J. Romero, J. Paley, J.M. Moret, S. Coda, F. Felici, L. Curchod, *Observer-Based Real-Time Control for the Poloidal Beta of the Plasma Using Diamagnetic Measurements in Tokamak Fusion Reactors,* 2011 50th IEEE Conference on Decision and Control and European Control Conference (CDC ECC 2011), Orlando, FL, USA, 12-15 December 2011, IEEE Conference on Decision and Control and European Control Conference, 7536-7542 (2011).

M. Silva, S. Alberti, F. Felici, T.P. Goodman, J.P. Hogge, L. Porte, T.M. Tran, M.Q. Tran, I. Pagonakis, *Millimeter Wave System Upgrades on TCV: Additional X3 Power and Fast ECE Polarizers,* 2011 Ieee/Npss 24Th Symposium On Fusion Engineering (Sofe), Chicago, IL, Jun 26-30, 2011, 2011 IEEE/NPSS 24Th Symposium On Fusion Engineering (Sofe), - (2011).

A.C.C. Sips, C.D. Challis, H. Weisen, P. Batistoni, J. Bizarro, F. Crisanti, L.G. Eriksson, J. Garcia, I. Jenkins, X. Litaudon, R. Neu, I. Nunes, J.-E. Contributors, *Scientific Preparation for Future D-T Campaigns at JET in Support of ITER,* Plasma Physics Controlled Fusion, Strasbourg, F, June 27 - July 1, 2011, ECA **35G**, O5.127 (2011).

B. Stepanov, P. Bruzzone, R. Wesche, S. Turt П, V. Corato, P. Decool, A. Devred, D. Bessette, A. Vostner, T. Boutboul, S. Lelekhov, W. Yu, *Test Results of Three Poloidal Field Superconducting Samples in Sultan,* MT 22, International Conference on Magnet Technology, Marseille, France, September 11-16, 2011 (2011).

D. Strauss, G. Aiello, R. Chavan, S. Cirant, M. Debaar, D. Farina, G. Gantenbein, T. Goodman, M.A. Henderson, W. Kasparek, K. Kleefeldt, J.D. Landis, A. Meier, A. Moro, B. Plaum, E. Poli, G. Ramponi, D. Ronden, G. Saibene, F. Sanchez, O. Sautter, T. Scherer, S. Schreck, A. Serikov, C. Sozzi, P. Spaeh, A. Vaccaro, H. Zohm, *Preliminary Design of the ITER ECH Upper Launcher,* 2011 Abstracts IEEE International Conference on Plasma Science, Chicago, IL, USA, 26-30 06 2011, 2011 Abstracts IEEE International Conference on Plasma Science, 1-1 (2011).

D. Testa, T. Panis, A. Fasoli, P. Blanchard, H. Carfantan, A. Goodyear, N. Mellet, S.E. Sharapov, D. Spong, J.-E. Contributors, *Measurement and Theoretical Modeling of the Damping Rate of Medium-N Toroidal Alfven Eigenmodes in JET,* 12th IAEA TCM on Energetic Particles in Magnetic Confinement Systems, Austin, Texas, USA, 8-10 September 2011, 12th IAEA TCM on Energetic Particles in Magnetic Confinement Systems (2011).

L. Thorndahl, S. Alberti, J.P. Hogge, F. Li, T.M. Tran, *Comparative Study of Dielectric Loaded Structures for Suppressing Gyro-Bwo Instabilities in Gyrotron Beam-Ducts (Bd) Using Hfss,* 2011 36th International Conference on Infrared, Millimeter, and Terahertz Waves (IRMMW THz 2011), Houston, TX, USA, 2-7 October 2011, 2011 International Conference on Infrared, Millimeter, and Terahertz Waves, 1-3 (2011).

D. Uglietti, C. Marinucci, *Design of a Quench Protection System for a Coated Conductor Insert Coil,* MT 22, International Conference on Magnet Technology, Marseille, France, September 11-16, 2011 (2011).

D. Uglietti, R. Wesche, B. Stepanov, P. Bruzzone, *Statistical Analysis of the Current-Sharing Temperature Evolution in Nb3Sn Cable-in-Conduit-Conductors for ITER,* MT 22, International Conference on Magnet Technology, Marseille, France,

September 11-16, 2011 (2011).

C. Wahlberg, J. Graves, *Pressure- and Q-Profile Effects on Ideal Infernal Modes in Tokamaks with an Extended Region of Low Magnetic Shear,* Plasma Physics Controlled Fusion, Strasbourg, F, June 27 - July 1, 2011, ECA **35G**, P5.089 (2011).

H. Weisen, Y. Camenen, A. Salmi, T. Versloot, P. Devries, M. Maslov, T. Tala, M. Berskens, C. Giroud, J.-E. Contributors, *Probable Identification of the Coriolis Momentum Pinch in JET,* Plasma Physics Controlled Fusion, Strasbourg, F, June 27 - July 1, 2011, ECA **35G**, O4.120 (2011).

R. Wesche, M. Boersch, P. Bruzzone, F. Holdener, E. Iten, N. Magginetti, S.A. March, D. Oertig, H. Quack, M. Vogel, *Development of Hts Current Leads for Industrial Fabrication,* MT 22, International Conference on Magnet Technology, Marseille, France, September 11-16, 2011 (2011).

R. Wesche, P. Bruzzone, S.A. March, M. Vogel, H. Ehmler, P. Smeibidl, *Design and Manufacture of 20 Ka Hts Current Leads for a Hybrid Magnet System,* Eucas 2011, The Hague, The Netherlands, September 18-23, 2011 (2011).

R. Wesche, D. Uglietti, P. Bruzzone, S.A. March, C. Marinucci, B. Stepanov, N.H. Glowa, *Development of Magnet Technologies for Hts Insert Coils,* Eucas 2011, The Hague, The Netherlands, September 18-23, 2011 (2011).

C.2 Seminars presented at the CRPP in 2011

Dr. Henri Weisen, CRPP-EPFL (détaché à JET), *"The scientific case for a possible new D-T campaign in JET"*

Dr. A. Pitzschke, CRPP-EPFL, CH, *"Pedestal Characteristics and MHD Stability of H-Mode Plasmas in TCV"*

Dr. T. Hansen, Department of Applied Physics, Eindhoven University of Technology, The Netherlands, *"Interaction between Low-energetic Plasmas and Hydrogenated Amorphous Carbon"*

Dr. T. Panis, CRPP-EPFL, CH, *"Direct measurements of the damping of Alfvén eigenmodes for an assessment of their stability limits in tokamak plasmas"*

N. Walkden, University of Bath, UK, *"The Effect of Toroidal Rotation on Ideal beta limits in tokamak Plasmas"*

D. Brunetti, Univ. degli Studi di Milano, Italy, *"Identification of tearing modes magnetic structure from ECE measurements"*

I. Cziegler, MIT, PSFC, USA. *"Edge Turbulence on Alcator C-Mod"*

A. Bogomolov, IOFFE Physico-Technical Inst., St-Petersburg, Russian Fed., *"Transport Processes Modeling in Globus-M Tokamak in Ohmic Mode and Additional Heating Mode (NBI)"*

Dr. D.D. Ryutov, Lawrence Livermore National Laboratory, USA, *"Axisymmetric mirrors: a game-changer in fusion research?"*

Dr. D.D. Ryutov, Lawrence Livermore National Laboratory, USA, *"Using intense lasers to simulate aspects of astrophysical accretion disks and outflows"*

Prof. P.K. Chattopadhyay, Inst. for Plasma Research, Bhat, Gandhinagar, India *"Initial Results from Basic Plasma Physics Experiment from Students Lab at IPR"*

Dr. R.A. Pitts, Divertor and Plasma Wall Interactions, ITER Organization, St Paul Lez Durance, F, *"Key physics and materials aspects of plasma-wall interactions in ITER"*

Dr. R. Nouailletas, IRFM, CEA Cadarache, F, *"Advanced control tools for improvement of tokamak operation"*

Prof. Cary Forest, Plasma Physics Group, Univ. of Wisconsin, Madinson, USA, *"Experimental Dynamos: From Liquid Metal to Plasmas"*

Dr. P. Angelino, Laboratory of Computational System Biotechnology, EPFL, Switzerland, *"A physicist in the cell - Or what a physicist can learn from biological systems"*

A. Altichieri, Consorzio RFX, Padova, Italy *"Helicity injection in RFX-mod: modelling and experimental realization"*

Dr. H. Weisen, CRPP-EPFL, détaché à EFDA-JET, *"Probable identification of the Coriolis momentum pinch in JET"*

F. Avino, Univ. of Roma "La Sapienza", Frascati ENEA Center, Italy, *"Alternative real-time density diagnostic: FTU Refractometer"*

G. Induni, Section de Physique, EPFL, Switzerland *"Theoretical study of electronic transport in TCV ELMy H-mode"*

Dr. M. Pedrozzi, Paul-Scherrer-Institute, Villigen, CH *"An overview of the SwissFEL project. A national hard X-ray Free Electron Laser facility at PSI"*

A. Talaei, Nuclear Science and Technology Research Institute (NSTR), Tehran, Iran, *"Influence of Admixture Gas on the Enhancement of Neutron Production in Plasma Focus Devices"*

Prof. A.A. Ivanov, Budker Institute of Nuclear Physics, Novosibirsk, Russian Federation, *"Megawatt Neutral Beam Injectors"*

R. Ragona, University of Turin, Italy, *"Analysis of a launching structure for heating thermonuclear plasmas at the Ion Cyclotron frequency"*

Prof. R.J. Goldston, Princeton Plasma Physics Laboratory, Princeton, USA *"Heuristic Drift-Based Model of the Power Scrape-Off Width in H-Mode Tokamaks"*

F. Felici, CRPP-EPFL, Switzerland, *"Nonlinear model-based optimization of actuator trajectories for plasma profile control"*

J. Garcia, CEA Cadarache, France, *"Conditions for the transition to advanced plasma regimes in tokamaks"*

Dr. H.B. Le, Laboratory of Conception and Integration of Systems (LCIS EA 3747) Grenoble Institute of Technology (Grenoble INP), France, *"Robust control for uncertain parameters systems: Low-order controllers design with robustness constraints System modelling for robust control"*

S. Gnesin, Dr. S. Coda, Ph. Marmillod, CRPP-EPFL, *"The TCV hard X-ray tomographic spectroscopy diagnostic"*

N. Patel, ITER-Support, India, *"Design and Analysis of various components of TOKAMAKs"*

Dr. M. Barnes, Oxford University, UK, *"Transport scalings for critically-balanced ITG turbulence in tokamaks"*

Dr. J.M. Reynolds Barredo, University of Alaska – Fairbanks, USA, *"Parareal: Time parallelization of plasma turbulence simulations"*

Dr. O. Sauter, CRPP-EPFL, *"Physics of Neoclassical Tearing Modes"*

S. Kim, National Fusion Research Institute, South Korea, *"Plasma-wall interaction research activities in KSTAR and SNU"*

Dr. D. Mazon, CEA Cadarache - DSM/IRFM, St Paul-Lez-Durance, F, *"Soft X-ray imaging techniques in tokamak plasmas: present status and possible future developments"*

Dr. R. Prater, General Atomics, San Diego, CA, USA *"Heating and Current Drive Systems for Support of Advanced Scenarios in DIII-D"*

Dr. L. Marot, Dept of Physics, University of Basel, Switzerland, *"Are coated films candidate for ITER's first mirrors?"*

Dr. N. Plihon, CNRS, Labo de Physique ENS Lyon, Lyon, France, *"A turbulent dynamo in the laboratory : the von-karman sodium dynamo"*

A. Mahfouf, Université de Paris 6, Paris, France, *"Core-SOL coupling of tokamak plasma with central rotation in limiter and divertor configurations"*

Z. Huang, Inst. für Plasmaforschung, Univ. Stuttgart, D, *"Probe measurement of electron temperature dynamics in TJ-K and ASDEX Upgrade"*

Dr. Y. Idomura, Japan Atomic Energy Agency, Japan, *"Momentum transport in full-f gyrokinetic simulations"*

Dr. W. Wuensch, CERN, CLIC RF Structure development program, Genève, *"CLIC – the study of a next-generation high-energy physics facility"*

S. Gnesin, CRPP-EPFL, *"Electron Cyclotron Heating and Suprathermal Electron Dynamics in the TCV Tokamak"*

P. Bohm, IPP-Prague, CZ, *"Tokamak COMPASS overview and Thomson scattering"*

Prof. S.I. Krasheninnikov, Univ. California, San Diego, USA, *"Multifaceted physics of edge plasma in magentic fusion devices"*

F. Jaulmes, York Plasma Institute, York, UK, *"Overview of transport in the plasma of magnetic confinement experiments dedicated to the production of fusion energy"*

Dr. N. Aiba, Japan Atomic Energy Agency, Plasma Theory and Simulation Group, *"Plasma rotation effect on edge localized MHD mode"*

Dr. N. Kirneva, NRC Kurchatov Institute, Moscow, RU, *"Confinement modification with the density increase in T-10 experiments with gas-puffing and ECRH"*

G. Merlo, Politecnico di Milano, I, *"Nanostructured materials for nuclear fusion applications"*

F. Braunmueller, IPP-Greifswald, D, *"Diagnostics for 2D-measurements of magnetic fluctuations and their application in Alfvén wave measurements"*

APPENDIX D External activities of CRPP Staff during 2011

D.1 National and international committees and ad-hoc groups

MEMBERSHIP

N. Baluc	Member of the HPC-FF board Member of the EFDA Scientific and Technical Advisory Committee (STAC) International Organizing Committee of the SOFT Conference (Symposium on Fusion Technology) International Advisory Committee of the ICFRM Conference (International Conference on Fusion Reactor Materials) IEA Annex II Executive Committee IEA Fusion Materials Agreement Executive Committee Swiss Society for Optics and Microscopy (SSOM) Task Coordinator of the subproject entitled 'Radiation-Resistant Materials' of the EXTREMAT Integrated Project (IP) of the 6th European Framework Programme
P. Bruzzone	International Magnet Technology Conference Organizing Committee European Magnet Expert Group 22st Magnet Technology Conference, Programme Committee SST-1 (India), Magnet Review Group Series Connected Hybrid Magnet, Project Review Group
B.P. Duval	TTG-rotation/transport working group chair, EU-TTG
A. Fasoli	Visiting Professor, MIT Physics Department EFDA Steering Committee ASDEX Upgrade Programme Committee, Germany International Tokamak Physics Activities: Energetic Particles Topical Group Scientific Committee, 12th IAEA Technical Meeting on Energetic Particles in Magnetic Confinement Systems, 2011 Expert for the Review of projects submitted to the French National Agency for Research (ANR) Member of Scientific Committee of the EFDA Transport Topical Group International Scientific Committee for the French Laboratory of Excellence in Plasma Science Evaluation of research programme of the University of Padua, Italy Chair of the Basic and astrophysical plasma of Programme Committee of EPS Conference 2011
Ivo Furno	Member of the SPS Committee
Ch. Hollenstein	Editorial Board Plasma Chemistry and Plasma Processing Kluwer Academic/Plenum Publisher Member of the IUVSTA Plasma Division
C. Marinucci	CHATS-AS, Board
A. Pochelon	Member of the Committee of the SWISS NUCLEAR FORUM Secretary and Member of the Swiss Physical Society Committee Member of the FORATOM Committee, in particular of the "Research and Development Task Force (R&D.TF)

	Associate member of IUPAP (International Union of Physics and Applied Phyiscs), Commission C16: Commission on plasma physics
O. Sauter	International Tokamak Physics Activities: MHD, Disruption and Control Topical Group Expert at panel for CNRS position at the University of Marseilles
R. Schäublin	Member of the board of the Swiss Society for optics and microscopy Member of the Program Committee of the ICFRM Conference (Int. Conf. on Fusion Reactor Materials)
P. Spätig	Member of the Program Committee of the ICFRM Conference (Int. Conf. on Fusion Reactor Materials)
M.Q. Tran	Director of the Inst. of Physics of Energy and Particle, EPFL Consultative Committee for the Euratom Specific Research and Training Programme in the field of Nuclear Energy, Fusion (CCE-FU) Chairman of the Technical Advisory Panel of the Joint Undertaking Fusion for Energy (F4E) (until June 2011) Swiss expert to the Governing Board of F4E Member of the Core Commission for nomination of Max-Planck Plasma Physics for Plasma Physics Committee of the International Symposium on Fusion Nuclear Technology Member of the Steering Committee of the Center of Competence on Energy and Mobility of the the CEPF Swiss delegate at the Fusion Power Coordinating Committee Member of the EU Delegation and vice-chair of ITER STAC until May 2011 Member of the Power Plant Physics and Technology Board
L. Villard	Member, Board of the High Performance Computing for Fusion, EFDA Special working group 1 of the IFERC-CSC Member, Standing Committee of the IFERC CSC
H. Weisen	Seconded to EFDA-JET CSU, programme department Member of the Diagnostics Working Group within the ITPA Member of the expert panel for evaluating PhD and post-doc research proposals submitted to the Fonds National de la Recherche, Luxembourg

PARTICIPATION

B. Duval	Remote Participation Users Group, EFDA-JET EU-TTG Meeting, Cordoba, Spain
Y.R. Martin	International Tokamak Physics Activity: "Transport and Confinement Modelling Topical Group" and "Edge and pedestal physics Topical Group"

D.2 Editorial and society boards

S. Alberti	Editorial Board International Journal Infrared Millimeter and Terahertz Waves Editorial Board IEEE Transaction on THz Science and Technology (Topical editor: THz plasma science and instruments)
S. Coda	Editorial Board of Plasma Physics and Controlled Fusion
Ch. Hollenstein	Editorial Board Plasma Chemistry and Plasma Processing Kluwer Academic/Plenum Publisher

J.B. Lister	Member of the International Advisory Board of Plasma Physics and Controlled Fusion
Y.R. Martin	Member of the EFDA Public Information Group (PIG) Chairman of the Association Vaudoise des Chercheurs en Physique
A. Pochelon	Auditor of the Swiss Physical Society Committee Set up of a "Network of Experts in the domain of Energy in Switzerland", Swiss Physical Society Committee
Ph. Spaetig	Member of the Advisory Editorial Board of Journal of Nuclear Materials

D.3 EPFL committees and commissions

N. Baluc	Commission Ecole Doctorale en Science et Génie des Matériaux Commission Ecole Doctorale en Physique
A. Fasoli	Président de la Commission Stratégique de la Physique, EPFL Direction de la Faculté FSB Comité de Coordination Joint Doctoral Initiative EPFL-IST Lisbon Conseiller d'études pour la Physique - Master
J-Ph. Hogge	Commission du Doctorat de la Section de Physique, FSB-EPFL
O. Sauter	Commission du Doctorat de la Section de Physique, FSB-EPFL
M.Q. Tran	Commission du Doctorat de la Section de Physique, FSB-EPFL Commission stratégique de la Section de Physique, EPFL Membre du Comité de Sélection du Prix de la meilleure thèse EPFL "Core Group" of the Master in Nuclear Engineering Programme
T.M. Tran	Groupe de travail technique du Comité de Pilotage HPC/MPC, EPFL
L. Villard	Délégué à la mobilité, Section de physique, FSB-EPFL Commission d'Ethique, EPFL Commission d’Enseignement de la Section de Physique, FSB-EPFL Groupe de travail technique HPC (High Performance Computing) – EPFL Steering Committee, HPC (High Performance Computing) – EPFL

APPENDIX E The basis of controlled fusion

E.1 Fusion as a sustainable energy source

Research into controlled fusion aims to demonstrate that it is a valid option for generating power in the long term future in an environmentally, politically and economically acceptable way. Controlled fusion is a process in which light nuclei fuse together to form heavier ones: during this process a very large amount of energy is released. For a fusion reactor it is planned to use the two isotopes of hydrogen: deuterium (D) and tritium (T), which fuse together much more readily than any other combination of light nuclei according to the following reaction:

$$D^2 + T^3 \rightarrow He^4 + n + 17.6MeV$$

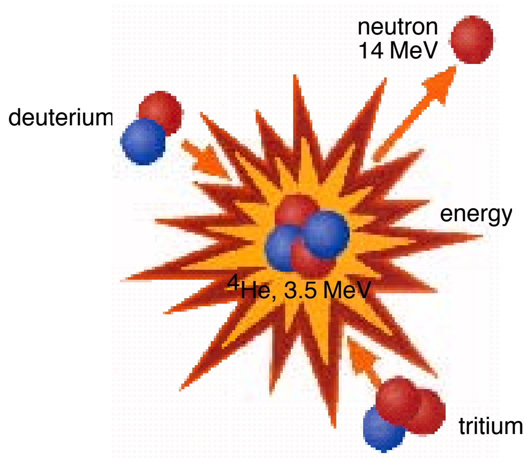

Fig. E.1 *Schematic of a fusion reaction between deuterium and tritium nuclei. The products are 3.5MeV ^{4}He, the common isotope of helium, and a 14MeV free neutron.*

The end products are helium and neutrons (n). The total energy liberated by fusing one gram of a 50:50% mixture of deuterium and tritium is 94000kWh, which is 10 million times more than from the same mass of oil. 80% of this energy is carried by the neutrons with an energy of 14MeV while the remaining 20% is carried by the helium nucleus. Most of this energy eventually becomes heat to be stored or converted by conventional means into electricity.

The temperature at which fusion reactions start to become significant are above a few tens of millions of degrees. For the D-T reaction, the optimal temperature is of the order of 70-200 million degrees. At such temperatures the D-T fuel is in the plasma state.

Deuterium is very abundant on the earth and can be extracted from water (0.034g/l). Tritium does not occur naturally, since its half-life is only 12.3 years, but it can be regenerated from lithium using the neutrons produced by the D-T fusion reactions. The two isotopes of natural lithium contribute to this breeding of tritium according to the reactions:

$$Li^6 + n \rightarrow He^4 + T^3 + 4.8MeV$$

$$Li^7 + n \rightarrow He^4 + T^3 + n - 2.5MeV$$

The relative abundance of the two lithium isotopes Li^6 and Li^7 are 7.4% and 92.6%, respectively. The known geological resources of lithium both in the earth and in the sea water are large enough to provide energy for an unlimited time.

E.2 Attractiveness of fusion as an energy source

The inherent advantages of fusion as an energy source are:

- The fuels are plentiful and their costs are negligible because of the enormous energy yield of the reaction;
- The end product of the reaction is helium, an inert, non-radioactive gas;
- No chain reaction is possible: the neutron emitted by the fusion process does not trigger subsequent reactions;
- Only a very small amount of fuel is present in the core of the reactor: the plasma weights a fraction of gram;
- Any malfunction would cause a quick drop of temperature and all fusion reactions would stop within seconds;
- No after-heat problem can lead to thermal runaway even if the case of a loss of coolant accident;
- None of the materials required by a fusion power plant are subject to the provisions of the non-proliferation treaties.

Its further potential advantages are:

- Radioactivity of the reactor structure, caused by neutrons, can be minimised by careful selection of low-activation materials resulting in a manageable quantity of long lived radioactive waste;
- The release of tritium in normal operation can be kept at a very low level. The inventory of tritium on the site can be sufficiently small so that even the worst possible accident could not lead to a harmful release to the environment requiring evacuation of the nearby population.

APPENDIX F Sources of Financial Support

In 2011, the work carried out at the CRPP and presented in this annual report was financed from several sources. The major financial support is provided by:

Swiss public institutions:

- the Ecole Polytechnique Fédérale de Lausanne (EPFL)
- the Conseil des Ecoles Polytechniques (CEPF)
- the Swiss National Science Foundation
- the Paul Scherrer Institute (PSI), which hosts the Supraconductivity and the Materials science activities
- the Swiss Secrétariat d'Etat à l'Education et à la Recherche (SER)
- the Swiss "Departement Fédéral de l'Intérieur" in the frame of the Broader Approach
- the Swiss "Commission pour la Technologie et l'Innovation" (CTI)

International public institutions:

- EURATOM
- ITER
  - ITER Organization
  - Domestic Agencies in China, Europe (F4E), Japan, Korea, Russia, USA
- Helmholtz-Zentrum Berlin, D

Private organisations

- Allper AG
- Atela SA
- Comadur SA
- Inspire AG
- OC Oerlikon Solar
- Ruag AG
- Sulzer Innotec AG
- Sulzer Metco AG
- Tetra Pak SA.
- WEKA AG

APPENDIX G Glossary

The following is a general purpose glossary for the field of controlled fusion and plasma physics.

Additional heating: Usually with reference to a plasma which is initially heated by a toroidal current induced in the plasma (ohmic heating), additional heating designates other means of heating a plasma (absorption of electromagnetic waves or of injected fast neutral particles).

Advanced Tokamak Scenarios: Tokamaks normally generate natural profiles of plasma current and plasma pressure. External non-inductive current drive and local control of the current and pressure profiles can allow access to enhanced regimes and even steady state operation, generally referred to as Advanced Tokamak Scenarios.

ALCATOR C-MOD: High field, high density tokamak at MIT (USA) with an elongated, diverted plasma and metallic walls.

Alfvén gap modes: The toroidal nature of tokamak plasmas produces gaps in the otherwise continuous spectrum of Alfvén waves, populated by discrete, weakly damped Alfvén gap modes. Under certain conditions these modes can be destabilised by resonant energy transfer from energetic particles, e.g. α-particles from fusion reactions.

Alfvén waves: A fundamental plasma wave, which is primarily magneto-hydrodynamic in character with an oscillation of the magnetic field and, in some cases, plasma pressure. In tokamaks, these waves are typically strongly damped. See also fast Alfvén wave.

Alfvén velocity: The velocity of propagation of Alfvén waves in the direction of the magnetic field; it is proportional to the magnetic field strength, and inversely proportional to the square root of the mass density.

alpha particle, or α-particle He^4: The nucleus of the helium atom, composed of two protons and two neutrons, is one of the two products of the DT fusion reaction (the other one is a neutron). The α-particles, being electrically charged, are trapped by the magnetic confinement field and therefore can release their energy to the plasma contrary to the neutrons which escape from the plasma and transfer their energy in the blanket surrounding the plasma core. The plasma heating which is provided by these α-particles as they slow down due to collisions is essential for achieving ignition.

Alternative lines: Magnetic confinement development other than the tokamak.

Analytic/Computational modelling: Analytic: algebraic solution of basic equations. Computational: numerical solution of basic equations.

Anomalous transport: Measured heat and particle loss is anomalously large compared with collisional theory of heat transport in toroidal plasmas.

ASDEX-Upgrade: Medium-sized Tokamak at Garching (Association Euratom-IPP, Germany) with an elongated, diverted plasma.

Aspect ratio: The ratio between the large radius and the small radius of a torus.

Auxiliary heating: See additional heating.

Ballooning instability: A local instability which can develop in the tokamak when the plasma pressure exceeds a critical value; it therefore constrains the maximum β that can be achieved. It is analogous to the unstable bulge which develops on an over-inflated tyre.

Beta (β): Ratio of plasma pressure to magnetic field pressure. One of the figures of merit for magnetic confinement: the magnitude of the magnetic field pressure determine the cost of the field coil that generates it; since fusion reactivity increases with the square of the plasma pressure, a high value of β indicates good performance. The highest values achieved in tokamaks reach 40% (START).

Beta-normalised (β_N): The ratio of plasma current (in MA) to the product of minor radius (in m) and magnetic field (in T) characterises the limit to the achievable β imposed by ideal MHD. β -normalised is the ratio of β (as a percentage) to the above ideal MHD parameter. Generally β_N ~3 should be achievable, but techniques for obtaining higher values have been found experimentally.

Blanket: A structure containing lithium or lithium compounds surrounding the plasma core of a fusion reactor. Its functions are to breed tritium, via lithium-neutron reactions, and to absorb most of the fusion energy to be used for electricity generation.

Bootstrap current: Theory developed in 1970 predicted that a toroidal electric current will flow in a tokamak which is fuelled by energy and particle sources that replace diffusive losses. This diffusion driven "Bootstrap current", which is proportional to β and flows even in the absence of an applied voltage, could be used to provide the poloidal magnetic field: hence the concept of a Bootstrap tokamak, which has no toroidal voltage. A Bootstrap current consistent with theory was observed many years later on JET and TFTR; it now plays a role in optimising advanced tokamaks.

Breakeven: The fusion performance of a power plant is denoted by Q, which is the ratio of the power released by fusion reactions to that used to heat the plasma. As a convention, scientific breakeven corresponds to Q=1 and ignition to Q=infinity. A fusion power plant would operate at Q~50.

Breeding ratio: The number of tritium atoms produced in the blanket of a fusion power station per tritium nucleus burned in the fusion plasma.

Burn: The fusion process of consuming DT fuel in a reactor, releasing energy.

CCE-FU: The Consultative Committee for the Euratom Specific Research and Training Programme in the field of Nuclear Energy, Fusion. Formerly the CCFP.

CEA: Commissariat à l'Energie Atomique, France. Partner in the Association EURATOM-CEA which operates the TORE SUPRA tokamak.

CFI: Committee on Fusion-Industry.

Charge exchange measurement: Measures the plasma ion temperature. Neutral atoms in the plasma (for example from a neutral beam) donate electrons to hot plasma ions, which are thereby neutralised. These hot atoms are no longer confined by the magnetic field and leave the plasma. Their energy is measured by a neutral particle analyser.

CIEMAT: Centro de Investigaciones Energéticas Medioambientales y Tecnológicas, Spain. Partner in the Association EURATOM-CIEMAT. Operates the flexible heliac stellarator TJ-II.

Classical transport: Collisions between the individual particles of a plasma allow them to move across the magnetic field. Theories which describe this mechanism are called “classical” (or “neo-classical” when additional effects due to the toroidal geometry are included). The measured heat and particle transport is usually higher than predicted by these theories.

Collisionality: Non-dimensional parameter, which is the inverse ratio of the mean free path of plasma particles between collisions to a characteristic length of the magnetic field configuration.

Compact torus: Class of closed magnetic configurations in which no material elements (coils, conductors or walls) need to link through the bore of the plasma torus. Thus the vessel of compact tori can be spherical or cylindrical.

COMPASS: COMPact ASSembly, a tokamak for studies of plasma stability, at Culham, UK (Association EURATOM-UKAEA). Originally with circular vessel (COMPASS-C), later with D-shaped vessel (COMPASS-D).

Confinement time: In a fusion plasma neither particles nor energy are perfectly confined. Particle confinement time is the time during which the particles, on average, stay confined. The energy confinement time, which is usually shorter than the particle confinement time, is defined in steady state as the ratio of the plasma energy content to the total power input to the plasma and is a measure of how fast a plasma would cool if there were no heating.

CRPP: Centre de Recherches en Physique des Plasmas. Fusion laboratories of the Association EURATOM-Swiss Confederation at the Ecole Polytechnique Fédérale de Lausanne and the Paul-Scherrer Institute, Villigen (CRPP-Fusion Technology).

Current drive (non-inductive): In a tokamak, plasma current can be driven inductively, with the toroidal plasma acting as a secondary winding of a transformer whose primary coil is at the central column of the device. Continuous current cannot be driven by transformer action. 'Non-inductive' current drive methods are applied either by injecting particles with directed momentum into the plasma or by accelerating electrons by electromagnetic waves so that they carry the current. Also being applied to control instabilities and to optimise confinement by modifying the current profile. The bootstrap effect also drives current.

Current profile (current distribution): The distribution of current density across the minor radius of the plasma.

Current ramp-up (down): The increase (decrease) of plasma current either at the start of operation or during operation.

Cyclotron frequency: Charged particles in a magnetic field have a natural frequency of gyration in the plane perpendicular to the magnetic field - the cyclotron frequency. For electrons in a tokamak, the cyclotron frequency is typically a few tens of GHz (28GHz per Tesla), and for ions, a few tens of MHz (7.5MHz per Tesla for deuterium).

Cylindrical approximation: An approximation to the true tokamak geometry in which the torus is straightened, so that the toroidal direction becomes the cylinder axis. There are two directions of symmetry: along the axis (the 'toroidal' direction) and about the axis (the 'poloidal' direction).

DCU: Dublin City University, Ireland. Partner in the Association EURATOM-DCU.

DEMO: Demonstration Reactor (the first device in the European fusion strategy intended to produce significant amounts of electricity).

Deuterium: A stable isotope of hydrogen, whose nucleus contains one proton and one neutron. In heavy water, normal hydrogen is replaced by deuterium. Sea water contains, on average, 34g deuterium per m^3. Deuterium plasmas are used routinely in present-day experiments; in a fusion power plant the plasma will consist of a mixture of deuterium and tritium which fuse more readily then two deuterium nuclei.

DG Research (DG RTD): The Directorate-General of the European Commission, Brussels, responsible for Research and Development. Formerly DG XII.

Diagnostic: Apparatus used for measuring one or more plasma quantities (temperature, density, current, etc.).

Diffusion, thermal (or particle): The random flow of heat (or particles) in the presence of a thermal (or density) gradient.

DIII-D: The largest operating US tokamak, run by General Atomics, San Diego. It has a flexible configuration and studies core and divertor physics with intense additional heating.

D-He^3: Deuterium-^{3}Helium: A potential fuel mix for fusion with low release of neutrons, but which would require a much higher fusion triple product ($nT\tau$) than DT to reach ignition. ^{3}Helium is an isotope of helium which is not available in appreciable quantities on Earth.

Disruption, Disruptive instability: A complex phenomenon involving MHD instability which results in a rapid release of energy to the wall and strong electromechanical forces in a tokamak. Plasma control may be lost, triggering a VDE (q.v.). This phenomenon places a limit on the maximum density, pressure and current in a tokamak.

Distribution function: Describes both the space and velocity distribution of plasma particles.

Divertor: A magnetic field configuration with a separatrix, affecting the edge of the confinement region, designed to remove heat and particles from the plasma, i.e. divert impurities and helium ash to divertor plates in a target chamber. Alternative to using a limiter to define the plasma edge.

Double null: See Single/double null divertors.

Drift kinetic theory: Kinetic theory which describes plasma processes which have spatial scales much greater than the particle Larmor radii.

Drift orbits: Particle motion is tied to straight magnetic field lines. However, electric fields and gradients of the magnetic field give an additional drift perpendicular to the magnetic field creating drift surfaces displaced from the magnetic surfaces.

Driven current: Plasma current produced by a means external to the plasma, inductively or non-inductively.

Driver: In inertial confinement fusion, the laser or particle beam system used to compress a target pellet.

DTE: The deuterium-tritium experiment at JET which in 1997 set new records for fusion power production. Followed the Preliminary Tritium Experiment of 1991.

ECCD: Electron Cyclotron Current Drive. Non-inductive current drive technique using directed electron cyclotron resonance waves.

ECE: Electron Cyclotron Emission. Radiation emitted by electrons as a result of their cyclotron motion around magnetic field lines. Used to measure electron temperature.

ECH: Electron-Cyclotron Heating. Radio wave heating near the resonance frequency (or its multiple) of the electron gyration in a magnetic field. In present and future machines ECH is at typically 60-170GHz, depending on the magnetic field strength in a machine.

EFDA: European Fusion Development Agreement. The organisational framework of the EU fusion activities for the exploitation of the JET Facilities, international collaboration (including ITER) and supporting technology.

EFET: European Fusion Engineering & Technology: a fusion technology oriented European Economic Interest Grouping.

Electron temperature: A measure of electron thermal energy in units of degrees or electron volts (1eV ~ 10^4 degrees Kelvin).

ELM: Edge localised mode. An instability which occurs in short periodic bursts during the H-mode in divertor tokamaks. It modulates and enhances the energy and particle transport at the plasma edge. These transient heat and particle losses could be damaging in a reactor.

ENEA: Ente per le Nuove Tecnologie, l'Energia e l'Ambiente, Italy. Partner in the Association EURATOM-ENEA.

Energetic particle: In terms of energy, the particles in a plasma can be divided into two classes. The more numerous thermal particles are characterised by a temperature typically in the range 1–30keV for modern tokamaks. The less numerous class of energetic particles has significantly higher energy up to several MeV. Energetic particles can be created by electric fields, fusion reactions, neutral beam injection or RF heating.

EPS: European Physical Society. Its Plasma Physics Division hosts the major European annual conference on Plasma Physics.

Error fields: The magnetic coils of a tokamak are designed to give the desired magnetic field configuration. The finite number of coils and imperfections in their construction lead to unwanted deviations from this configuration known as error fields. These could lead to disruptions and are of particular concern for larger tokamaks.

EXTRAP T-II: External Trap II, a medium-sized reversed field pinch (RFP) at the Royal Institute of Technology, Stockholm (Association EURATOM-NFR), built for RFP transport and shell stabilisation studies in support of RFX.

EURATOM: European Atomic Energy Community.

Faraday rotation: The rotation of the plane of polarisation of light passing through a magnetised plasma.

Fast Alfvén wave: The fast Alfvén wave exists over a broad frequency spectrum, from the ion cyclotron range of frequencies (ICRF) where its character is electromagnetic, down to magnetohydrodynamic frequencies. Its velocity is comparable to the Alfvén velocity. The fast Alfvén wave is used routinely for high-power (~20MW) ICRF heating on JET, as it is efficiently absorbed in the plasma by the mechanism of ion cyclotron resonance. Although usually stable in tokamaks, the wave can be excited by energetic ion populations.

Fast wave current drive: Current drive produced by a fast wave. The wave can penetrate the plasma more easily than a lower hybrid wave.

Feedback: Use of measurements of plasma parameters to control the parameters, shape or profiles of the plasma to obtain desired conditions.

Field lines, Flux surfaces: Imaginary lines marking the direction of a force field. In a tokamak these define a set of nested toroidal surfaces, to which particles are approximately constrained, known as flux surfaces.

Field reversed configuration: A compact torus with a strongly elongated plasma. The plasma is contained in a cylindrical vessel inside a straight solenoid. The confining magnetic field usually has only a poloidal component. Not to be confused with reversed field pinch.

FIR: Far infra-red (e.g. wavelength ~ 0.2 to 1mm). FIR lasers are used to measure the magnetic field and plasma density.

"Fishbones": Rapid bursts of MHD activity sometimes observed when neutral beam heating is used in tokamaks (fishbone refers to the shape of the bursts in oscillating magnetic field when plotted as a function of time).

First wall: The first material boundary that surrounds the plasma. Today, the first wall in many machines is protected by low-Z materials (such as carbon tiles, boron or beryllium coating). Future tokamaks will require metallic walls.

Flat-top current: Constant current during quasi-stationary operating conditions.

Fokker-Planck Code: A computer code to calculate the velocity distribution of plasma particles allowing for collisional relaxation and plasma heating. Calculates distribution functions (q.v.).

FOM: Stichting voor Fundamenteel Onderzoek der Materie (Foundation for basic investigations of matter), The Netherlands. Partner in the Association EURATOM-FOM.

FTU: Frascati Tokamak Upgrade, a high density, high current tokamak at Frascati, Italy (Association EURATOM-ENEA).

Fusion triple product: Product of (ion) density, (ion) temperature and energy confinement time. A measure of the proximity to break-even and ignition.

Fusion product: The product of a fusion reaction, for example an α-particle or neutron in a deuterium-tritium plasma.

Fusion reactivity: Fusion reaction rate. For present typical tokamak conditions, it increases with the square of the density and the ion temperature of the plasma.

Full wave theory: Wave theory which includes complete accounting of wave energy (transmitted, reflected and absorbed, including energy transferred to other waves) for studying RF heating.

FZK: Forschungszentrum Karlsruhe, Germany. Partner in the Association EURATOM-FZK, active in fusion technology and, with the development of gyrotrons, in plasma engineering.

FZJ: Forschungszentrum Jülich GmbH, Germany. Partner in the Association EURATOM-FZJ, operating the tokamak TEXTOR.

GSI: Gesellschaft fuer Schwerionenforschung, Darmstadt, Germany. Studying heavy-ion physics, and driver physics with possible application for inertial confinement fusion.

Gyro-kinetic theory: Version of kinetic theory in which the Larmor radius is not assumed to be small. An essential theory for investigating fine-scale instabilities which might be responsible for driving turbulence, which may in turn be responsible for anomalous transport.

Gyrotron: Device used for generating high power microwaves in the electron cyclotron range of frequencies (50 - 200GHz). This UHF wave is mostly used to heat the plasma at the electron cyclotron resonance frequency. It also could be used to diagnose the plasma.

Heliac: Stellarator configuration with a central toroidal coil around which the plasma column is wound helically. Because of its high capability of investigating a wide range of stellarator configurations, it is used for TJ-II.

Helias: Optimised stellarator configuration, used with modular coils for Wendelstein VII-X (Germany) and SHEILA (Australia).

H-mode: A High confinement regime that has been observed in tokamak plasmas. It develops when a tokamak plasma is heated above a characteristic power threshold, which increases with density, magnetic field and machine size. It is characterised by a sharp temperature gradient near the edge (resulting in an edge “temperature pedestal”), ELMs and typically a doubling of the energy confinement time compared to the normal “L” regime. Today, a variety of high confinement modes have been identified in divertor and in limiter configurations (e.g. the I-mode), which, in part, have been obtained by special tailoring of the radial plasma current profile.

H-transition (or L-to-H transition): Transition into the H-regime from the L-regime, usually quite sudden, at a certain threshold power of additional heating and specific plasma parameters.

Halo currents: See Vertical Displacement Event.

Helicity injection: The helicity of a toroidal plasma is related to a linkage of toroidal and poloidal magnetic fluxes, and is approximately conserved throughout a discharge. If additional helicity can be injected, the plasma current could be sustained or even increased.

Helium ash: Fusion reactions in a deuterium-tritium plasma produce energetic α-particles (helium nuclei), which heat the plasma as they slow down. Once this has happened, the α-particles have no further use: they constitute helium ash, which dilutes the fuel and must be removed to maintain a burning plasma.

High beta (β): Condition in which the plasma energy is a significant fraction of the energy in the magnetic field. An alternative measure is the ratio between the plasma energy and the energy in the poloidal magnetic field, the poloidal β.

High field ECH launch: Electron cyclotron waves can be launched from the inside of the plasma torus. This allows higher density plasma to be heated.

Hydrogen: The lightest element; the nucleus consists of only one proton, the atomic shell of one electron. Isotopes of hydrogen, with one or two additional neutrons in the nucleus, are deuterium and tritium respectively.

IAEA: International Atomic Energy Agency (of the United Nations), Vienna, Austria. The ITER-EDA is undertaken under the auspices of the IAEA.

ICE: Ion Cyclotron Emission. Observed in JET and TFTR as a suprathermal signal, apparently driven by collective instability of energetic ion populations such as fusion products and injected beam ions.

ICF: Inertial Confinement Fusion. Intense beams of laser light or light or heavy ion beams are used to compress very rapidly and heat tiny target pellets of fusion fuel to initiate fusion burn in the centre. Sufficient fusion reactions must occur in the very short time before the fuel expands under its own pressure. The inertia of the pellet's own mass determines the time scale during which fusion reactions occur, hence the name inertial confinement.

Ideal: In the context of MHD, 'ideal' implies that the magnetic field and the plasma always move together. For this to occur, the electrical resistivity of the plasma must be negligible.

Ideal internal kink modes: An MHD instability of the central region of a tokamak. This, or its close relative the resistive internal kink mode, may be involved in the Sawtooth disruptions which occur in most Tokamaks.

IEA: International Energy Agency (of the OECD), Paris, France. Implementing agreements for international collaboration on specific topics in fusion have been set up in the frame of the IEA.

Ignition condition: Condition for self-sustaining fusion reactions: heat provided by fusion α-particles replaces the total heat losses. External sources of plasma heating are no longer necessary and the fusion reaction is self-sustaining. Ignition is not required for energy gain in a power station. Retaining a level of external heating or current drive will be required to control the plasma pressure and current profiles, to optimise the performance, leading to a so-called "driven burn".

Impurities: Ions, other than the basic plasma ion species, which are unwanted as they lose energy by radiation and dilute the plasma.

Impurity screening: The prevention of impurities from entering the plasma.

Internal kink: A type of MHD instability that can occur within the central region of the plasma (where $q < 1$) reducing the peak temperature and density.

Internal Reconnection Event (IRE): An instability which breaks magnetic field lines and reconnects them with a different topology to reduce the system to a lower energy state - associated with the operating limits of spherical tokamaks.

Ion Bernstein wave: A wave which only exists in a hot plasma and is supported by the ions. It propagates at right angles to the magnetic field, when it is undamped, at harmonics of the ion cyclotron frequency. There is also an electron Bernstein wave which propagates at harmonics of the electron cyclotron frequency.

Ion Cyclotron Current Drive (ICCD): Non-inductive current drive using ICRH.

Ion Cyclotron Resonance Heating (ICRH)/Ion Cyclotron Resonance Frequencies (ICRF): Additional heating method using RF waves at frequencies (~ 20-50MHz) matching the frequency at which ions gyrate around the magnetic field lines.

IPP: Max-Planck-Institut fuer Plasmaphysik, Garching, Germany. Partner in the Association EURATOM-IPP, operating the tokamak ASDEX-Upgrade and the stellarator Wendelstein VII-AS. Also has sites in Berlin and in Greifswald, where the construction of the large superconducting stellarator Wendelstein VII-X is in progress. The name is also used for the Czech Republic Association.

IR: Infra Red part of the electromagnetic spectrum.

IRE: Internal Reconnection Event.

IST: Instituto Superior Técnico, Portugal. Partner in the Association EURATOM-IST.

ISTTOK: Tokamak, for study of non-inductive current drive, at the Instituto Superior Técnico (IST), Lisbon, Portugal.

ITER: International Thermonuclear Experimental Reactor (the next step as a collaboration between EURATOM, Japan, China, India, Korea, the Russian Federation and the USA, under the auspices of the IAEA). After a conceptual design phase - CDA (1988-1990), and engineering design activities (ITER-EDA, 1992-2001), now under the Coordinated Technical Activities (CTA).

JAEC: Japan Atomic Energy Commission, Tokyo, Japan.

JAEA: Japan Atomic Energy Agency. Headquarters in Tokyo, Japan.

JET: Joint European Torus. The largest tokamak in the world, sited at Abingdon, UK. Operated as a Joint Undertaking (JET Joint Undertaking), until the end of 1999. The scientific exploitation of the JET facilities is now guaranteed by the Euratom fusion Associations within the EFDA framework. The operation of the facility is the responsibility of the Association Euratom-UKAEA.

JT-60U: Japanese tokamak at Naka. The largest Japanese tokamak and second largest operating experiment after JET, but not designed for use with D-T fuel.

keV: Kilo-electronvolt. Energy which an electron acquires passing a voltage difference of 1000 volts. Also used to measure the temperature of a plasma (1 keV corresponds to 11.8 million degrees Kelvin).

Kinetic instability: Oscillation which is unstable as a result of the energy distribution of ions or electrons.

Kinetic theory: A detailed mathematical model of a plasma in which trajectories of electrons and ions are described. More complex than fluid and two-fluid theories, it is necessary in the study of RF heating and some instabilities, particularly when energetic particles are involved.

L-H transition: Change from L regime to H regime (usually quite sudden).

L-mode: As opposed to the H mode. Regime with degradation of confinement, in additionally heated plasmas, with respect to plasmas heated ohmically by the plasma current.

Langmuir probe: Electrical probe inserted into the edge of a plasma for measurements of density, temperature and electric potential.

Larmor radius: Radius of the gyratory motion of particles around magnetic field lines.

Large scale ideal modes: A large scale mode has a wavelength which is a significant fraction of the plasma dimensions and assumes ideal MHD.

Laser ablation: Use of lasers to produce a sudden influx of impurities into the plasma from a solid surface.

Last closed flux surface: The boundary separating those magnetic field lines that intersect the wall (open lines) from the magnetic field lines that never intersect the wall (closed lines).

Lawson criterion: The value of the confinement time multiplied by the ion density (at the required temperature) which must be exceeded in a fusion reactor to reach ignition.

Limiter: A material surface within the tokamak vessel which defines the edge of the plasma and thus avoids contact between the plasma and the vessel. A pumped limiter can also be used to remove heat and particles and is an alternative exhaust system to the divertor.

LLNL: Lawrence Livermore National Laboratory, Livermore, USA.

Locked modes: MHD modes that cease rotating (though they can still grow).

Low-activation materials: Materials which do not develop high, long-lived radioactivity under neutron irradiation.

Low aspect ratio: Low ratio of major to minor radius of the torus.

Lower hybrid current drive (LHCD): Non-inductive current drive using lower hybrid waves.

Lower hybrid heating (LHRH): Plasma heating by radio frequency waves at the "lower hybrid" resonance frequency in the plasma. Typical frequencies are a few GHz.

Lower hybrid (LH) wave: A plasma wave of frequency between the ion and electron cyclotron frequencies. It has a component of electric field parallel to the magnetic field, so it can accelerate electrons moving along the field lines.

Magnetic axis: The magnetic surfaces of a tokamak form a series of nested tori. The central 'torus' defines the magnetic axis.

Magnetic Confinement Fusion (MCF): Confinement and thermal insulation of a plasma within the reactor core volume by the action of magnetic fields. In toroidal magnetic confinement, usually both toroidal and poloidal components of the magnetic field are needed (the field lines are threaded like the filaments of a cable which is bent into a ring).

Magnetic islands: Islands in the magnetic field structure caused either by externally applied fields or internally by unstable current or pressure gradients. See tearing magnetic islands.

Magnetic surfaces (flux surfaces): In toroidal magnetic confinement, the magnetic field lines lie on nested toroidal surfaces. The plasma pressure, but not the amplitude of the magnetic field, is a constant on each magnetic surface.

Magneto-acoustic cyclotron instability: This instability results from an exchange of energy between the fast Alfvén wave (or magneto-acoustic wave) and an ion Bernstein wave which has a source of free energy through the presence of a population of energetic (non-thermal) ions, e.g. fusion products. The instability occurs for propagation perpendicular to the equilibrium magnetic field.

Major radius: The distance from the tokamak symmetry axis to the plasma centre.

Marfe: A localised and radiating thermal instability sometimes observed near the edge of tokamak plasmas.

Marginal Stability: Close to the transition from stability to instability.

MAST: Mega Amp Spherical Tokamak at Culham (Association EURATOM-UKAEA), twice as big as START. Began operation in 1999.

MeV: Mega-electronvolt, unit for nuclear energies. Energy which an electron acquires passing a voltage difference of 1 million volts.

MHD (Magnetohydrodynamics): A mathematical description of the plasma and magnetic field, which treats the plasma as an electrically conducting fluid. Often used to describe the bulk, relatively large-scale, properties of a plasma.

MHD instabilities: Unstable distortions of the shape of the plasma/magnetic field system.

Microinstabilities: Instabilities with characteristic wave-lengths similar to the ion Larmor radii, rather than to the tokamak dimensions. These are thought to be responsible for the fine scale turbulence in tokamaks, and hence anomalous transport.

Minor radius: Half the small diameter of the tyre-shaped toroid.

Mirnov coils: Pick-up coils at the edge of the plasma for measuring the time variation of magnetic fields arising from instabilities.

Mirror: A linear magnetic confinement concept with a weaker magnetic field in a central region and with strong fields at both ends which reflect contained particles by the mirror effect. Some variants exist to increase the magnetic field in all directions from the centre or to improve the closure of the bottlenecks. The Tandem Mirror confinement concept also involves electrostatic fields.

MIT: Massachusetts Institute of Technology, Boston, USA. Operates the high-field divertor tokamak ALCATOR C-MOD.

Mode: A resonant wave or oscillation in a plasma. Also used as a synonym for an operating regime.

Mode number: Characterises the wavelength of a mode normalised to the device size.

Monte Carlo code: A statistical technique used in numerical calculations where events may occur many times, each with a certain probability.

Motional Start Effect (MSE): The measurement of shifts and splitting of spectral lines emitted from particles moving in a local electric field. This can be interpreted to give the local magnetic field inside the tokamak if the particle velocity is known, and is a major diagnostic on some tokamaks to deduce the current profile.

MPQ: Max-Planck-Institut fuer Quantenoptik, Garching, Germany. Active, within its programme, in ICF (laser fusion) related physics. Partially supported by Euratom, for a “keep in touch activity” in ICF.

Negative ion beam: To produce neutral beams, negative ions (obtained by the addition of electrons to neutral atoms) are accelerated and then neutralised before entering the plasma. The efficiency of creating neutral beams from positive ions is too low at the beam energy required for a fusion power station, of the order of 1 MeV.

Neo-classical theory: Classical collisional plasma transport theory, corrected for toroidal effects. The neoclassical theory predicts the existence of the bootstrap current.

Neo-classical tearing mode: The magnetic island produced by a tearing mode perturbs the bootstrap current which further amplifies the island and degrades confinement or leads to a disruption.

NET: Next European Torus, a design for the Next Step which had been prepared by the NET team (located at the Association EURATOM- IPP in Garching) and which largely influenced the ITER design.

Neural network: A computer algorithm that uses incoming data to derive plasma parameters, having previously been "trained" on a series of examples of a non-linear input-output mapping.

Neutrons: Neutral particles in the nucleus. Products of Deuterium-Tritium and other fusion reactions.

Neutral beams: Since charged particles cannot easily penetrate the magnetic confinement fields of the plasma, high energy beams of neutral atoms are injected into the plasma for fuelling, heating and current drive. Within the plasma, the atoms of the beam are ionized and are then confined.

Neutron multiplier: The fusion of deuterium and tritium consumes one tritium nucleus per reaction, producing one neutron. Since in the blanket of a power station not every neutron reacts with lithium to produce a new tritium atom, a neutron multiplying element may be used in the blanket to enhance the tritium production so as to make the power station self-sufficient in tritium supply.

Next Step: The next experimental device in the strategy of the European Fusion Programme. Presently pursued via the ITER EDA, with a European activity as a fall-back option. The generic name for an experimental reactor with a long pulse burning plasma at high fusion gain.

NFR: Naturvetenskapliga Forskningsrädet (Natural Science Council), Sweden. Partner in the Association EURATOM-NFR.

NIFS: National Institute for Fusion Science, Nagoya, Japan.

NRIM: National Research Institute for Metals, Sakura-mura, Japan.

Non-inductive heating and current drive: See additional heating and current drive.

NSTX: Spherical tokamak at Princeton, USA. A similar size to MAST, but of different design. Started operation in 1999.

Ohmic heating (OH): The resistive heating resulting from a current flowing within the plasma corresponding to the heating of a wire by a current flowing through it. Ohmic heating in a tokamak is insufficient to reach thermonuclear temperatures since, contrary to a wire, the resistance of a plasma decreases strongly with increasing temperature, thus making Ohmic heating weak at high temperatures.

ORNL: Oak Ridge National Laboratory, USA.

Operating limits: See tokamak operating boundaries.

Optimised shear: Adjusting the current profile to optimise tokamak.

PbLi: Eutectic lithium-lead alloy considered for use as blanket breeding material.

Peeling mode: An edge MHD instability which exists when the current density at the plasma edge is non-zero. It may be associated with ELMs.

Pellet: In inertial confinement concepts, the fuel is contained in tiny spheres, called pellets, which are compressed by laser or particle beams. In magnetic fusion, pellets of frozen hydrogen, deuterium, tritium, accelerated up to several kilometres per second, are used to refuel the plasma and to obtain very high densities.

PIREX: Proton Irradiation Experiment, material test facility (Association Euratom-Switzerland, CRPP-FT, PSI, Villigen, CH).

Plasma: State of matter above a few thousand degrees where atoms are broken into their constituents, ions and electrons, thereby creating an electrically conducting medium. Plasmas can therefore interact strongly with electric and magnetic fields.

Plasma confinement: Retention of plasma energy or particles within a given region, including the heat and particle losses from the plasma.

Plasma parameters: Physical quantities which characterise the plasma and which must be measured experimentally, such as current, density, temperature, confinement time, β.

Plasma pressure: Proportional to the product of plasma density and temperature. There is an electron and an ion pressure and the plasma pressure is the sum of the two. In magnetic confinement devices, this pressure is counterbalanced by magnetic pressure.

Plasma shape: Describes the plasma vertical cross-section, circular, elongated, D-shape, diverted, single null, double null.

Polarimetry: Measurement of the rotation of the plane of polarisation of light passing through a magnetically confined plasma; used to measure the local magnetic field and thus the safety factor (see Faraday rotation).

Poloidal field: Component of the magnetic field perpendicular to the toroidal direction and the major radius. The poloidal field is essential for confinement and is generated in a tokamak by the plasma current and the external coils.

Power threshold: The L-H transition and improved performance regimes related to reversed shear occur when the power exceeds a certain threshold value - the power threshold.

PPPL: Princeton Plasma Physics Laboratory, New Jersey, USA.

Preliminary Tritium Experiment (PTE): Three plasma discharges on JET, November 1991, into which a significant amount of tritium was injected for the first time in a tokamak. The power liberated from fusion reactions (~ 2MW for ~ 2 seconds) was in accordance with expectations. Followed by the more ambitious DTE in 1997.

Profile: Variation of plasma parameters with minor radius.

Profile control: Controlling the profiles of pressure, density or current, in order to control instabilities.

PSI: Paul-Scherrer-Institut, Villigen, Switzerland, active, in muon physics among others fields. The Association EURATOM-Swiss Confederation has their fusion technology activities working in superconductor and materials technology located at Villigen.

Pumped divertor: Divertor field lines directed into a pumped chamber surrounding the target plate.

q, q_{95}: See Safety factor.

Q: Ratio of fusion power to total additional heating power. At Q= , no external power is required and the plasma is said to be ignited. A power station should operate with Q~50 to be economical.

Radial electric field: Arises when there is a charge imbalance in the plasma.

Radio frequency (RF) heating: Heating with waves in the radiofrequency range at resonance frequencies of the plasma (see ECH, ICRH, LHH).

Reflectometry: Use of reflected microwaves to measure plasma density.

Relaxation: The evolution of a plasma to a lower energy state.

Resistive ballooning modes: A class of ballooning mode which would be stable in the absence of resistivity, but can be unstable in its presence. Related to tearing modes, but topologically different.

Resistive instability: Instability due to diffusion and rearrangement of magnetic field lines. When the plasma resistivity is small, these instabilities have a slow growth rate.

Resistivity: The tendency to resist the flow of electric current, thereby dissipating energy. Plasmas are very good conductors of electric current, so that their resistivity can often be neglected. In this case, 'ideal' magnetohydrodynamics may be applied.

Resonant ions/electrons: Resonance occurs when one of the characteristic frequencies of particle motion in the plasma (for example, the cyclotron frequency) matches the frequency of some applied perturbation (for example, an RF wave).

Resonant magnetic perturbation (RMP): An externally applied magnetic perturbation matched to the spatial structure and optionally the frequency and phase of an instability.

Reverse Field Pinch (RFP): A toroidal magnetic confinement device, similar to a tokamak, in which the poloidal and toroidal fields are of comparable magnitude. Capable of higher plasma current and pressure for a given external magnetic field. They require a conducting shell close to the plasma for stabilisation.

Reverse (magnetic) shear: In a tokamak the current density is usually greatest at the magnetic axis, in which case the safety factor increases from the centre to the edge of the plasma. Using non-inductive current drive and/or the bootstrap current the current density can be made to increase away from the centre. In this “reverse shear” case, the safety factor has a minimum away from the plasma centre. Using reverse or low shear (“optimised shear”) some tokamaks, notably DIII-D and TFTR in the US and more recently JT-60U in Japan and JET, have shown greatly improved plasma performance. Reverse shear is an attractive option for advanced tokamak scenarios.

RF: Radio-Frequency.

RFX: Reversed Field pinch Experiment at CNR-Padova, Italy (Association EURATOM-ENEA).

RISØ: Forskningscenter Risø, Denmark. Partner in the Association EURATOM-RISØ.

Rotational transform: Measure of the ratio of poloidal to toroidal flux defining the pitch of the helical field lines. The q-value of the tokamak is proportional to the reciprocal of the rotational transform.

RTP: Rijnhuizen Tokamak PETULA, for study of transport in a plasma, at Nieuwegein (Rijnhuizen), the Netherlands (Association EURATOM-FOM). Ceased operation in 1998, the activities of the Association being transferred to TEXTOR, as part of the Tri-lateral Euregio Cluster.

Runaway electron: An electron with a very high energy has a decreasing probability of colliding with another charged particle and of losing its energy. Such a particle then gains more and more energy in the electric field of a tokamak, reaching 10's of MeV.

Safety factor: Number of turns the helical magnetic field lines in a tokamak make round the major circumference for each turn round the minor circumference, denoted q. Has no connection with the ordinary sense of “safety” other than q=1 surfaces are ideally unstable. For diverted plasmas q goes to infinity at the separatrix, so instead q_{95} is used to describe the safety factor near the edge, which is the safety factor of the plasma surface which contains 95% of the poloidal flux.

Sawtooth: A cyclically recurring instability which causes an energy loss from the central region of tokamak discharges. The temperature periodically falls abruptly, then slowly recovers. The jagged trace produced by plotting temperature against time gives the instability its name.

Sawtooth crash: The rapid collapse of the central temperature in a tokamak during a sawtooth cycle.

Scaling laws: Empirical or theoretical expressions for how various plasma phenomena (eg confinement, power threshold, etc) vary with tokamak parameters. They are particularly used for predicting the performance of future tokamaks.

Scrape-off-layer (SOL): The residual plasma between the "edge" of the plasma (defined by the limiter radius or the separatrix) and the tokamak vessel wall.

Semi-empirical: A theoretical approach in which the behaviour of some key quantities is deduced from experiment, rather than a priori.

SEAFP: The Safety and Environmental Assessment of Fusion Power is an extensive study conducted by several teams in the associated laboratories, NET, industry and the JRC, published in June 1995.

SEAL: The Safety and Environmental Assessment of Fusion Power Long-term is a programme, launched in 1995, being undertaken for the European Commission in the framework of the Fusion Programme.

Separatrix: Magnetic surface at which the rotational transform vanishes and the safety factor becomes infinite.

Shear: The safety factor usually varies from magnetic surface to magnetic surface across the plasma cross-section; this variation is measured by the non-dimensional quantity called "shear". Also refers to the variation of plasma flow (flow shear). If the type of shear is not specified, it usually means magnetic shear.

Single/double null: Points of zero poloidal magnetic field where the separatrix crosses itself are the X-points or nulls. Usually sited above and/or below the plasma. Tokamak divertor configurations have either one or two nulls.

Single fluid model: The set of equations which represent a plasma as a magnetised, electrically conducting fluid with the usual fluid properties of viscosity, thermal conductivity, etc. The possibility of distinct behaviour of electrons and ions (i.e. 2 "fluids") is excluded.

Small aspect ratio: Same as Low aspect ratio.

Spectroscopy: The detection and analysis of the spectrum of radiation emitted by a plasma. This can yield information about temperatures, impurities, rotation, using different parts of the electromagnetic spectrum (IR, visible, VUV, XUV, etc.)

Spherical tokamak (ST): A very low aspect ratio tokamak - it appears almost spherical, though topologically it remains a torus with a centre column. The spherical tokamak is being further investigated, with larger experiments, MAST and NSTX.

Spheromak: A spherical plasma in which comparable toroidal and poloidal currents flow. The toroidal current is not driven by transformer action.

Stability theory: The theory of how small perturbations to a system evolve in time. Spontaneous growth is due to instability. Instabilities can saturate at some small amplitude, in which case they may degrade confinement, or grow uncontrollably, in which case the equilibrium is lost leading to a disruption.

START: Small Tight Aspect Ratio Tokamak, a "spherical" tokamak with a very small aspect ratio at the Association EURATOM-UKAEA (Culham). This very fat ring-shaped configuration showed experimentally a lesser tendency to disruptions and is efficient in its use of magnetic energy. Ceased operation in 1998, replaced by MAST.

Start-up assist: Assisting plasma formation to cross a range of plasma temperature at which impurities radiate strongly, with the aim of minimising the start-up delay and transformer requirements, usually using ECH.

STAC: Scientific and Technical Advisory Committee set up by EURATOM.

Steady state power plant: A continuously (as opposed to cyclically) operated power plant.

Stellarator: Closed configuration having the shape of a three-dimensionally distorted ring in which the plasma is confined principally by an externally generated magnetic field (produced by non-planar coils outside the plasma vessel). The coils can be arranged in a modular fashion. Stellarators do not need a transformer; they need an additional heating system for the plasma start-up. Due to the fact that no toroidal plasma current is needed to maintain the confinement configuration, they naturally provide steady state operation.

SULTAN: Supra Leiter Test ANlage. Large Superconductor Test Facility, CRPP at PSI Villigen, Switzerland (Association EURATOM-Swiss Confederation).

Super Alfvénic velocity: A velocity greater than the Alfvén velocity. In a tokamak, only energetic particles have super Alfvénic velocities; because they satisfy this condition, they may resonantly transfer their energy to magnetohydrodynamic modes, which may grow as a result (eg TAE modes).

Superthermal radiation: Electromagnetic radiation produced by energetic particles, as opposed to thermal particles.

Survey spectrometer: An instrument which gives information concerning the radiated spectrum over a large range of frequencies.

TAE modes: Toroidal Alfvén Eigenmodes. One class of Alfvén gap modes.

Target plates: See Divertor.

TCV: "Tokamak à Configuration Variable", for study of elongated and strongly shaped plasmas, at Lausanne, Switzerland (Association EURATOM-Swiss Confédération).

TEKES: Technology Centre Finland. Partner in the Association EURATOM-TEKES.

Tearing magnetic islands: The disturbance caused by a tearing mode which alters the topology of the confining magnetic field and causes transfer of heat across the affected region.

Tearing mode: A class of resistive MHD instability which has been predicted theoretically in tokamaks and positively identified in experiments.

Temperature pedestal: In an H-mode discharge there is a region of steep temperature gradient at the plasma edge. The temperature at the top of this steep gradient region is the temperature pedestal.

Tesla: Unit of magnetic field strength (more exactly the magnetic induction). $1T = 1Vs/m^2 = 10{,}000$Gauss.

TEXTOR: Torus Experiment for Technology Oriented Research. Tokamak at Jülich, Germany (Association EURATOM-FZJ). Refurbished and upgraded, in 1994, as TEXTOR-94.

TFTR: "Tokamak Fusion Test Reactor" at Princeton, the largest US device with a major campaign using deuterium-tritium fuel from 1993 - 1997. Ceased operation in March 1997.

Thermal cycling: Successive heating and cooling of materials can lead to cracks or rupture, particularly at boundaries between materials that expand at different rates.

Thermal particles: As a result of collisional energy exchange, the energy of most plasma particles falls within a Maxwellian distribution which is described by a single temperature (typically 1-30keV for tokamaks). These are the thermal particles, as distinct from energetic particles which lie outside the thermal distribution.

Thomson scattering diagnostic: Diagnostic to measure temperature and density by detecting laser light scattered and Doppler shifted by the thermal plasma electrons.

Tight aspect ratio: Same as Low aspect ratio.

TJ-II: A heliac stellarator at Madrid, Spain (Association EURATOM-CIEMAT). (TJ-IU was a torsatron at CIEMAT, built and operated in preparation for TJ-II).

Tokamak: Magnetic configuration with the shape of a torus. The plasma is stabilised by a strong toroidal magnetic field. The poloidal component of the magnetic field is produced by an electrical current flowing toroidally in the plasma. This current is induced via transformer action and, for steady state, must be maintained by non-inductive current drive and by self-generation of bootstrap current inside the plasma.

Tokamak operating boundaries: The set of plasma parameters, beyond which it is impossible to operate a tokamak. Careful choice of plasma cross-sectional shapes and current and pressure profiles can increase the operating regime.

TORE SUPRA: Large tokamak with superconducting toroidal magnetic field coils and a circular plasma cross-section at the Association EURATOM-CEA in Cadarache, France. It features long high total energy plasmas.

Toroidal Alfvén Eigenmodes: See TAE modes.

Toroidal field: The component of the magnetic field along the major circumference of the torus. The largest magnetic field component in a tokamak.

Toroidal stability: Stability analysis taking account of effects due to the toroidal geometry. These are sometimes neglected to identify possible instabilities, but must usually be included for accurate predictions of stability boundaries.

Toroidal turbulence code: A turbulence code which includes effects due to the toroidal geometry.

TOSKA: Large testing facility for superconductors (Association EURATOM-FZK, Karlsruhe, Germany).

Transformer drive: The use of a transformer action to induce plasma current.

Transport: The processes by which particles and energy move across magnetic surfaces.

Transport barrier: In certain operational scenarios (e.g. the H-mode or ITB-mode) a region of low transport exists giving rise to a steep local pressure gradient. Such a region is referred to as a transport barrier.

Transport scaling: The magnitude of heat transport may be expressed, empirically or theoretically, in terms of a simple functional dependence on a few plasma parameters. This allows us to model how the heat transport varies (scales) in response to changes in the value of these parameters.

Trapped particles: The outside (large major radius) of a tokamak plasma has a lower magnetic field than the inside. Particles with low velocity parallel to the magnetic field compared with the velocity perpendicular to the magnetic field may not enter the higher field (inside) region and become trapped on the outside. They are not free to circulate toroidally but instead bounce back and forth, performing so-called banana orbits.

Tri-lateral Euregio Cluster (TEC): A collaboration between the Associations Euratom-FZJ, -FOM and –Etat Belge, to exploit the TEXTOR tokamak at FZJ, Julich, Germany.

Tritium: An isotope of hydrogen, whose nucleus consists of one proton and two neutrons. Tritium is unstable to radioactive decay with a half-life of 12.3 years. Due to its rapid decay, tritium is almost absent on earth. For a fusion reactor, tritium will be produced in the breeding blanket surrounding the core of a fusion power station. Special tritium-handling technology is required whenever the use of deuterium-tritium plasmas is contemplated and has been developed on TFTR and JET.

Tritium inventory: The amount of tritium contained in a fusion power station or in a specified part of it.

Turbulence: Randomly fluctuating, as opposed to coherent, wave action. For example, the turbulent water beneath a waterfall can only be described in terms of its averaged properties, such as the scale and duration of fluctuations; whereas a more systematic description can be given to waves on the surface of a still pond.

Turbulent transport: Anomalous heat transport associated with plasma turbulence.

Two-fluid model and multi-fluid model: The extended set of equations which represent a plasma as interpenetrating and interacting fluids of electrons and ions, impurity ions etc.

UKAEA: United Kingdom Atomic Energy Authority. Partner in the Association EURATOM-UKAEA which operates the tokamak COMPASS-D and the spherical tokamak MAST. Also charged with the operation of the JET facilities under EFDA.

Vertical Displacement Event (VDE): An event which arises when control of the plasma is lost and the plasma moves vertically. It can lead to a “halo current” in components which surround the plasma resulting in large, potentially damaging, forces on these components. The forces are much larger in larger tokamaks and are therefore of particular concern for JET and ITER.

VUV: The “Vacuum Ultra Violet” range of the electromagnetic spectrum.

Warm plasma refuelling: Fuelling of plasma using medium energy particles or particle clusters.

WEC: World Energy Council.

WENDELSTEIN VII-AS: Advanced stellarator, at Garching, Germany (Association EURATOM-IPP).

WENDELSTEIN VII-X: Large advanced superconducting stellarator, optimised to produce a reactor-relevant plasma configuration, designed at Garching. Construction is in progress at Greifswald, Germany (Association EURATOM-IPP).

X-point: See single/double null.

XUV: The "Extreme Ultra Violet" range of the electromagnetic spectrum. Shorter wavelengths than VUV.

<u>Acknowledgement:</u> This glossary was adapted from the "Glossary of fusion terms" by UKAEA Culham, UK, and from the glossary of "Fusion programme evaluation", 1996, EUR 17521, European Commission.